UNIVERSITY OF LIVERPOOL

Investigation of the molecular basis for p53-mediated metabolic regulation in head and neck cancer

Thesis submitted in accordance with the requirements of the University of Liverpool for the degree of Doctor in Philosophy by

Emad Abduljalil Abdulghani Anaam

November 2021

I. Abstract

Reprogramming energy metabolism, also known as the Warburg effect, has received considerable attention recently as a potential therapeutic target to improve the low survival outcomes of Squamous Cell Carcinoma of the Head and Neck (SCCHN). New evidence has demonstrated that loss-of-function mutations in *TP53*, the most commonly mutated gene in SCCHN, promotes the Warburg effect, but how this is mediated is unknown. The aims of this thesis were primarily to use a panel of SCCHN cell lines with defined p53 status (including two sets of isogenic cell lines) and microplate-based extra-cellular oxygen and proton flux analysis to examine in detail whether the exhibited metabolic phenotype is determined by the status of p53. Secondary aims were to investigate the mechanism that underlies this role of p53 which could lead to the identification of novel potential therapeutic strategies for SCCHN. RNAi and plasmid transfection were used to manipulate the expression of TIGAR (*TP53*-inducible glycolysis and apoptosis regulator), a potential target mediator of the p53-responsive cellular machinery that regulates glucose metabolism, to try to identify the role that TIGAR play in the Warburg effect with respect to changes in metabolic phenotype and sensitivity to potential therapeutic agents. Metabolic profiling of SCCHN cells using microplate-based extra-cellular oxygen consumption and acidification measurements have shown that wild type *TP53* SCCHN cells display higher oxygen consumption rates (OCR) compared to cells harbouring mutant *TP53*, while cells harbouring mutant *TP53* showed significantly higher extracellular acidification rates (ECAR) in comparison to wild type *TP53* cells. This indicates that the p53 status is a dominant determinant of metabolic reprogramming in SCCHN. My results also show that although TIGAR knockdown promotes glycolytic functions in wild type p53 cells, it promotes both mitochondrial and glycolytic functions in p53-null cells, but not in mutant p53 cells, which may suggest an alternative mechanism or a possible role of gain of function (GOF) that regulates the role of TIGAR in the absence of wild type p53. In addition, although TIGAR knockdown shows no significant change in the balance between glycolysis and mitochondrial respiration in p53-null and mutant p53 cells, it changes the balance towards aerobic glycolysis in wild type p53 cells, which indicates that the TIGAR role in the metabolic switch toward glycolysis is primarily regulated by p53. I also found that TIGAR-knockdown-mediated increase in glycolysis results in sensitising the wild type p53 SCCHNs to radiotherapy. Thus, it is plausible to speculate that identifying TIGAR inhibitors may prove to be a beneficial approach to treatment in the future.

II. Acknowledgement

First and foremost, I would like to express my deepest gratitude to my supervisors, Professor Mark Boyd and Dr Nikolina Vlatković, for giving me the opportunity to work on this project and for all the help, encouragement and support I have had from the first day.

I would like to thank the University of Liverpool and Cara team for all of their help and support in funding this project.

I would also like to thank Dr Amy Chadwick from the Department of Molecular and Clinical Pharmacology for her invaluable assistance with the Seahorse XFe96 instrument.

It was a long journey with many challenges and difficulties that I was able to overcome thanks to the friendly work environment and the assistance and support I received from all the former and current members of our research group, as well as all staff and colleagues in the Cancer Research Centre, which made it a truly enjoyable experience.

I thank my wife Sameeha for the constant support, love and encouragement throughout the years of research. Achieving this PhD would not have been possible without her. This also applies to my son Sam; whose smile sometimes was more than enough to keep me sane and optimistic.

I thank my parents and my sisters and brothers for always being there for me every time I needed them.

I hope the coming days will bring peace and happiness to my home country, Yemen.

III. Disclaimer

All the experiments, results and conclusions embodied in this thesis, except for mycoplasma testing, STR profiling and Sanger sequencing, are the work of the author. Preparing samples for mycoplasma testing, STR profiling and Sanger sequencing was done by the author as detailed in Appendix (chapter 6). The mycoplasma testing was performed as a service at the University of Liverpool, with the assistance of Mr Steven Hoang. STR profiling was performed as a service at the University of Liverpool, with the assistance of Dr Lakis Liloglou (University of Liverpool). Sanger sequencing was performed as a service by Source BioScience lab (Nottingham, UK).

This thesis was written entirely by the author under the guidance of supervisors, Professors Mark Boyd and Dr Nikolina Vlatković.

IV. Table of Contents

V. List of Figures

VI. List of Tables

VII. Abbreviations

2-DG	2-Deoxy-d-glucose
2PG	2-Phosphoglycerate
3PO	[3-(3-pyridinyl)-l-(4-pyridinyl)-2-propen-l-one]
4EBP1	4E-binding protein 1
6-AN	6-Aminonicotinamide
6-PGD	6-Phosphogluconate dehydrogenase
AIF	Apoptosis-Inducing factor
AJCC	American Joint Committee on Cancer
AMPK	Adenosine monophosphate-activated protein kinase
APAF1	Apoptotic protease activating factor 1
ATG	Autophagy-related gene
ATP	Adenosine triphosphate
BAX	BCL2 associated X, apoptosis regulator
BBC3	BCL2 binding component 3
BH3	Bcl-2 homology 3
BID	BH3 interacting-domain death agonist
CBP	CREB-binding protein
CDK	Cyclin-Dependent Kinase
CDKN	Cyclin-Dependent Kinase Inhibitor
CT	Computerized tomography
CTD	C-terminal domain
DBD	DNA-binding domain
DCA	Dichloroacetate
DDR	DNA damage responses
DISC	Death-inducing-signalling-complex
DR5	Death Receptor 5
DRAM	DNA Damage Regulated Autophagy Modulator
ECAR	Extracellular Acidification Rates
EGF	Epidermal Growth Factor
EGFR	Epidermal Growth Factor Receptor
EIF4E	Eukaryotic Translation Initiation Factor 4E
EIF4G	Eukaryotic Translation Initiation Factor 4G
ENO	Enolase
ETC	Electron transport chain
F1,6BP	Fructose-1,6-bisphosphate
F2,6BP	Fructose-2,6-bisphosphate
FADD	Fas-associated death domain protein

FBPase-2	Fructose-2,6-bisphosphatase
FDA	Food and Drug Administration
FDG	2-[fluor-18] fluoro-2-deoxy-D-glucose
G6PD	Glucose-6-phosphate dehydrogenase
GADD45	Growth arrest and DNA-damage-inducible protein 45 gene
GDP	Guanosine diphosphate
GLUT	Glucose transporter
GOF	Gain of Function
GSH	Glutathione
GTP	Guanosine-5'-triphosphate
HDI	Human Development Index
HIF	Hypoxia-Inducible Factor
HK	Hexokinase
HPV	Human Papillomavirus
IGF	Insulin-like growth factor
IGFBP	IGF-binding protein
IHC	Immunohistochemistry
IL-6	Interleukin 6
IR	Ionising Radiation
ISH	*In situ* hybridization
kDa	Kilodalton
LDH	Lactate dehydrogenase
MAPK	Mitogen-activated protein kinases
MCT-1	Monocarboxylate transporter 1
Mieap	Mitochondria-eating protein
MOMP	Mitochondrial outer membrane permeabilisation
MPC	Mitochondrial pyruvate carrier
MRI	Magnetic resonance imaging
mRNA	Messenger ribonucleic acid
mTOR	Mammalian target of rapamycin
NADH	Nicotinamide adenine dinucleotide
NF-κB	Nuclear Factor Kappa-Light-Chain-Enhancer of Activated B Cells
NMR	Nuclear magnetic resonance
NTD	N-terminal domain
OCR	Oxygen Consumption Rates
p14ARF	Alternate Reading Frame Protein
p53C	p53 core domain
PCNA	Proliferating cell nuclear antigen
PCR	Polymerase-chain-reaction

PDC	Pyruvate dehydrogenase complex
PDH	Pyruvate dehydrogenase
PDK	Pyruvate dehydrogenase kinase
PDPK1	3-phosphoinositide-dependent protein kinase-1
PEP	Phosphoenolpyruvate
PET	Positron emission tomography
PFK	Phosphofructokinase
PFKFB	6-phosphofructokinase/fructose-2,6-biphosphatase
PGAM	Phosphoglycerate mutase
PI3K	Phosphoinositide 3-kinase
PIP3	Phosphatidylinositol (3,4,5)-trisphosphate
PKM2	Pyruvate isoform kinase M2
PMAIP1	Phorbol-12-myristate-13-acetate-induced protein 1
POLA1	DNA polymerase alpha 1
PPP	Pentose phosphate pathway
pRb	Retinoblastoma Protein
PRR	Proline-rich region
PTEN	Phosphatase and tensin homolog
PUMA	p53 upregulated modulator of apoptosis
RE	Response element
RNAi	RNA Interference
ROS	Reactive oxygen species
RR	Relative risk
RT	Radiotherapy
SCC	Squamous Cell Carcinoma
SCCHN	Squamous Cell Carcinoma of the Head and Neck
SCO2	Cytochrome c oxidase assembly protein
SEER	Surveillance Epidemiology and End Results
SH3	Src homology 3 domains
STAT	Signal transducer and activator of transcription
TAD	Transactivation domain
TCA	Tricarboxylic acid cycle
TGF	Transforming growth factor
TIGAR	*TP53*-Inducible Glycolysis and Apoptosis Regulator
TKI	Tyrosine Kinase Inhibitors
TNFR	Tumour necrosis factor receptor
TNM	Tumour-Node-Metastasis
TSC2	Tuberous sclerosis protein 2

1. Introduction

Squamous Cell Carcinoma of the Head and Neck (SCCHN) is the most common type of head and neck cancer (1), which is the eighth most common cancer worldwide (2). The poor survival rates of SCCHN have not increased remarkably, despite advanced surgical techniques, new chemotherapeutic drugs and improvements in radiotherapy, within the last three decades, with the best improvement occurred in cancer of the oral cavity (3–5).

The most common molecular alterations in SCCHN are the mutations of the tumour suppressor gene *TP53* (6), which plays a pivotal role in the metabolic regulation of SCCHN by promoting mitochondrial respiration and limiting glycolytic flux through multiple mechanisms, including the regulation of the *TP53*-inducible glycolysis and apoptosis regulator (TIGAR)(7). However, the mechanisms through which p53 regulates glucose metabolism in SCCHN are not fully understood and research is needed to understand the role of p53-mediated metabolic regulation in determining the response to therapeutic agents currently used to treat these cancers, and also to enable the development of novel future therapeutic strategies. In this introduction, I will review some of our current understanding of the molecular basis of SCCHN, the role and function of p53, and also glucose metabolism in cancer and the function of TIGAR.

1.1. Squamous cell carcinoma of the head and neck

1.1.1. Definition and regional anatomy

The term "head and neck cancer" refers to a broad heterogeneous set of epithelial malignancies that vary in natural history, treatment, and prognosis (8,9). It includes cancers of the paranasal sinuses, the salivary glands and the upper aerodigestive tract (Figure 1.1.) (8,9). The major common feature of head and neck cancers in addition to the proximity of anatomical location is the fact that approximately 95% of these malignancies are squamous cell carcinomas (squamous cell carcinomas of the head and neck or SCCHN)(9) and these are thus the exclusive focus of this thesis.

Squamous cell carcinoma (SCC) is a type of malignant epithelial tumour that develops following squamous metaplasia in the surface squamous epithelium or ciliated respiratory epithelium (10). SCCHN tumours arise from the mucosal surfaces of the

upper aerodigestive epithelium of four major anatomical locations: the oral cavity, the oropharynx, larynx and hypopharynx, and are classified based on these major anatomical subsites of origin (Figure 1.1.)(8). Despite the fact that nasopharyngeal carcinomas are histologically classified as squamous cells, they are distinct in their aetiology, epidemiology, and clinical behaviour, and are therefore not typically grouped together with SCCHN (9). Infection with the Epstein–Barr virus (EPV) is the most common cause of nasopharyngeal cancer, as the EBV genome is present in approximately 90% of nasopharyngeal cancer cases (11). Aside from alcohol and tobacco use, a number of other risk factors have been linked to the development of nasopharyngeal cancer, including the consumption of salt-preserved foods and exposure to wood-fire smoke (12). The disease behaviour of nasopharyngeal cancer is different from SCCHN as well. Approximately 90% of nasopharyngeal cancer patients develop lymphadenopathy and 50% of patients have bilateral lymph node involvement (13). The treatment strategies are also different due to the proximity of the base of the skull, which makes surgical resection with an acceptable margin impossible (14).

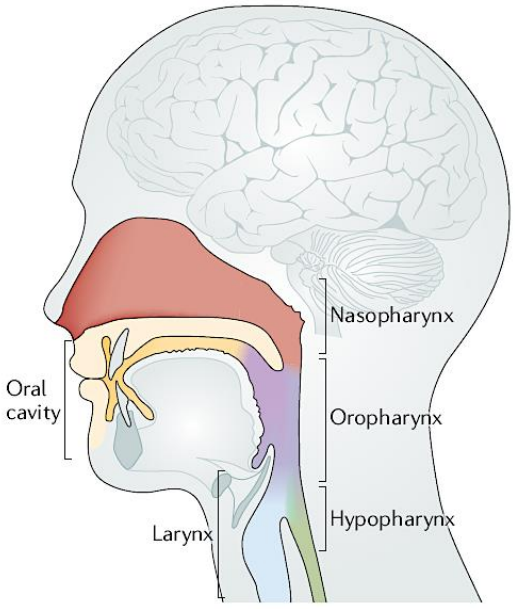

Figure 1.1.: Major anatomical subsites of squamous cell carcinoma of the head and neck. A diagrammatic depiction shows the four major anatomical subsites of the SCCHN. Histologically, nasopharyngeal carcinomas are squamous cells. However, these tumours exhibit distinct aetiological, epidemiological characteristics, and are not commonly grouped with SCCHN (15).

1.1.2. Epidemiology and risk factors

SCCHN is the sixth most prevalent cancer in the world with more than 700,000 new cases and accounts for 4% of all new cancer cases reported in 2018 worldwide. Males represent more than 80% of all SCCHN patients, and SCCHN accounts for 6% of all male cancer patients worldwide (16). The worldwide incidence rate is roughly 8.8 per 100,000 males and 5.1 per 100,000 females (17). In addition, SCCHN is the seventh most common cause of cancer-induced mortality worldwide with more than 358,000 annual deaths giving a mortality of 50%, which is responsible for 4% of all cancer-related deaths (16). Males represent 76% of total mortalities and SCCHN patients account for 5% of total cancer-related death among men worldwide (16). The mortality rate of SCCHN is approximately 7.3 per 100,000 for males and 3.2 per 100,000 for females (17).

In the United Kingdom (UK), SCCHN is the eighth most prevalent cancer, with more than 12,200 new cases annually, accounting for 3% of all new cancer cases (18). Males represent 70% of all new cases in the UK (18). In addition, SCCHN is the 16th most common cause of cancer death in the UK, with more than 4000 deaths every year, accounting for 2% of all cancer-related deaths (18). 71% of all SCCHN deaths in the UK are males (18).

Regional variations in incidence rates of SCCHN are primarily influenced by a number of demographics, environmental, lifestyle and biological risk factors.

1.1.2.1. Demographic factors

The incidence of SCCHN is influenced by gender and there is a strong male preponderance in SCCHN. SCCHN is the eighth most common cancer in women and the fifth in men. The male to female ratio varies depending on the site of the disease, as males are 2.3 times more likely to develop oral cancer, and over six times more likely to develop pharyngeal and laryngeal cancer than females (2). Interestingly, this ratio has been decreasing over time, most likely due to the increased number of female smokers (the role of tobacco smoking in SCCHN epidemiology will be reviewed in 1.1.2.2.1.).

In addition, there is wide geographical variation in the incidence and anatomic distribution of SCCHN around the world, suggesting a strong environmental component to demographic differences and exposure to risk factors (19). In men, the incidence of SCCHN is highest in Papua New Guinea (40.9 per 100,000) and Sri Lanka (24.5 per

100,000), and lowest in China (1.1 per 100,000) and Indonesia (1.5 per 100,000)(20). In women, the highest incidence is in Papua New Guinea (26.3 per 100,000) and Bangladesh (16.8 per 100,000) and the lowest incidence was reported in China (0.7 per 100,000)(20). Moreover, laryngeal cancer is relatively rare in women in comparison with men, with 0.86 new cases per 100,000 women worldwide in comparison with 4.64 per 100,000 men (21). About 53% of the SCCHN cases occur in countries with very high or high human development index (HDI), whose population represents only 20% of the global population. Although the incidence of oral cancer is on the decline in developing countries, there has been an increase in the incidence of the oral cavity and pharyngeal cancers in many developed countries, as is the case, for example, in southern and eastern European countries (9,10). Almost one-quarter of the new cases and one-third of the deaths from cancers of the oral cavity and pharynx occur in India, despite accounting for only 18% of the global population (17).

In addition, the prevalence of SCCHN is strongly linked to age, with a median age of diagnosis of 59-69 years (9). However, there has been an increase in the incidence of oral cavity cancer, particularly cancers of the tongue, in people under the age of 40 (9,10). SCCHN incidence is also higher among black people than white people most likely to be due to the greater rates of smoking and alcohol intake in blacks, whereas the rates of SCCHN are roughly equal in the absence of alcohol and tobacco in both races (19). Other socioeconomic factors, including income and education, are also all strongly linked with variations in SCCHN incidence. For example, a study of the associations between community income and cancer incidence in Canada and the United States found that the incidence rates of SCCHNs in males were higher in poorer communities, as the age-standardised incidence rate of SCCHN was 36-37 per 100,000 in poorer communities compared to 15-17 per 100,000 in communities with four times the income (9).

In the United Kingdom, the incidence of SCCHN has increased by 20%, (by 17% in males, and by 24% in females) over the last decade. Around 22% of all new SCCHN cases in the UK are diagnosed in people aged 75 and over, and most of the UK cases occur in the larynx (18). The age-specific incidence of SCCHN in both females and males in the UK population is depicted in Figure 1.2.

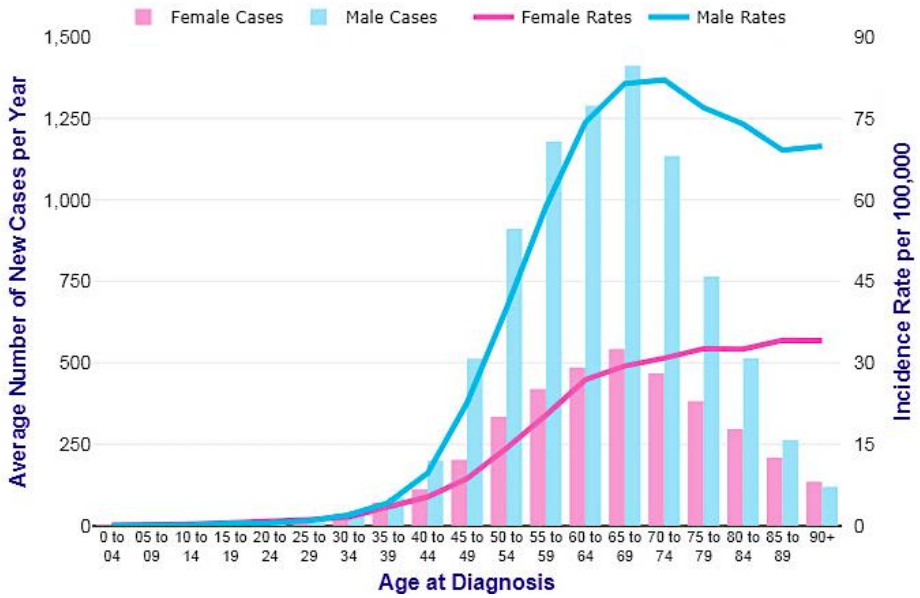

Figure 1.2.: The age-specific incidence of SCCHN in women and men in the UK between 2015 and 2017. Graphs illustrating both the total number of new cases per year (bars) and the age-specific incidence per 100,000 population (lines). There is a strong male preponderance in almost all age groups, with a substantial rise in incidence beginning at age 40 and peaking in the seventh decade. The figure is reproduced from the Cancer Research UK website (https://www.cancerresearchuk.org)(18)

1.1.2.2. Risk factors

Although tobacco smoking and alcohol consumption are the key risk factors for SCCHN worldwide (see below 1.1.2.2.1.)(19), betel quid chewing has been identified as a major exogenous risk factor for SCCHN in some East Asian countries, such as India, Sri Lanka and the Philippines (19). In addition, epidemiological studies show that a subset of SCCHN has a strong connection to the human papillomavirus (HPV)(see section 1.1.2.2.2.) (19). In addition to these risk factors, SCCHN risk is predisposed by hereditary disorders such as Fanconi anaemia and some other less well-understood genetic susceptibility (19).

1.1.2.2.1. ***Tobacco and alcohol consumption***

As stated in section 1.1.2.2. the major risk factors of SCCHN are tobacco smoking and alcohol intake. Essentially, carcinogens and the genotype of the affected individual are constantly interacting, eventually leading to cancer through a series of molecular alterations.

Individuals frequently combine tobacco and alcohol use, making it difficult to distinguish the separate effects of tobacco and alcohol on SCCHN incidence. Although nearly three-quarters of SCCHN cases are related to tobacco and/or alcohol intake, only a small proportion of smokers and drinkers develop SCCHN (9). The relative risk for SCCHN increases with the intensity (cigarettes per day) and the duration of smoking (pack-years). Furthermore, females are at a higher risk of SCCHN than males exposed to the same amount of tobacco (22). Despite these strong associations, 5 to 30 per cent of SCCHN cases arise in non-smokers (23). Similar to tobacco smoking and alcohol intake, the use of oral or nasal smokeless tobacco, such as the chewing of betel quid or areca nut or oral snuff, is also a strong risk factor for SCCHN cancers. More than 25% worldwide, and more than 50% in Sudan and India, of all cancers among smokeless tobacco smokers are cancers of the oral cavity. However, there is a weaker association between smokeless tobacco and the prevalence of larynx cancers (19).

1.1.2.2.2. *Human papillomavirus (HPV)*

Although the majority of SCCHNs are negative to infection with high-risk (oncogenic) types of human papillomavirus (HPV), a subset of SCCHN cancers, in particular those of the oropharynx, are caused by infection with high-risk types of HPV. A review of 60 studies by Kreimer et all (2005) found that 35.6% of oropharyngeal SCCHNs (95% CI, 32.6-38.7), 24.0% of laryngeal SCCHNs (95% CI, 21.8-26.3) and 23.5% of oral SCCHNs (95% CI, 21.9-25.1) are HPV positive (24). HPV are a family of circular DNA viruses that includes over 100 types that infect and replicate in mucosal epithelial cells (25).

The HPV genome is comprised of a non-coding regulatory region and early and late genes (19). Three proteins (E5, E6, and E7) coded by the early (E) open reading frames of the high-risk HPV genomes are oncogenic proteins because of their ability to abrogate the function of the p21, p53, and pRb proteins, which predisposes the cell to genomic instability resulting in defects in cell cycle regulation, DNA repair and apoptosis (Figure 1.3.)(19).

Because of the rising interest in vaccination and the encouraging effects(26), HPV^{+ve} SCCHN is going to increasingly become a rarity in the UK and worldwide with vaccination programmes, HPV^{-ve} will be the exclusive focus of this thesis.

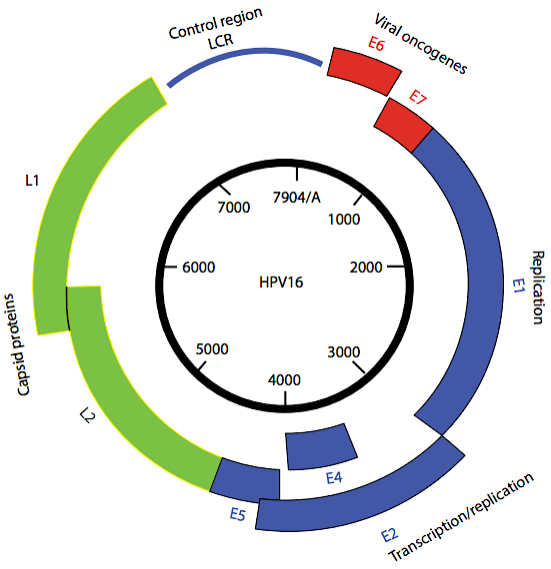

Figure 1.3.: The structure an HPV genome. A schematic representation of the HPV genome showing the early genes (*E1, E2, E4, E5, E6* and *E7*), and the late genes (*L1* and *L2*). *E5*, *E6*, and *E7* code oncoproteins. The figure is reproduced from reference (11).

1.1.2.3. SCCHN outcomes

Whilst the overall survival rates of SCCHN have not changed much in the past three decades, this fact conceals some very significant differences depending upon disease subsite and whether or not the disease is associated with carcinogens and or oncogenic virus infection (HPV). The 5-year overall survival rate of SCCHN varies from 28% to 82%, with the wider range being attributed to differences in geographical location and the prevalence of risk factors (19). According to statistics from the Surveillance Epidemiology and End Results (SEER) website, the combined SCCHN 5-year survival rate for all stages and all races in the United States was about 59% between 1995 and 2001, which is one of the lowest 5-year survival rates among all cancers (27). In addition, this wide range in survival rate also depends on race, stage, and anatomical subsite with the worse survival rates observed for cancers of the hypopharynx (19). In Europe, SCCHN has a 5-year overall survival rate of 42%, ranging from 54% in patients younger than 45 years to 35% in patients older than 75 (28). So clearly, there is an urgent need to find new ways to improve patient outcomes. The main reasons for such low survival rates are likely to be the high percentage of patients diagnosed in advanced stages, the lack of sensitive and specific markers for early detection and the failure of many tumours to respond to current standards of care such as chemo-radiation, as well as the lack of knowledge of the underlying mechanisms of SCCHN carcinogenesis which obstructs the

development of more effective treatment approaches and for this reason, I will next consider the molecular basis of SCCHN disease.

1.1.3. Molecular carcinogenesis

Many genetic and epigenetic events are involved in the gradual acquisition of a malignant phenotype in SCCHN, including abnormal function, loss of function and altered expression of molecules that control cell proliferation, signalling, survival, angiogenesis and the cell cycle. Elucidating and understanding the basic molecular mechanisms underlying SCCHN carcinogenesis may help to develop novel strategies for diagnosis, prevention and treatment of disease (29), including the development of monoclonal antibodies targeting surface antigens expressed on tumour cells or small molecule tyrosine kinase inhibitors (TKI), or methods to manipulate or reintroduce the *TP53* gene, the most mutated gene in SCCHN (30). Recent studies using genome sequencing in SCCHNs have shown a high frequency of alterations in a number of genes that contributes to cellular homeostasis including *TP53*, *RB*, *HRAS*, *PIK3*, *mTOR* and *AKT* (6,31). In the following sections, I will briefly discuss the most frequent genetic alterations in SCCHN.

1.1.3.1. Molecular alterations in SCCHN

The accumulation of genetic and epigenetic alterations in SCCHN, as stated in section 1.1.3., which include changes in oncogenes and tumour suppressors, lead to dysplasia, carcinoma in situ and invasive tumours (19). There is a potential contribution of alterations in many tumour suppressor genes in SCCHN, such as *TP53* (discussed in detail in 1.2.), p16 (cyclin-dependent kinase inhibitor 2A or *CDKN2A*), which is responsible for G1 cell cycle regulation, the alternative reading frame tumour suppressor *P14ARF*, which is responsible for MDM2 mediated degradation of p53 (32).

1.1.3.1.1. *TP53*

The protein product of the *TP53* gene is a transcription factor that acts as a potent tumour suppressor (33). p53 protein regulates the activity of multiple functions that control cell cycle, genome stability and apoptosis (33)(discussed in detail in 1.2.2.). p53 regulates cell division by preventing cells from growing and proliferating in an uncontrolled manner (33). Almost all tumours lose the normal function of the *TP53* gene, either due to upregulation of negative regulators of *TP53* function, or gene mutations or

deletions. Loss of heterozygosity for the *TP53* locus has been identified in approximately 60% of SCCHNs (see section 1.2.)(34).

1.1.3.1.2. *pRb*

The retinoblastoma protein (pRb), encoded by the first tumour suppressor gene to be identified (*RB1*), regulates cell cycle progression (35). The active (dephosphorylated) pRb binds to the transcription factor E2F protein, which is part of a heterodimeric transcription complex, thereby inhibiting E2F-mediated transcription of other cyclins, including E and A and genes essential for G1/S progression, such as DNA polymerase alpha (*POLA1*), leading to cell cycle arrest at G1 and inhibiting cells from entering the S phase (Figure 1.4.)(35).

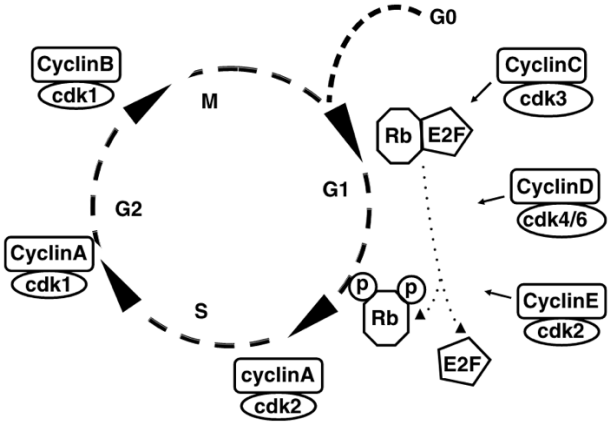

Figure 1.4.: The role of pRb in the cell cycle. pRb protein bind to the transcription factor E2F protein, blocking E2F transactivity and inhibiting E2F-mediated transcription of other cyclins in G0 and early G1. In late G1, pRb is inactivated by cyclin-CDK-mediated phosphorylation, releasing E2F, allowing the transcription of genes essential for G1/S progression. The figure is reproduced from reference (35).

Inactivating pRb, by cyclin-CDK-mediated phosphorylation, results in E2F release and activation which enables cells to initiate the synthesis of DNA (35). The loss of pRb functions, caused either by chromosomal mutations in the *RB1* gene or altered activity of upstream regulators, allows cells to progress through the cell cycle and is common in most types of human cancer (35). In SCCHN tumours, lack of pRb expression has been reported at a variable rate (11-66%) (36,37), but *RB1* mutations are usually rare (36).

1.1.3.1.3. *NF-κB*

The key role of the nuclear factor kappa B (NF-κB) is regulating the expression of genetic programs involved in immune responses, and it is a crucial component of the

intracellular regulatory circuits that control proliferation and survival (38). The expression and function of NF-κB is often altered in SCCHN. NF-κB promotes the expression of the antiapoptotic protein Bcl-2 in SCCHN, and NF-κB protein levels rise steadily with increasing invasiveness and tumour aggressiveness (39).

1.1.3.1.4. *TGF-β*

Transforming growth factor-beta (TGF-β) plays a dual role in epithelial malignancies, including SCCHN. During the early stages of carcinogenesis, TGF-β acts as a potent tumour suppressor, thus attenuation of the TGF-β signalling pathway enhances *de novo* tumour development. However, TGF-β promotes also tumour development at later stages (40).

1.1.3.1.5. *EGFR*

The abnormal activity of the epidermal growth factor receptor (EGFR) family has been associated with the development and growth of many types of tumours including 80-90% of all SCCHNs (41). This family of genes is essential for many normal cellular processes, such as differentiation, cell proliferation, and survival (42). The predominant mechanism that leads to overexpression of these kinases is thought to be an increase in EGFR transcription, with no apparent change in the stability of its mRNA (41). Amplification of the EGFR gene was also identified in SCCHN, with more than 12 copies per cell (43). The activated form of EGFR plays a role in inducing a number of downstream signalling events that contribute to abnormal cell growth and metastatic potential of SCCHN, such as the phosphatidylinositol-3-kinase (PI3K)/ serine/threonine kinase 1 (AKT)/mammalian target of rapamycin (mTOR) pathway, as wells as Ras and STAT signalling pathways. These biochemical pathways are often persistently active in SCCHN (see section 1.1.3.3.)(44).

1.1.3.2. Cell cycle regulation

Loss of a functional p16 gene contributes to avoiding the replicative stress-induced senescence and to the loss of ability to suppress abnormal growth (45). p16 is a tumour suppressor protein that functions through its activity as a cyclin-dependent kinase (CDK) inhibitor. The normal function of p16 is to inhibit CDK4/Cyclin D and CDK6/Cyclin D complexes by binding to either CDK4 or CDK6 and preventing their association with D-type cyclins. These complexes normally control cell cycle progression

by inhibiting the growth-inhibiting activity of pRb (Figure 1.4.). Disassociation of CDK4/Cyclin D and CDK6/Cyclin D complexes by p16 also leads to Cyclin D degradation, resulting in termination of its cell cycle regulation activities toward the end of the G1 phase (45). Alterations in p16 were reported in 19-33% of SCCHN tumours (46–48).

1.1.3.3. Signalling pathways

The abnormal function of many components involved in signalling pathways, including the STAT family of proteins, mTOR, Phosphatase and tensin homolog (PTEN), AKT, and PI3Ks signalling pathways, is a frequent event in SCCHN (49).

1.1.3.3.1. *STAT protein family*

SCCHN tumours display considerably elevated levels of the activated (phosphorylated) forms of STAT3, which is the most prominent STAT molecule in SCCHN among seven identified members of this family (50). This family of proteins play an important role as intracellular transcription factors that regulate the expression of genes that promote cellular growth, as well as a number of transcription-regulating cytokines implicated in the growth and immune responses, such as IL-6 (50). STAT3 targets cell cycle regulators such as *CCND1*, *CCND3*, *MYC* and antiapoptotic genes such as *BCL2* and promotes tumour cell proliferation and survival. Reciprocally, studies showed that suppressing STAT3 activity leads to inhibiting SCCHN growth (50).

1.1.3.3.2. *Ras family*

The *RAS* family of proto-oncogenes encode small GTPase proteins involved in cellular signal transduction (51). Activation of Ras proteins subsequently activates other proteins, which ultimately turn on genes involved in cell differentiation, growth, and survival. Hotspots mutations in the Ras family (*HRAS*, *NRAS* and *KRAS*) result in the loss of the ability to hydrolyse GTP to GDP, which thus leads to constitutive activation of Ras proteins (52). These mutations are one of the most common types of oncogene mutations in SCCHN, accounting for more than 4% of cases worldwide (53). In addition, overexpression of the normal alleles of *RASs* genes has also been reported in SCCHN (54).

1.1.3.3.3. *PTEN and PI3K/AKT/mTOR signalling pathway*

Genetic alterations of PTEN, a lipid phosphatase that plays a role in tumour suppression, occur in 5-10% of SCCHN lesions. In addition, loss of expression of this enzyme occurs in 30% of SCCHN cases which may represent a prognostic predictor of poor clinical outcome (55). This enzyme dephosphorylates phosphatidylinositol (3,4,5)-trisphosphate (PIP3), converting it into PIP2. PIP3 is an important substrate for the Protein Kinase B (AKT) and 3-phosphoinositide-dependent protein kinase-1 (PDPK1) signalling pathway which is essential for cellular growth, migration, and survival. The phosphorylation and activation of the AKT signalling pathway, mediated by PI3K, is an early event in most cases of SCCHN and is detected in approximately half of the preneoplastic tongue lesions (56). PTEN-mediated inactivation of PIP3 decreases AKT activity and limits its ability to bind to the membrane which results in significant inhibition of tumour growth (57).

The AKT signalling pathway also contributes to cell growth and proliferation through mTOR-mediated activation of eukaryotic translation initiation factor 4E (eIF4E), an essential protein translation initiation factor. AKT indirectly activates mTOR, which phosphorylates the 4E-binding protein 1 (4EBP1), releasing eIF4E which in turn bind to eukaryotic translation initiation factor 4G (eIF4G), stimulating translation initiation of a subset of genes required for cell growth (58). Amplification of the *EIF4E* gene is often associated with malignant progression of SCCHN, as well as increased protein expression, with more than six times the risk of local recurrence in surgical margins of eIF4E-positive SCCHN tumours (59).

1.1.4. Diagnosis and staging

Prompt diagnosis of tumours is critical to successful therapeutic intervention in SCCHN as in other cancers, and depends on the early recognition of signs and symptoms (1,8). In general, a number of considerations are in the diagnosis of SCCHN, including investigation of symptoms, findings of physical examination, radiographic examinations, endoscopy and histological study (8). The physical examination of the patient is often based on the investigation of the main aetiology of symptoms in the early stages of SCCHN through a complete evaluation of the oral cavity, pharynx, and lymph nodes (1,8). Nasolaryngoscopy is used to carefully examine the nasal cavity, the base of the tongue, hypopharynx, and larynx (8). Symptoms such as hoarseness and dysphagia may be

associated with impaired swallowing, as well as oral or pharyngeal masses or ulcers, and sometimes with vocal cord paralysis. Tongue pain and sore throats can also be associated with neck mass (1,8). Diagnosis may also include other symptoms such as earache or mouth bleeding (1,8). When any suspicious lesion is confirmed by physical examination, a biopsy is taken for subsequent histological examination, and the cancer is confirmed or denied (8).

When cancer is confirmed, the therapeutic approaches are determined based on the accurate staging of SCCHN. Oncologists often use the American Joint Committee on Cancer (AJCC) and the Tumour-Node-Metastasis (TNM) classifications. The staging criteria for both systems differ depending on the site of origin and require a direct visual evaluation that includes radiographic studies, such as magnetic resonance imaging (MRI) or computerized tomography (CT) or both, as well as endoscopy. However, these classifications do not include the biological or pathological aspects of tumorigenesis (60). Early stages (I and II) of SCCHN typically involve smaller tumours without prominent involvement of lymph nodes. Later stages (III and IV) include locally advanced disease and invasion of surrounding structures or an increased number of involved lymph nodes, with distant metastasis often identifying stage IV (8).

At initial assessment, chest imaging is routinely performed and second primary lung cancer or lung metastasis can be detected, especially in patients with locally advanced SCCHN (8). However, the frequency of distant metastatic dissemination in SCCHN remains relatively low and can be predicted by several factors including the location of the primary tumour (particularly the hypopharynx, which is most likely to metastasise), histological grade, advanced T- and N-classification and the ability to achieve locoregional control. Lung accounts for approximately 70% of distal metastatic disseminations in SCCHN, with a lower frequency to bone and liver, as well as to the mediastinal lymph nodes (61). In addition, the use of positron emission tomography (PET) with 2-[fluor-18] fluoro-2-deoxy-D-glucose (FDG) in the diagnosis of SCCHN has increased due to the ability of this technique to detect metastases. Recently, hybrid PET/CT scanning technology has become the technique of choice for identifying malignant lesions in SCCHN due to its advantage over either technique alone in preventing the misinterpretation of FDG PET results (62).

In oropharyngeal cancer, an assessment of HPV status is often required for staging given the consensus that HPV-driven oropharyngeal squamous cell carcinoma represents a

distinct entity from HPV-negative disease. This assessment typically includes polymerase-chain-reaction (PCR) or *in situ* hybridization (ISH) techniques to determine the presence and levels of HPV DNA or RNA. Immunohistochemistry (IHC) testing for cellular p16 expression, which is increased in HPV positive cases only due to E7 oncoprotein-mediated inactivation of pRb, is often used in the first instance if HPV involvement is suspected, and this is then followed up with molecular tests (63).

1.1.5. Treatment and prognosis

Radiotherapy (RT) and surgery are the most common treatment options for SCCHN, and both are indicated, either as primary or adjuvant therapy, in 74 % of all cases (64). Treatment differs depending on the anatomical site, surgical accessibility, and the stage of the disease, as well as the geographical variations in practice (65).

Treatment of patients with stage I or II disease, who make up about a third of SCCHN patients, aims to reduce morbidity and preserve function either using surgery alone or RT alone. These approaches lead to effective oncologic control and increased long-term survival rates in about 70 to 90% of cases, and are sufficient to cure 30-40% of stage I or II SCCHN patients (8,66). The choice of treatment depends on the accessibility to the anatomical subsite, and therefore, surgery is the treatment of choice for oral cavity cancers (8). Surgery is associated with higher cure rates and reduced morbidity in oral cancer as well as the benefits of avoidance of the late toxic effects of radiation. Oropharyngeal cancers may be managed with primary surgery or radiotherapy, while radiotherapy has an established role in laryngeal preservation for patients with laryngeal cancer (8). Given the complex anatomy of the head and neck and the proximity to vital organs, proton radiotherapy has recently gained increasing importance in the treatment of SCCHN due to its physical properties that allow better sparing of proximal healthy tissues and organs at risk when compared to conventional photon radiotherapy (reviewed in (67–69))

The main approaches to treating stage III or IV patients, who make up more than 60% of SCCHN patients, are surgery, RT and chemotherapy. The aims of therapy must be individualised. Choosing initial therapy, and the sequencing and administration of therapy and combinations of methods require experience due to the complex considerations of morbidity, adverse effects, and preservation of function (70,71). The concurrent administration of chemotherapy and radiotherapy (chemoradiotherapy) has

provided a major advance in the treatment of advanced stages of SCCHN, providing excellent locoregional control of more advanced SCCHN primary tumours. Chemoradiotherapy is recommended for SCCHN patients with good outcome status who have advanced laryngeal or hypopharyngeal cancer without cartilage involvement. However, patients with persistent or recurrent disease or severe functional impairment are typically treated by salvage laryngectomy (8,65,66).

Standard chemotherapy for SCCHN includes the use of platinum compounds such as cisplatin or carboplatin in combination with RT or other drugs. Other treatment options include the use of taxane-based combinations, which are highly effective in chemotherapy for locally advanced SCCHN. In addition, EGFR inhibitors, including cetuximab, are novel therapeutic agents for SCCHN and are currently undergoing further clinical research to study the efficacy of their combination with radiotherapy (72). However, the treatment of SCCHN continues to be constrained by the relatively limited therapeutic options.

1.2. *TP53* tumour suppressor gene

The *TP53* gene is part of a small family of related proteins that also includes p63 and p73. This gene integrates many signals that control cellular and organismal life and death, and it is activated in response to a number of oncogenic stress signals, resulting in tumour growth inhibition (73). *TP53* is mutated in nearly half of all human cancers, including SCCHN, and has 280 cancer-associated mutations, the largest number of such mutations among all known genes (73).

1.2.1. Structure of p53

TP53 is an approximately 20 kilobase pair gene located on chromosome 17p13.1, and consists of 11 exons, of which exons 2-11 encode the p53 protein (74). The active form of the resulting p53 protein is a tetramer, with four identical 393-residue chains. The structure of full-length p53 can be dissected into three major domains (74)(Figure 1.5.).

The first domain is the N-terminal domain (NTD) which contains amino acid residues 1–93 and is subdivided into the transcription activation subdomain (TAD)(amino acid residues 1-61) and the proline-rich region (PRR) (amino acid residues 62–93) (75). The

TAD is a complex binding site for a multitude of interacting proteins, such as the negative regulators MDM2/MDM4, the transcriptional coactivators p300/CBP (CREB-binding protein), and components of the transcription machinery (76).

The PRR links the TAD to the DNA binding domain (DBD) and it comprises five PXXP motifs (P is proline and X is any amino acid) that mediate multiple protein-protein interactions in transmitting anti-proliferative signals downstream of the p53 protein by binding to Src homology 3 domains (SH3)(76,77). However, there is a comparatively poor understanding of the exact role of the PRR (76,77).

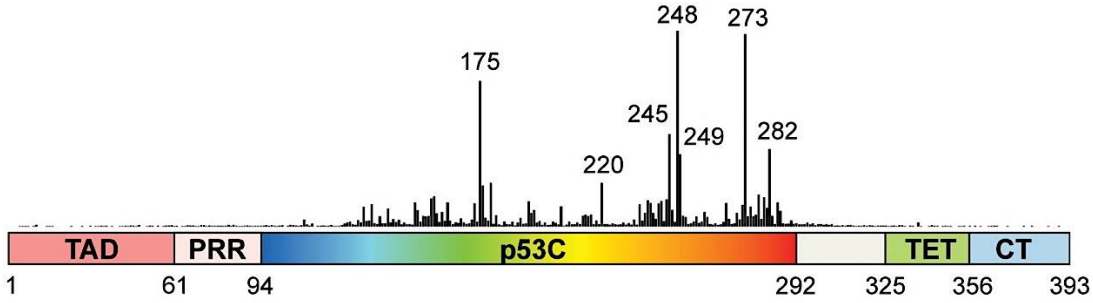

Figure 1.5.: The multidomain structure and mutation hotspots of p53 protein. The p53 protein consists of the N-terminal domain, which is subdivided into N-terminal transactivation domain (TAD) and proline-rich region (PRR), the central DNA-binding domain (DBD), labelled here as the p53 core domain (p53C), where most of the cancer-associated p53 mutations occur, and the C-terminal domain, which is subdivided into a flexible linker, the tetramerisation domain (TET) and the extreme C-terminal domain (CT). Hotspot mutations are all located within the DBD. The figure is reproduced from reference (76)

The second domain is the DNA-binding domain (DBD), or core domain (p53C), which spans amino acid residues 94–292. The DBD is responsible for binding p53 to specific sequences in DNA (78). Importantly, the majority of *TP53* mutations occur in highly conserved regions of the DBD, causing DNA binding to be lost or altered. (p53 mutations are further discussed in 1.2.5.)(79). The third domain is the C-terminal domain (CTD) which is a large natively unfolded region containing amino acid residues 293-393, mostly essential amino acids (primarily lysine)(80). This domain binds DNA in a non-specific way (76). It is subdivided into a flexible linker (residues 292-325) that links DBD to CTD, a tetramerization domain (TET)(residues 326-355) and the extreme C-terminus regulatory domain (CT)(residues 356-393)(76).

1.2.2. Functions of p53

The development of around half of human cancers is attributed to the loss of function of the p53 tumour suppressor pathway (81), which primarily functions as a transcription factor regulating the expression of around 4000 p53-responsive genes (82). These responsive genes have a p53 response element (RE) made up of a sequence of DNA to which p53 binds with high specificity and affinity (83). These genes regulate various functions including the regulation of the cell cycle, oxidative stress, senescence, DNA repair, angiogenesis, cell migration, metabolism and apoptosis (84). Studies have shown that many tumours harbouring wild type p53 lack the ability to induce or respond to the expression of p53 (85).

p53 is stabilised and activated in response to a number of stress signals that include DNA damage, loss of normal growth and survival signals, telomere attrition, hypoxia, and activation of oncogenes (85). p53 plays a role in preventing tumour cell growth through its ability to induce a number of different responses to stress signals at several points during tumour progression, followed by integration of various signals, for example, some may be pro-survival, others pro-apoptotic or pro-arrest and so on, which essentially regulates the fate of the cell towards life or death (85).

The transcriptional activation by p53 is typically achieved by direct sequence-specific DNA binding (83). In addition, indirect suppression by p53 can occur by either binding to another transcription factor and suppressing a gene without p53-specific REs, or by the p53-mediated activation of CDKN1A (also known as p21), which prevents the formation of the cyclin D/CDK4 complex and ultimately leads to suppression of S-phase genes (83). The results of p53 activation depend on a number of factors, including the state of the cell, the type of tissue, the existence of other oncogenic changes in the cell, as well as the type and intensity of the stimulation (86). In response to acute DNA damage signals, p53 can cause cell cycle arrest that can allow time for DNA repair. Alternatively, p53 can promote apoptosis permanently eliminating damaged cells. Both responses prevent tumour development by inhibiting the replication of cells that undergo oncogenic changes (86).

In addition, *TP53*-related proteins *TP63* and *TP73* genes encode many isoforms, which can mimic wild type p53 to some degree and activate a subset of target genes shared with wild type p53 due to the high similarity between the DBDs for all three proteins

(87). In the absence of p53, p73 may thus play an essential role in maintaining genome integrity by suppressing aneuploidy and polyploidy (87). However, both p63 and p73 also have distinct additional activities not shared with wild type p53, and affect many important biological processes, most notably development and differentiation (87). Inactivation of p63 and p73 function disrupts the cell cycle and prevents apoptosis, promoting cell proliferation (87).

In the following sections of this chapter, the role of p53 as a tumour suppressor gene involving cell cycle arrest, senescence, apoptosis and autophagy in response to DNA damage signals will be discussed in more detail. Moreover, recent studies have shown that p53 also plays a key role in metabolic regulation (88), and this will be discussed in more detail in section 1.3.2.

1.2.3. Role of p53 as a tumour suppressor

1.2.3.1. Cell cycle arrest

The cell cycle consists of a coordinated sequence of events, to produce two cells. However, it is accepted to say that DNA synthesis and mitosis consist of distinct phases: G1 or the first gap phase (between mitosis and the initiation of nuclear DNA replication); S or the DNA synthesis phase (nuclear DNA replication); G2 or the second gap phase (between the synthesis of nuclear DNA replication and mitosis); and M (mitosis). This sequence of phases results in duplication of DNA content and other cell components and ultimately cell division (Figure 1.4.)(89).

Cell cycle progression is regulated by a sequence of cellular activities, and p53 plays an important role in this regulation. Basically, the activation and inactivation of the CDKs at a number of checkpoints promote cell cycle progression by forming complexes with proteins of the cyclin family that are synthesized and degraded at certain points in the cell cycle (89,90). Four CDKs have been clearly demonstrated to regulate cell cycle progression. Progression through G1 depends on CDK4 and CDK6 that bind to cyclin D and cyclin E, while progression through S, G2 and M phases depends on the CDK2 and CDK1 that bind to cyclin A and cyclin B. Indeed, each cyclin is synthesised at the specific stage of the cell cycle it promotes, in response to different molecular signals such as DNA damage signals, and has no catalytic activity, whereas CDKs are expressed throughout the cell cycle and are inactive in the absence of a partner cyclin (89,90). Once activated

by its respective cyclin, the cyclin-CDK complex activates or inactivates target proteins, by phosphorylation, to coordinate entry into the next phase of the cell cycle. These phosphorylated proteins control specific processes during cycle division, including microtubule formation and chromatin remodelling (89,90). Cell cycle checkpoints, G1/S and G2/M maintain the accuracy of the sequenced events of the cell cycle and ensure that the current phase is completed before the next phase begins. This enables cell cycle arrest that allows repairing the damaged DNA prior to the continuation of the cell cycle (89,90).

In response to DNA damage, p53 induces cell cycle arrest through a number of pathways. For example, p53 transcriptionally activates the expression of p21, which in turn binds to and potently inhibits a number of cyclin-CDK complexes, including CDK4/6-cyclin D1, CDK1/2-cyclin A, CDK1- cyclin B1 and CDK2- cyclin E, thus preventing phosphorylation of substrates of those cyclin-dependent kinases and ultimately leading to cell cycle arrest at both G1/S and G2/M checkpoints (91). Moreover, p21 binds to and inhibits the activity of proliferating cell nuclear antigen (PCNA), which is an auxiliary factor for DNA polymerases in DNA replication and DNA repair, that further contributes to cell cycle arrest at the G1/S transition (91).

In addition, p53 transcriptionally activates the growth arrest and DNA-damage-inducible protein 45 gene (*GADD45*) following some genotoxic stresses. This gene is involved in inducing cell cycle arrest at the G2/M checkpoint by inhibiting the activity of the cyclin CDK1/cyclin B1 complex (92). Another gene, Reprimo (*RPRM*), has also been implicated in the regulation of the G2/M checkpoint, and has moreover, been shown to be positively regulated by p53. The expression product of this gene is a cytoplasmic, highly glycosylated protein that interferes with CDK1/cyclin B1 complex activity by inhibiting both CDK1 activity and nuclear translocation of cyclin B1 and thus contributes to cell cycle arrest in the G2 phase (93).

1.2.3.2. Apoptosis

Apoptosis, or programmed cell death, is a critical component of various processes which are essential for the preservation of healthy organisms, including normal cell turnover/cellular homeostasis and the proper functioning and development of the immune system (94). The inactivation of apoptosis is a factor in many human conditions including many types of cancer and is considered to be one of the fundamental hallmarks

of cancer (95). Apoptosis occurs either normally as a homeostatic mechanism for regulating cell populations in tissues and during development and ageing, or as a defensive mechanism such as in cell damage or as in immune reactions including the elimination of self-antigen-recognising lymphocytes during thymic development, and cell-mediated cytotoxicity (94). Apoptosis can be triggered by a wide variety of stimuli and physiological and pathological conditions, including irradiation and chemotherapy (94), and is characterised by a series of distinct morphological changes accompanied by energy-dependent biochemical mechanisms which are closely regulated by a large number of pro- and anti-apoptotic proteins (94).

Apoptosis occurs through two main pathways that are linked together: the intrinsic, or mitochondrial, pathway and the extrinsic, or death receptor, pathway (reviewed in (94)). Molecules in one of these two pathways can affect the other (94). Interestingly, the extrinsic pathway requires the involvement of members of the tumour necrosis factor receptor family (TNFR), including the cell-surface receptor Fas (CD95, Apo-1) and death receptor 5 (DR5), which have a characteristic common cytoplasmic region of 80–100 amino acids that forms motif known as the death domain that is involved in the transduction of the apoptotic signals (96). This death domain binds and activates the associated Fas-associated death domain protein (FADD) (96). This leads to a cascade of activation of caspases, such as caspase-3 and caspase-8, by forming of the death-inducing-signalling-complex (DISC), which ultimately promotes apoptosis (96).

On the other hand, the intrinsic pathway is triggered in response to DNA damage and is associated with mitochondrial membrane depolarisation which leads to the release of cytochrome c from the intermembrane space of the mitochondria into the cytoplasm (97). The release of cytochrome c is induced by p53 through the activation of target genes that encode the Bcl-2 homology 3 (BH3)-only proteins, including the Bcl2 modifying factor (*BMF*), the p53 upregulated modulator of apoptosis (*BBC3* or *PUMA*), the BH3 interacting-domain death agonist (*BID*) and the phorbol-12-myristate-13-acetate-induced protein 1 (*PMAIP1* or *NOXA*) (97). Upon release, cytochrome c binds to the apoptotic protease activating factor 1 (Apaf1) to form a large protein structure known as the apoptosome (97). The expression of Apaf1 is also induced by p53 through a response element within the *APAF1* promoter. Once this complex is formed, caspase-9 is activated and promotes the activation of caspases-3, -6 and -7 (97).

There is a third apoptotic pathway involving cytotoxic T lymphocytes, which eliminate the transformed cells by releasing granules containing perforin, a pore-forming cytolytic protein, and granzymes, which are serine proteases that can cleave a number of apoptotic effectors (98). Granzyme B cleaves and activates the initiator caspases 8 and 10, and the executioner caspases 3 and 7 which trigger apoptosis (98). Granzyme B can also cleave Notch 1, Bid, fibroblast growth factor receptor-1 (FGFR-1) and a number of other proteins that mediate apoptosis (98). The three apoptotic pathways converge at the mitochondrial outer membrane (MOM), leading to mitochondrial outer membrane permeabilization (MOMP) which results in the release of cytochrome C (94). Once released, cytochrome C activates the caspase cleavage cascade, which ultimately results in the fragmentation of DNA and the degradation of cytoskeletal and nuclear proteins (94).

p53 is a major obstacle to tumorigenesis due to its role as a major regulator of cellular responses to stress, with the result that the normal activity of p53 has typically to be removed or inhibited to allow tumour development (99). Many general factors influence p53 to induce cell cycle arrest or apoptosis, including the cell type, the p53 expression levels, the oncogenic status of the cell and the intensity and the type of stress signal which includes DNA damage, growth factor deprivation, hypoxia and cytokine deprivation (100). Given the function of p53 in apoptosis and the role of apoptosis in determining the response to cancer therapy, it has been assumed that the p53-deficient cells are resistant to apoptosis and therefore to cancer treatments (101). However, many studies have shown that programmed cell death can occur independently of p53, such as the p53-independent induction of pro-apoptotic proteins Fas, PUMA, DR5 and Noxa, the degradation of the anti-apoptotic protein Bcl-2, the p53-independent cytotoxic drug-induced apoptosis pathway which is controlled by p73, E2F and the checkpoint kinases Chk1 and Chk2, and the stimulation of apoptosis by ROS through the NF-κB-mediated transcription of FasL (102). Furthermore, a study of a number of cancer cell lines has shown that mutant p53 cells retain their ability to induce apoptosis (102).

1.2.3.3. Autophagy

The regulation of apoptosis is closely related to the regulation of another crucial process determining the outcome of cell death decisions, autophagy. Autophagy is an important process during development and in several pathological conditions including

tumorigenesis (103). In contrast to apoptosis, which depends on the activation of caspases that cleave multiple target proteins (see section 1.2.3.2.), autophagy is a lysosomally regulated, caspase-independent process that maintains quality control of cellular content by sequestering long-lived proteins and organelles into double-membrane vesicles, known as autophagosomes, that fuse with lysosomes to form the autophagolysosome (104). In autophagolysosomes, the engulfed organelles and long-lived proteins are hydrolysed, and the resulting amino acids and other macromolecular precursors can be reused by the cell (104).

Whilst the process is not fully understood, it is believed that apoptosis and autophagy are both regulated by common regulators, including p53 (105). p53 plays a dual role in regulating autophagy. In response to stress, nuclear p53 stimulates autophagy, hence allowing cells to cope with stress, by increasing the expression of DNA damage regulated autophagy modulator (DRAM), a direct p53 target gene that encodes a lysosomal membrane protein that induces accumulation of autophagosomes. p53 can also induce transcription of autophagy-related genes (ATGs) such as sestrin 1 and 2, which activate adenosine monophosphate-activated protein kinase (AMPK), and thus induce autophagy through AMPK-mediated inhibition of mTOR, a negative regulator of autophagy (106). However, cytoplasmic p53 can relocalise to mitochondria and inhibit autophagy, thereby promoting apoptosis, by binding and activating Bcl-2 family proteins (as discussed in 1.2.3.2.)(106).

1.2.3.4. Senescence

Senescence is a prolonged and irreversible cell-cycle arrest that occurs in response to cellular ageing (107). Senescence is also an in adaptative response to various sources of cellular events, such as responses to cytokines, oxidative damage, irradiation, chemotherapy, activated oncogenes, ROS depletion, which trigger DNA damage responses (DDR)(107,108). Senescence is manifested by the acquisition of different phenotypic alterations, including morphological changes and metabolic reprogramming, chromatin remodelling, and the secretion of pro-inflammatory factors (107). In cancer, senescence is a physiological anti-tumour response that protects cells against oncogenic insults (109).

Whereas transient stimuli only trigger a transient cell cycle arrest, enabling the cell to repair the damage, senescence appears to necessitate a stable stimulus, and more

intense stimuli can lead instead to apoptosis (109). The stressor intensity threshold between senescence and apoptosis has also been shown to vary by cell type, with several types of cells being more prone to follow one fate over the other (109).

p53 is an important player in senescence, and it can be activated in a DDR-dependent or DDR-independent manner (110). The p53-mediated cellular senescence response depends on a number of factors including stress intensity and duration, p53 concentration, as well as post-transcriptional modifications (111).

The p53/p21 (see section 1.2.3.1.) and p16/pRb (see section 1.1.3.2.) tumour suppressor pathways are the most extensively studied pathways in the regulation of cellular senescence (108). The p53/p21 pathway is important for the onset of senescence and it has been shown to be involved in several cancer types, including SCCHN (108), whereas p16 and the pRb family of proteins appears to play a key role in the maintenance of senescence (108).

Given this role of p53 in the induction of senescence and the loss of tumour-suppressing function of p53 in a large number of cancers, cellular senescence is thought to be a key mechanism for tumour suppression (112). Consistent with this, reactivating p53 in tumours has been shown to induce senescence-mediated tumour regression (113).

1.2.4. Regulation of p53

All cells are subjected to DNA damage, and maintaining DNA integrity is, therefore, an important activity for cells. One of the most important proteins necessary to maintain genetic integrity is the transcription factor p53. Although p53 has no role in DNA repair, cells need homoeostasis of p53 levels to regulate many of the cellular processes that determine the balance between repair of damaged DNA or the elimination of cells with potentially oncogenic lesions (114). p53 is regulated by antagonising activities of two genes, the mouse double minute 2 homolog (*MDM2*) and the related gene *MDM4* (*MDMX*)(115), through several mechanisms.

Following stress induction, a number of mechanisms, including post-translational modifications, physical sequestration, and degradation, lead to targeted disruption of the interaction between p53 and MDM2 (116). One of the post-translational modifications that contribute to the activation of p53 in response to cellular stress is

phosphorylation. Stress-induced phosphorylation of Ser395 (by ATM kinases) and Tyr394 (by c-Abl) on MDM2 prevents Mdm2-p53 interaction (117,118). In addition, phosphorylation of several p53 sites (for example Thr18, Ser15 and Ser20) disrupts the MDM2-p53 interaction and significantly reduces MDM2 binding, resulting in p53 stabilisation (119–122). However, recent in vivo evidence suggests that phosphorylation alone may not be sufficient to activate p53 (123–127), and other evidence has indicated that phosphorylation is not required for p53 activation in response to a number of specific types of cellular stress (123,128–130). Acetylation is another post-translational modification that leads to activation of the transcriptional activity of p53. MDM2 acetylation by CBP/p300 contributes to the disruption of the p53-MDM2 interaction (131). In addition, acetylation of six key C-terminal lysines of p53, which are the predominant sites for MDM2-mediated ubiquitination and subsequent degradation, prevents the p53-MDM2 interaction, because MDM2 cannot ubiquitinate acetylated p53 (132,133). Another stress-induced mechanism of p53 stabilization is through the physical sequestration of MDM2 by the alternate reading frame protein p14arf (ARF), an oncogenic stress-induced tumour suppressor. Activated ARF disrupts the p53-MDM2 interaction and sequesters MDM2 in the nucleolus (134–136). In addition, studies have also shown that ARF can directly inhibit the E3 ubiquitin ligase activity of MDM2 (137,138). The third mechanism for p53 stabilisation is the degradation of MDM2. MDM2 has inherent self-ubiquitination activity due to its E3 ligase activity (139,140). In resting cells, self-ubiquitination is inhibited by the deubiquitinase herpesvirus-associated ubiquitin-specific protease (HAUSP) (141,142), whereas cellular stress promotes disrupts the stability of the MDM2-HAUSP complex and promotes MDM2 auto-ubiquitination and degradation (143,144).

In the resting state, MDM2 binds to the TAD, keeping p53 in a latent state and with a low abundance, reducing the capacity of the tumour suppressor to activate gene transcription (115). p53 can induce transcription of MDM2, which in turn regulates p53 levels by mediating the ubiquitylation, through its function as an E3-ubiquitin ligase for p53, and subsequently promoting the degradation of the p53 in 26S proteasomes, generating an autoregulatory feedback loop (Figure 1.6.)(145,146). In addition, the overlap between the MDM2-binding region of the p53 TAD and parts of the binding site for the transcriptional coactivator p300 is another essential part in the regulation of p53. p300 is an enzyme with a histone acetyltransferase activity that regulates the transcription of genes by relaxing chromatin structure, allowing histone proteins to bind less tightly to DNA. p300 also can acetylate nonhistone targets, such as specific lysine

residues in the C-terminal region of p53. The binding of p300 may protect p53 from proteasomal degradation by MDM2. Conversely, the TAD binding region can be occupied by MDM2 and thus prevent the binding of the p300 coactivator or components of the transcription machinery (76). Similarly, MDMX, which was originally discovered through its homology to MDM2, negatively regulates p53, but it lacks the E3-ligase activity (unlike MDM2 it does not possess a function RING domain). It can achieve this by inhibiting p53 transcriptional activity, for example by competing for binding and thus inhibiting the p300-mediated acetylation of p53, and it can also promote increased MDM2-mediated ubiquitylation and degradation of p53, by forming heterodimers with MDM2 that appear to exhibit increased ability to modify p53 (145,147).

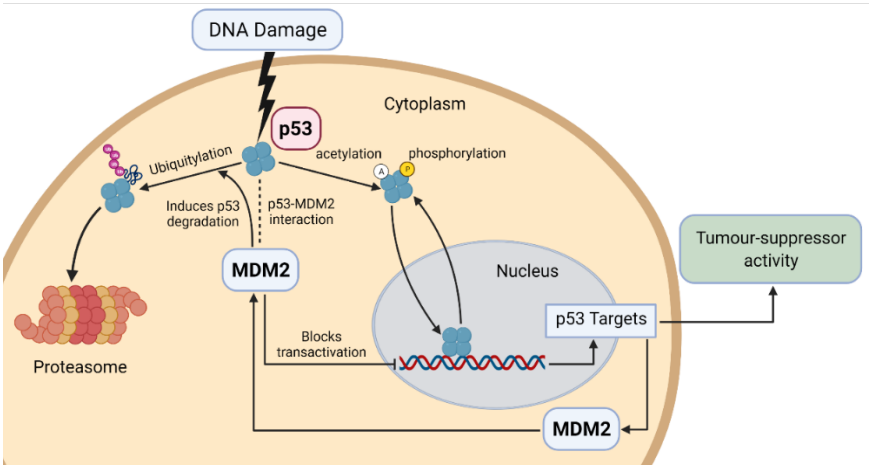

Figure 1.6.: MDM2-mediated regulation of p53. p53 stimulates the expression of MDM2, which in turn suppresses p53 activity by blocking its transcriptional activity and stimulating its ubiquitination and degradation, generating an autoregulatory feedback loop. DNA damage stimulates p53 phosphorylation-mediated activation which prevents p53 binding to MDM2. The figure is reproduced from reference (148).

1.2.5. *TP53* mutations

Activation of p53 in response to a variety of stress signals causes the transactivation of several target genes that regulate many biological processes, provoking a number of complex responses that are dependent on many intrinsic and extrinsic factors (discussed in 1.2.2.)(149). *TP53* mutations in cancer are most commonly missense mutations in the DBD, and these typically result in the loss of the wild type function (such as loss of transcriptional regulation capacity) and are often manifested by stable full-length but non-functional protein (150). Cancer cells with *TP53* mutations typically express high but heterogeneous levels of mutated p53 protein, sometimes with new biochemical and biological properties that may lead to gain of function (150). The

majority of p53 mutations result in a loss of the ability to bind DNA in a sequence-specific manner and activate transcription of p53 target genes, and thus, the signalling pathways that p53 regulates (149).

TP53 mutations are the most frequent genetic alteration in all the human cancers, with mutated *TP53* being reported in almost 50% of all cancers (151). According to sequencing studies, missense mutations that occur within the DBD represent 75% of p53 mutations, and 31% of these occur in one of seven hotspot codons (152). This high percentage of mutations in the DBD of p53 in human cancers emphasises the importance of the DNA-binding function of p53 in the tumour suppressor function of the gene (149). These p53 missense mutations are usually loss-of-function (LOF) mutations, where the abrogated DNA-binding function of p53 compromises its ability to transactivate the transcription of the target genes necessary for regulating cellular processes, such as promoting cell-cycle arrest, DNA repair and apoptosis (discussed in 1.2.3.), and so contributes to tumour formation and progression (153). Although these mutations may affect only one of the two p53 alleles with the other allele remaining wild type, many of the common DBD mutant p53 proteins exert dominant-negative effects on the coexpressed wild type protein by forming mixed tetramers, which greatly reduces the DNA binding affinity of the tetramer and thus the capability of transactivation, resulting in the cell losing the wild type function even if one wild type allele is preserved (153). However, this heterozygosity is usually transient, as *TP53* mutation in one allele is frequently followed by deletion or mutation of the remaining wild type allele during cancer progression, also known as loss of heterozygosity (LOH). Loss of p53 function is not the only outcome of *TP53* mutations, as there is also evidence that some specific p53 mutants acquire new activities that are not present in the wild type protein. These activities, also known as gain-of-function (GOF), can actively contribute to various aspects of tumour progression (153).

GOF mutant p53s have a number of biological and biochemical functions that are distinct from those of wild type p53. Many GOF mutant p53s, including those with hotspot mutations: R175H, R248Q, R248W, R249S, R273C, R273H, R282W, were found to modulate the expression of several genes, such as *MYC*, *FAS*, *EGFR*, and also a number of genes that encode many ribosomal proteins (154). Mutant p53 protein is also expected to be implicated in many additional GOF activities that are characteristic of cancer cells such as inflammatory responses, biosynthetic activates, resistance to chemotherapeutic drugs, as well as energy metabolism (155,156). Whilst there has been a considerable

amount of work in recent years aimed at investigating p53 GOF it is an area that is not well understood and clearly more work is needed to reveal the full impact of GOF on tumorigenesis (157).

TP53 GOF mutations either specifically affect the recognition of DNA through altering the amino acid sequence that is directly involved in DNA binding function (DNA-contact mutations) or alter DNA binding (presumably thus changing specificity) by exposing the amino acids residues that are normally hidden within the DBD (conformational mutations)(153). Studies have shown that the conformational mutations in p53 hotspots R175, G245, R249 and R282 and DNA-contact mutations in hotspots R248 and R273, all have an altered DNA-binding function (158). Studies have also shown that depletion of GOF mutant p53 reduces cell proliferation and colony formation capacity and induces the expression of p53-dependent apoptotic and repair genes, and thus reduces the resistance to chemotherapeutic drugs (157,159).

1.2.6. p53 as a predictive biomarker

Given that p53 is an important regulator of apoptosis through a number of effector genes such as *BAX*, *BCL2*, and *FAS* (as previously discussed in 1.2.3.2.), the fact that this gene is the most frequently mutated gene in human cancer (as discussed in 1.1.3.) was the premise of several studies that investigated the role of p53 in determining the response to the cytotoxic effects of ionising radiation (IR) and cancer drugs (160).

Early studies using embryonic fibroblasts from p53 knockout mice showed that p53 (-/-) cells were resistant to ionising radiation and various anticancer drugs *in vitro* and *in vivo* (161). This lack of responsiveness was explained by the inability of cells to undergo apoptosis in response to DNA damage (161) and these findings suggested a direct role for p53 in modulating susceptibility to anticancer drugs (160). Many subsequent studies have used various tumour cell lines to further investigate this observed correlation between p53 status and response to exposure to these agents.

Overall, it has been shown in several studies that the presence and characteristics of p53 mutations influence the clinical outcomes of cancer therapy. Studies in cells have lent further support for these conclusions. For example, one study that examined the nature of the relationship between p53 status in 60 human cancer cell lines and responsiveness

to 123 different chemotherapeutic drugs found that cells with wild type p53 were more susceptible to growth inhibition by the majority of drugs examined (162). Many other studies have supported the idea that p53 mutations reduce the sensitivity to anticancer drugs in a variety of cancers (160), including male germ cells (163) and colorectal tumours (164,165). In contrast, other studies have shown no correlation between p53 status and chemosensitivity in breast cancer (160) and ovarian cancer (166,167). Similarly, the correlation between p53 status and resistance to ionising radiation is not completely clear and may not be the same for all cell types (160,168).

In vivo, mutant p53 mouse models showed substantially increased radiation resistance (169,170). Nonetheless, in clinical studies, p53 mutations have most commonly been found to be associated with reduced radiosensitivity and worse prognosis in many human cancers (171–173).

In SCCHN, a landmark study of 560 patients has shown that p53 mutations in tumour DNA are associated with reduced post-surgery survival (RR, 1.4; 95% CI, 1.1 to 1.8; P=0.009)(174). Other studies have found a similar correlation between p53 status and response to radiation therapy, as measured by treatment failure and survival, with a higher rate of treatment failure in mutant p53 tumours (171,175,176).

Whilst the above shows that there is some uncertainty in clinical studies of the impact of p53 mutations on treatment responses and outcomes, the overwhelming body of evidence suggests that loss of functional p53 contributes to anticancer drug and radiation resistance.

1.3. Glucose metabolism in cancer

Glucose metabolism is an essential cellular process for meeting the continuous high demand for energy represented by ATP production, and it is typically reprogrammed in rapidly proliferating normal cells to achieve this goal (177). This process is regulated by signalling pathways that are regulated by a number of internal and external factors, including nutrient levels, growth factors, oxygen, pH, proto-oncogenes, as well as tumour suppressor genes (177). Given the critical role that cellular energy metabolism plays in cellular proliferation and survival, it is one of the key processes involved in the transformation of cells from normal to neoplastic (177). Reprogramming energy

metabolism has recently emerged as an identified "hallmark of cancer" with a major effect on tumour proliferation, progression, resistance to therapy and survival (177,178). In tumour cells, the metabolism process is adapted so that different metabolic activities either directly participate in the transformation process or indirectly support the biological processes that promote tumour growth (179). As a result, metabolic reprogramming has gained in importance as a potential target for cancer treatment, and thus the focus of this thesis will be on increased aerobic glycolysis (the Warburg effect), which is the most prevalent and well-studied metabolic reprogramming feature in many types of cancer.

1.3.1. Principle and molecular basis of the "Warburg Effect"

In 1857, Louis Pasteur found that in the absence of oxygen, the pathway we now know as oxidative phosphorylation is inhibited, and cells turn to glucose consumption, or as we now know as glycolysis, to generate energy (Pasteur effect)(180). In the 1920s, physiologist Otto Warburg made his seminal observation that tumour cells, unlike normal cells, use fermentation to metabolise glucose instead of relying solely on respiration (or as we now know it: the mitochondrial oxidative phosphorylation pathway or electron transport chain) even in oxygen-rich environments (Warburg effect)(181).

Basically, glycolysis provides cancer cells with different substrates for biosynthesis pathways (for example through the pentose phosphate pathway), allowing cancer cells to adapt to hypoxic conditions and promote redox homeostasis by increasing antioxidant levels and decreasing reactive oxygen species levels (ROS)(182). However, the Warburg effect appears to be paradoxical because, while being a faster metabolic pathway in comparison to oxidative phosphorylation, glycolysis is a less efficient metabolic pathway for generating ATP (183).

Glycolysis is a catabolic process that produces two reduced nicotinamide adenine dinucleotide (NADH) and two ATP molecules from the conversion of one molecule of glucose to two molecules of pyruvates. In the oxidative phosphorylation pathway, pyruvate is oxidised to CO_2 and H_2O in the presence of oxygen, which results in generating approximately 36 molecules of ATP. In the absence of oxygen, pyruvate is converted into lactic acid in the anaerobic glycolysis pathway. However, Warburg observed that glucose can be converted to lactic acid even in the presence of oxygen,

(178). In this phenomenon, proliferating cells tend to express glycolytic enzymes and glucose transporters in excess of the machinery required to oxidise pyruvate, suggesting that glucose is preferentially converted to lactate without loss of respiration (179). Numerous studies have since investigated the Warburg effect, and it has been demonstrated in a wide variety of tumours. Recently, the significance of several primary oncogenic signalling pathways in reprogramming cancer cell metabolism established links between metabolic changes in cancer cells and the causative changes that determine the cancer phenotype (184). Hanahan and Weinberg have recently updated their landmark paper from 2000, adding "deregulated cellular energetics" to the hallmarks of cancer (95,185).

However, the causal association between aerobic glycolysis and cancer progression remains unclear (183), and it can show significant differences between different types of cancers, based on the tissue of origin and genotype (186). This highlights the need for cancer-specific metabolic perturbations studies to investigate these differences (179). Moreover, it is reasonable to say that the most studied metabolic phenotype of cancer is the Warburg effect (187), and consequently will be the focus throughout the remainder of this thesis.

Indeed, Warburg originally proposed that increased lactate production and reliance on glycolytic metabolism is a compensation mechanism for energy deficiency caused by respiration damage (181). However, numerous studies have failed to demonstrate this hypothesis (188). Instead, many studies have demonstrated that mitochondrial respiration activities are essential for tumour development and are frequently unimpaired in cancer cells (189). Furthermore, the acquisition of the Warburg effect as a metabolic phenotype by rapidly dividing normal cells to meet the requirements of rapid proliferation supported the idea that aerobic glycolysis is the preferred phenotype under conditions of rapid cellular expansion, as observed in embryonic stem cells and lymphocytes, rather than a malignancy-specific feature (187). This idea led to the adoption of a new perspective on metabolic regulation in cancer cells which considers the molecular mechanisms and intracellular signalling regulation that drive the acquisition of this metabolic phenotype by cancer cells, especially with more evidence has emerged that mutations in oncogenes and tumour suppressor genes have a direct impact on metabolism (179,187). However, the molecular mechanisms by which cancer cells initiate and maintain the Warburg effect remain unclear and vary by tumour type (187,190).

The transcriptional upregulation of glucose transporters and glycolysis pathway enzymes in many malignancies is one of the well-studied mechanisms that support the complex link between the acquisition of the Warburg effect metabolic phenotype and the oncogenic changes in cancer tissues (187). Among these critical oncogenic events that are responsible for the transcription of several genes, three main mechanisms controlling cell metabolism were studied extensively more than others: the activation of *HIF* and *MYC* or the inactivation of *TP53* (187).

The hypoxia-inducible factor 1 (HIF-1)-containing transcription factor complex is a transcriptional factor that is activated in hypoxic conditions and induces adaptive responses to hypoxia through controlling the transcription of a number of genes responsible for angiogenesis, apoptosis, and metabolic reprogramming (180). In addition, germline mutations in nuclear-encoded Krebs cycle enzymes, fumarate hydratase (FH) and succinate dehydrogenase (SDH), which act as tumour suppressors, have been shown to result in accumulation of fumarate and succinate in tumour and overexpression of HIF-1 (191). Studies have found that HIF-1 induces transcription of nearly every enzyme in the glycolysis pathway (180). HIF-1 upregulates pyruvate dehydrogenase kinase (PDK)(192), which phosphorylates and inhibits pyruvate dehydrogenase complex (PDC), the enzyme responsible for introducing pyruvate into the mitochondria, leading to the accumulation of pyruvate and thus increasing its conversion to lactate by lactate dehydrogenase (LDH), another enzyme that is upregulated by HIF-1 (180). Studies have recently demonstrated that HIF-1 can be activated independently of hypoxia in a number of human cancers by a number of oncogenic and tumour suppressor mutations (180).

PDK is also regulated by the *MYC* proto-oncogene, which is another important transcriptional factor that regulates the expression of different metabolic genes and controls the metabolic phenotype in cancers, including the Warburg effect (193). MYC upregulates several metabolite transporters and enzymes required for glucose metabolism, increasing glucose influx through the glycolytic pathway (193). Studies found that MYC deregulation is a frequent oncogenic event, which is linked with various metabolic changes including attenuating the entry of pyruvate into the tricarboxylic acid cycle (TCA) and enhancing the Warburg effect (reviewed in (193)).

The role of p53 in regulating metabolism has received increased attention in recent years (182). p53 enhances oxidative phosphorylation by promoting the expression of SCO2, an essential protein for cytochrome c oxidase assembly (Complex IV) of the electron transport chain, which is the primary site of cellular oxygen utilisation (194). p53 also suppresses glycolysis by upregulating TIGAR, which limits glycolytic flux downstream of the third step in glycolysis pathways (194) (discussed in detail in 1.4.2.). In addition to SCO2 and TIGAR, studies have suggested that p53-mediated regulation of glucose metabolism may be dependent on other transcriptional targets, which is discussed in greater detail in the next section of this chapter.

1.3.2. The role of p53 in Warburg Effect

It has recently become apparent that many oncogenesis-related events are associated with the complicated processes involved in the metabolic regulation mechanisms, suggesting that these events may be implicated in metabolic reprogramming, albeit those mechanisms are not fully understood (184). One of these fundamental oncogenesis-related events that may be involved in metabolic reprogramming is the loss of function of p53, which is highly important in SCCHN tumorigenesis (see section 1.2.2.1.). Recent studies revealed that p53 is involved in mitochondrial respiration, glycolytic activity balance and maintenance of metabolic homeostasis (184).

As stated in section 1.3.1., p53 regulates both oxidative phosphorylation and glycolysis through numerous mechanisms, which may involve modulating the activity of subsidiary metabolic pathways (see Figure 1.7.). It has been shown that p53 plays a role in pyruvate metabolism through activation of PDC, by suppressing the expression of the PDC inactivator, PDK, and thus converting pyruvate to acetyl CoA (195). In addition, p53 can also inhibit glycolysis by decreasing cellular uptake of glucose through downregulation of glucose transport molecules, GLUT1 and GLUT4 (184). p53 also suppresses the expression of monocarboxylate transporter-1 (MCT-1), a protein that sustains elevated rates of glycolysis by increasing lactate flux under hypoxic conditions (195). Additionally, the increased transcription of Parkin, an E3 ubiquitin ligase, is one of the mechanisms by which p53 promotes mitochondrial respiration. This enzyme ubiquitinates pyruvate isoform kinase M2 (PKM2), which increases the expression of PDH, and thus increases the cellular level of CoA and reduces the glycolytic rate (195).

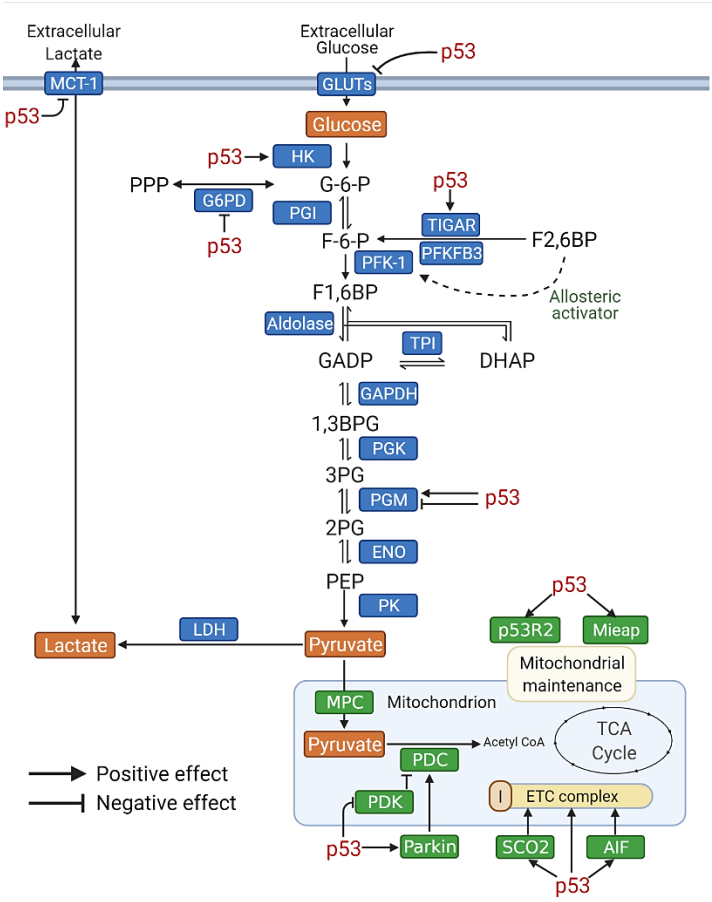

Figure 1.7.: Proposed outline of p53-mediated metabolic regulation. p53 promotes mitochondrial respiration (green) and restricts glycolysis (blue) through various mechanisms, including inhibiting the expression of glucose transporters and promoting the expression of TIGAR. The figure is reproduced from reference (196) .

Furthermore, p53 enhances mitochondrial respiration by mitochondrial quality control which includes maintenance of mitochondrial integrity as well as repairing and removing the damaged mitochondria through induction of mitochondria-eating protein (Mieap), which induces the accumulation of lysosomal proteins within mitochondria in response to mitochondrial damage (197). p53 also maintains mitochondrial homeostasis by regulating the mitochondrial biomass and the stability of mitochondrial DNA through direct induction of the ribonucleotide reductase small subunit p53R2 in response to DNA damage, enabling dNTP supply for DNA repair (198).

In addition to direct regulatory effects that normally suppress a glycolytic phenotype, p53 exerts indirect regulatory effects by interacting with many other important metabolic regulatory pathways. p53 can suppress the transcriptional activity of NF-κB pathway by inhibiting the subunits of IκB kinase (IKKα and IKKβ), which activates NF-

κB. This results in decreased glucose transporters expression, and thus a reduction in glycolytic flux (199). Additionally, the activities of PI3K/AKT/mTOR pathways, key regulators of cellular metabolism, are inhibited by p53 activation which promotes the transcription of four negative regulators of PI3K/AKT/mTOR pathways: IGF-binding protein-3 (IGFBP3), PTEN, the β subunit of AMPK, and tuberous sclerosis protein 2 (TSC2). This results in cell growth inhibition, glycolysis suppression, and likely p53-directed autophagy and apoptosis (200). Furthermore, p53 negatively regulates aerobic glycolysis through suppressing HIF-1 activities (discussed in 1.3.1.), either directly by upregulating ubiquitylation and degradation (201), or indirectly by promoting the expression of sestrins 1 and 2, which induces AMPK activity (202), an inhibitor of HIF-1 pathway (203).

Whilst much of the literature on p53 and p53-metabolic effects are in accord, some contradictory metabolic roles of p53 have been described. For instance, the fact that the promoters for hexokinase-II and phosphoglycerate mutase (PGAM), two enzymes involved in the glycolysis pathway, contain p53-responsive elements (204), through which p53 has been shown to both inhibit and promote the pentose phosphate pathway (PPP) flux, respectively (196)(Figure 1.7.). Studies have also shown that whereas p53 is involved in the destabilisation of PGAM in fibroblasts (205), p53 transcriptionally activates a PGAM muscle-specific isoform in cardiocytes (206). Although the exact reasons for these opposing p53 responses are unknown, it is widely recognised that p53 does not function in the same manner in all tissues or cancers that arise from them (207). As a result, p53-mediated metabolic regulation is likely tissue-specific (196), which emphasise yet again the importance of cancer-specific study of metabolic regulation mechanisms.

Despite a few apparently contradictory effects, p53 appears to generally play a role in regulating the balance between mitochondrial respiration and glycolytic activity, with loss of function possibly implicating in the acquisition of the unbalanced malignant metabolic phenotype. Recent studies have reported that the oncogenic GOF properties acquired by some mutant forms of p53 (discussed in section 1.2.5.) may contribute in additional ways to tumorigenesis through mechanisms related to metabolic regulation. However, the underlying mechanisms of these effects remain poorly understood (208–212). For example, one of these GOF properties of mutant p53 proteins in SCCHN is their ability to specifically inhibit the activation and signalling of AMPK, an enzyme that is upregulated by wild type p53 (208), which results in an increase in glycolytic aerobic

capacity (213). These findings revealed an important role for mutant p53 in mediating metabolic changes in cancer, which provides a novel mechanism explaining the mutant p53 GOF in tumorigenesis.

1.3.3. Evidence for metabolic reprogramming in SCCHN

While aerobic glycolysis is probably the best-documented tumour cell metabolic phenotype, it is not observed in all cancers (214). Two studies found an increase rather than a decrease in oxidative phosphorylation in chronic lymphocytic leukaemia (215) and breast cancer (216), while other studies found that glutaminolysis is predominant in glioblastoma (217) and cervical cancer (218). Additionally, prostate cancers have been found to rely on lipids and other energetic molecules, instead of aerobic respiration, for energy production (219). In line with this, the use of FDG-PET uptake in the diagnosis and monitoring of tumours, although important, shows a broad clinical variance among the different types of tumours, as FDG-PET show negative results in up to 30% of tumours (220). This again highlights the importance of a comprehensive study of metabolism for each specific type of cancer to develop effective metabolism-targeting therapeutic strategies. The majority of the metabolic studies in SCCHN, until recently, have only focused on limited expression analysis of transporters and enzymes of metabolic pathways, instead of providing a detailed picture of the metabolic phenotype or investigating the characteristics of dynamic metabolic flux (7)

As stated previously, the loss of wild type p53 activity is one of the primary oncogenic events that may lead to metabolic reprogramming in SCCHN, and mutations in *TP53* play an important role in SCCHN tumorigenesis with 60-85% of SCCHN cases harbouring mutations (6). Moreover, *TP53* mutations are linked to more aggressive and treatment-resistant SCCHN phenotypes (174)(Discussed in 1.1.3.).

Overexpression of GLUT-1 has been consistently observed in SCCHN in comparison to GLUT-1 levels in normal or benign tissues (221–223). In addition, one study found GLUT-1 overexpression in SCCHN in early pre-neoplastic lesions (223), while another study linked overexpression of both GLUT-1 and GLUT-3 to a poor prognosis (224). Since GLUT expression has a biochemical and clinical correlation with FDG-PET uptake, reflecting the capacity for glucose uptake, high FDG-PET uptake in SCCHN has been found to be reliable in predicting long-term survival and useful for identifying patients who need more aggressive treatment (224). This supports the notion that increased

levels of GLUT are indeed associated with a functional tumour phenotype: increased tumour glycolysis, which in turn is associated with poorer outcomes.

However, other metabolic mediators in SCCHN have received less attention than GLUT expression and function, and only a few studies have focused on enzymatic expression in the metabolic pathways of SCCHN. Two studies, for example, have found that the enhanced expression of (PDK-1) in SCCHN leads to inhibitory phosphorylation of the PDH subunit α (PDHα) (as described in 1.3.1.) which in turn inhibits PDC activity (Figure 1.7.), promoting the Warburg effect metabolic profile and associated malignant phenotype; increasing tumour invasiveness and also growth (225,226).

A number of studies have examined tumour lactate concentrations as a biomarker of glycolytic activity in SCCHN. One study of 40 patients found high pre-treatment tumour lactate levels in SCCHN, which was associated with a low two-year survival rate of 35%, compared to 90% in SCCHN patients with low pre-treatment lactate levels ($p<0.0001$) (227). These findings are in agreement with those of a recent prospective 15-year follow-up study of 17 patients that found a correlation between high lactate levels in SCCHN and a decrease in both post-surgery and post-irradiation overall survival ($p= 0.04$) and recurrence-free survival ($p=0.02$)(228). Consistent with this, two *in vivo* studies have suggested that tissue lactate content may contribute to radioresistance and can be used to monitor the response to radiation in SCCHN (229,230). Another recent analysis of SCCHN cell lines using nuclear magnetic resonance (NMR) spectroscopy observed a substantial increase in lactate levels in comparison with normal tissue, which indicates increased glycolysis and acquisition of the glycolytic phenotype (231).

Given the close regulatory relationship between p53 and TIGAR, it is surprising that the role of TIGAR in SCCHN tumorigenesis has not received much attention, especially considering the fact that p53 is the most mutated gene in the disease, and that TIGAR-mediated p53 regulation of metabolic reprogramming has been reported in breast cancer (30), colon cancers (31), and glioblastoma (32). An *in vitro* study of SCCHN cells using SCC-61 cells treated *in vitro* with fractionated radiation followed by performing tumour selection to generate a matched model of radiation resistance (radiation-sensitive and radiation-resistance cells) showed that radioresistant cells exhibit increased levels of expression of TIGAR and a decrease in oxidative phosphorylation compared to radiosensitive cells. Although this study used only two cell lines without defining the *TP53* status, preventing any conclusions about the regulatory relationship

between *TP53* and *TIGAR* expression in SCCHN cells (232), it may suggest a further investigation of a potential role of TIGAR in increasing radioresistance in SCCHN. TIGAR is discussed in more detail in 1.4..

1.3.4. Targeting Warburg effect in cancer therapeutics

Based on the role that the Warburg adaptation plays in tumorigenesis (discussed previously in 1.3.1. and 1.3.2.), metabolic reprogramming could potentially be exploited to treat cancer. Bonnet et al. have recently demonstrated that switching the metabolism of cancer cells from the glycolytic phenotype to oxidative phosphorylation led to the induction of cell death (233). Despite the expected limitations of treatment with glycolysis inhibitors because of the expected toxicity to the metabolism of normal, rapidly dividing cells such as lymphocytes, which also undergo similar metabolic reprogramming (as discussed earlier in 1.3.1.), studies have shown that targeting glycolysis has no effect on the survival of these normal cells due to their ability to metabolise alternative substrates, such as glutamine, through the TCA (234). Indeed, some treatment strategies with glycolysis inhibitors are currently being evaluated in preclinical models and in clinical trials (235,236). Figure 1.8. summarises the main metabolic perturbations and potential therapeutic targets studied to date in SCCHN.

One of the most obvious therapeutic approaches to target tumour metabolism is inhibiting enzymes of the glycolytic pathway. Although the anti-proliferative effects of 2-deoxy-D-glucose (2-DG), a competitive inhibitor of glucose-6-phosphate which is the product of the first step of glycolysis, have been demonstrated in many preclinical studies (237), early clinical tests limited the use of this drug either due to toxicity associated with hypoglycaemia (238), or insufficient therapeutic effects to prevent disease progression at lower doses (239,240). 2-DG has shown selective cytotoxicity in SCCHN cells, both *in vitro* and *in vivo*, and potentiated the effects of conventional therapy, implying that the tumour survival of these SCCHN models is glycolysis-dependent (241–243). However, significant variations in response among the SCCHN cell lines were reported in other *in vitro* studies (244,245). Two studies from the same research group investigated the importance of glucose metabolism in determining the response to therapy in SCCHN. The first study demonstrated that glucose, not glutamine, is the main energy source in SCCHN cells and that 2-DG-mediated glucose deprivation resulted in an increase in cell death in SCCHN cells (245). The second study used two isogenic SCCHN derived cell lines from the same patient, one harbours mutant *TP53* and the other

harbours wild type *TP53*. Fluorescence-based extracellular flux analysis showed that mutant *TP53* cells exhibit a different metabolic phenotype than that of wild type *TP53* cells, with apparently lower use of oxidative phosphorylation and higher use of glycolysis by mutant *TP53* cells (246). It was also observed, using clonogenic assay, that 2-DG-mediated inhibition of glycolysis potentiates the effects of IR in mutant *TP53* cells, without similar effects in wild type *TP53* cells, which suggested that *TP53* status may be a key determinant in metabolic phenotyping of SCCHN, and indicated for the first time that *TP53* may play an important role in determining the response of SCCHN cells to glucose deprivation-based therapies (246).

Another potential therapeutic target in the glycolysis pathway is 6-phosphofructo-2-kinase/fructose-2,6-biphosphatase (PFKFB)(247). Overexpression of PFKFB was observed in a number of extremely aggressive human carcinomas, causing elevated levels of fructose-2,6-bisphosphate (F2,6BP)(247), which allosterically activates PFK-1, the catalyser of the third step of the glycolysis pathway (247). 3PO, [3-(3-pyridinyl)-l-(4-pyridinyl)-2-propen-l-one], has recently been identified as a PFKFB inhibitor, which suppresses glycolysis and tumour growth in a variety of cancer cells *in vitro* and *in vivo* (248).

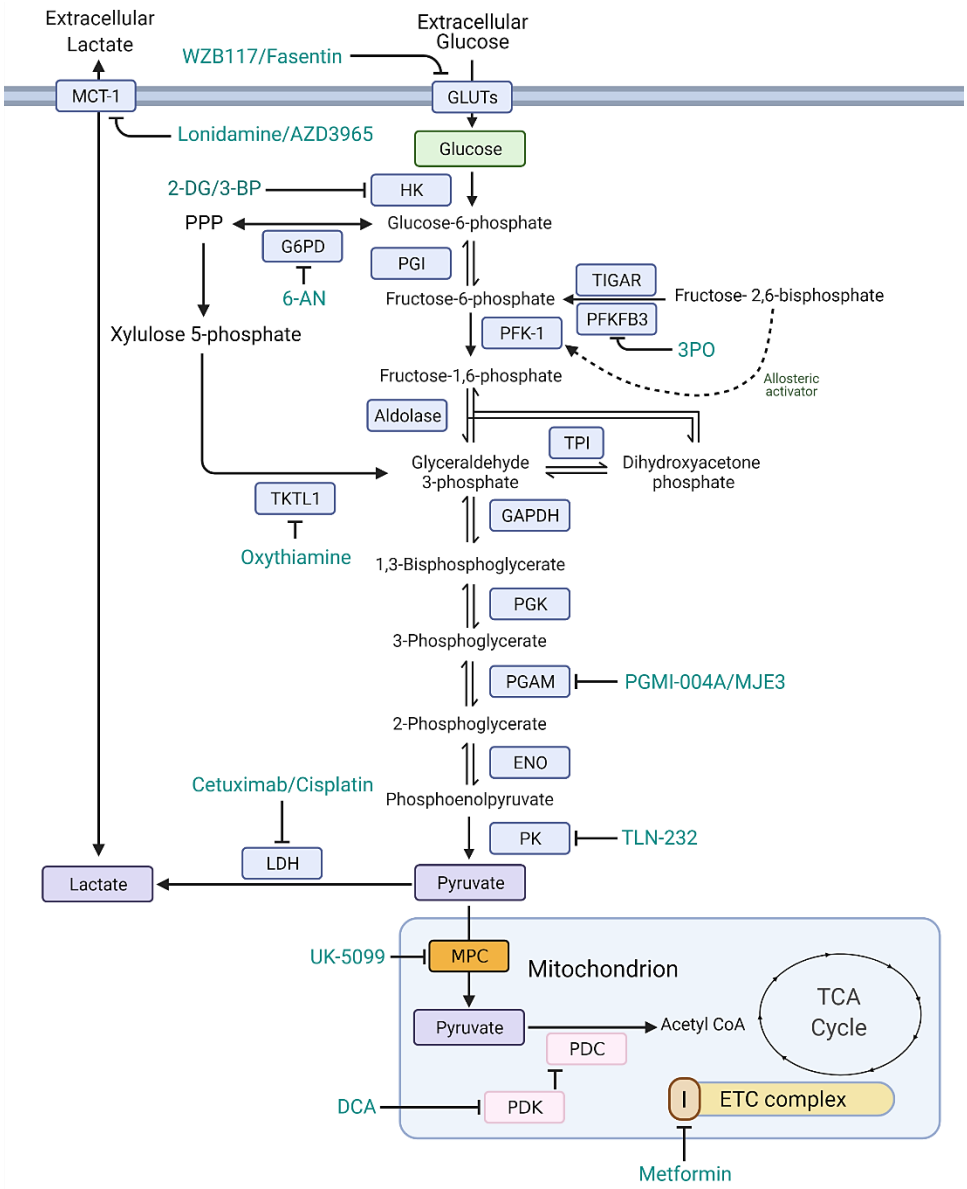

Figure 1.8. The potential therapeutic targets of the glycolysis pathway in SCCHN. According to the evidence available to date, SCCHN, particularly in advanced and treatment-resistant diseases, exhibits the Warburg effect (increased aerobic glycolysis). Recent evidence has also demonstrated that loss of wild type p53 function contributes to this metabolic switch. The potential therapeutic targets in the metabolic switch toward glycolysis include suppressing the glycolysis pathway by inhibiting HK (using 2-DG) or PFKFB (using 3PO), suppressing the PPP by inhibiting G6PD (using 6-AN) and enhancing the conversion of pyruvate into Acetyl CoA in TCA by inhibiting PDK (using DCA). All abbreviations are included in the abbreviations list. The figure is reproduced from the references (249–253).

Promoting the mitochondrial oxidative phosphorylation in human cancer cells, and thus redirecting cell metabolism away from glycolysis and inducing apoptosis, has received increasing interest as another potential cancer treatment strategy. One of the ways to redirect the cell metabolism away from glycolysis is by activating PDH. PDH is typically phosphorylated and relatively inactive in cancer cells due to overexpression of PDKs, a

family of kinases that negatively regulates PDH function by phosphorylating it. *In vitro* and *in vivo* studies have shown that the PDK inhibitor dichloroacetate (DCA) promotes PDH hypophosphorylation and thus increases mitochondrial oxidative phosphorylation, induces apoptosis, and inhibits cancer cell proliferation (226,233,254).

The outcomes of clinical studies targeting glycolysis indicate that oxidative stress is the main mechanism underlying the cytotoxic effects that result from this inhibition, suggesting that secondary metabolic pathways that prevent oxidative stress, such as the PPP, could be used as potential therapeutic targets for cancer treatment. *In vitro* studies have shown that inhibiting the first step of the glycolysis pathway using 2-DG induces perturbations in surrogates of oxidative stress, such as a significant increase in ROS levels (246), lower cellular reduction potential (245), and a lessened proportion of GSH (241). This conclusion is supported by results from experiments that used simultaneous treatment with N-acetyl cysteine, a thiol antioxidant, which was found to reverse both the cytotoxic effects of glycolytic inhibition and indicators of oxidative stress (241,245,246). In addition, rapidly proliferating tumour cells abundantly require pentoses and NADPH, the main product of the PPP, for their roles in nucleic acid synthesis and oxidative stress prevention, respectively. Indeed, tumour cells are known to upregulate the PPP by promoting the expression of G6PD, which controls the oxidative component of the PPP, and transketolase, which controls the nonoxidative component (255,256). Thus, both enzymes are promising therapeutic targets in cancer treatment since inhibition of these would be expected to render cells more sensitive to the toxic effects of ROS and create nucleotide shortages incompatible with rapid proliferation. 6-Aminonicotinamide (6-AN) is one candidate drug that could have therapeutic potential since it inhibits G6PD, causing oxidative stress and sensitises cancer cells to both radiation and cisplatin (257,258). A recent study that used a preclinical matched model of radiation resistance SCCHN cells (radiation-sensitive and radiation-resistance cells) showed an increased dependence on glycolysis in the radioresistant cells group in comparison with the radiosensitive cells group. This study also showed an increase in PPP flux as evidenced by higher expression of TIGAR and key PPP enzymes as well as elevated levels of NADPH in the radioresistant cells group (232). These findings not only support the potential therapeutic benefit of targeting PPP flux, but also imply that TIGAR-mediated p53 regulation of SCCHN metabolism is indeed an area that needs to be investigated further and could be a potential target for therapy, given the association between *TP53* status and acquisition of glycolytic phenotype in tumours. TIGAR will discuss in more detail in the following chapter.

1.4. *TIGAR*

A seminal study in 2006 identified *TP53*-induced glycolysis and apoptosis regulator (TIGAR) as a novel transcriptional target of p53 that plays a direct and significant role in regulating the glycolysis pathway (259).

1.4.1. Structure of *TIGAR*

The discovery of TIGAR was made through an analysis of gene expression by computer-based microarray data following the activation of p53 (259,260). The human TIGAR gene (also known as C12orf5) is 38 kilobase pair gene consisting of six exons and located on chromosome 12p13-3. The gene promoter contains two p53 binding sites: BS1, which is located upstream of the first exon and BS2, which is located within the first intron. BS2 is significantly more effective than BS1 in binding p53 (259).

TIGAR protein consists of 270 amino acids with a molecular weight of 30 kDa (259). The protein contains a bisphosphatase active centre which requires two histidine residues (H11 and H198) and one glutamic acid residue (E102) for its enzymatic activity (the catalytic triad)(259). This domain has similarities with the catalytic domains of PGAM enzymes (259,261), and especially with the bisphosphatase domain of the isoform products of the four genes (PFKFB1–4) which encode the glycolytic enzyme PFK-2/FBPase-2 (259,261). PFK-2/FBPase-2 is a bifunctional protein that comprises a kinase domain within the amino-terminus and a bisphosphatase domain at the carboxy-terminus. This bifunctional enzyme both regulates the intracellular synthesis and decreases cellular levels of F2,6BP, through the activity of PFK-2 and FBPase-2, respectively. It was found that decreasing TIGAR expression using RNAi results in elevated levels of F2,6BP levels and increased glycolytic rates (259). It was also found that exogenously driven overexpression of TIGAR had comparable effects to that observed following expression of a truncated form of PFK-2/FBPase-2 expressing only the bisphosphatase domain (FBPase-2), including the reduced levels of F2,6BP, the decreased glycolysis rates and the enhanced PPP flux and resistance to oxidative stress (259). Thus, TIGAR appears to be a functional FBPase enzyme. However, it is noteworthy that the FBPase catalytic activity of TIGAR is several orders of magnitude lower than that of the FBPase-2 component of PFK-2/FBPase-2 isoenzymes, the significance of this is unclear (262).

The essential regions for catalytic activity within the FBPase-2 domain are well preserved in TIGAR (259), including the characteristic RHG motif, an N-terminal region conserved among the PGAM family (263), and the catalytic triad of H, E, and H residues (264)(Figure 1.9.).

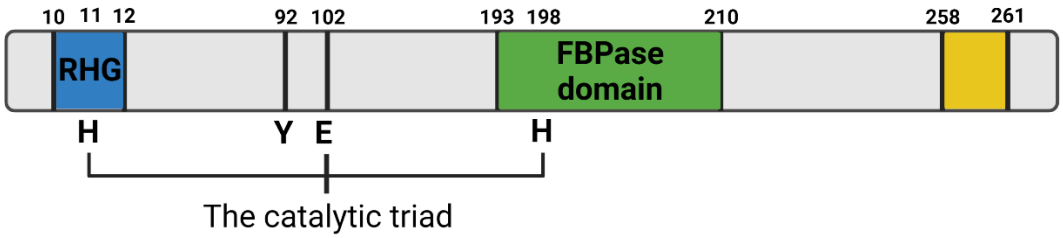

Figure 1.9.: The functional regions in TIGAR protein structure. TIGAR protein structure includes the characteristic RHG signature of the PGAM family (residues 10-12), the catalytic triad which consists of the histidine residues 11 and 198 and the glutamic acid residue 102 and responsible for maintaining the activity of the FBPase-2 domain, tyrosine 92 which interferes with TIGAR-dependent NADPH production, and the 258–261 domain that is responsible for the mitochondrial localization and the phosphatase-independent stimulation of HK-II. The figure is reproduced from reference (265).

The TIGAR-triple mutant H11A/E102A/H198A (TIGAR-TM mutant) was generated to determine whether these three amino acids are the active sites for a putative bisphosphatase activity (259). Mutations in these three amino acids have been observed to abrogate the capacity of TIGAR to decrease the F2,6BP levels (259).

1.4.2. TIGAR functions

As described in 1.4.1., the catalytic domain of TIGAR has similarities with the bisphosphatase domain of PFKFB, which possesses FBPase-2 activity and catalyses the de-phosphorylation of F2,6BP to F6P. F2,6BP is a potent positive allosteric effector of PFK-1, which catalyses the conversion of F6P to F1,6BP and thus, drives glycolysis (259). F2,6BP also suppresses gluconeogenesis through its activity as an inhibitor of FBPase-1, the enzyme that opposes the activity of PFK-1 by converting F1,6BP to F6P (266). Therefore, the effect of TIGAR acting as an FBPase-2 is to reduce F2,6BP levels and so decrease the activity of PFK-1. The increase in F6P that results from TIGAR also increases the activity of FBPase-1, with the net effect being to reduce glycolytic flux at the third step of the glycolysis pathway (Figure 1.10.)(259).

As stated in 1.2.3.1., the p53-promoted decrease in ROS levels help to maintain genomic stability and protect the genome from oxidative damage which has been shown to play a crucial role in promoting tumours (267). One of the consequences of TIGAR activity in suppressing glycolysis is that TIGAR indirectly plays a role in the regulation of redox homeostasis by enhancing the rate of the PPP, which generates NADPH and thus contributes to increased glutathione (GSH) synthesis and this promotes the scavenging of ROS (259). In addition, intermediate metabolites of the PPP, such as ribose-5-phosphate and NADPH, are essential precursors for DNA biosynthesis and repair, thereby allowing cell survival and thus protecting against ROS-sensitive apoptotic responses, such as those regulated by p53 (268).

Function of TIGAR is most clearly seen under conditions of metabolic stress, including hypoxia (269). The limited role of TIGAR in normal condition allows cells to avoid excessive PPP flux and increases pyruvate entry into mitochondria and the generation of ROS (270).

Studies have also identified phosphatase-independent functions of TIGAR (271). Interestingly, TIGAR has been found to induce cell cycle arrest and promote DNA repair by inhibiting the expression of the cyclins and CDKs involved in pRb phosphorylation (see section 1.1.3.1.2.) in a p21-independent manner, and thus stabilise the pRb–E2F complex and induce cell cycle arrest (272).

It was found that localization of TIGAR to the mitochondria occurs only under hypoxia condition, which results in a significant interaction of HK-II (an isoform of Hexokinase found at the outer membrane of mitochondria) with TIGAR (270). Stimulating HK-II results in increased glycolytic flux and the availability of glycolytic intermediates for use in the PPP (273,274), which suggests that TIGAR can positively regulate the PPP through both an enzymatic (in normoxia) and non-enzymatic activity (in hypoxia)(273,274).

Although the regulatory relationship between p53 and TIGAR has been studied in several cancers, an alternative mechanism that regulates TIGAR in the absence of p53 has also been suggested. A study of tumour cell lines found relatively high expression of TIGAR in some p53-null cells, which clearly demonstrated that the expression of TIGAR is not exclusively p53-dependent (259).

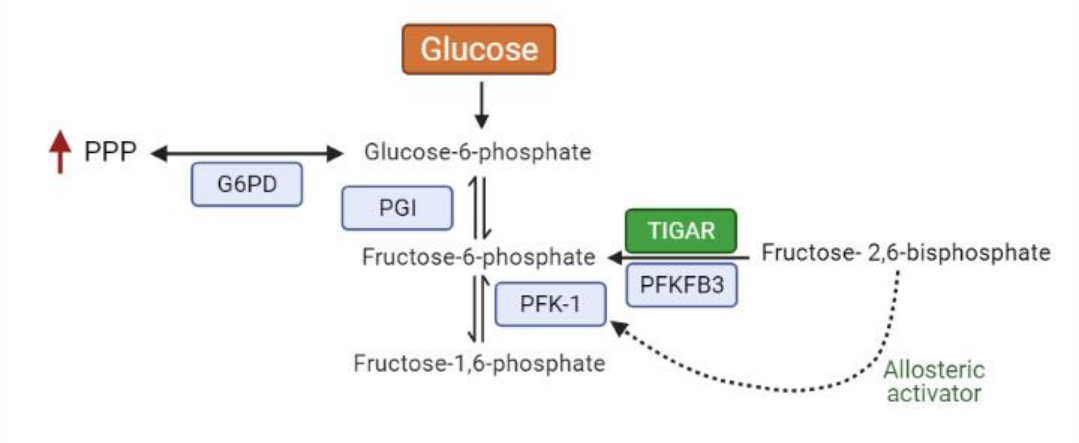

Figure 1.10. Functions of TIGAR. TIGAR redirects the glycolytic pathway toward the PPP by reducing F2,6BP levels, reducing ROS levels, inhibiting autophagy and promoting nucleotide synthesis. TIGAR has phosphatase-independent activities including stimulating HK-II in the mitochondria and inhibiting the expression of the cyclins and CDKs involved in pRb phosphorylation, inducing cell cycle arrest and DNA repair. The figure is reproduced from reference (271).

1.4.3. Role of TIGAR in cancer

In tumour progression, the remodelling of metabolic pathways may help regulate redox homeostasis and provide intermediates required for cell growth (275). TIGAR has been observed to be upregulated in cells under a variety of stress conditions, such as ischemia and hypoxia (273,276), and is found to be highly expressed in a number of cancers (277). It is believed that TIGAR has a dual function contributing to carcinogenesis, due to its role in inhibiting glycolysis as well as its ability to suppress both autophagy and apoptosis (mechanisms are discussed in 1.2.3.3. and 1.2.3.2., respectively)(278).

TIGAR function as a p53 target gene (previously discussed in 1.4.2.) indicates that TIGAR may play a role in suppressing tumours through its function in lowering F2,6BP levels and inhibiting glycolysis as well as enhancing DNA repair through cell cycle regulation and promoting the oxidative phosphorylation function of mitochondria (275).

On the other hand, TIGAR also promotes the PPP, which results in the generation of NADPH and supports the cellular antioxidant function to inhibit oxidative stress and apoptosis, thus TIGAR has the potential to contribute to carcinogenesis (275). This role is also linked to stimulation of HK-II, as stated in 1.4.2., which maintains mitochondrial membrane potentials and promotes the reduction of ROS in hypoxic conditions (275). ROS are key mediators in TIGAR-mediated suppression of autophagy (265). Under

conditions of starvation and metabolic stress, TIGAR was found to have the ability to indirectly inhibit autophagy, as measured by the accumulation of GFP-tagged LC3 probes which is a marker protein involved in the formation of autophagosomes. This role of TIGAR in limiting autophagy under conditions of starvation and metabolic stress was found to be correlated with its role in stimulating NADPH production and lowering ROS through the PPP (269). These observations were consistent with outcomes of TIGAR knockdown studies that reported increased ROS levels and induced apoptosis and autophagy in different types of cancers (279–281).

The functions identified for TIGAR, such as promoting gluconeogenesis and the PPP and suppressing ROS, are at least compatible with TIGAR contribution to tumour suppression and yet at the same time imply a potential contribution to carcinogenesis-related events. Indeed, the fact that TIGAR is regulated, at least in some settings, by the tumour suppressor p53, the ultimate "Guardian of the Genome", further supports this notion (282). Data from different systems indicate that cell type, as well as the nature of the stresses examined, greatly influence the results in studies of TIGAR function. Accordingly, this thesis focuses on one cell type to characterise the function of TIGAR in SCCHN cells with defined p53 status. It is hoped that in so doing, reliable information leading to a better understanding of the role of TIGAR, and also of p53, in carcinogenesis can be obtained. Ultimately, of course, such studies are aimed at increasing our understanding so that new ideas can inform therapeutic approaches that will lead to better outcomes for patients.

1.5. Aims

As stated in Section 1.1.5, radiotherapy is the cornerstone of SCCHN treatment, and is recommended for 74% of SCCHN patients at any stage during treatment, either as monotherapy or as adjuvant therapy. There is a need to increase treatment effectiveness and enhance survival outcomes in SCCHN patients. Hence, it is necessary to identify new treatment approaches and one such approach is to focus on attempting to increase radiosensitivity. Alterations in cellular metabolism are now widely recognised as a critical hallmark of cancer, offering an attractive potential therapeutic target, particularly since there is evidence that such changes may impact radiation sensitivity. There is undeniable heterogeneity in normal metabolic homeostasis among cancers, which may be due to various oncogenic and tissue-specific events that drive tumorigenesis in a variety of cancers, including SCCHN. As such, there is a need for comprehensive studies of metabolism for each specific type of cancer to develop effective metabolism-targeting therapeutic strategies. However, early studies of SCCHN metabolism were limited and often yielded contradictory findings. Recent studies have indicated that *TP53* is a critical determinant of cancer cell metabolic reprogramming in SCCHN. However, the exact mechanisms through which *TP53* status determines the switch from mitochondrial respiration towards increased glycolysis in the presence of oxygen in SCCHN are still not fully understood. Through this switch, cancer cells use glycolysis even under normoxic conditions to produce energy and it is thought that one reason for this is to avoid excessive ROS accumulation, one of the main products of mitochondrial respiration which mediates apoptosis and DNA damage. Understanding how these mechanisms work could lead to identifying critical elements of p53-mediated metabolic regulation as potential therapeutic targets.

Thus, the aims of this study were:

1- To investigate the role that the *TP53* status plays in determining the metabolic phenotype in SCCHN.
2- To investigate the potential role that target mediators play in the p53-responsive machinery that regulates different parts of SCCHN metabolism.
3- To determine whether drugs targeting glycolysis could have a role in improving the response to radiation which might provide a means to enhance radiotherapy in SCCHN.

2. Materials and Methods

2.1. List of materials

2.1.1. Laboratory equipment

Product	Manufacturer
CellRad x-ray irradiator	Faxitron
Evos FL Cell Imaging System	AMG
Mini-PROTEAN® Tetra Vertical Electrophoresis Cell	Bio-Rad
Mr Frosty™ freezing container	Thermo Scientific
Refrigerated Centrifuge	Thermo Scientific™
Refrigerated microcentrifuge (5424R)	Eppendorf
Trans-Blot Turbo Transfer System (Bio-Rad)	Bio-Rad
Ultrapure Water (18.2 MΩ) System	Avidity Science

2.1.2. Consumables

Product	Manufacturer
10%, Acrylamide:Bis-acrylamide, 37.5: precast protein gels of 10 or 15 wells	Bio-Rad
96-well black-bottom plates	Sigma-Aldrich
Cell culture dish (100mm x 20mm)	Starlab
Cell culture flask (25cm2, 75cm2)	Thermo Fisher Scientific
Cell culture plate (6-well)	Thermo Fisher Scientific
Cell culture plate (96-well), flat-bottom	Starlab
Cell scraper	Greiner Bio-One
Centrifuge micro tubes (o.5, 1 and 2ml)	Eppendorf
Centrifuge tubes (15 and 50 ml)	Greiner Bio-One
Cryovials	Thermo Fisher Scientific
Filtered tips (10, 200 and 1000µl)	Starlab
Gel loading tips	Starlab
Gloves What type	StarGuard
Immun-Blot® PVDF membrane	Bio-Rad
Microloop® sterile plastic inoculating loop	MWE
Multichannel pipetting reservoir	Starlab

Parafilm™ M laboratory wrapping film	Bemis
Pipette tips (10, 200 and 1000µl)	Scientific Laboratory Supplies
Pipettes (5, 10, and 25 ml)	Greiner Bio-One
Spectrophotometer cuvettes	VWR
Sterile disposable scalpel	Swann-Morton
Sterile filter bottles (0.22 µm filter) and cap	Corning
Sterilin™ standard 90mm Petri dish	Thermo Scientific
Syringe (20ml, 50ml)	BD Plastipak Luer-Lok™
Syringe filter (pore size 0.22µm)	Fisher Scientific
Virkon	Fisher Scientific
XFe96 cell culture microplates	Agilent
XFe96 sensor cartridges	Agilent

2.1.3. Chemicals and biological reagents

Product	Manufacturer
Acrylamide (#1490-OP)	Calbiochem
Agar powder for microbiology (#009002-18-0)	Formedium
Ammonium persulfate (APS)(#7727-54-0)	Sigma-Aldrich
Aprotinin (#10236632103)	Roche
Blotting grade blocker, non-fat dry milk (#1706404)	Bio-Rad
Blue Prestained Protein Standards (#1610373)	Bio-Rad
Bovine serum albumin (BSA)(#11413164)	Fisher scientific
Bromophenol blue (#B0126)	Sigma-Aldrich
Buffer solution pH 10, Carbonate buffer (#258600025)	Acros Organics
Buffer solution pH 4, Phthalate buffer (#10675492)	Fisher scientific
Buffer solution pH 7, Phosphate buffer (#10448273)	Acros Organics
Calcium chloride (#10043-52-4)	Sigma-Aldrich
Clarity Western ECL (#1705061)	Bio-Rad
Collagen (#C2249)	Sigma-Aldrich
Crystal Violet (#C581-25)	Fisher scientific
D-glucose	Sigma-Aldrich
Dimethyl sulfoxide (DMSO)(#10499683)	Fisher scientific
DNase-free RNase A (#79254)	QIAGEN
Ethanol (absolute)(#10610813)	Fisher scientific
Ethanol (molecular biology grade)(#5197)	Sigma-Aldrich
Ethylenediaminetetraacetic acid (EDTA)(#03620)	Sigma-Aldrich
EveryBlot blocking buffer (#12010020)	Bio-Rad
Glutaraldehyde (#BP25484)	Fisher Scientific
Glycerol (#G5516)	Sigma-Aldrich

Glycine (#10061073)	Fisher Scientific
HEPES (#H3375)	Sigma-Aldrich
Hydrogen chloride (HCl)(#320331)	Sigma-Aldrich
Isopropanol (#10315720)	Fisher Scientific
Kaleidoscope™ Prestained Protein Standard (#1610375)	Bio-Rad
Leupeptin (#11017128001)	Roche
Lipofectamine 2000 transfection reagent (#11668019)	Invitrogen
Luria broth (LB)(#L3397)	Sigma-Aldrich
Methanol (HPLC grade)(#10675112)	Thermo Fisher Scientific
MTT (3-(4,5-dimethylthiazol-2-yl)-2,5-diphenyl tetrasodium bromide)(#M6494)	Thermo Fisher Scientific
N, N, N', N'-tetramethylenediamine (TEMED)(#0761)	VWR
PBS, pH 7.4 (#10010023)	Gibco
PBS, Phosphate Buffered Saline, 10X Solution (#10649743)	Fisher scientific
Pepstatin (#10253286001)	Roche
Phenylmethylsulphonyl fluoride (PMSF)(# 11359061001)	Sigma-Aldrich
Ponceau S (#P7170)	Sigma-Aldrich
Protein assay dye reagent (#5000002)	Bio-Rad
Proteinase K (#P2308)	Sigma-Aldrich
Sodium chloride (NaCl)(#10428420)	Fisher Scientific
Sodium dodecyl suphate (SDS)(#28312)	Fisher Scientific
Sodium hydroxide (NaOH)(#10675692)	Fisher Scientific
Super Optimal broth with Catabolite repression (SOC) media (#S1797)	Sigma
Transfer buffer (#1610734)	Bio-Rad
Tris base (#648310)	Calbiochem
Triton X-100 (#T8787)	Sigma-Aldrich
Trypsin-EDTA solution (#T4049)	Sigma-Aldrich
Tween-20 (#P1379)	Sigma-Aldrich
XF calibrant solution (100840-000)	Agilent
XL1-Blue competent cells (200249)	Agilent
β-mercaptoethanol (M6250)	Sigma-Aldrich

2.1.4. Cell culture basal media and supplements

Product	Manufacturer
Dulbecco's Modified Eagle Medium (DMEM), high glucose (4500 mg/L glucose) (#D5796)	Sigma-Aldrich
Dulbecco's phosphate buffered Saline (PBS)(# D8537)	Sigma-Aldrich

Fetal bovine serum (FBS)(#F7524)	Sigma-Aldrich
L-Glutamine (#G7513)	Sigma-Aldrich
Non-Essential Amino Acids (#11140050)	Gibco
Opti-MEM™ I Reduced Serum Medium (#31985062)	Gibco
Penicillin/Streptomycin-Solution (P/S) 10,000U penicillin and 10mg streptomycin per ml (100X)(# P4333)	Sigma-Aldrich
Sodium pyruvate (#S8636)	Sigma-Aldrich
XF DMEM-based medium, pH 7.4 (#103575-100)	Seahorse Bioscience

2.1.5. Kits

Product	Manufacturer
CyQUANT® cell proliferation assay kit (#C7026)	Invitrogen
DNeasy® Blood & Tissue Kit (#69504)	QIAGEN
QIAprep Spin Miniprep Kit (#27104)	QIAGEN
Trans-Blot Turbo RTA Midi 0.2 µm PVDF Transfer Kit (##1704273)	Bio-Rad

2.1.6. Oligonucleotides

Product	Manufacturer
siGENOME Human *TIGAR* SMARTpool siRNA (M-020597-01-0005)	Dharmacon™
siGENOME Human *TIGAR* set of 4 siRNAs (MQ-020597-01-0002)	Dharmacon™
siGENOME Human *TIGAR* individual siRNA#2 (D-020597-02-0020)	Dharmacon™
siGENOME Human *TIGAR* individual siRNA#3 (D-020597-03-0020)	Dharmacon™
siGENOME Non-targeting siRNA (D-001210-01-50)	Dharmacon™
siGENOME *TP53* siRNA (D-003329-05-0050)	Dharmacon™

2.1.7. Plasmids

Product	Manufacturer
Myc-DDK-tagged-Human TIGAR open reading frame 5 clone	OriGene
pCMV6-AN-Myc-DDK Mammalian Expression Vector (#PS100016)	OriGene
pEGFP-N3 plasmid	Addgene
pCMV-Neo-Bam MDM2	Addgene
VP1.5 vector sequencing primer	OriGene
XL39 vector sequencing primer	OriGene

2.1.8. Reagents used in western blotting

SLIP (Stuart Linn Immunoprecipitation) buffer:

- 50mM HEPES (pH 7.5)
- 150mM NaCl
- 10% (v/v) glycerol
- 0.1% (v/v) Triton X-100
- 0.5mg/ml BSA

4x protein sample loading buffer:

- 0.25 M Tris (pH 6.8)
- 8% (w/v) SDS
- 40% (v/v) Glycerol
- 4 mg/ml Bromophenol blue
- 1% (v/v) β-mercaptoethanol
- Diluted with H_2O to make 2x and 1x sample buffer.

Tris-glycine electrophoresis running buffer:

- 25mM Tris, pH 8.3
- 250mM glycine
- 0.1% (w/v) SDS

Tris-glycine transfer buffer:

- 20% 10x Tris/glycine buffer for western blots (10x premixed electrophoresis buffer contains 25 mM Tris pH 8.3, 192 mM glycine, pH 8.3 following dilution to 1x with water)
- 20% Methanol 100%
- 60% H_2O

Ponceau S solution:

- 0.2% (w/v) Ponceau S
- 5% (v/v) acetic acid

PBS/tween:

- 10x PBS diluted with H_2O to make 1x
- 0.1% (v/v) Tween-20

2.1.9. Antibodies

Product, clone or catalogue number, final concentration and manufacturer
MDM2 (IF-2), mouse monoclonal antibody, final concentration of 3µg/ml (#OP46, Calbiochem®)
Myc/c-Myc Antibody (9E10), mouse monoclonal antibody, used at a 1:500 dilution (#sc-40, Santa Cruz)
p53 (DO-1), mouse monoclonal antibody, final concentration of 1µg/ml (#OP43, Calbiochem®)
TIGAR (E-2), mouse monoclonal antibody, final concentration of 1µg/ml (#sc-166290, Santa Cruz)
Vinculin, mouse monoclonal antibody, final dilution of 1:10 000 (#V9131, Sigma-Aldrich)
Sheep anti-mouse antibody, used at a 1:2500 dilution (#RPN4201, GE Healthcare)
Donkey anti-rabbit antibody, used at a 1:5000 dilution (#NA934, GE Healthcare)

2.1.10. Drugs

Product, stock preparation and manufacturer

2-deoxy-D-glucose (2-DG) product code needed for all (#D8375, Sigma-Aldrich)
Stock solution prepared by dissolving to 1M in DMSO. Stored at -20°C for six weeks.

(2E)-3-(3-Pyridinyl)-1-(4-pyridinyl)-2-propen-1-one (3PO) (#SML1343, Sigma-Aldrich)
Stock solution prepared by dissolving to 5mM in DMSO. Stored at -20°C for six weeks.

6-aminonicotinamide (6-AN) (#A68203, Sigma-Aldrich)
Stock solution prepared by dissolving to 2mM in DMSO. Stored at -20°C for six weeks.

Antimycin A (#A8674, Sigma-Aldrich)
Stock solution prepared by dissolving to 2mM in 95% (w/v) ethanol. Long-term storage was at -20°C.

Carbonyl cyanide 4-(trifluoromethoxy)phenyl-hydrazone (FCCP) (#C2920, Sigma-Aldrich)
Stock solution prepared by dissolving to 10mM in 95% (w/v) ethanol. Kept at -20°C long-term storage.

Dichloroacetate (DCA) (#347795. Sigma-Aldrich)
Stock solution prepared by dissolving to 0.1M in DMSO. Stored at -20°C for six weeks.

Oligomycin (#75351. Sigma-Aldrich)
Stock solution prepared by dissolving to 5mM in 95% (w/v) ethanol. Kept at -20°C long-term storage.

Plasmocin™ (#ant-mpt, Invivogen)
A final working concentration of 50µg/ml was used and prepared freshly on each occasion.

Rotenone (#R8875, Sigma-Aldrich)
Stock solution prepared by dissolving to 2mM in 95% (w/v) ethanol. Kept at -20°C long-term storage.

UK-5099 (#PZ0160, Sigma-Aldrich)
Stock solution prepared by dissolving to 10mM in DMSO. Kept at 4°C long-term storage.

Kanamycin (#60615, Sigma-Aldrich)

Stock solution prepared by dissolving to 25 mg/ml in dH_2O. Filtered using 0.22-micron syringe filter and stores at -20°C

2.1.11. Instruments

Product	Manufacturer
BioPhotometer	Eppendorf
CellDrop™ automated cell counter	DeNovix
ChemiDoc™ Touch Imaging System	Bio-Rad
GelCount™ colony analyser	Oxford Optronix
NanoDrop™ One/One^C Microvolume UV-Vis Spectrophotometer	Thermo Scientific
Spark® multimode microplate reader	TECAN
SpectraMax Plus 384 Microplate Reader	Molecular Devices
XFe96 instrument	Seahorse Bioscience

2.1.12. Software

Product	Manufacturer
GelCount	Oxford Optronix
GENtle	Magnus Manske
Image Lab	Bio-Rad
Image Lab Touch	Bio-Rad
Inkscape 0.91	Inkscape Project
Mendeley 1.17.10	Elsevier
MS Office 365	Microsoft
NanoDrop 1000 Software V3.8	Thermo Scientific
PRISM® 9	GraphPad
SoftMax Pro	Molecular Devices
SparkControl™	TECAN
Seahorse Wave Desktop	Agilent

2.2 Cell culture

2.2.1. Cell lines

All the parental cell lines used in this work were University of Michigan squamous cell carcinoma cell lines (UM-SCC), and were kindly provided by Professor Thomas E. Carey (University of Michigan Medical School) (283). These cell lines show a close similarity of genetic and molecular cytogenetic data *in vitro* with primary tumours (284).

Genetically modified derivatives of UM-SCC-17A cells, stably expressing short-hairpin RNA (shRNA) specific for p53 (shp53) or empty vector control (lenti), and genetically modified derivatives of UM-SCC-1, transduced with an empty vector (pBABE), wild type *TP53*, or various *TP53* mutations (R175H, C176F, or R282W), were produced in the lab of Professor J. Myers (University of Texas MD Anderson Cancer Center, TX, USA) using standard cloning and transfection techniques, as detailed in the reference (285). Briefly, the RNAi derivative cell lines generated by the Myers laboratory were produced as follows: cells were infected with a green fluorescent protein (GFP)-tagged empty lentiviral vector or a recombinant derivative encoding an shRNA against p53 (shp53) before being cultured for several passages, and then sorted using flow cytometry. Derivatives of UM-SCC-1 cells expressing *TP53* constructs (wild type, R175H, C176F, and R282W) were also generated by the Myers laboratory as follows: RNA was extracted from cell lines known to express these mutants. Then reverse transcription of PCR (RT-PCR) was performed using primers specific to *TP53*. Standard cloning techniques were used to insert the purified resulting products into a pBABE retroviral vector containing a puromycin-resistance cassette and the resulting vectors were verified by Sanger sequencing. After transfection and packaging in 293T cells, the viral supernatant was centrifuged, and the cellular debris was removed. Then, the viral supernatant was added to UM-SCC-1 cells in combination with polybrene (to enhance the efficiency of infection). After 1 passage, the cells underwent selection with puromycin (285).

Table 2.1. shows a summary of the included parental cell lines, accompanied by details of the SCCHN subsite of origin, type of lesion, reported *TP53* status and type of mutation if any, p53 phenotype and the reported HPV status.

Table 2.1.: Parental cell lines used in this study.

Cell Line	Subsite of Origin	Type of Lesion	Reported *TP53* Status	p53 phenotype	Reported HPV Status	Primary References
UM-SCC-1	Floor of mouth	Primary	Null, Splice site mutation	Loss of Function	Negative	(283,285,286)
UM-SCC-5	Supraglottis	Primary	Mutant: V157F	Dominant-Negative Activity; Gain of Function	Negative	(283,286–290)
UM-SCC-10A	True vocal cord	Primary	Mutant: G245C	Dominant-Negative Activity; Gain of Function (weak)	Negative	(283,286,287,291–293)
UM-SCC-11A	Supraglottis	Primary: pre-treatment biopsy	Wild type	Wild type	Negative	(294–296)
UM-SCC-11B	Supraglottis	Primary: post-chemotherapy surgery	Mutant: C242S	Loss of Function	Negative	(283,286,287,291,295)
UM-SCC-17A	Supraglottis	Primary	Wild type	Wild type	Negative	(283,286,291)
UM-SCC-17As	Supraglottis	Primary	Wild type	Wild type	Negative	(283,286,291)
UM-SCC-81B	Tonsil	Metachronous primary	Mutant: H193R	Dominant-Negative Activity	Negative	(283,286–288,295)

2.2.2. Cell medium and growth environment

Cells were grown in Nunc™ cell culture treated flasks with filter caps (Thermo Fisher Scientific) of various sizes (T25, T75) under standard conditions in a humidified cell incubator at 37°C with 5% CO_2. All cell lines were maintained in Dulbecco's modified Eagle medium (DMEM) high glucose (4500 mg/L glucose) supplemented with 10% fetal bovine serum (FBS), 100 U/ml penicillin and 100 µg/ml streptomycin, 2 mM L-glutamine and 1% Non-Essential Amino Acids.

2.2.3. Cell sub-culture technique

All cell culture methods were performed under sterile conditions at all times in order to avoid contamination. All tissue culture work was carried out in Class II laminar flow tissue culture cabinet. Cell culture medium and nutritional supplements were purchased in sterile bottles, stored as required, and the outside of the containers was disinfected with ethanol before being placed in the tissue culture cabinet. The equipment required for cell culture was typically supplied sterile, and additionally sterilised before each session by exposure to ultraviolet radiation for 10 minutes inside the cabinet. All cells were tested every four weeks for mycoplasma contamination, as described in section 5.1.2.

All the cell lines used in this study were grown as adherent monolayers on cell culture-treated surfaces. Sub-culture, or passage, of cells was performed on a regular basis to ensure that cells were maintained at optimal health, as once cells reach the maximum confluence in the culture vessel, death can occur due to overcrowding and associated stress.

Once cells reach approximately 70-90% confluence, the cells were trypsinised and passaged. All media, PBS and trypsin were warmed in a 37°C water bath for 1 hour before use with cell cultures. Media was aspirated from the culture vessel and the cell monolayer was washed once with phosphate-buffered saline (PBS) pH 7.4 at room temperature (RT), typically 10 ml when using a T75 tissue culture flask. PBS was then aspirated before an appropriate volume of trypsin-EDTA, typically 3 ml when using a T75 tissue culture flask, was added to the monolayer and the culture vessel was returned to the cell incubator at 37°C. The culture vessel was agitated as needed to facilitate the detachment of cells, which was assessed by examination under light microscopy. Cell lines required incubation times of 2 to 10 minutes depending upon the line. Once sufficiently detached, the trypsin-EDTA was neutralised by the addition excess of complete media, typically 8 ml when using a T75 tissue culture flask. A volume of cells was added to a new culture vessel based on the cell split ratio, which was in turn determined by the growth characteristics of the individual cell line. For example, slow-growing cell lines were usually split in a ratio of 1:3, while rapidly proliferating cell lines were split in a ratio of 1:20. An appropriate volume of fresh media was added - typically to a total volume of 10 ml when using a T75 flask. Cells were routinely subcultured once every 7 days. Media changes were made every 2-3 days by aspirating

the old media and adding an appropriate volume of fresh warmed complete media, typically 10 ml when using a T75 flask. The seeding densities and volumes of media and trypsin-EDTA used for different culture vessels are shown in Table 2.2.

Table 2.2.: Cell culture seeding densities and volumes

Culture vessel	Number of cells (seeding range)	Volume of media	Volume of Trypsin-EDTA
75 cm^2 flask	5 x 10^5 – 1 x 10^6	10 ml	3 ml
25 cm^2 flask	3 x 10^5 – 5 x 10^5	5 ml	1 ml
100 mm dish	5 x 10^5 – 1 x 10^6	10 ml	2 ml
35 mm dish	1.5 x 10^5 – 3 x 10^5	3 ml	300 µl
6-well plate	5 x 10^4 – 2.5 x 10^5	2 ml	200 µl
96-well plate	8 x 10^3 – 1 x 10^4	100 µl	N/A
XFe Cell Culture 96-well Microplate	5 x 10^3 – 1.6 x 10^4	80 µl	N/A

N/A = not applicable

2.2.4 Cryopreservation and recovery of the cell stocks

Cell stocks were cryopreserved in liquid nitrogen at -196°C. In order to preserve cells by cryopreservation, cells were harvested by trypsin as previously described (section 2.2.3.). The cell suspension was then centrifuged at 300 × g for five minutes at 4°C. The supernatant was aspirated and cells were resuspended at a concentration of 1x10^6/ml of freezing media before being transferred to Nunc™ cryovials. The freezing medium was always freshly prepared by adding 10% DMSO dropwise to 90% FBS. To avoid prolonged exposure of cells to toxic concentrations of DMSO, handling of cells was performed rapidly during freezing and thawing of cells. The cryovials were placed in a pre-cooled Thermo Scientific™ Mr Frosty™ freezing container containing a sufficient amount of 100% isopropyl alcohol, which allows for a consistent cooling rate of approximately 1°C per minute. After cooling in a -80ºC freezer for 24-48 hours, the cryovials were transferred to the liquid nitrogen tank for long term storage.

To recover cells from stocks preserved in liquid nitrogen, cryovials were taken from a liquid nitrogen tank and thawed immediately at 37 °C in a water bath. Since DMSO is cytotoxic at concentrations above 0.5%, cells were resuspended in a T75 tissue culture flask with at least 25 ml of pre-warmed media which was sufficient to dilute the 0.1 ml of DMSO contained in each frozen stock to less than 0.5%. Once the cells had adhered

to the flask surface, typically the following day, the media was changed as previously described (section 2.2.3).

All cell lines used were authenticated using STR profiling and were regularly certified negative for mycoplasma contamination as detailed in appendix 6.1.1. and 6.1.2.

2.3. Metabolic profiling using microplate-based extracellular flux analysis

2.3.1. Principle of microplate-based extracellular flux analysis

Metabolic profiling assays were performed using extracellular flux (XF) analysis with the XFe96 instrument (Seahorse Bioscience), which is a high-throughput system that can perform accurate and reproducible measurements of the rate of change in dissolved oxygen, to demonstrate oxygen consumption rate (OCR), and pH, to demonstrate the extracellular acidification rate (ECAR), in the media surrounding cultured living cells using a unit of two sensors embedded in a disposable sensor cartridge. The sensor cartridge comprises 96 units, each of which has a plastic sleeve containing two embedded biosensors immersed in cell culture medium and four drug-delivery ports (Figure 2.1.). The embedded sensors are solid-state fluorescent optical and can detect precise changes resulting from cellular metabolism (297) in an isolated microchamber of media above cell monolayer in a 96-well tissue culture microplate over pre-set time cycles (Figure 2.2.). One of the biosensors is sensitive to oxygen concentration, and the other to proton content. During the assay, the fibre optics emit light that excites the embedded fluorophores and can read back the change in fluorophore emission due to the change in oxygen and protons (Figure 2.2.). Baseline readouts of OCR in pmol/min and ECAR in mpH/min are surrogate measurements of oxidative phosphorylation and glycolysis respectively. The four drug-delivery ports allow for the addition of inhibitors, stimulators, or substrates to the cell culture medium during a specifically designed stress test, which will be detailed further in sections 2.4.6. and 2.4.7.

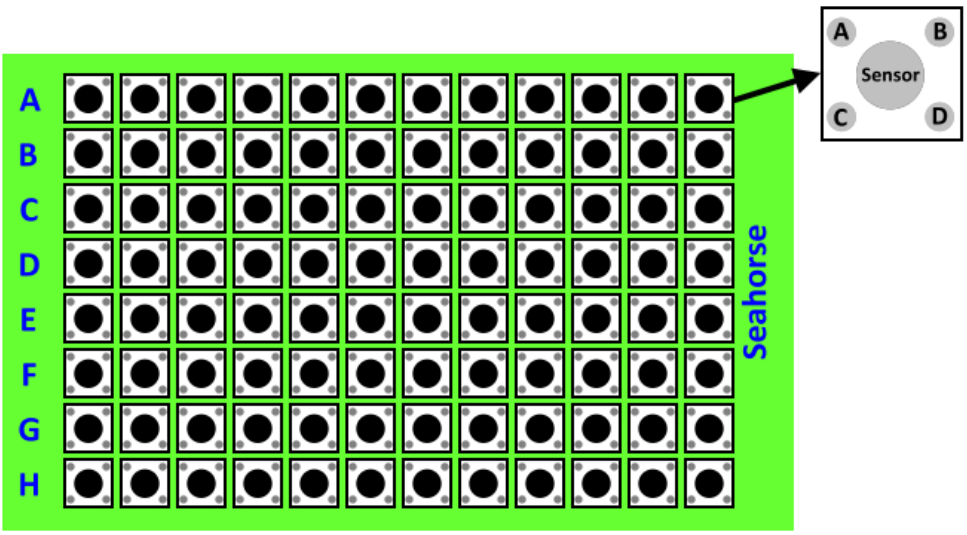

Figure 2.1.: Illustration of the Extracellular Flux Assay sensor cartridge. The XFe96 cartridge comprises 96 units of a central sensor and four injection ports. The ports A-D are loaded with stress test compounds. Sensor contains two optical fluorescent biosensors probes to detect changes in O_2 and H^+.

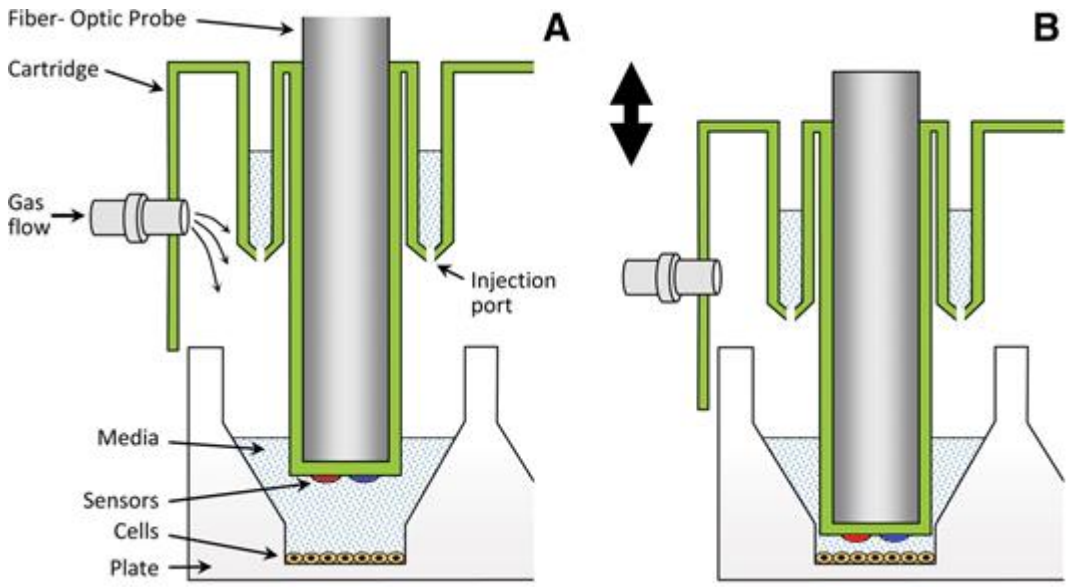

Figure 2.2.: A schematic of the XFe sensor cartridge unit. Two distinct polymer-embedded fluorophores sensitive to O_2 and H^+ (red and blue) are embedded within each sensor probe. The fibre optic bundles emit light that excites the fluorophores, and the emitted light is measured by a detector t within the XFe96 instrument. Lowering the cartridge from the upper (A) to the lower (B) position traps the cells in a small transient chamber that allows for accurate and reproducible measurements. The figure is reproduced from (298).

2.3.2. Media preparation

A DMEM-based medium was utilised for both mitochondrial and glycolytic stress tests (detailed in sections 2.3.6.1. and 2.3.6.2. respectively). This medium is formulated with 5 mM HEPES and is pre-adjusted to pH 7.4. In comparison to bicarbonate buffers, HEPES has a better ability to maintain physiological pH despite variations in carbon dioxide concentration caused by aerobic respiration. Using bicarbonate buffers could have a significant impact on cellular metabolism because bicarbonate acts as a nutrient, permits intracellular pH fluctuations (299) and alters kinase signalling (300). XFe media is glucose-, sodium bicarbonate-, sodium pyruvate- and glutamine-free, which allow for specific customisation of the assay medium. In addition, the omission of phenol red from this medium allows for accurate and precise measurement of absolute pH value by the XFe Analyser. For the glycolytic stress tests, media was supplemented with 2mM L-glutamine only, while for the mitochondrial stress tests 10mM of D-glucose and 2mM of sodium pyruvate were also added. Media was then adjusted to pH 7.4 and sterile filtered. These media will be referred to as "Seahorse glycolytic assay medium" and "Seahorse mitochondrial assay medium" throughout this study.

2.3.3. Hydration of the XFe96 sensor cartridge

To prepare the XFe96 sensor cartridge for any Seahorse assay, a hydration step should be performed 24 hours before the assay by adding 200uL of XF calibrant solution to each well in the XFe96 calibration microplate before placing the sensor cartridge into the microplate. Following this, the cartridge-calibration microplate was incubated overnight in a non-CO_2 incubator at 37°C.

2.3.4. Preparation of the XFe96 microplate

24 hours before the assay, the microplate wells were coated with collagen to assure better attachment and incubated at 37°C with 5% CO_2 for 30 minutes before removing the excess collagen and washing the wells twice with 100 ul of sterile PBS pH 7.4. cells. Cells were harvested using trypsin-EDTA, as described in section 2.2.3., and cellular concentrations were determined by means of three independent cell counts using a CellDrop™ automated cell counter (DeNovix Inc.). A cell suspension with a pre-determined cell density in DMEM media was prepared to give a total volume of 80ul per well. Cells were then seeded in each well of the XFe96 microplate, with the

exception of the background control wells. Plates were left to rest at room temperature in the tissue culture hood for 20 minutes to promote even cell distribution and reduce edge effects (301). Following this, cell adherence was checked using a light microscope, and the microplate was incubated overnight at 37°C with 5% CO_2 to allow for cell attachment.

Cell seeding titrations were used to determine the optimal cell seeding densities for each individual cell line. Visual assessment using light microscopy was used first with the aim of achieving evenly distributed cells at 50-90% confluence within each well to generate metabolic rates in the desirable/dynamic range of the instrument on the day of assay. Basal OCR and ECAR values were then obtained to evaluate several cell seeding densities to determine the optimal seeding density that achieves the target values of 20-160 pmol/min for OCR and 10-90 mpH/min for ECAR, as per the manufacturer's guidelines. Seeding densities used for each cell line are shown in Table 2.3.

Depending on the assay type, relevant compounds were prepared on the day of the assay and added to the injection ports in the pre-hydrated XF sensor cartridge (see sections 2.4.6. and 2.4.7.). This cartridge/calibration plate was then used to calibrate the XFe96 instrument.

Table 2.3.: Seeding densities used for each cell line in XF assays.

Cell Line	Number of Cells/Well
UM-SCC-1 (and derivative lines)	8,000
UM-SCC-5	10,000
UM-SCC-10A	10,000
UM-SCC-11A	16,000
UM-SCC-11B	8,000
UM-SCC-17A (and derivative lines)	9,000
UM-SCC-17As	11,000
UM-SCC-81B	9,000

Before running the assay, light microscopy was used to confirm cell attachment to the XFe96 microplate. The media was then aspirated and the cells were carefully washed with 100ul of pre-warmed relevant assay media to ensure all FBS-containing media

was removed. Subsequently, 175µl of relevant assay media was added per well and the integrity of the monolayer was re-checked. The plate was then left to equilibrate for one hour in the non-CO_2 incubator at 37°C before being loaded into the pre-calibrated XFe96 instrument. According to the manufacturer's instructions, the 1-hour incubation in a non-CO_2 atmosphere is necessary for de-gassing the plate and the cell culture of any residual CO_2 that may disrupt the assay.

2.3.5. Setting the XFe96 instrument

All assay designs, calibrating, mixing and measuring steps described in this thesis were set up and executed using the XFe96 analyser and Wave software (Seahorse Bioscience), and all subsequent data analysis was carried out using Wave software.

2.3.6. The principle of XFe stress tests

Cells generate energy in the form of ATP by a combination of two main metabolic pathways: oxidative phosphorylation and glycolysis. Glycolysis converts glucose to pyruvate, through a series of enzymatic reactions, which can then be reduced to lactate or oxidised to generate ATP through the tricarboxylic acid cycle (TCA cycle) and the mitochondrial electron transport chain (ETC). Amino acids and fatty acids can also be broken down to acetyl CoA, pyruvate, and other intermediates for ATP production. The various compounds used in XFe stress tests to examine the bioenergetic profile of cells are shown at their respective sites of action in Figure 2.3. The electron flow in the mitochondrial ETC is represented by block arrows, and will further be detailed in 2.3.6.1 and 2.3.6.2

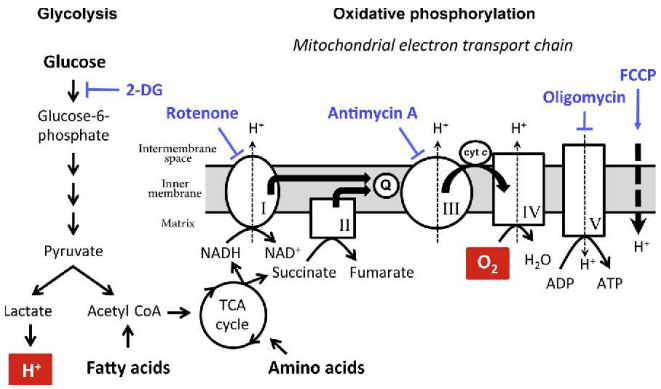

Figure 2.3.: A schematic of cellular bioenergetic pathways. Two main metabolic pathways are used by cells to generate energy in the form of ATP: glycolysis (left) and oxidative phosphorylation (right). XFe

stress tests use various compounds to interfere with energy generation pathways at their respective sites of action as described in detail in 2.4.6.1 and 2.4.6.2. The figure is reproduced from (302).

2.3.6.1. Mitochondrial stress test

The mitochondrial stress test allows for the assessment and quantification of mitochondrial bioenergetic activity through the sequential addition of compounds that affect oxidative phosphorylation function (303). Cells were sequentially treated with three mitochondrial stressor compounds in the following order: oligomycin, FCCP, and a combination of antimycin-A and rotenone. 8x, 9x and 10x stock concentrations respectively, of each of these compounds, were prepared in Seahorse mitochondrial assay media and added to injection ports A (oligomycin), B (FCCP), and C (antimycin-A/rotenone) in all the designated stress test wells. These starting concentrations achieve the desired working concentrations in the microplate wells upon injecting equal volumes of 25µl. The desired working concentrations of both rotenone and antimycin-A were 1µM, while careful titration was required to determine the working concentrations of oligomycin and FCCP because the effects of these compounds can vary between different cell types, and relatively minor differences in concentration can affect the final measurement (297,304). Data obtained during optimising the working concentration of oligomycin and FCCP is presented in section 3.2.1.

For this test, the instrument was programmed to perform three baseline OCR measurements before the first stressor, oligomycin, was delivered to each well and three measurement cycles were performed. Oligomycin inhibits ATP synthase (ETC complex V) and decreases OCR, which can be used to distinguish between the amount of oxygen consumed for ATP synthesis and the amount needed to overcome the natural proton leak across the inner membrane of mitochondria (297,304). This addition inhibits the generation of oxidative energy, thereby abolishing the oxygen consumption unrelated to proton leak (Figure 2.4.). In the third step of the test, FCCP was delivered to each well, followed by three more measurement cycles. FCCP is an ionophore that uncouples the mitochondria from the ETC by disrupting ATP synthesis through transporting hydrogen ions across the inner mitochondrial membrane instead of through the proton channel of ATP synthase, forcing the mitochondria to increase electron flow, and thus oxygen consumption, in order to maintain the membrane potential (297). This leads to dissipating mitochondrial membrane potential that produces a rapid and uncontrolled intake of energy and oxygen without the production

of ATP, resulting in a maximal increase in OCR that can be used to calculate the spare respiratory capacity of cells (297,304)(Figure 2.4.). In the final step of this test, rotenone and antimycin-A were added before three measurement cycles were performed. These compounds are ETC complex I and III inhibitors respectively, which completely shut down the mitochondrial respiration when used in combination, allowing for the detection of non-mitochondrial residual respiration, which needs to be subtracted from the previous measurements (297,304)(Figure 2.4.).

The raw data were normalised before being analysed using the Seahorse XF mito stress test generator (Agilent Technologies), and normalised OCR values were used to calculate the mitochondrial profile parameters based on equations shown in Table 2.4. Results presented are from 3 independent experiments, with 3-6 replicate wells for each condition.

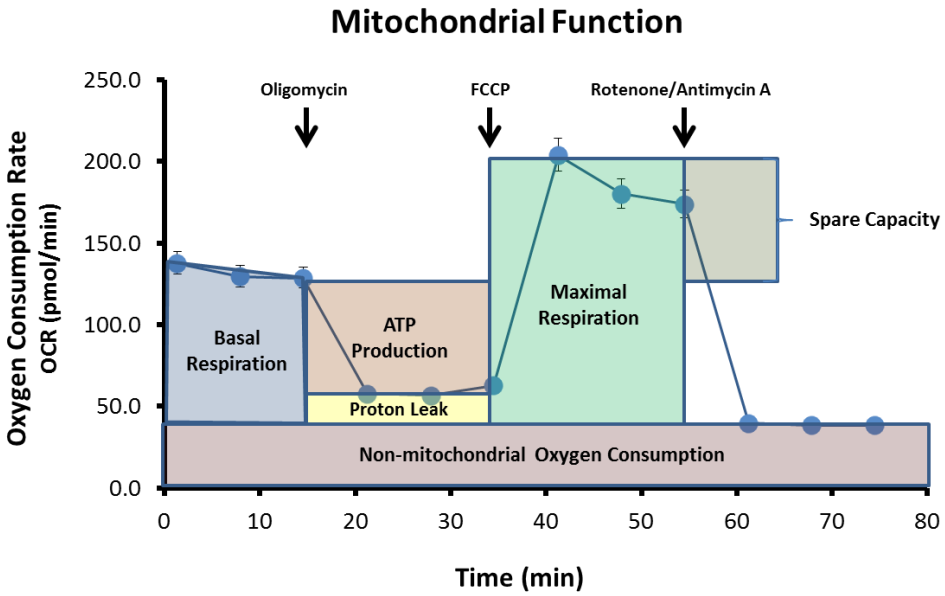

Figure 2.4.: A read-out of mitochondrial function from the mitochondrial stress test. An illustration of the sequential delivery of the three stressors (oligomycin, FCCP, and a mixture of antimycin A and rotenone) and the metabolic parameters calculated based on this test (basal respiration, ATP-related respiration, proton leak-related respiration, maximal respiration, spare respiratory capacity and non-mitochondrial respiration). The figure is reproduced from (305)

Table 2.4.: Equations used to calculate the mitochondrial function parameters

Parameter Value	Equation
Basal Respiration	(Last rate measurement before the first injection) - (Non-Mitochondrial Respiration Rate)
Maximal Respiration	(Maximal rate measurement after FCCP injection) – (Non-Mitochondrial Respiration)
Spare Respiratory Capacity	(Maximal Respiration) – (Basal Respiration)
ATP production	(Late rate measurement before Oligomycin injection) – (Minimum rate measurements after Oligomycin injection)

2.3.6.2 Glycolytic stress test

The glycolytic stress test involves the sequential delivery of three compounds that affect the glycolytic function to facilitate the derivation of key glycolytic parameters. These injected compounds are D-glucose, oligomycin, and 2-deoxy-D-glucose (2-DG)(297,304). 8x, 9x and 10x stock concentrations of each of these compounds, respectively, were first prepared in Seahorse glycolytic assay media, such that upon injection of 25µl, final working concentrations of 10mM D-glucose and 50mM 2-DG were achieved in all the designated stress test microplate wells, including the allocated control wells. As stated previously, the relevant data obtained during optimising the working concentration of oligomycin is presented in section 3.2.1.

This test was programmed to take three cycles of baseline measurements in a glucose-free medium before the delivery of a saturating concentration of glucose to each well and three cycles of measurements were taken. This enables the cells to rapidly utilise and catabolise glucose to pyruvate through the glycolytic pathway, which results in producing ATP, NADH, water and extrusion of protons into the surrounding medium causing an increase in ECAR. The glucose-induced response is detected as the rate of glycolysis under basal conditions (297,304)(Figure 2.5.). Oligomycin was delivered in the next step of the test and further three measurement cycles were taken. As detailed previously, oligomycin functions as an ATP synthase inhibitor in ETC that decreases mitochondrial ATP production causing a reduction in the ATP/ADP ratio, thus stimulating glycolysis and shifting the energy production towards a more glycolytic state to maintain energy requirements. This results in an increase in ECAR reflecting the cellular maximal glycolytic capacity (297,304)(Figure 2.5.). Finally, 2-DG was delivered to each well and three final measurement cycles were performed. 2-DG is a

stable glucose analogue that cannot undergo conversion to glucose-6-phosphate and thus competitively inhibits glycolysis through competitive binding to hexokinase, the first enzyme in the glycolytic pathway, resulting in a substantial decrease in ECAR (297,304). The decreased ECAR reflects the combined glycolytic acidification rate of basal and reserve glycolysis, while the post-2-DG residual ECAR is attributable to cellular processes other than glycolysis and is subtracted from previous measurements (Figure 2.5.).

The raw data were normalised before being analysed using the Seahorse XF glyco stress test generator, and normalised ECAR values were used to calculate the glycolytic profile parameters based on equations shown in Table 2.5. Results presented are from 3 independent experiments, with 3-6 replicate wells for each condition.

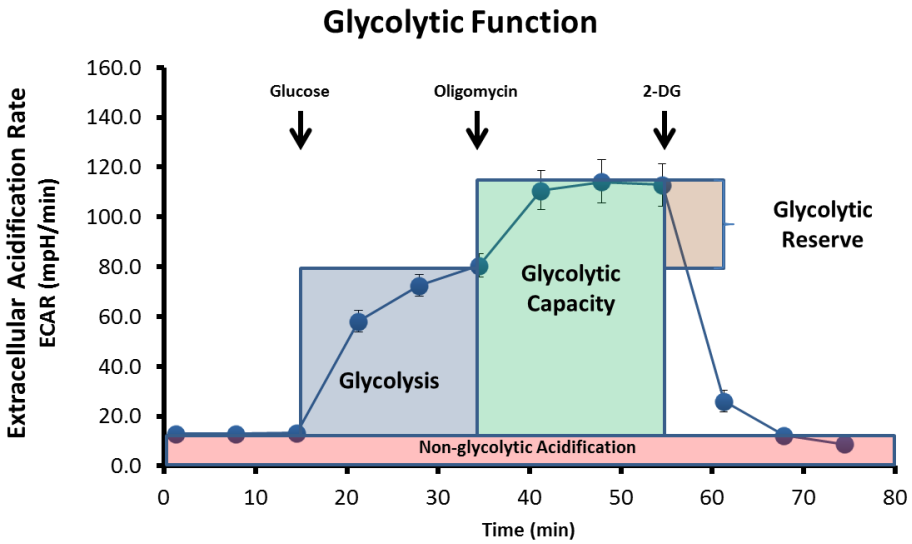

Figure 2.5.: A read-out of glycolytic function from the glycolytic stress test. An illustration of the sequential delivery of three compounds (glucose, oligomycin, and 2-DG) and the glycolytic parameters calculated based on this test (basal glycolysis, maximal glycolysis, spare glycolytic capacity, and non-glycolytic acidification). The underlying mechanisms are described in more detail in the text. The figure is reproduced from (305).

Table 2.5. Equations used to calculate the glycolytic function parameters

Parameter Value	Equation
Glycolysis	(Maximum rate measurement before oligomycin injection)-(Last rate measurement before glucose injection)
Glycolytic capacity	(Maximum rate measurement after oligomycin injection)-(Last rate measurement before glycose injection)
Glycolytic reserve	(Glycolytic capacity)-(Glycolysis)
Non-Glycolytic acidification	Last rate measurement prior to glycose injection

2.3.7. Post-treatment metabolic profiling

Cells were seeded at optimised densities shown in Table 2.3. in an XFe96 cell culture microplate with 80µl of complete growth medium and left to adhere for 6 hours. Cells were then treated with vehicle control (DMSO) or IC_{50} of 2-DG, 6-AN, 3PO, UK-5099, and DCA, as well as various combinations of these drugs for 24 hours, before Mito and Glyco stress tests were carried out.

2.3.8. Normalisation to cellular DNA content

To enable the comparison of metabolic measurements between cell lines, post-transfection or post-treatment, normalisation of the OCR and ECAR data was necessary. Consequently, following completion of all mitochondrial and glycolytic stress tests, the XFe microplate was removed from the instrument and the media removed from each of the wells, before the microplate was stored at -80°C for future normalisation.

At a later date, typically within one week, the cell culture plate was allowed to thaw for 20 minutes on ice then transferred to room temperature, fresh reagents were prepared as outlined later, and the DNA content in each of the microplate wells was determined to facilitate normalisation of data to DNA content. Measurement of total DNA content was performed using the CyQUANT® cell proliferation assay kit as per the manufacturer's instructions and experiments were carried out in Corning® 96-well black-bottom plates. Lysis buffer was prepared using 9.5ml of a solution containing 180mM NaCl in 1mM of EDTA and 0.5ml of stock cell lysis buffer from the CyQUANT® kit. Next, 28.6 µl of DNase-free RNase A was added to 9.971 ml of this lysis buffer, and 100µl of this final solution was then added to each well of the XFe96 microplates,

including the background wells. The microplates were then placed on an orbital shaker for one hour at room temperature to extract cellular DNA. Following the lysis step, the lysed cells and the content of the background wells were transferred to the pre-designated wells of the 96-well black-bottom plate. Subsequently, dye solution was prepared by diluting 50 µl of the CyQUANT® GR stock solution in a total volume of 10 ml of CyQUANT® kit lysis buffer diluted in nuclease-free distilled water before 100 µl were added to each well. Standard curve for DNA content was generated by preparing DNA standards using the stock DNA standard from the CyQUANT® kit diluted in lysis buffer without RNase A to the following concentrations: 0, 10, 50, 100, 200, 400, 600, 800, and 1000ng/ml in a total volume of 200 µl directly in the designated wells in the 96-well black-bottom plate. The plate was then left for two minutes prior to measurement using a Spark® multimode microplate reader, on which relative fluorescence units (RFU) were measured at excitation and emission wavelengths of 480nm and 520nm respectively. DNA concentrations were calculated as ng/ml using linear quantitation and the values obtained were then divided by five to be converted from ng/ml to ng of DNA by accounting for the final measured volume of 200µl.

2.4. siRNA transfection

RNA interference (RNAi) is a conserved cellular response to double-stranded RNA (dsRNA) and is the process by which dsRNA mediates the silencing of gene expression – via the induction of sequence-specific degradation of complementary mRNA, or through the inhibition of translation (306). siRNA-based RNAi has proved to be an effective gene-silencing tool that enables the silencing (albeit typically only partial) of a specific gene to be rapidly linked with a loss-of-function phenotype – thereby providing an effective means by which to validate critical components of a cellular pathway such as proliferation and metabolism (306).

Knockdown of p53 and TIGAR expression was performed by RNA interference using specific small interfering ribonucleic acid (siRNA) oligonucleotides. Each siRNA consists of 21 nucleotides designed to knockdown target gene expression. Non-targeting siRNA (siCONT), siRNA specific to p53, a smartpool of siRNAs specific to TIGAR, and four siRNA oligonucleotides targeting different regions of TIGAR were all obtained from Dharmacon (GE Healthcare, USA). The sequences of the siRNAs used are detailed in Table 2.6.

Table 2.6. Sequences of siRNAs used

siRNA	Sequence 5' to 3'
Non-targeting siRNA	GGACGCAUCCUUCUUAAUU
p53 siRNA	GGACAUACCAGCUUAGAUU
TIGAR siRNA #1	AAUCACAGCUCUAAAGUUA
TIGAR siRNA #2	GAUAUGACGGUAAAGUAUG
TIGAR siRNA #3	GAAAUACGGGGUUGUAGAA
TIGAR siRNA #4	GAGUCACGGUGCUUACAUG

24 hours before siRNA transfection, $8x10^5$ - $1x10^6$ cells were cultured in a complete DMEM medium in a 100mm dish and were incubated at 37°C and 5%CO_2. At 30-50% confluence, cells were transiently transfected in accordance with the manufacturer's protocol by introducing siRNA to cells using Lipofectamine 2000 transfection reagent (Invitrogen). Two separate tubes were used to prepare the transfection mixture, one containing 30uL of Lipofectamine 2000 diluted in 1.5 ml of OptiMEM, a serum-free medium. The second tube contained the desired volume of siRNA diluted in 1.5 ml of OptiMEM medium. The two tubes were separately incubated for 5 min at room temperature before being combined, gently mixed by pipetting up and down, and incubated for 20 min at room temperature. The complete media was replaced with 7 ml of antibiotic-free media and cells were transfected with siRNA by adding the 3 ml mixture dropwise to the dish for a final concentration of 25-75 nM siRNA.

To control for potential off-target effects of the siRNA treatment, a commercially available nontargeting control siRNA (siCONT) was taken as a negative control, and a validated siRNA specific to p53 was used as a positive control (Dharmacon - GE Healthcare, USA). Untransfected cells were incubated with 30uL of Lipofectamine 2000 diluted in 3ml of OptiMEM media (mock transfection). Six hours after transfection, media was replaced with complete media and cells were incubated for 24 hours before being seeded for various assays for further 24 hours. 48 hours after transfection, the knock-down efficiency was monitored by analysing protein expression using western blotting (as described in 2.9.).

2.4.1. Evaluation of TIGAR siRNAs

siGENOME SMART pool (Dharmacon), containing a mixture of four distinct siRNAs targeting TIGAR mRNA, was tested in UM-SCC-11A cell line for 24 and 48 hours to test the time required to achieve an efficient reduction of protein expression of TIGAR. In the next step, the four individual siRNAs were tested separately under identical conditions for 48 hours and it was decided to use only the two most efficient TIGAR siRNA oligonucleotides for further experiments. For optimisation of siRNA concentration, three different concentrations of the most efficient siRNA oligonucleotides were transfected into cells. For each cell line transfected, it was decided to perform all further experiments at the lowest concentration that achieved efficient inhibition of protein expression since no better results could be seen with a higher concentration. All data obtained from the optimisation of TIGAR siRNAs are shown in 3.2.2.1.

2.5. Plasmid transfection

Commercially available plasmids to express MDM2, Green fluorescent protein (GFP) and TIGAR proteins or to deliver an empty backbone were used in this study (as listed in 2.1.7.). A plasmid encoding Myc-DDK-tagged-Human TIGAR open reading frame (ORF) 5 (NCBI accession number NM_020375) was purchased from OriGene, USA. The plasmid was then isolated, purified and sequenced before being used in this study. Methods used for bacterial transformation, plasmid purification and transfection are described in the next sections. All plasmid maps are provided in Appendix 6.3.

2.5.1. Bacterial transformation

The process of introducing foreign DNA into a bacterial cell is known as transformation. Bacterial transformation with plasmids is an important means for storing and replicating plasmids, and nearly all plasmids carry both a bacterial origin of replication and an antibiotic resistance gene for use as a selectable marker in bacteria.

Chemically competent Escherichia coli cells (XL1-Blue competent cells) were transformed with Myc-DDK-tagged-Human TIGAR cDNA containing plasmid in accordance with the manufacturer's instructions.

Bacterial cells were removed from storage at -80°C, thawed on ice for approximately 20-30 mins. 20µl of cells was mixed with 0.34 µl of β-mercaptoethanol and incubated on ice for 10 minutes with a gently flicking every two minutes. β-mercaptoethanol degrades carbohydrates on the cell surface, allowing DNA to get closer to the membrane prior to heat shock. 5µl of DNA containing 0.5 µg of TIGAR DNA plasmid was added into the mix and this was then incubated on ice for 30 minutes, before being placed into a 42°C water bath for 45 seconds. The mixture was then incubated on ice for 2 minutes before being transferred to a 5ml round bottom high clarity Falcon tube. 180 µl of Super Optimal broth with Catabolite repression (SOC) media was added, and the mixture was left in a 37°C shaking incubator for 1 hour at 225 RPM to permit expression of the bacterial antibiotic resistance proteins encoded in the plasmid backbone. In the meantime, LB-Agar plates were prepared by mixing 15g of agar and 25g of LB broth in 1l of distilled water. The mixture was autoclaved for at least 30 min under 20 psi at a temperature of at least 121°C. Agar was cooled to 60°C, and 1 ml of 25 mg/ml of kanamycin was added and evenly distributed throughout the agar to make a final concentration of 25 ug/ml. Agar was poured in close proximity to a Bunsen flame in a total volume of 10-15 ml in a 90mm petri dish. Dishes were left to solidify for 30 minutes at room temperature. The bacterial mixture was removed from the shaking incubator and 50µl was plated on one agar dish and the rest on a second dish. Dishes were incubated at 37°C overnight. The next day, autoclaved Luria-Bertani (LB) broth (25 g/L) was supplemented with a final dilution of 25 µg/ml kanamycin at 60°C next to the flame before a single colony from a freshly streaked agar dish was picked and inoculated using a sterile plastic inoculating loop. The mixture was loosely capped and incubated at 37°C for 18 hours in a shaking incubator at 160 RPM. Bacterial growth, which is characterized by a turbid haze in the media, was monitored visually, and a bacterial glycerol stock was made for long-term storage of transformed bacteria at −80°C by mixing the bacterial culture with an equal volume of 50% (v/v) sterile glycerol.

2.5.2. Plasmid DNA purification

TIGAR plasmid DNA was extracted and purified from E. coli cultures using a QIAprep Spin Miniprep Kit and quantified using NanoDrop™ One/One^{C} Microvolume UV-Vis Spectrophotometer according to the manufacturer's instructions.

Six ml of the bacterial overnight culture in LB broth was centrifuged at 4,500 RPM (Thermo Scientific 400R refrigerated centrifuge), 4°C for 15 minutes to pellet the bacteria. Pellets were resuspended in 250 µl of the resuspension buffer PI (50mM Tris-Cl, 10 mM EDTA, 100µg/ml RNase A, pH 8.0) and transferred to a 2 ml microcentrifuge tube. 250 µl of alkaline lysis buffer P2 (1% SDS (w/v), 200mM NaOH) was then added and mixed thoroughly for no more than 5 minutes. 350µl of neutralization buffer N3 (3.0 M potassium acetate, pH 5.0) was added and mixed immediately and thoroughly, then the mixture was centrifuged at 13,000 RPM (Eppendorf 5424R refrigerated microcentrifuge), 4°C for 10 minutes. 800µL of the supernatant was applied to the QIAprep 2.0 spin column and centrifuged for 1 minute. The flow-through was discarded and the column was washed firstly with 0.5 ml of buffer PB which include a low concentration of chaotropic salts to remove residual proteins and pigments, then with 0.75 ml of buffer PE, an ethanol wash to remove the salts. The flow-through was discarded from each of the two washing steps and the residual wash buffer was removed by further centrifugation at 13,000 RPM (Eppendorf 5424R refrigerated microcentrifuge) for 1 minute. The column was placed in a clean 1.5 ml microcentrifuge tube and 50 µl of the elution buffer EB (5 mM Tris/HCl, pH 8.5) was applied to the centre of the column to release the desired DNA from the column. The column was let stand for 1 minute before being centrifuged for 1 min. The purified plasmid was quantified and the purity monitored using a NanoDrop spectrophotometer at 260/280 nm wavelengths.

2.5.3. Preparing samples for sequencing

Sanger sequencing of TIGAR plasmid used in this study was performed as a service by Source BioScience lab (Nottingham, UK). Samples were prepared in our lab as follow: TIGAR plasmid was diluted with the elution buffer (EB) to a final concentration of 1µg/µl. The VP1.5 (forward, with sequence 5' GGACTTTCCAAAATGTCG 3') and XL39 (reverse, with sequence 5' ATTAGGACAAGGCTGGTGGG 3') vector sequencing primers were spun down at high speed for 10 seconds and suspended using 10µl of TE buffer (10 mM Tris, 0.1 mM EDTA, pH 8.0) to a final concentration of 10 pmol/µL. Primers were stored at 4°C overnight. Next day, primers were diluted in TE buffer to a final concentration of 3.2 pmol/µL and 6µl was used in sequencing. Sanger sequencing of TIGAR plasmid used in this study is provided in Appendix 6.4.

2.5.4. Transient transfection

The transient transfection technique was used to transfect cells with plasmid expression vectors. Plasmid vectors delivered in this manner are gradually lost and/or diluted out of the cell after a few divisions. 24 hours before plasmid transfection, $8x10^5$ - $1x10^6$ of cells were cultured in a complete DMEM medium in a 100 mm dish and cells were incubated at 37°C and 5%CO_2 until approximately 60% confluent. Cells were then transiently transfected using Lipofectamine 2000 transfection reagent in accordance with the manufacturer's protocol. Two separate tubes were used to prepare the transfection mixture, one containing 20uL of Lipofectamine 2000 diluted in 1.5 ml of pre-warmed OptiMEM. The second tube contained 1-5 µg of plasmid (TIGAR, MDM2 or empty vector) and 0.3-0.5µg of pEGFP-N3 plasmid diluted in 1.5 ml of pre-warmed OptiMEM medium. The two tubes were separately incubated for 5 min at room temperature before being combined, gently mixed by pipetting up and down, and incubated for 20 min at room temperature. The complete media was replaced with 7 ml of antibiotic-free media and cells were transfected with plasmids by adding the 3ml mixture dropwise to the dish for a final optimised concentration of 0.1-0.5µg/ml plasmid. To monitor the efficiency of plasmid transfection, a pCMVneobam MDM-2 plasmid previously used and published in our lab was taken as a positive control for the methodology, and pCMV6-AC mammalian expression vector was used as an empty vector control. Untransfected cells served as blank control and were incubated with 20uL of Lipofectamine 2000 diluted in 3ml of OptiMEM media (mock transfection). Six hours after transfection, media was replaced with 10 ml of complete media and cells were incubated for 24 hours at 37°C and 5% CO_2 before were seeded for various assays for further 24 hours. 48 hours after transfection, transfection efficiency was measured by fluorescence microscopy, to detect expression of EGFP expressed from the pEGFP-N3 plasmid using an Evos FL Cell Imaging System (AMG, USA). 48 hours after transfection, transfection efficiency was measured by fluorescence microscopy, to detect expression of EGFP expressed from the pEGFP-N3 plasmid using an Evos FL Cell Imaging System (AMG, USA). Images were taken by brightfield and fluorescence microscopy and were used to semi-quantify fluorescence intensities in 3 fields per condition using ImageJ software. Protein expression was monitored by western blotting.

2.6. MTT proliferation assay

The growth inhibitory effects of the inhibitors and candidate drugs used in this study were evaluated using an MTT (3- [4,5-dimethylthiazol-2- yl]-2,5-diphenyltetrazolium bromide) cell viability assay. The MTT assay is a rapid colorimetric assay that relies on mitochondrial function as a surrogate indicator of mitochondrial-dependent cell viability. The viable cells contain the mitochondrial NAD(P)H-dependent oxidoreductases and dehydrogenases which are capable of cleaving the tetrazolium ring in MTT, reducing yellow MTT into a purple formazan precipitate. Active mitochondria are required for this process, and even newly dead cells do not cleave large amounts of MTT (307). The purple formazan crystals formed can be dissolved with DMSO, and absorbance at 570nm with a reference filter of 620nm can be used as a surrogate indicator of the viability of cells treated with MTT.

To study cell viability using the MTT assay, cells were grown to 80-90% confluence in T75 cell culture flasks and then harvested using trypsin-EDTA as described in section 2.2.3. Cell concentrations were then determined using the mean from three independent cell counts from a CellDrop™ automated cell counter (DeNovix Inc.). $8x10^3$ cells were then seeded in 96 well plates CytoOne (Starlab, UK) using a multichannel pipette with a total volume of 100µl added to each well and incubated overnight at 37°C with 5% CO_2 to allow for cell attachment. The following day, media from each well was carefully aspirated and replaced with desired concentrations of drugs in a total volume of 100µl of media. An equal concentration of DMSO in DMEM media was added to negative control wells, and wells containing DMSO in DMEM media with no cells were used as a blank. After the treatment time course, 20µl of 5 mg/ml MTT stock (diluted in PBS [pH 7.4], 0.2µm filtered and stored protected from light at -20 °C) to give a final concentration of 1mg/ml, was added to each well using a multichannel pipette and the 96-well plate was incubated at 37 °C with 5% CO_2 for four hours. Following incubation, all of the liquid was carefully aspirated from each well and 100µl of DMSO and 12µl of Sorensen's glycine buffer (0.1 M glycine, 0.1 M NaCl adjusted to, pH 10.5, with 1 M NaOH) were added to dissolve the purple formazan precipitate and to adjust the pH-dependent absorption spectrum (308), respectively. The plate was sealed and agitated on an orbital plate shaker at room temperature for 15 minutes. Optical absorbance measurements at 570nm and 630nm were taken using a SpectraMax Plus 384 Microplate Reader (Molecular Devices, USA). The absorbance values corresponded to the number of viable and metabolically active cells. Readings of negative control

(DMSO-only-treated cells) and untreated cells were compared first to assure the minimal cytotoxic effect of DMSO (with no more than 0.5% inhibition). Blank readings were subtracted from all readings to determine the final absorbance of the cells, and the percentage cell viability was calculated as percentage growth relative to cell viability of DMSO-only-treated control wells, as follows:

$$\textbf{Cell viability\%} = \frac{(\mathbf{OD1}^{570nm} - \mathbf{OD1}^{630nm}) - (\mathbf{OD2}^{570nm} - \mathbf{OD2}^{630nm})}{(\mathbf{OD3}^{570nm} - \mathbf{OD3}^{630nm}) - (\mathbf{OD2}^{570nm} - \mathbf{OD2}^{630nm})} x100$$

As OD1, OD2, OD3 represent the optical density readings of treated cells, blank and DMSO-only-treated cells wells, respectively.

2.6.1. IC_{50} determination

$5x10^3$ cells were seeded in 96 well plates CytoOne (Starlab, UK) using a multichannel pipette (Gilson, USA) with a total volume of 100µl added to each well and incubated overnight at 37°C with 5% CO_2 to allow for cell attachment. After 24h, cells were exposed to different concentrations of candidate drugs in triplicate wells. At the end of each exposure time (24, 48h and 72 hours), an MTT assay was performed as described above. The IC_{50} value, which represents the drug concentration that reduced the absorbance observed by 50% of the value observed in control cells, was calculated with a nonlinear regression method using Hill's variable slope (four parameters) dose-response log fit in Prism 9 software (GraphPad, USA). Each experiment was performed in triplicate for each treatment condition, and at least three independent experiments were conducted. The IC_{50} concentrations of the candidate drugs were then used in subsequent experiments.

2.7. Clonogenic survival assay

A clonogenic assay was utilised to assess the radiosensitivity effect on colony formation following exposure to certain drugs and controls. In this assay, a colony is defined as a collection of ≥50 cells, which represents more than five cell divisions (309).

Cells were harvested, counted, seeded into 3.5 cm dishes, and incubated overnight at 37°C with 5% CO_2 to allow for cell attachment overnight. At 30-50 % confluence, cells were transfected with TIGAR siRNA or non-targeting siRNA (siCONT) for 48 hours (as described in 2.4.). After 48 hours, cells were treated with either DMSO (as a vehicle only

control) or the IC_{50} of 2-DG; 6-AN; 3PO; UK-5099 and DCA for one hour. Cells were then were exposed to low-LET X rays (100 kV) at doses of 0Gy (untreated), 2Gy, 4Gy, or 6Gy at room temperature using a CellRad x-ray irradiator (Faxitron®, USA) pre-set to produce 3 Gy per minute. Subsequent to irradiation, cells were washed in 1 ml PBS, before being harvested by adding 200 µl of trypsin-EDTA. 800 µl of media was added to neutralise trypsin, and cell suspension concentrations were determined as described previously. Cells were seeded in 2 ml of complete media at two different cell densities in triplicate for each treatment condition in 6-well plates, as shown in Table 2.7. Plates were then incubated at 37°C, 5% CO_2 for 15 days to enable colony visualisation. Three independent experiments were conducted. Following 15 days of incubation, media was aspirated from all 6-well plates and each well was washed with 2 ml of cold PBS before applying colonies were fixed and stained using a 2ml of 0.5 % w/v crystal (methyl) violet in 6 % v/v glutaraldehyde in H_2O for one hour at room temperature. Subsequently, the crystal violet/glutaraldehyde solution was removed, and plates were washed by immersion in cold H_2O. After air drying overnight, colonies were counted and colony images were obtained using GelCount™ colony analyser (Oxford Optronix, UK) and the optimised counting settings (309).

Table 2.7. Clonogenic assay seeding densities for each IR dose.

IR (Gy) dose	0 Gy	2 Gy	4 Gy	6 Gy
Seeding densities	500	1000	2000	4000
	1000	2000	4000	8000

The plating efficiency (PE) was calculated from non-treated conditions as fellow:

$$PE=\frac{\text{number of colonies}}{\text{number of cells seeded}}$$

Plating efficiencies of control groups (0 Gy) of all treatment conditions are shown in Table 2.8.

The surviving fraction (SF) was calculated for each treatment condition based on the number of colonies formed after treatment and the plating efficiency, as follow:

$$SF=\frac{\text{number of colonies}}{\text{number of cells seeded x PE}}$$

Survival parameters to generate treatment-dose survival curves for treatment conditions were then derived from fitting the data using the linear-quadratic-model (LQ-Model) and were calculated in the formula Y = exp (-1*(A*X + B*X^2)), where Y is survival following a given dose of IR (X), A represents the linear parameter and B represents the quadratic parameter, using Prism 9 (GraphPad, USA).

Table 2.8. Plating efficiencies of control groups (0 Gy) of all treatment conditions (%)

		DMSO		2-DG		6-AN	
		PE%	SEM	PE%	SEM	PE%	SEM
UM-SCC-1 pBABE	siCONT	7.7	0.3	3.7	0.5	3.0	0.5
	TIGAR siRNA	14.2	0.1	3.3	0.4	14.8	0.6
UM-SCC-1 WT-p53	siCONT	10.0	0.5	8.9	1.9	8.4	0.9
	TIGAR KD	9.1	0.4	7.2	2.8	7.7	1.8
UM-SCC-1 R175H-p53	siCONT	10.8	1.6	3.5	0.2	9.3	0.7
	TIGAR KD	30.1	1.6	12.2	1.6	7.3	1.2

		3-PO		UK-5099		DCA	
		PE%	SEM	PE%	SEM	PE%	SEM
UM-SCC-1 pBABE	siCONT	1.1	0.3	4.0	0.5	2.4	1.1
	TIGAR siRNA	2.7	0.3	8.8	0.9	8.4	1.1
UM-SCC-1 WT-p53	siCONT	8.6	1.4	8.7	2.5	8.3	0.4
	TIGAR KD	7.4	0.9	7.4	0.4	7.9	2.6
UM-SCC-1 R175H-p53	siCONT	3.2	1.4	7.6	3.0	11.9	0.8
	TIGAR KD	9.5	1.6	18.3	1.3	16.7	1.3

2.8. Western blotting

2.8.1. General principle of western blotting

Western blotting, also known as immuno-blotting, is a technique, which is used for the detection of specific proteins in a studied sample. Proteins are first separated by size using SDS-PAGE gel electrophoresis and then immobilised by transfer to a membrane, which is probed with antibodies raised specifically to the proteins of interest.

2.8.2. Protein quantification

Protein was quantified using the Bradford Assay. Cells were harvested by trypsinisation or by scraping as specified and pelleted by centrifugation at 300 x g for five minutes at 4°C as described previously. The pellets were washed with 1ml of PBS, transferred to Eppendorf® 1.5ml microcentrifuge tubes, and the cells were again pelleted by centrifugation and the supernatant aspirated as before. The pellets were then frozen at -80°C prior to further processing. On the day of sample processing, cell pellets were thawed on ice and lysed by resuspension in an appropriate volume of SLIP buffer supplemented with the following protease inhibitors (hereafter referred to as lysis buffer): aprotinin (2µg/ml), leupeptin (0.5µg/ml), pepstatin A (1µg/ml) and phenylmethylsulphonyl fluoride (PMSF) (1mM in 100% ethanol). Samples were then incubated on ice for 10 minutes, centrifuged for 10 minutes at 16,000 RPM (Eppendorf 5424R refrigerated microcentrifuge) at 4°C, before the supernatant was transferred to a clean microcentrifuge tube. In the interim, protein standards were prepared for the Bradford assay. Firstly, a solution of 20mg/ml BSA in lysis buffer was prepared and a serial dilution was performed to produce six further standards of the BSA concentrations: 10, 5, 2.5, 1.25, 0.625, and 0.3125mg while lysis buffer only was used as a blank. 2µl of each of the standards or the blank was then added to 1ml of protein assay dye reagent diluted 1:5 with H_2O and vortexed for 10 seconds. 2µl of each of the protein samples was added to 1ml of protein assay dye reagent in pre-chilled microcentrifuge tubes. A standard curve was prepared on a BioPhotometer using the standard serial dilutions and the Bradford program which was pre-set measures absorbance at 595nm. A coefficient of variability value (CV value) of less than 5% was deemed an acceptable level of calibration. Following the generation of the standard curve, the protein concentrations were determined based on the prepared standard curve using the BioPhotometer. Samples were then diluted in adjusted volumes of 1X, 2X and 4X sample buffers to make 50µg of total protein to a total volume of 20µl. These samples were then frozen at -80°C prior to gel electrophoresis.

2.8.3. Sodium dodecyl sulphate-polyacrylamide gel electrophoresis (SDS-PAGE)

Sodium dodecyl sulphate–polyacrylamide gel electrophoresis was used to separate proteins based on their apparent relative size. The percentage of acrylamide used in the separating gel was 10% chosen based on the size of proteins to be resolved. All gels and buffers were prepared freshly immediately before use. In a part of this study, the

separating and stacking gels were prepared as detailed in Table 2.9. while 10% Mini-PROTEAN® TGX™ Precast Protein Gels of 10 or 15 wells (Bio-Rad, USA) were used in other experiments. To prepare gels, glass slides for making 0.75mm thick gels were assembled, the separating gel poured into the gap, overlaid with H_2O, and allowed to polymerise. Once the gel had set the water was poured off and the stacking gel was poured, a 10-well plastic comb was inserted, and the gel was left to polymerise.

Following polymerisation, the comb was removed and the gels, with the assembled glass slides, were placed in an electrophoresis tank filled with tris-glycine electrophoresis running buffer specified in 2.1.8. The previously prepared protein samples were retrieved from the -80°C freezer and were denatured by heating in a heat block at 95°C for five minutes, then vortexed, before 20µl of each sample was loaded into the designated wells, alongside a Precision Plus Protein™ All Blue Prestained or Kaleidoscope™ Prestained Protein Standards ladder (Bio-Rad, USA). SDS-PAGE was performed using a Mini-PROTEAN® Tetra Vertical Electrophoresis Cell (Bio-Rad, USA) run at 150V for one hour.

Table 2.9.: **Composition of SDS-PAGE gels** (to make a total volume of 10ml).

Reagent	Separating Gel 10%	Stacking Gel
H_2O	4.8ml	7.225ml
40% acrylamide mix Acrylamide Bis-acrylamide, 37.5:1	2.5ml	1.275ml
1.5M Tris (pH 8.8)	2.5ml	-
1M Tris (pH 6.8)	-	1.25ml
10% (w/v) SDS	100µl	100µl
10% (w/v) APS	100µl	100µl
TEMED	8µl	10µl

2.8.4. Protein detection

Following SDS-PAGE, proteins were transferred onto an Immun-Blot® PVDF Membrane (Bio-Rad) using a Trans-Blot Turbo Transfer System (Bio-Rad). Firstly, two packs-of-six pre-cut absorbent filter papers were pre-soaked in transfer buffer specified in 2.1.8., while PVDF membrane was activated in methanol 100% for a few minutes. Next, the gel electrophoresis apparatus was dismantled, and the gel was removed from between the glass slides. The stacking gel was discarded, and the PVDF membrane was equilibrated in transfer buffer for two minutes. The PVDF membrane

was placed on the top of a pack of filter papers, and the separating gel was then placed on the top of the PVDF membrane. Another pack of filter paper was placed on the top of the gel to complete the assembly. This was then placed in a transfer cassette, which was then placed in the Trans-Blot Turbo Transfer System. The system was designed to enable the negatively charged proteins on the gel to run in the direction of the PVDF membrane. The transfer was performed at 25 V for 13 minutes.

Subsequently, the transfer apparatus was dismantled, and the membrane was stained briefly with Ponceau S to ensure the transfer of proteins was successful. Figure 2.6. shows a representation of a PVDF membrane stained with Ponceau S and the bands of the two protein ladders used in this study. The membrane was washed three times using PBS-Tween 0.1% for 5 minutes to remove the Ponceau S stain before being cut horizontally, with the help of protein ladders bands, into strips based on the size of proteins of interest. To block non-specific antibody binding, the membrane was blocked either in 5% (w/v) non-fat dry milk (Bio-Rad) in PBS/Tween solution for one hour or in EveryBlot Blocking Buffer (Bio-Rad) for 10 minutes, at room temperature.

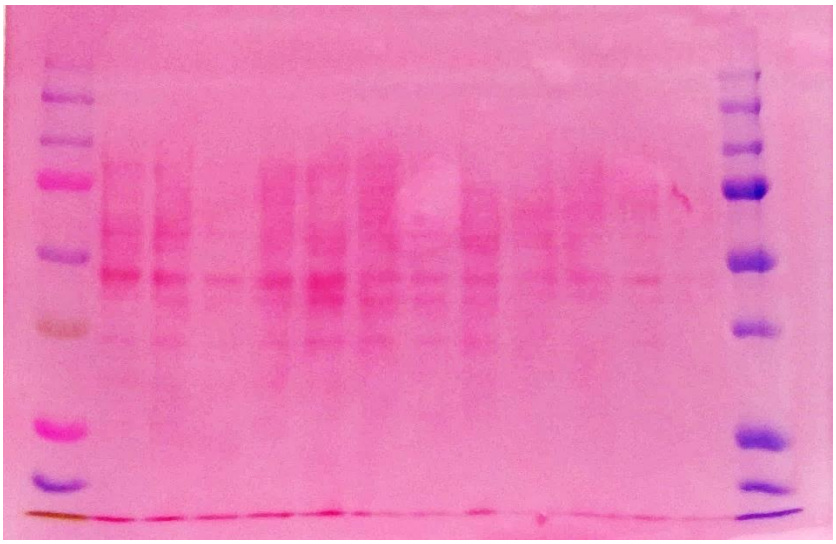

Figure 2.6. A representation of a PVDF membrane stained with Ponceau S. Visualising the protein bands by staining the membrane with Ponceau S to ensure the transfer of proteins was successful. The bands on the left and the right are of the two protein ladders used in this study: Kaleidoscope™ (left) and All Blue (right) Prestained Protein Standards ladders (Bio-Rad, USA).

For western blotting, the blocking buffer was removed, and each protein was probed separately by incubating the appropriate membrane strip with the corresponding primary antibodies diluted in blocking buffer (section 2.1.4.) overnight at 4°C on a 3D gyratory shaker. The membranes were then washed three times with PBS/Tween 0.1%

for 15 minutes, after which horseradish peroxidase (HRP)-conjugated secondary antibodies diluted in blocking buffer (section 2.1.4.) raised to the relevant primary antibody species were applied and the membranes incubated for a further hour at room temperature. Next, the membranes were washed three times as previously, before being transferred into dry trays. A 1:1 mix of the two substrates of the luminol-based signal enhancer Clarity Western ECL (Bio-Rad) was then applied (typically 2ml per membrane) for five minutes, and the signal was detected by chemiluminescence and imaged using ChemiDoc™ Touch Imaging System (Bio-Rad).

2.8.5. Densitometry

To determine the intensity of signals from western blotting, signal intensity was estimated by performing densitometry using Image Lab software (Bio-Rad), and images were analysed to determine the protein expression. The signal intensity for each sample was calculated by subtracting the sum intensity of only the total background from the sum intensity of each sample (Figure 2.7.). Normalised data to the corresponding loading control protein signals of the appropriate samples are shown for each protein expression experiment in this study.

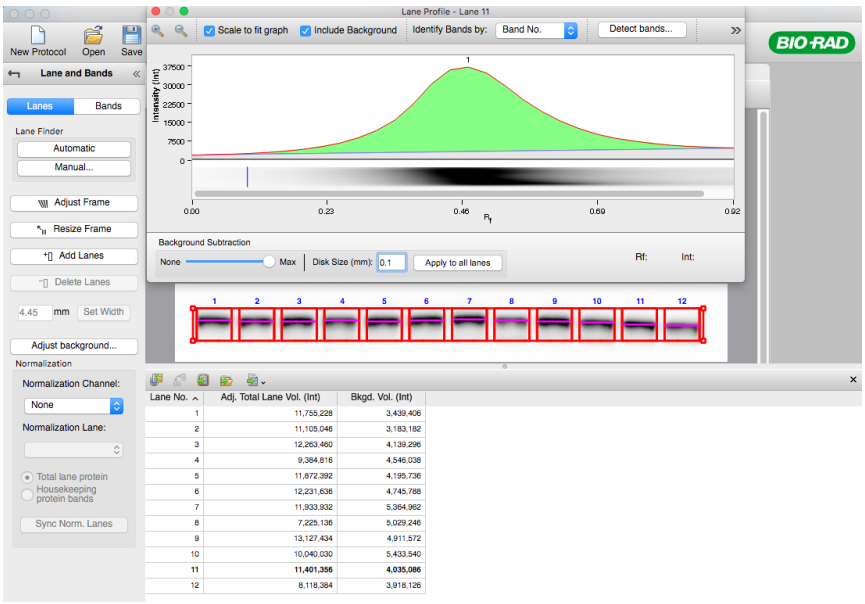

Figure 2.7. Analysis of luminol-based signal intensity using Image Lab software (Bio-Rad). Lanes were manually or automatically selected, bands were detected, the signal background was adjusted and subtracted from the total signal intensity, and the total volume of each band was automatically calculated.

3. Results

3.1. Investigating the metabolic phenotype in SCCHN

3.1.1. Introduction

As discussed in section 1.3, although metabolic alterations are today a hallmark of cancer and have recently begun to receive increased attention, metabolic profiling and primary studies of metabolic alterations have not received much attention in SCCHN. In addition, detailed studies of the role of p53-mediated metabolic regulation in SCCHN and the genes involved have been very limited. As stated in 1.4.3., the role that TIGAR plays in the regulation of glycolysis, as one of the p53-regulated genes, has gained importance in cancer studies recently, however, only a handful of studies have investigated this role in SCCHN (213,310,311). Furthermore, only a few studies have examined the role that glycolytic pathway inhibitors may play in improving the therapeutic response in SCCHN. Indeed, some of these studies have produced conflicting results and did not provide a clear picture of the metabolic profile in SCCHN and the role that p53 plays in SCCHN metabolic regulation (241–243).

Given the importance of metabolic alterations as a hallmark of cancer, and the variations in metabolic profiles between different types of cancers, the aim of this section is to explore the metabolic phenotype in SCCHN. This was achieved through the use of Seahorse high-sensitivity microplate-based extracellular flux (XFe96) metabolic assays that allow for reliable and repeatable quantitative metabolic analysis as well as providing real-time metabolic phenotype information. By measuring the OCR and ECAR at basal levels and following sequential injection of substrates and inhibitors used in mitochondrial and glycolytic stress tests, as detailed in sections 2.3.6.1. and 2.3.6.2., the following parameters can be calculated: basal respiration, maximal respiration, spare respiratory capacity, ATP production, glycolysis, glycolytic capacity, glycolytic reserve and non-glycolytic acidification.

3.1.2. Optimising the concentration of compounds for injection during XFe96 metabolic assays

Before conducting Seahorse XFe assays, it was essential to optimise the measurement conditions for the analysis of SCCHN cell lines used in this study. To begin, as previously

stated in section 2.4.5., cell seeding titrations were performed for each of the cell lines to determine the optimal seeding densities. The aim was to achieve evenly distributed cells at 50-90% confluence in each well on the day of the assay, and to obtain basal OCR and ECAR values of 20-160 pmol/min and 10-90 mpH/min respectively, as per the manufacturer's guidelines. The cell seeding densities that resulted were previously summarised in Table 2.3.

The concentrations of oligomycin and FCCP were then titrated as the following step in the optimisation process. This is because the effects of these compounds can vary between different cell types, and even minor variations in concentration can significantly affect the final results (297,304). Optimisation assays were performed using the mitochondrial stress assay described in 2.3.6.1. For oligomycin, OCR measurements were taken at baseline (at the measurement point 3) and following the addition of oligomycin at the following concentrations: 0.5, 0.75, 1 and 1.25 µM (at the measurement point 4). These concentrations were chosen based on the manufacturer's recommendations and were also consistent with concentrations that used in studies using other SCHNN cell lines (246,312). The resulting OCR responses in three SCCHN cell lines selected depending on their p53 status are shown in Figure 3.1. Given that 1µM was the lowest concentration to consistently induce a maximal decline in OCR, together with the fact that dose-dependent responses appeared to be substantially conserved among SCCHN cell lines, this concentration of oligomycin was selected for use in all subsequent XF assays.

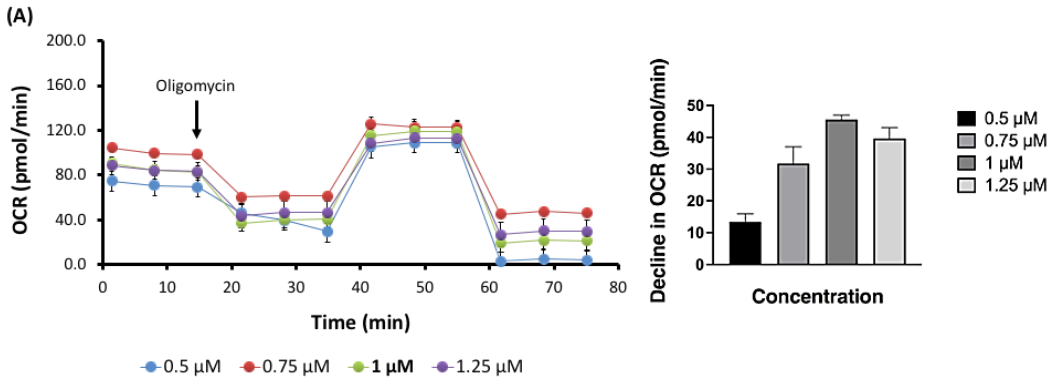

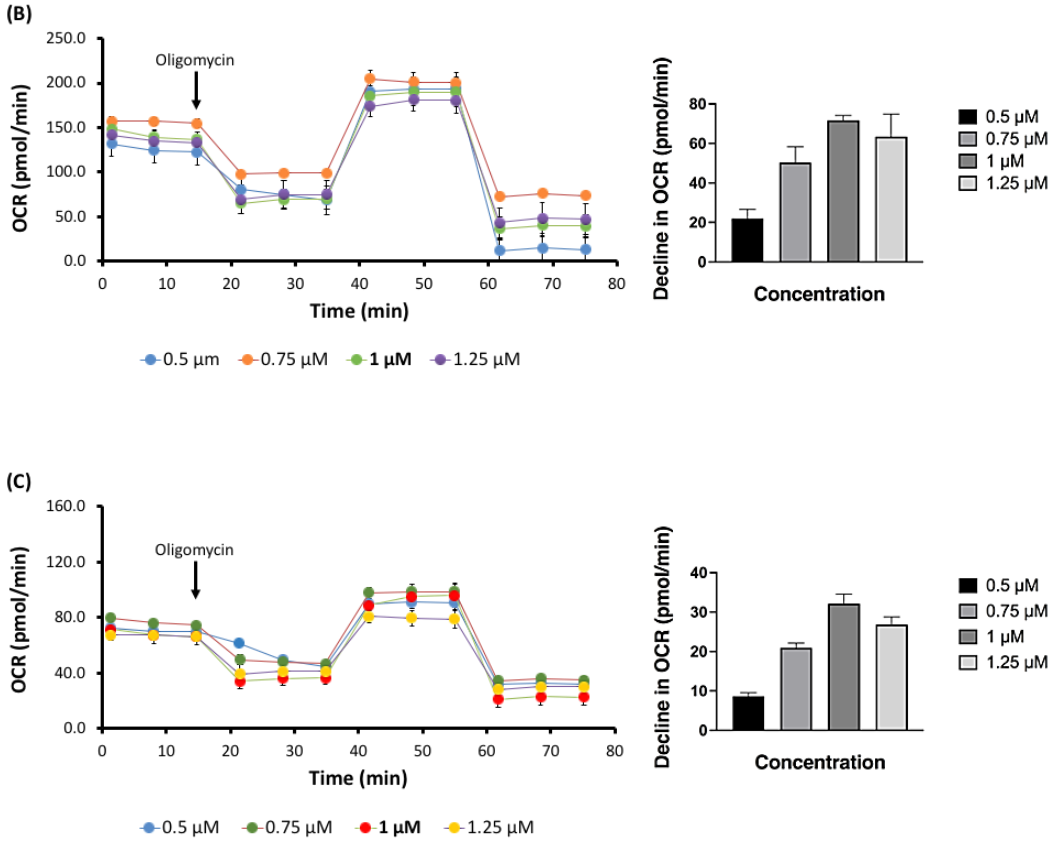

Figure 3.1. Titration of oligomycin for XFe metabolic profiling assays. Left: Measurement of OCR following administration of 0.5, 0.75, 1 and 1.25µM oligomycin (at the indicated time point on each graph) in three selected SCCHN cell lines depicted separately: (A) UMSCC-1 pBABE (p53-null cell line), (B) UMSCC-17A (wild type p53 cell line) and (C) UMSCC-11B (mutant p53). Right: a representation of decline in OCR following the administration of the indicated concentration of oligomycin in each cell line. 1µM was the lowest concentration to consistently induce a maximal decline in OCR, and thus was used in the subsequent experiments. Titration was performed in hextuplets. Data are shown as the mean of decline in OCR (pmol/min) from three experiments (n=3) ± SEM.

Following oligomycin titration, optimisation assays for FCCP concentrations were performed. OCR was measured at baseline (at the measurement point 3) and following the addition of FCCP at the following concentrations: 0.125, 0.25, 0.5, 0.75, 1.0 and 2µM (at the measurement point 4). These concentrations were selected on the basis of the manufacturer's guidelines and published studies (246,312). The resulting OCR measurements in three SCCHN cell lines, selected based on their p53 status, are shown in Figure 3.2. Given that 0.5µM was the lowest concentration to consistently induce a maximal increase in OCR, together with the fact that dose-dependent responses appeared similar between SCCHN cell lines, this concentration of FCCP was selected for use in all subsequent XF assays.

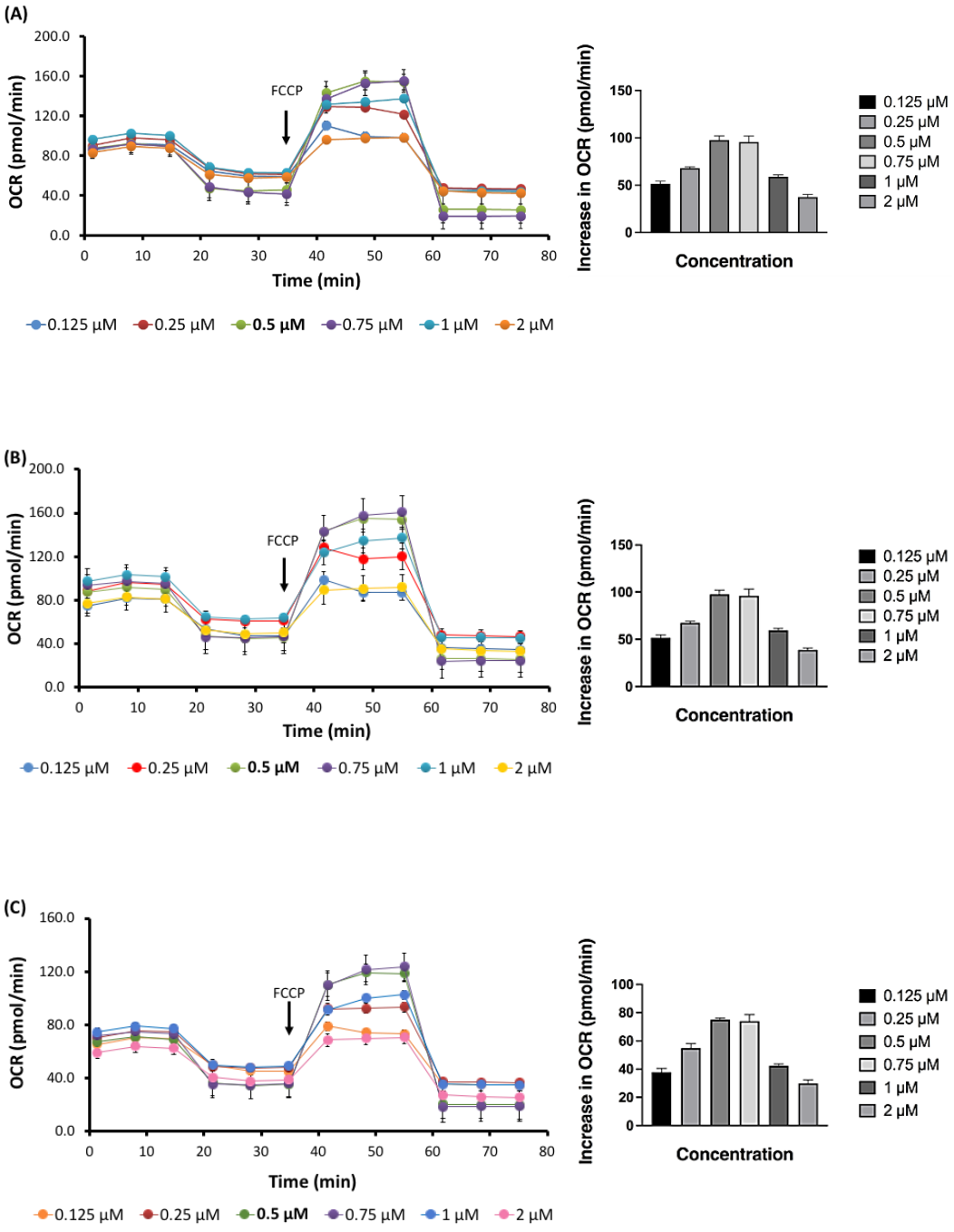

Figure 3.2.: Titration of FCCP for XFe metabolic profiling assays. Left: Measurement of OCR following administration of 0.125, 0.25, 0.5, 0.75, 1 and 2µM FCCP (at the indicated time point on each graph) in three selected SCCHN cell lines depicted separately: (A) UMSCC-1 pBABE (p53-null cell line), (B) UMSCC-17A (wild type p53 cell line) and (C) UMSCC-11B (mutant p53). Right: a representation of the increase in OCR following the administration of the indicated concentration of FCCP in each cell line. 0.5 µM was the lowest concentration to consistently induce a maximal increase in OCR, and thus was used in the subsequent experiments. Titration was performed in hextuplets. Data are shown as the mean of increase in OCR from three experiments (n=3) ± SEM.

3.1.3. Investigating the role of TP53 status in the metabolic phenotype of SCCHN cells

Prior to exploring any potential relationship between metabolic profile and *TP53* status, the *TP53* status of the panel of SCCHN cell lines used in this study was confirmed using western blotting analysis. Two sets of isogenic cell lines were used as well as a panel of mutant and wild type p53 SCCHN cell lines. Figure 3.3. shows the western blotting analysis of p53, MDM2 and TIGAR status in a panel of 15 SCCHN cell lines detailed in section 2.2.1.1. Western blot analysis shows that TIGAR expression and some of the MDM2 expression in SCCHN cells used is due to p53 activity. All cells expressing wild type p53 (UM-SCC-1 WT-p53 in panel (A), UM-SCC-17A and UM-SCC-17A lenti in panel (B) and UM-SCC-17As and UM-SCC-11A in panel (C)) show a marked increase in TIGAR expression when compared to p53-null cells or cells expressing mutant or knockdown p53. Figure 3.3. also show relatively high expression of MDM2 in UM-SCC-17A and isogenic derivative harbouring lenti empty vector as well as the sub-cell line UM-SCC-17As (both 17A and 17As are derived from the same patient but morphologically distinct and 17As cells grow more slowly (313)) when compared to the p53 knockdown derivative, UM-SCC-17A shp53. Cells with homozygous/ loss of heterozygosity (LOH) p53 mutations (UM-SCC-11B and UM-SCC-81B) show higher p53 and MDM2 expression when compared to cells with heterozygous p53 mutations (UM-SCC-5 and UM-SCC-10A)(Figure 3.3. panel C).

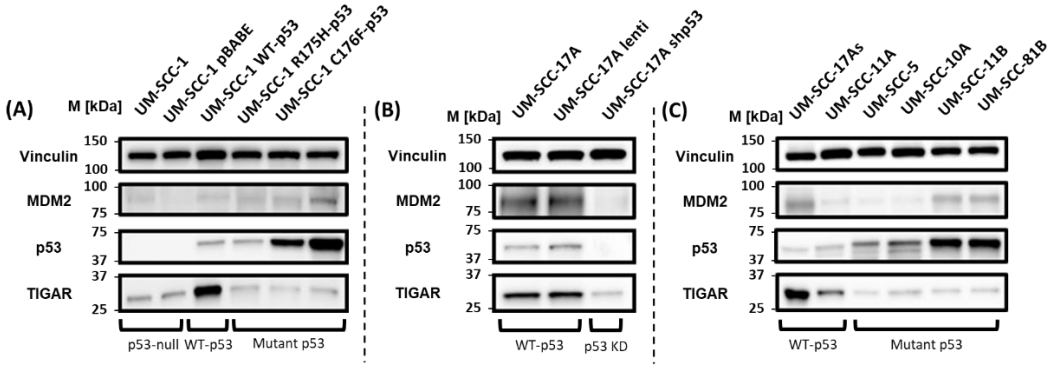

Figure 3.3.: Western blot analyses of MDM2, p53 and TIGAR expression levels in selected mutant and wild type *TP53* SCCHN cells. Cells from each cell line were harvested and lysed as described in section 2.8.3. Protein samples were prepared and loaded into gels, and specific antibodies were used for detection as detailed in section 2.1.9. Vinculin was used as a loading control. The migration of protein standards of the indicated approximate molecular weights is shown in kDa. Blots for the p53-null cell line UM-SCC-1 and derivatives are shown first (A), and subsequently for the wild type p53 cell line UM-SCC-17A and derivatives (B), and finally, a panel of mutant and wild type p53 SCCHN cell lines (C). All cells expressing

wild type p53 (UM-SCC-1 WT-p53 in panel (A), UM-SCC-17A and UM-SCC-17A lenti in panel (B) and UM-SCC-17As and UM-SCC-11A in panel (C)) show marked increase in TIGAR expression. UM-SCC-17A and isogenic derivative harbouring lenti empty vector, as well as sub-cell line UM-SCC-17As, show relatively high expression of MDM2 when compared to the p53 knockdown derivative, UM-SCC-17A shp53. Cells expressing LOH mutant p53 (UM-SCC-11B and UM-SCC-81B) show higher levels of p53 and MDM2 expression when compared to cells expressing heterozygous mutant p53 (UM-SCC-5 and UM-SCC-10A). Cell lines details are shown in 2.2.1.1.

To identify the metabolic phenotype of UM-SCC-1 cell line and isogenic derivatives and to explore any potential correlations between metabolic profile and *TP53* status, Seahorse XFe mitochondrial and glycolytic stress tests were performed, as described in sections 2.3.6.1. and 2.3.6.2., respectively. As stated in 2.2.1., UM-SCC-1 is an endogenously p53-null cell line while genetically modified derivatives are transduced with either an empty vector (pBABE), or vectors expressing wild type *TP53*, or specific *TP53* mutations (R175H, C176F, or R282W). Outputs from the mitochondrial stress test for UMSCC-1 and isogenic derivatives are shown in Figures 3.4. and 3.5., while outputs from glycolytic stress tests are shown in Figures 3.6. and 3.7.

In Figure 3.4., outcomes of mitochondrial stress tests show a marked increase in the mitochondrial function in cell lines that harbour wild type *TP53* or the partially functional C176F mutation of p53 (287,314–317) in comparison with the *TP53*-null parental cell line UM-SCC-1, and the derivative cell lines that harbour the empty vector (pBABE) or the non-functional R175H and R282W mutations of p53. Figure 3.5. shows the absolute normalised values of the mitochondrial stress test parameters, with cell lines that harbour wild type or partially functional p53 showing a significant increase in basal respiration, maximal and spare respiratory capacity as well as ATP production.

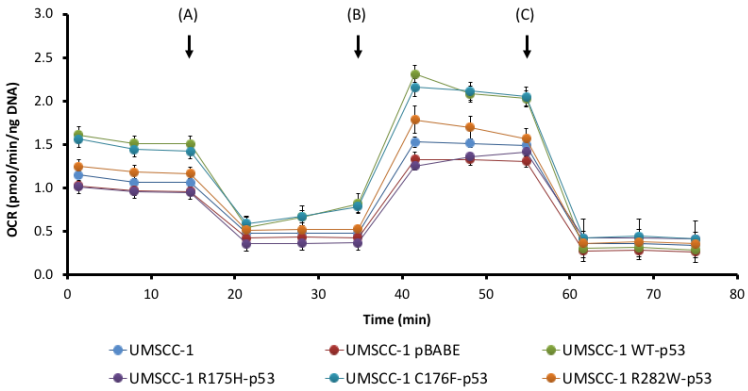

Figure 3.4.: Changes in the metabolic profile of UM-SCC-1 and derivative cell lines in the mitochondrial stress test. UM-SCC-1, UM-SCC-1 pBABE, UM-SCC-1 WT-p53, UM-SCC-1 R175H-p53, UM-

SCC-1 C176F-p53, and UM-SCC-1 R282W-p53 cell lines were subjected to mitochondrial stress test, as described in 2.3.6.1. Points A, B, and C on the graphs refer to the injections time points of 1µM oligomycin, 0.5µM FCCP and 1µM rotenone and antimycin-A, respectively. Post-injection changes in the mitochondrial function were used to calculate the mitochondrial respiration parameters as described in Table 2.4. and are shown in Figure 2.4. Derivative cell lines that harbour the wild type *TP53* or the partially functional C176F mutation in p53 show a marked increase in the mitochondrial function in comparison to the p53-null parental cell line and other p53-mutant derivatives. OCR readings were obtained from three experiments (n=3), each experiment was performed in hextuplet. Data are presented as mean OCR (pmol/min), normalised to DNA content (ng DNA) as described in 2.3.8. Means of individual data were used to derive overall means. Error bars represent SEM.

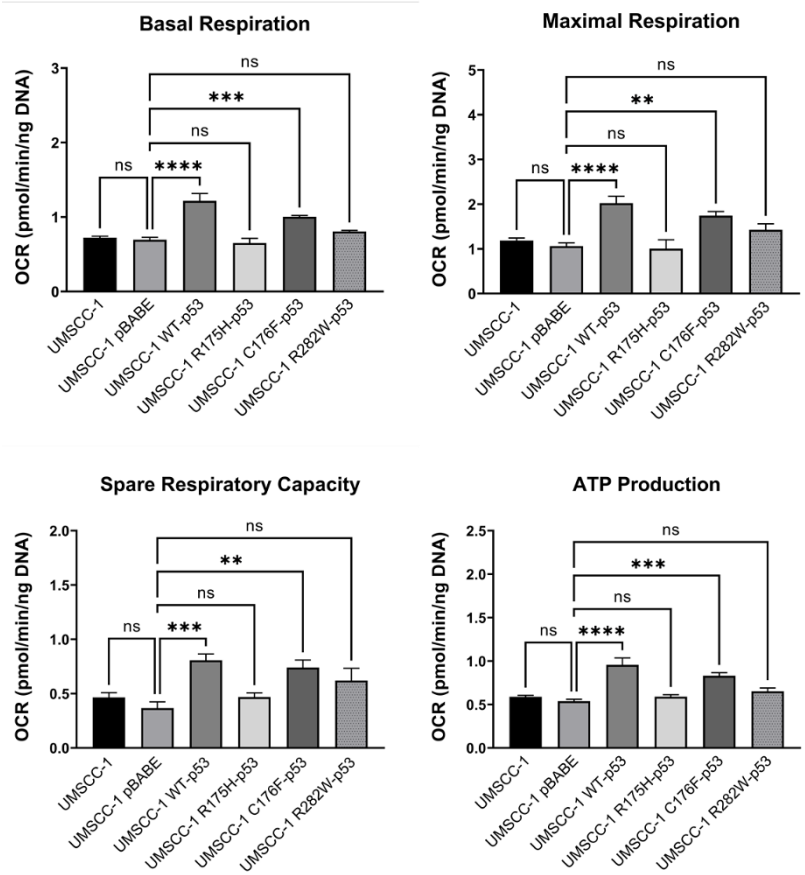

Figure 3.5.: The mitochondrial respiration parameters for UM-SCC-1 and derivatives. Absolute data derived from mitochondrial stress tests was normalised to DNA content for all cell lines (Figure 3.4.), and the absolute values for basal respiration, maximal respiration, spare respiratory capacity and ATP production were calculated as described in section 2.3.6.1. Values for basal respiration, maximal respiration, spare respiratory capacity and ATP production were all significantly greater in the wild type *TP53* cell line in comparison with the *TP53*-null parental cell line UM-SCC-1, while the derivative cell line that harbours the partially functional C176F mutation in *TP53* shown a less significant increase in these values. Means of individual data were used to derive overall means. Error bars represent SEM. Statistical analysis: a one-way ANOVA with Dunnett's test. (ns) $p > 0.05$, (*) $p \leq 0.05$, (**) $p \leq 0.01$, (***) $p \leq 0.001$, (****) $p \leq 0.0001$.

In Figure 3.6. outcomes of the glycolytic stress test show that forced expression of wild type p53 in the p53-null parental cell line UM-SCC-1 resulted in a marked decrease in the glycolytic function following the injection of glucose at the time point (A), with no significant difference found between all cell lines in the following injection steps. The glycolytic parameters obtained from Figure 3.6. were calculated and are presented in Figure 3.7. Although it wasn't measured in the mitochondrial stress assay medium, OCR means in UM-SCC-1 wild type p53 cells were higher (1.54±0.4) in comparison with OCR means in p53-null empty vector cells (1.24±0.11).

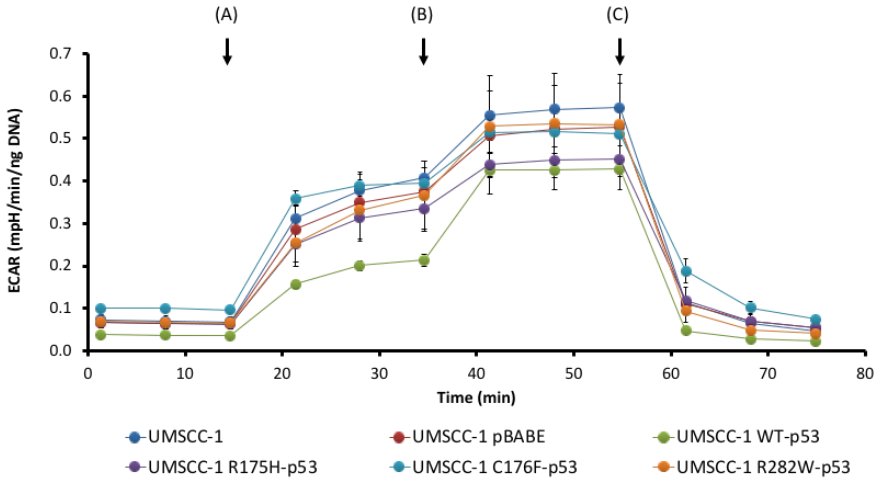

Figure 3.6.: Changes in the metabolic profile of UM-SCC-1 and derivative cell lines in the glycolytic stress test. UM-SCC-1, UM-SCC-1 pBABE, UM-SCC-1 WT-p53, UM-SCC-1 R175H-p53, UM-SCC-1 C176F-p53, and UM-SCC-1 R282W-p53 cell lines were subjected to glycolytic stress test, as described in 2.3.6.2. Points A, B, and C on the graphs refer to the injections time points of 10mM D-glucose, 1µM oligomycin and 50mM 2-DG, respectively. Post-injection changes in the glycolytic function were used to calculate the glycolytic parameters as described in Table 2.5. and are shown in Figure 2.5. A derivative cell line that harbours the wild type *TP53* shows lower levels of glycolysis (injection point A) in comparison to the p53-null parental cell line and other p53-mutant derivatives, with no marked differences between all cell lines after injection point B and C. ECAR readings were obtained from three experiments (n=3), each experiment was performed in hextuplet. Data are presented as mean ECAR (mpH/min), normalised to DNA content (ng DNA) as described in 2.3.8. Means of individual data were used to derive overall means. Error bars represent SEM.

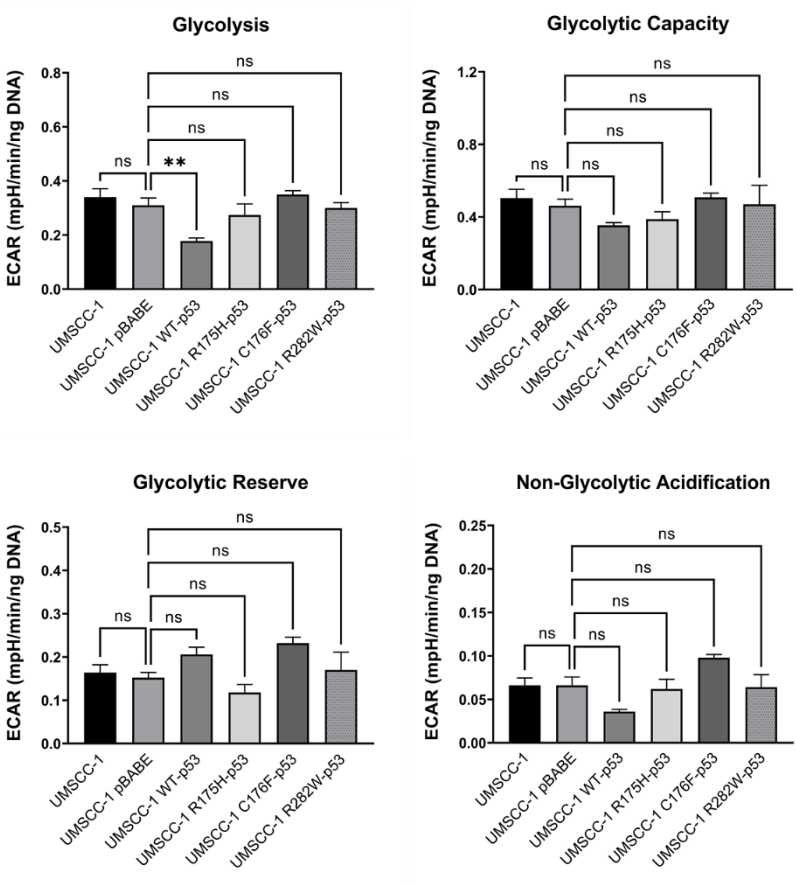

Figure 3.7.: The glycolysis parameters for UM-SCC-1 and derivatives. Absolute data derived from glycolytic stress tests was normalised to DNA content for all cell lines (Figure 3.6.), and the absolute values for glycolysis, glycolytic capacity, glycolytic reserve and non-glycolytic acidification were calculated as described in section 2.3.6.2. Values for glycolysis were significantly lower in the derivative cell line that harbours wild type *TP53* in comparison with the *TP53*-null parental cell line UM-SCC-1, while the derivative cell lines that harbour R175H, C176F and R282W mutations of *TP53* shown no significant differences. No significant differences were found in values for glycolytic capacity, glycolytic reserve and non-glycolytic acidification in all cell lines in comparison with the parental cell line, UM-SCC-1. Means of individual data were used to derive overall means. Error bars represent SEM. Statistical analysis: a one-way ANOVA with Dunnett's test. (ns) $p > 0.05$, (*) $p \leq 0.05$, (**) $p \leq 0.01$, (***) $p \leq 0.001$, (****) $p \leq 0.0001$.

These results show that forced expression of wild type p53 in the p53-null cell line, UM-SCC-1, results in a metabolic shift from lower use of mitochondrial respiration with a higher dependence on glycolysis to a marked increase in mitochondrial respiration associated with a lower dependence on glycolysis, without noticeable effect on glycolysis capacity and glycolysis reserves. Although the metabolic profiles of the derived cell lines expressing mutant p53 were similar to that of the parental cell line in glycolytic function, partial conservation of p53 function in the derived cell line

expressing the C176F mutant of p53 showed a significant increase in mitochondrial respiration function.

Further investigation was needed to determine whether these observations could be consistent with the changes in the metabolic profile of cells that endogenously express wild type p53 and whether inhibiting the expression of p53 would alter the metabolic profile, indicating a possibly deterministic function for p53 in this process. Seahorse XFe mitochondrial and glycolytic stress tests were performed, as described in sections 2.3.6.1. and 2.3.6.2., respectively, to identify the metabolic phenotype of UM-SCC-17A cell line and isogenic derivatives to explore any potential similarities in the correlation between the metabolic profile and *TP53* status observed in UM-SCC-1 cell line and isogenic derivatives. As described in 2.2.1., UM-SCC-17A is an endogenously wild type p53 cell line while genetically modified derivatives have been generated that either stably harbours an empty vector control (lenti) or a short-hairpin RNA (shRNA) specific for p53 (shp53). Outputs from the mitochondrial stress test for UMSCC-17A and isogenic derivatives are shown in Figure 3.8., while outputs from glycolytic stress tests are shown in Figure 3.9.

Figure 3.8. panel (I) presents the outcomes of mitochondrial stress tests, showing highly active mitochondrial function in the wild type parental cell line UM-SCC-17A and the derivative cell line that harbours empty vector (lenti), while stable p53 knockdown (shp53) results in low active mitochondrial function. Panel (II) shows the absolute normalised values of the mitochondrial parameters, with stable p53 knockdown results in a significant decrease in basal respiration, maximal and spare respiratory capacity as well as ATP production.

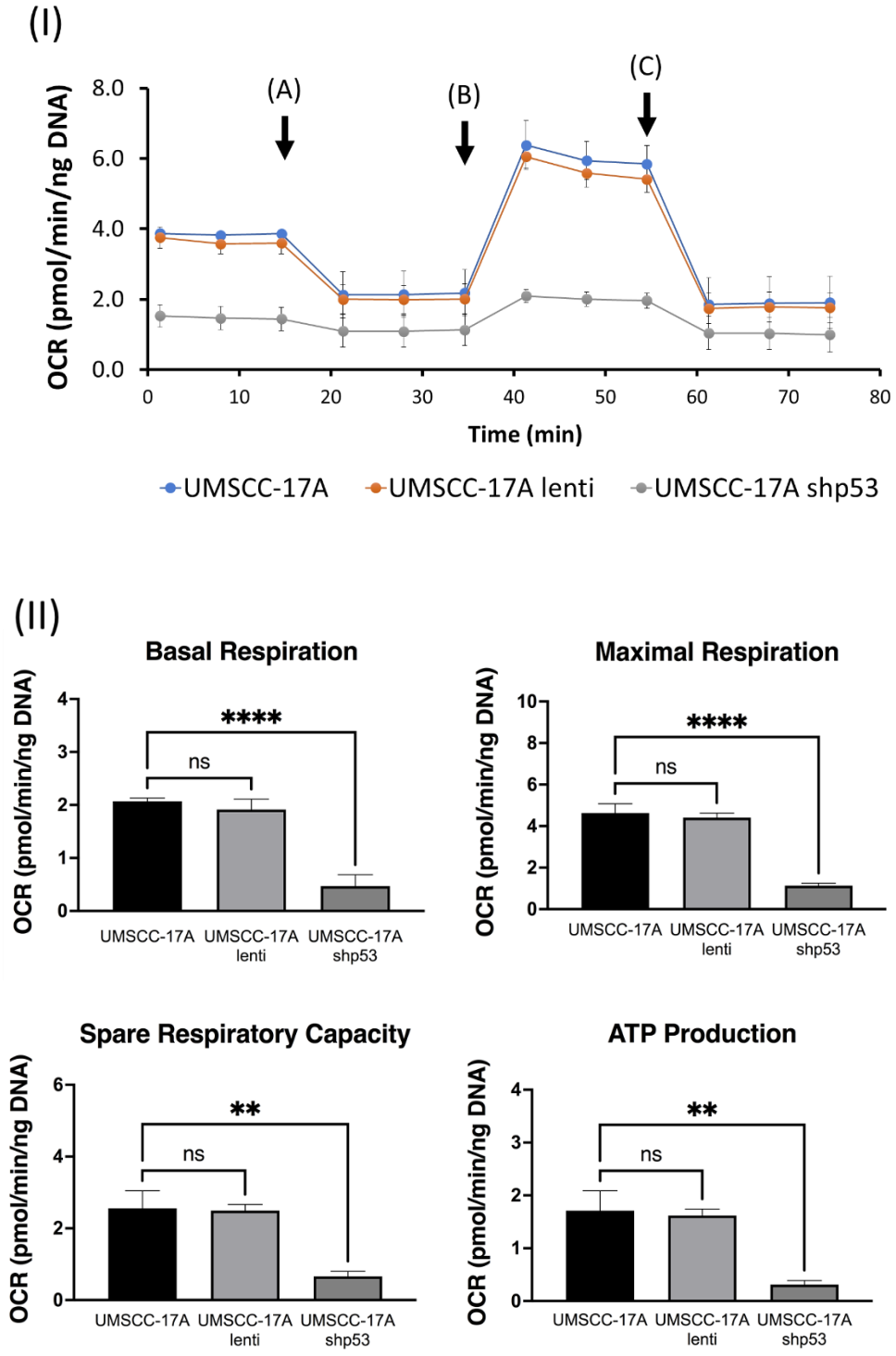

Figure 3.8.: The metabolic profile of UM-SCC-17A and derivative cell lines in the mitochondrial stress test. (I) Changes in the metabolic profile of UM-SCC-17A and derivative cell lines in the mitochondrial stress test. UM-SCC-17A, UM-SCC-17A lenti and UM-SCC-17A shp53 cell lines were subjected to mitochondrial stress test, as described in 2.3.6.1. Points A, B, and C on the graphs refer to the injections time points of 1μM oligomycin, 0.5μM FCCP and 1μM rotenone and antimycin-A, respectively. Post-injection changes in the mitochondrial function were used to calculate the mitochondrial respiration parameters as described in Table 2.4. and are shown in Figure 2.4. A derivative cell line that expresses shRNA specific for p53 shows a marked decrease in the mitochondrial function in comparison to the wild

type p53 parental cell line and the derivative that expresses empty vector (lenti). **(II)** The mitochondrial respiration parameters for UM-SCC-17A and derivatives. Absolute data derived from mitochondrial stress tests was normalised to DNA content for all cell lines, and the absolute values for basal respiration, maximal respiration, spare respiratory capacity and ATP production were calculated as described in section 2.3.6.1. Values for basal respiration, maximal respiration, spare respiratory capacity and ATP production were all significantly greater in the wild type *TP53* parental cell line and the derivative that express lenti empty vector in comparison with the derivatives that expresses shRNA specific for p53. OCR readings were obtained from three experiments (n=3), each experiment was performed in hextuplet. Data are presented as mean OCR (pmol/min), normalised to DNA content (ng DNA) as described in 2.3.8. Means of individual data were used to derive overall means. Error bars represent SEM. Statistical analysis: a one-way ANOVA with Dunnett's test. (ns) $p > 0.05$, (*) $p \leq 0.05$, (**) $p \leq 0.01$, (***) $p \leq 0.001$, (****) $p \leq 0.0001$.

In Figure 3.9. (I), outcomes of the glycolytic stress test show that p53 knockdown resulted in a significant increase in the glycolytic function following the injection of glucose at the time point (A), with no significant difference found between all cell lines in the following injection steps. Glycolytic parameters obtained from (I) were calculated and presented in (II). Consistent with results from Figures 3.7., p53 knockdown results in a significant increase in glycolysis in comparison with the parental cell line, UMS-CC- 17A and the derivative cell line that harbours the empty vector control (lenti), with no significant changes in other glycolytic parameters. Although it wasn't measured in the mitochondrial stress assay medium, normalised OCR means in UM-SCC-17A lenti (wild type p53) cells were higher (2.04±0.11) in comparison with OCR means in p53 knockdown empty vector cells (0.51±0.33).

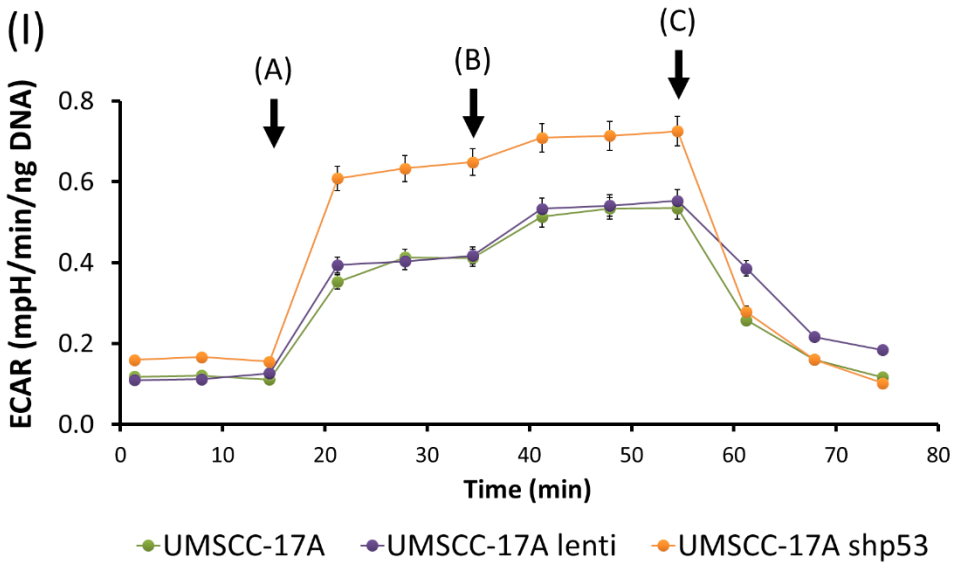

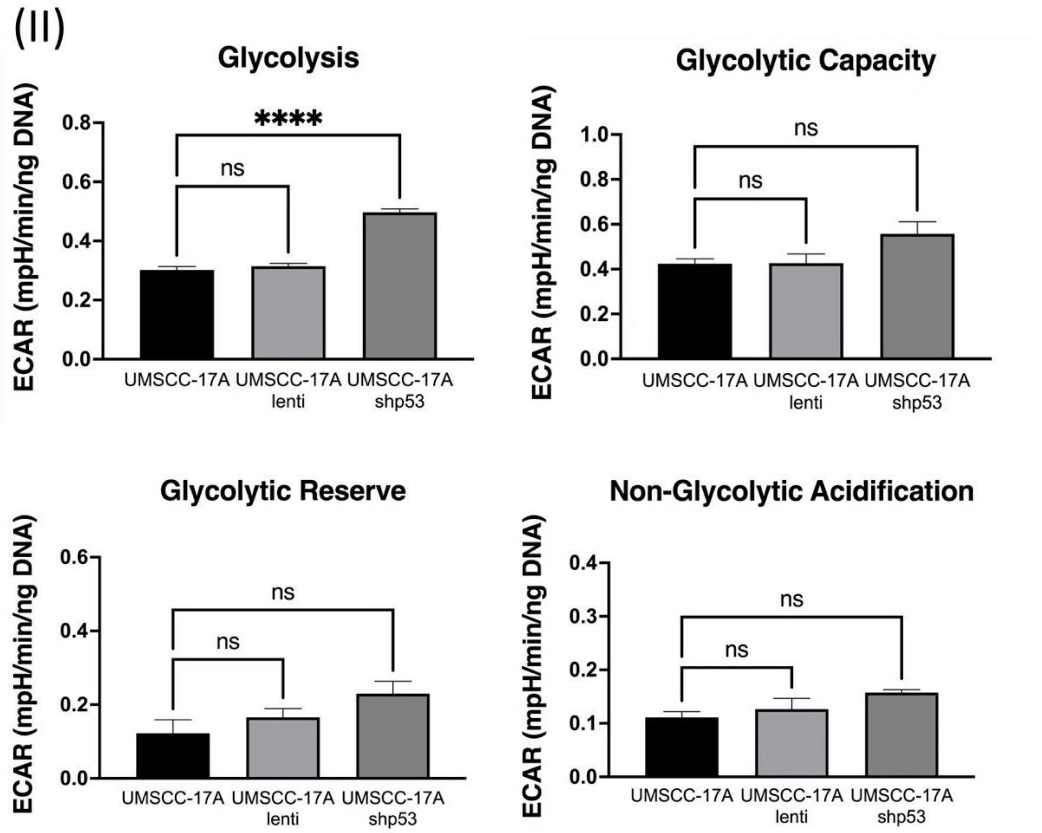

Figure 3.9.: The metabolic profile of UM-SCC-17A and derivative cell lines in the glycolytic stress test. (I) Changes in the metabolic profile of UM-SCC-17A and derivative cell lines in the glycolytic stress test. UM-SCC-17A, UM-SCC-17A lenti and UM-SCC-17A shp53 cell lines were subjected to glycolytic stress test, as described in 2.3.6.2. Points A, B, and C on the graphs refer to the injections time points of 10mM D-glucose, 1μM oligomycin and 50mM 2-DG, respectively. Post-injection changes in the glycolytic function were used to calculate the glycolytic parameters as described in Table 2.5. and are shown in Figure 2.5. A derivative cell line that expresses shRNA specific for p53 shows a marked increase in the glycolytic function following the injection of glucose at time point A in comparison to the wild type p53 parental cell line and the derivative that harbours empty vector (lenti), while no marked changes in response to inhibition of mitochondrial ATP production following the injection of oligomycin at time point B. **(II)** The glycolysis parameters for UM-SCC-17A and derivatives. Absolute data derived from glycolytic stress tests was normalised to DNA content for all cell lines, and the absolute values for glycolysis, glycolytic capacity, glycolytic reserve and non-glycolytic acidification were calculated as described in section 2.3.6.2. The derivative cell line that expresses shRNA specific for p53 shows a significant increase in values for glycolysis in comparison to the wild type p53 parental cell line and the derivative that harbours empty vector (lenti), while no significant differences are shown in values for glycolytic capacity, glycolytic reserve and non-glycolytic acidification. ECAR readings were obtained from three experiments (n=3), each experiment was performed in hextuplet. Means of individual data were used to derive overall means. Data are presented as mean ECAR (mpH/min), normalised to DNA content (ng DNA) as described in 2.3.8. Error bars represent SEM. Statistical analysis: a one-way ANOVA with Dunnett's test. (ns) $p > 0.05$, (*) $p \leq 0.05$, (**) $p \leq 0.01$, (***) $p \leq 0.001$, (****) $p \leq 0.0001$.

Given the variation in the metabolic profiles and *TP53* status between different types of cell lines, we further expanded our work from the limited metabolic profiling of a parental cell line with isogenic derivatives to use a panel of SCCHN cell lines with a range of *TP53* variants to investigate the observed role of *TP53* status as a determinant in the metabolic profile in SCCHN. A panel of SCCHN cell lines with different *TP53* variants, as detailed in Table 2.1. were used together to examine and compare the changes in metabolic profile using mitochondrial and glycolytic stress tests, as described in 2.3.6.1. and 2.3.6.2., respectively.

To enable comparison of metabolic profiling between cell lines, outputs from the mitochondrial stress tests for all cell lines are shown in Figure 3.10., with 10 pmol/min/ng DNA used as a maximum value of OCR on the Y-axis. Outcomes of mitochondrial stress tests show highly active mitochondrial function in all cell lines that express wild type p53 in comparison with the endogenously p53-null cell lines or the cell lines that express mutant or have knockdown of p53. Figure 3.11. shows the absolute normalised values of the mitochondrial parameters, calculated using the changes in mitochondrial function in the mitochondrial stress test, shown in Figure 3.10. A marked increase in basal respiration, maximal and spare respiratory capacity, as well as ATP production, was observed in cell lines with endogenous or forced expression of wild type p53 in comparison with the endogenously p53-null cell lines or the cell lines that express mutant or knockdown p53.

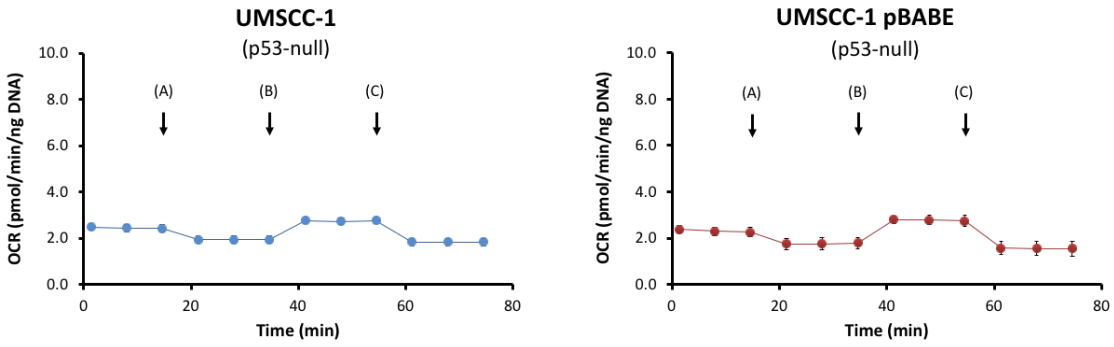

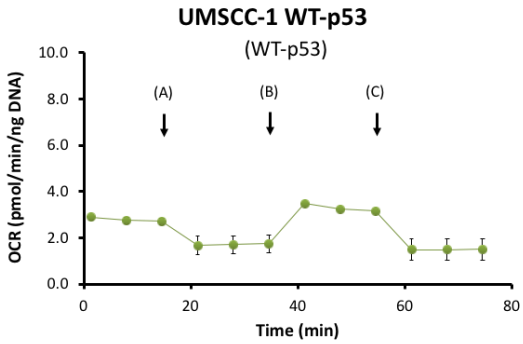
UMSCC-1 WT-p53
(WT-p53)
OCR (pmol/min/ng DNA)
(A)
(B)
(C)
Time (min)

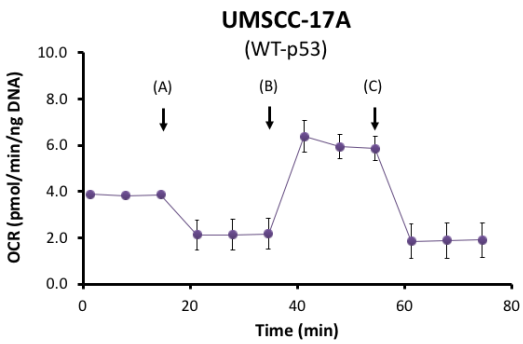
UMSCC-17A
(WT-p53)
OCR (pmol/min/ng DNA)
(A)
(B)
(C)
Time (min)

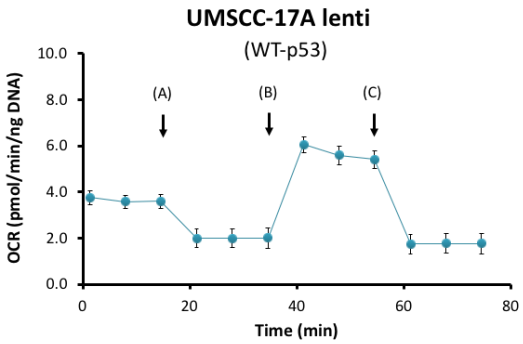
UMSCC-17A lenti
(WT-p53)
OCR (pmol/min/ng DNA)
(A)
(B)
(C)
Time (min)

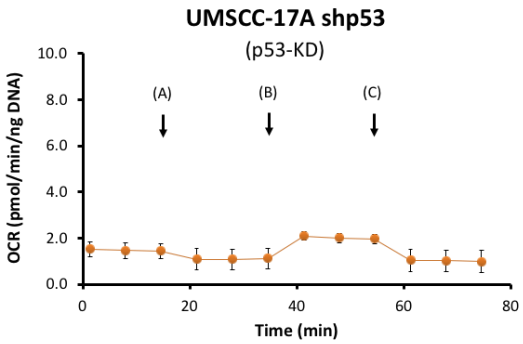
UMSCC-17A shp53
(p53-KD)
OCR (pmol/min/ng DNA)
(A)
(B)
(C)
Time (min)

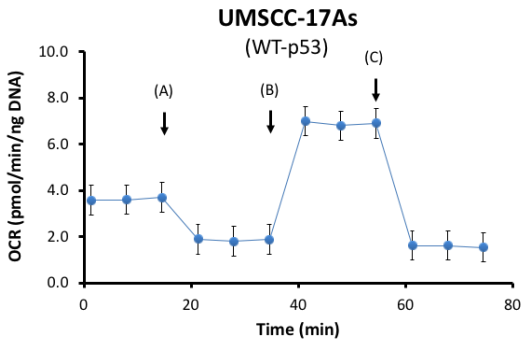
UMSCC-17As
(WT-p53)
OCR (pmol/min/ng DNA)
(A)
(B)
(C)
Time (min)

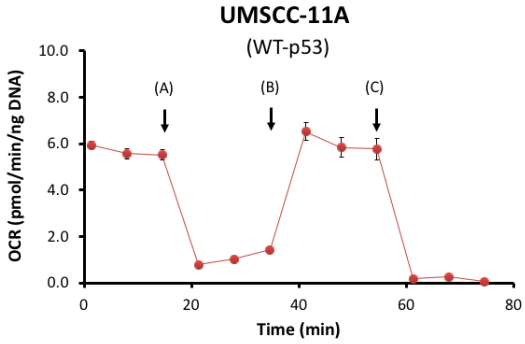
UMSCC-11A
(WT-p53)
OCR (pmol/min/ng DNA)
(A)
(B)
(C)
Time (min)

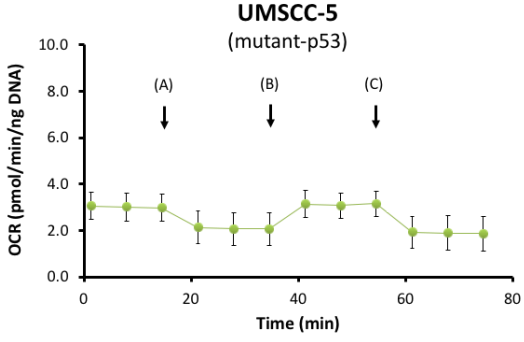
UMSCC-5
(mutant-p53)
OCR (pmol/min/ng DNA)
(A)
(B)
(C)
Time (min)

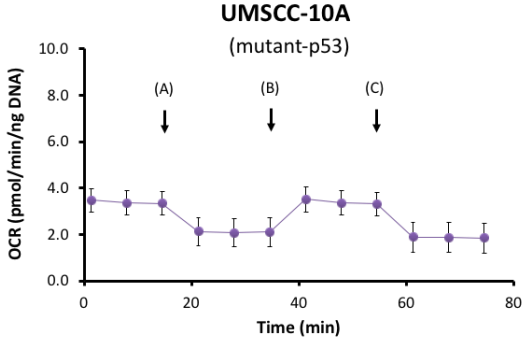
UMSCC-10A
(mutant-p53)
OCR (pmol/min/ng DNA)
(A)
(B)
(C)
Time (min)

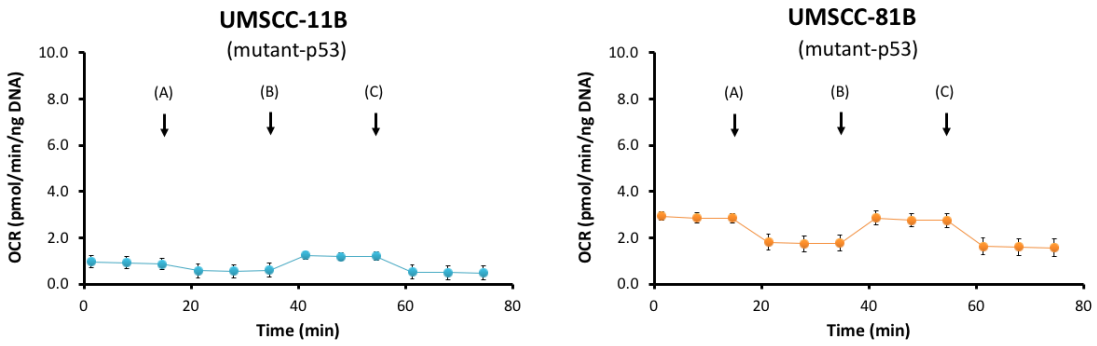

Figure 3.10.: Comparative changes in the metabolic profile of a panel of SCCHN cell lines in the mitochondrial stress test. Outputs from the mitochondrial stress tests for all cell lines are shown, with 10 pmol/min/ng DNA was used as a maximum value of OCR on the Y-axis. Cell lines indicated in each panel were subjected to the mitochondrial stress test, as described in 2.3.6.1. Points A, B, and C on the graphs refer to the injections time points of 1µM oligomycin, 0.5µM FCCP and 1µM rotenone and antimycin-A, respectively. Post-injection changes in the mitochondrial function were used to calculate the mitochondrial respiration parameters as described in Table 2.4. and are shown in Figure 2.4. OCR readings were obtained from three experiments (n=3), each experiment was performed in hextuplet. Data are presented as mean OCR (pmol/min), normalised to DNA content (ng DNA) as described in 2.3.8. Error bars represent SEM.

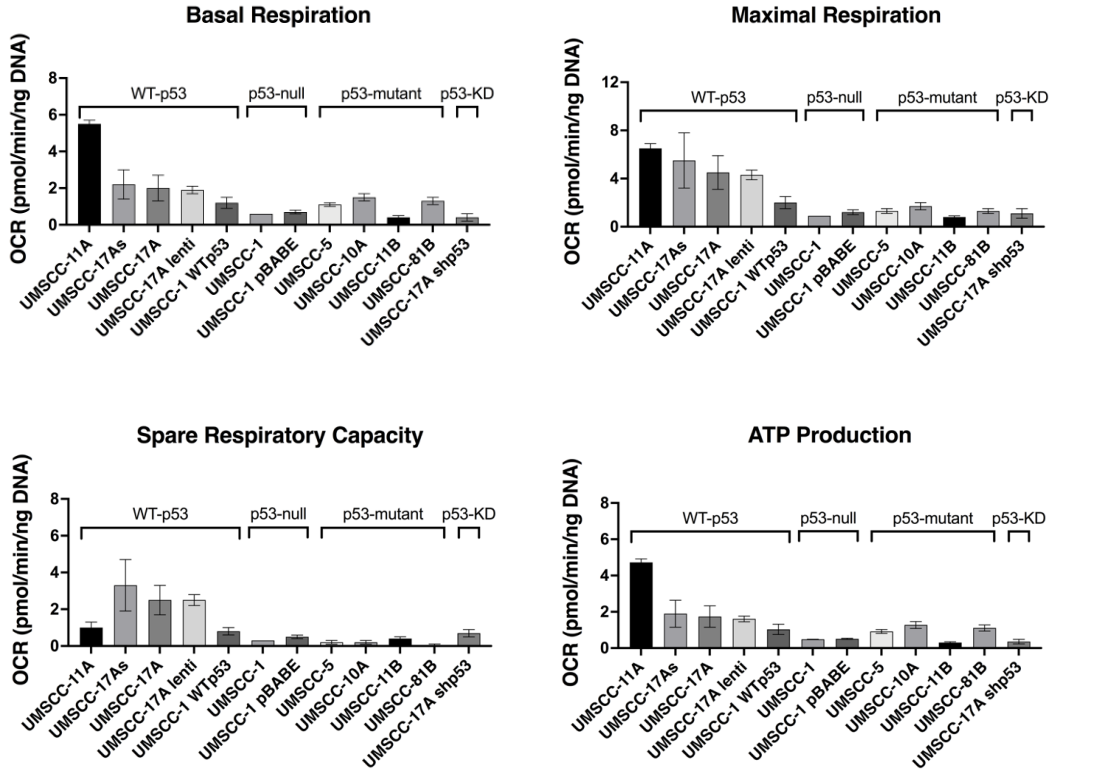

Figure 3.11.: The mitochondrial respiration parameters for a panel of SCCHN cell lines. Absolute data derived from mitochondrial stress tests was normalised to DNA content for all cell lines (Figure 3.10.), and the absolute values for basal respiration, maximal respiration, spare respiratory capacity and ATP

production were calculated as described in section 2.3.6.1. To enable comparison, outputs were reordered based on p53 status. Error bars represent SEM.

Similarly, outputs from the glycolytic stress tests for all cell lines are shown in Figure 3.12., with 1.2 mpH/min/ng DNA was used as a maximum value of ECAR on the Y-axis. Figure 3.13. shows the absolute normalised values of the glycolytic parameters, calculated using the changes in the glycolytic function in glycolytic stress test, shown in Figure 3.12. A significant increase in glycolysis is observed in the endogenously p53-null cell lines or the cell lines that express mutant or knockdown p53 in comparison to cell lines with endogenous or forced expression of wild type p53 (detailed in Table 3.1.). No distinct pattern was observed for the levels of glycolytic capacity and glycolytic reserve nor for non-glycolytic acidification.

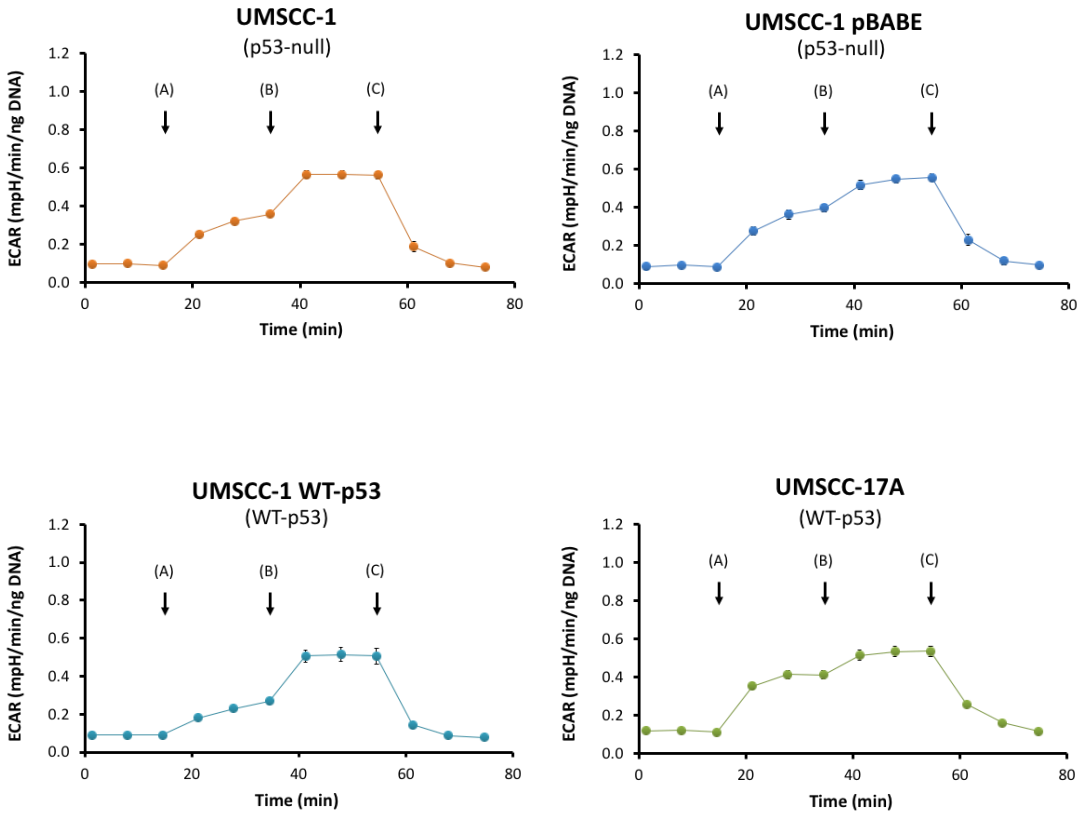

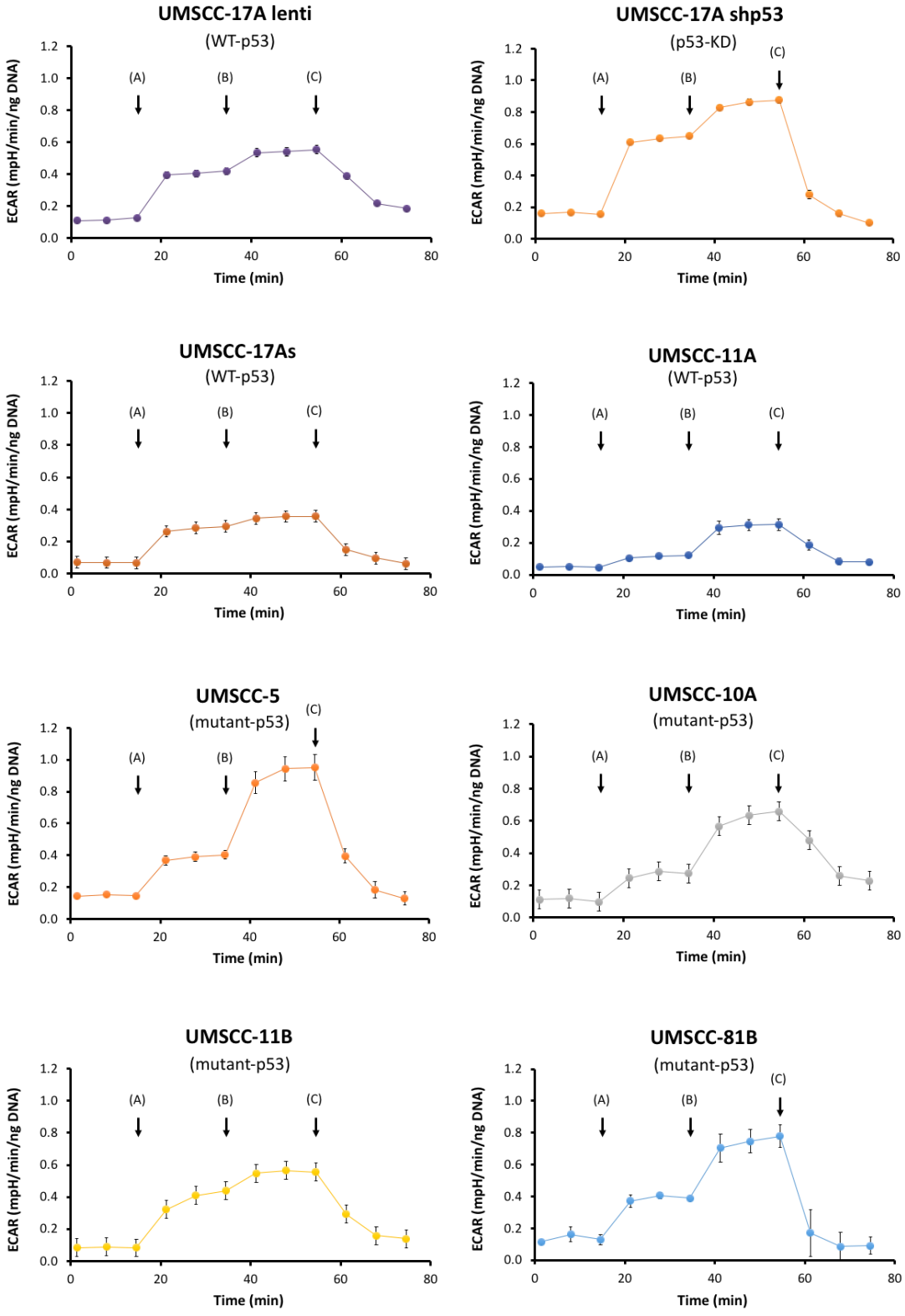

Figure 3.12.: Comparative changes in the metabolic profile of a panel of SCCHN cell lines in the glycolytic stress test. Outputs from the glycolytic stress tests for all cell lines are shown, with 1.2 mpH/min/ng DNA was used as a maximum value of ECAR on the Y-axis. Cell lines were subjected to the glycolytic stress test, as described in 2.3.6.2. Points A, B, and C on the graphs refer to the injections time points of 10mM D-glucose, 1μM oligomycin and 50mM 2-DG, respectively. Post-injection changes in the glycolytic function were used to calculate the glycolytic parameters as described in Table 2.5. and are

shown in Figure 2.5. ECAR readings were obtained from three experiments (n=3), each experiment was performed in hextuplet. Data are presented as mean ECAR (mpH/min), normalised to DNA content (ng DNA) as described in 2.3.8. Error bars represent SEM.

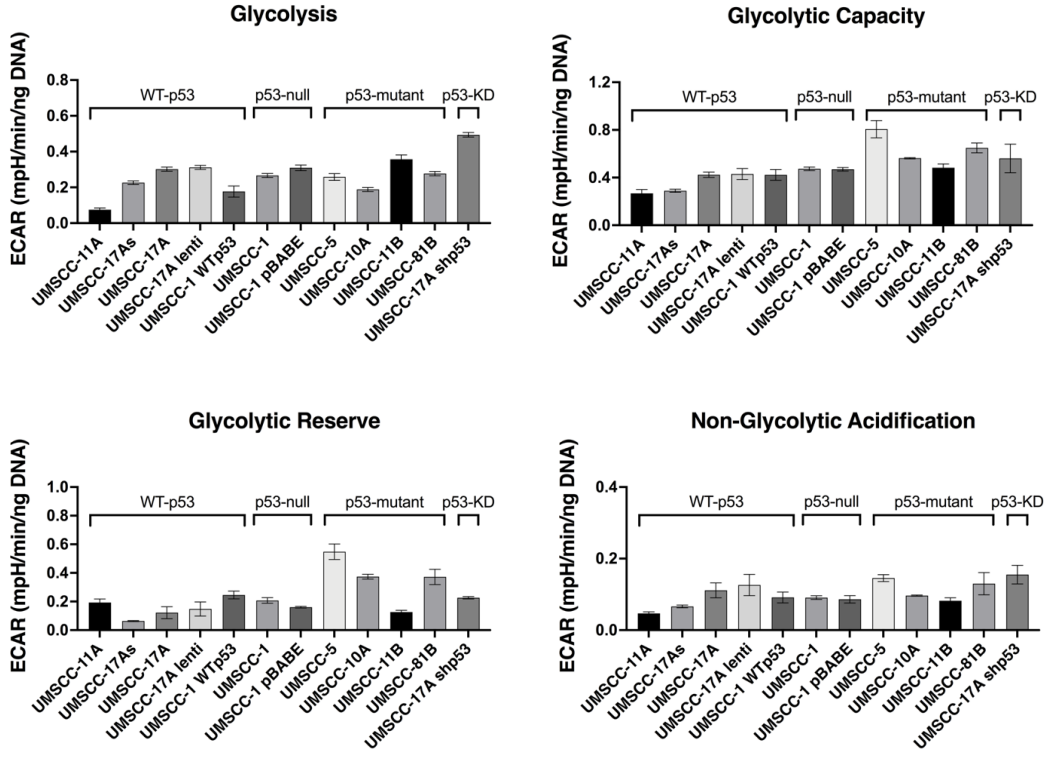

Figure 3.13.: The glycolytic parameters for a panel of SCCHN cell lines. Absolute data derived from glycolytic stress tests was normalised to DNA content for all cell lines (Figure 3.12.), and the absolute values for glycolysis, glycolytic capacity, glycolytic reserve and non-glycolytic acidification were calculated as described in section 2.3.6.2. To enable comparison, outputs were reordered based on p53 status. Error bars represent SEM.

Table 3.1.: The means of absolute values of glycolysis measured in a panel of SCCHN cell lines, based on TP53 status

	Cell line	TP53 status	Mean	SEM
Wild type	UMSCC-11A	Wild type	0.07	0.010
	UMSCC-17As	Wild type	0.23	0.010
	UMSCC-17A	Wild type	0.30	0.012
	UMSCC-17A lenti	Wild type	0.31	0.011
	UMSCC-1 WTp53	Wild type	0.18	0.031
Compromised	UMSCC-1	p53-null	0.27	0.011
	UMSCC-1 pBABE	p53-null	0.31	0.016
	UMSCC-5	Mutant p53	0.26	0.019
	UMSCC-10A	Mutant p54	0.19	0.011
	UMSCC-11B	Mutant p55	0.36	0.025
	UMSCC-81B	Mutant p56	0.28	0.012
	UMSCC-17A shp53	p53 knockdown	0.49	0.013

Having analysed the panel of cell lines in detail, the metabolic profiling data obtained from mitochondrial and glycolytic stress tests shown were used to examine the potential role of p53 in determining the metabolic profile in SCCHN cells based on the observations previously shown in Figures 3.10. and 3.12. The data from all cell lines were combined into two groups based on *TP53* status: the first group includes all cell lines with endogenous or forced expression of wild type p53 and will be referred to as the WT-p53 group, while the second group includes endogenously p53-null cell lines or the cell lines that express mutant or knockdown of p53 expression and will be referred to as the compromised p53 group.

In Figure 3.14. panel (I), basal readings and post-injection changes in the metabolic profile of the two groups of SCCHN cell lines in the mitochondrial stress test clearly shown a highly active mitochondrial function in the wild type p53 group in comparison with the compromised p53 group (null/mutant/knockdown). The wild type p53 group displays significantly higher levels of basal respiration, maximal and spare respiratory capacity as well as ATP production in comparison with the compromised p53 group, Figure 3.14. panel (II).

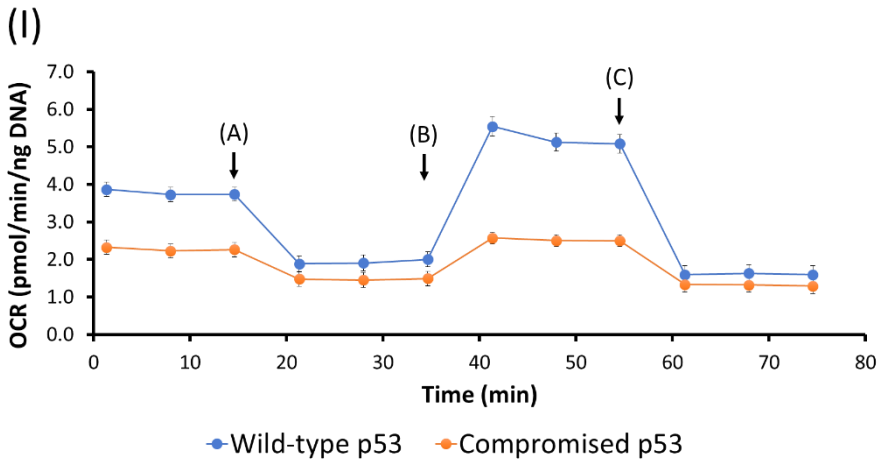

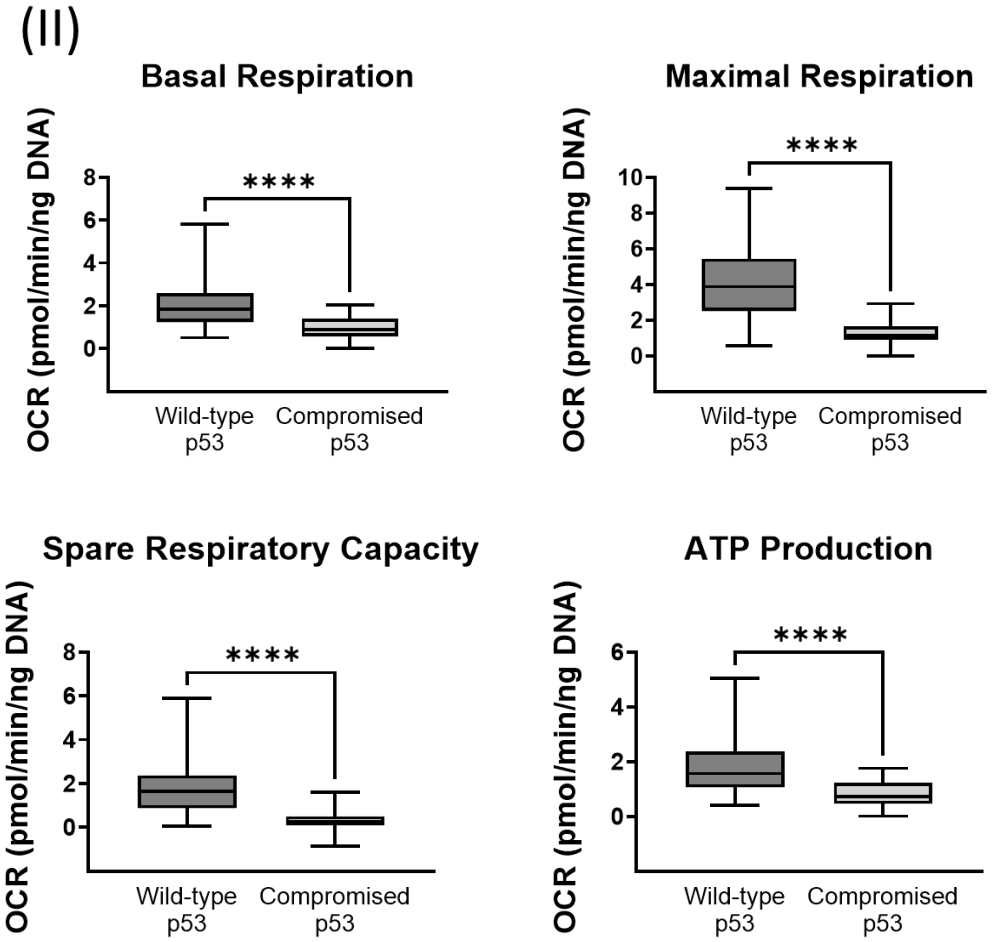

Figure 3.14.: The potential role of p53 status in changing the mitochondrial function of SCCHN. Changes in the mitochondrial function shown in Figure 3.11. were processed into two distinct groups based on the p53 status. Points A, B, and C on the graphs refer to the injections time points of 1µM oligomycin, 0.5µM FCCP and 1µM rotenone and antimycin-A, respectively. **(I)** displays a highly active mitochondrial function in the wild type p53 group in comparison with the compromised p53 group (null/mutant/knockdown), both at the basal level and following the injection of stressors. **(II)** Basal readings and post-injection changes in the mitochondrial function, shown in (I), were used to calculate the absolute normalised values of the mitochondrial respiration parameters as described in Table 2.4. and are shown in Figure 2.4. Means of individual data were used to derive overall means. Error bars represent SD. Statistical analysis: Mann-Whitney U test. (ns) $p > 0.05$, (*) $p \leq 0.05$, (**) $p \leq 0.01$, (***) $p \leq 0.001$, (****) $p \leq 0.0001$.

In Figure 3.15. panel (I), basal readings and post-injection changes in the metabolic profile of the two groups of SCCHN cell lines in the glycolytic stress test clearly shown higher glycolytic activity in the compromised p53 group (null/mutant/knockdown) in comparison with wild type p53 group following the injection of glucose with no further changing following stimulating glycolysis by inhibiting ATP production (at time point B) or following the inhibition of glycolysis (at time point C). The compromised p53

group displays significantly higher levels of glycolysis, with no significant difference in the values for glycolytic capacity, glycolytic reserve and non-glycolytic acidification in comparison with the wild type p53 group, Figure 3.15. panel (II).

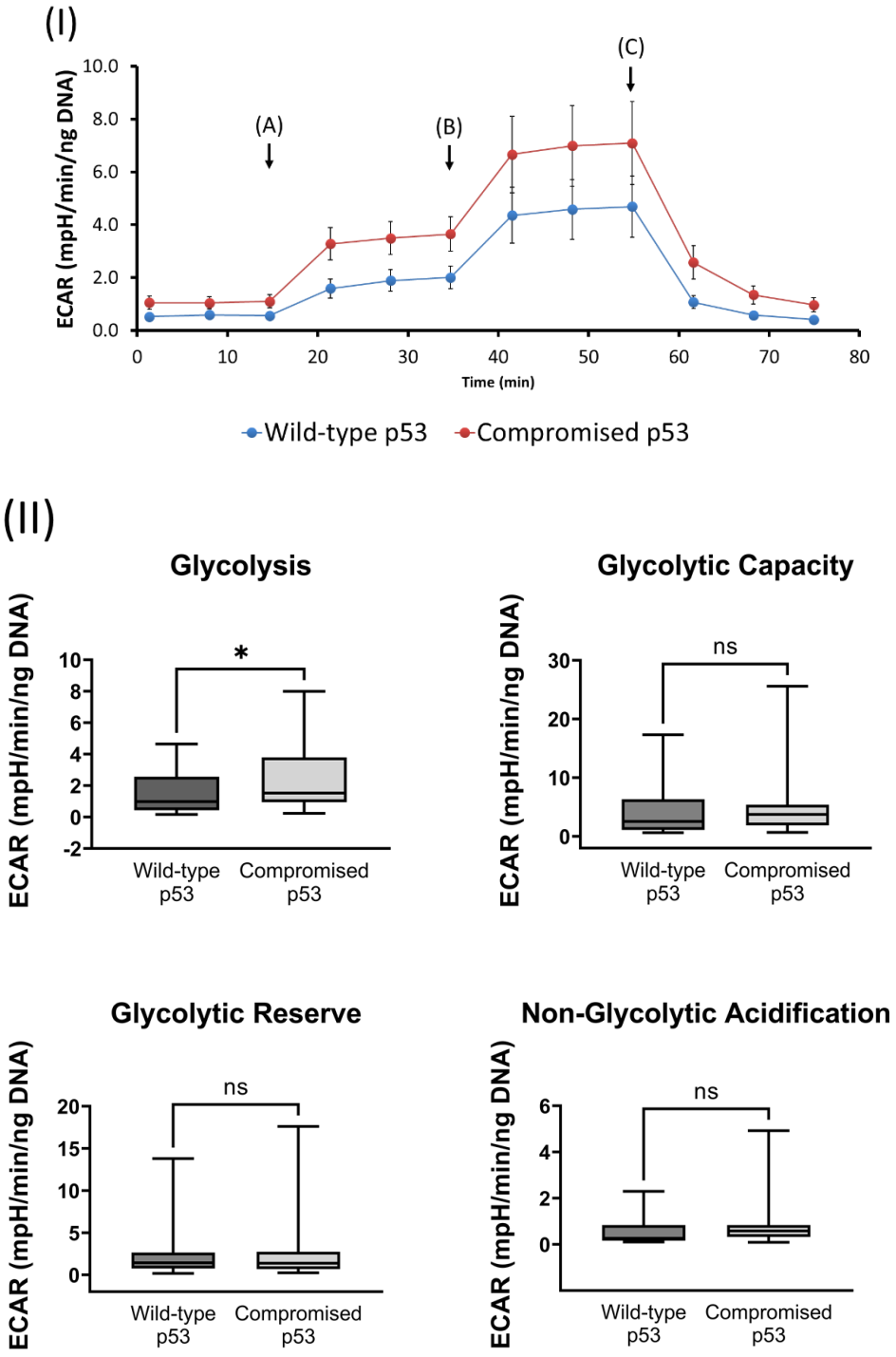

Figure 3.15.: The potential role of p53 status in changing the glycolytic function of SCCHN. Changes in the glycolytic function shown in Figure 3.13. were processed into two distinct groups based on the p53 status. Points A, B, and C on the graphs refer to the injections time points of 10mM D-glucose, 1μM

oligomycin and 50mM 2-DG, respectively. **(I)** displays a highly active glycolytic function in the compromised p53 group (null/mutant/knockdown) in comparison with the wild type p53 group following the injection of glucose at time point A, with no clear difference in the glycolytic profile following the injection of oligomycin or 2-DG at the time point (B) and (C), respectively. **(II)** Basal readings and post-injection changes in the glycolytic function, shown in (I), were used to calculate the absolute normalised values of the glycolytic parameters as described in Table 2.5. and are shown in Figure 2.5. Means of individual data were used to derive overall means. Error bars represent SD. Statistical analysis: Mann-Whitney U test. (ns) $p > 0.05$, (*) $p \leq 0.05$, (**) $p \leq 0.01$, (***) $p \leq 0.001$, (****) $p \leq 0.0001$.

The cell lines in the compromised p53 group showed lower respiratory activity and higher glycolytic activity than the cell lines in the wild type group, and thus they display a phenotype in line with the Warburg effect. The pattern of metabolic profiles observed suggests that by combining analysis of measurements of glycolysis and of respiratory activity, it may be possible to predict the *TP53* status of the samples being analysed. To further examine the "Warburg effect" or the metabolic phenotype, a value derived from the ratio of basal glycolysis/basal respiration was ascribed to each cell line. This ratio was first utilised in Warburg studies as an indicator of rapid tumour progression and proliferation (318) and it has since been used in a number of studies (319–322). This results in clear dichotomisation of cells into p53 wild type and p53 compromised groups, with similar results in the isogenic cell lines used in this study (Figure 3.16.).

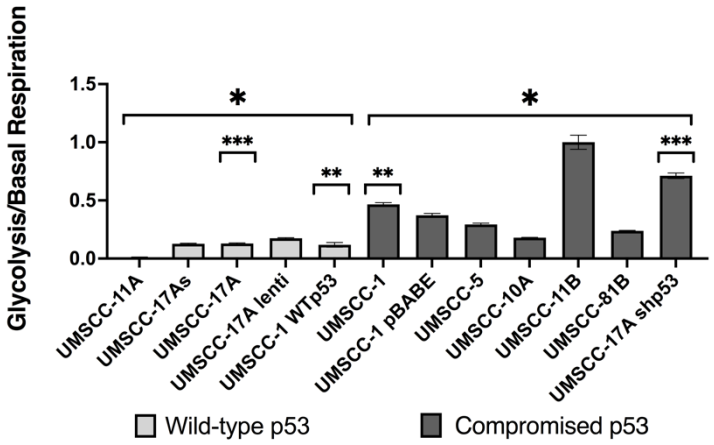

Figure 3.16.: Warburg effect in a panel of SCCHN cell lines. The increased aerobic glycolysis of each cell line can be assessed by ascribing a value derived from the glycolysis/basal respiration ratio as an indicator of the Warburg effect. This ratio dichotomised the cell lines into p53 wild type and p53 compromised groups, as discussed before, demonstrated significantly higher values in the p53 compromised group (*p = 0.028), indicative of increased dependence on glycolysis, while significant lower values are typical of wild type p53 cells with higher use of oxidative phosphorylation. Direct comparison of the isogenic cell lines showed a similar pattern. Forced expression of wild type p53 in the endogenously p53-null parental

cell line, UM-SCC-1, resulted in a marked decrease in dependence on glycolysis (**$p < 0.001$), while a UM-SCC-17A derivative that contains a lentiviral vector expressing a shRNA specific for p53 shows a significant increase in dependence on glycolysis in comparison with the parental cell line, UM-SCC-17A (***$p < 0.001$). Statistical analysis: Mann-Whitney U test was used to compare between p53 wild type and p53 compromised groups, while Student's t-test was used to compare between isogenic derivatives. Means of individual data were used to derive overall means. Error bars represent SEM.

3.1.4. Conclusion

Taken together, the data presented in this section demonstrate a marked highly active mitochondrial function in cell lines expressing wild type p53, whether that be endogenous or exogenously driven. This high mitochondrial activity was observed in the basal levels and also following induction of spare respiratory capacity by uncoupling ATP synthesis from the ETC (Figures 3.4., 3.8., 3.10., 3.14.). On the other hand, cells that express compromised p53 function, including p53-null, mutant or wild type p53 knockdown, consistently exhibited a distinct metabolic phenotype (which clearly resembles that described by Warburg) to that of wild type *TP53* cell lines, with lower active mitochondrial function and greater levels of glycolysis (Figures 3.6., 3.9., 3.12., 3.15.). It is noteworthy that no marked differences were observed in glycolytic capacity and reserves based on p53 status (Figures 3.7., 3.9., 3.13., 3.15.). These findings clearly link p53 function to the maintenance of metabolic diversity and robust mitochondrial function, with levels of glycolytic reserves comparable to those shown in cells that express compromised p53 function which show a greater dependence on glycolysis.

Interestingly, the data also show that cells with partially-functional mutant p53 (C176F) maintained relatively robust mitochondrial function (Figures 3.4., 3.5.). These cells also exhibit more active glycolytic function than wild type p53 cells and exhibit comparable levels of activity to the glycolytic function observed in cells with both p53-null and GOF mutant p53 (Figures 3.6., 3.7.). This indicates that the robust mitochondrial function in SCCHN cells is substantially linked to functional p53, whereas the switch toward aerobic glycolysis is a result of loss of wild type p53 function rather than any oncogenic GOF properties possessed by a specific *TP53* mutation. These findings were consistent with data obtained from p53-null cells forcibly expressing wild type p53 (Figures 3.5., 3.7.) and wild type p53 cells that stably expressing short-hairpin RNA specific for p53 (Figures 3.8., 3.9.).

Evaluating the balance between mitochondrial respiration and glycolysis in this panel of SCCHN cell line and by ascribing to each cell line a value derived from the ratio of normalised basal glycolysis/basal respiration, as a simplified depiction of the Warburg effect, results in clear dichotomisation of cells into a p53 wild type and p53 compromised groups. These results together provided clear proof of the importance of *TP53* status as a determinant of the metabolic phenotype in SCCHN. As discussed in 1.3.4., despite a recent trend in cancer research to investigate the metabolic pathways as potential targets for improving the therapeutic response in cancer, metabolic studies of SCCHN remain few and are generally relatively simplified with a limited tendency to investigate the link between the metabolic phenotype and major oncogenic events, such as loss of p53 function (323–326). Thus, the results presented in this section contribute to an improved understanding of an important process in head and neck carcinogenesis.

3.2. Investigation of the potential role of TIGAR in the regulation of SCCHN metabolism

3.2.1. Introduction

As discussed in 1.3.2., loss of function of wild type p53 is one of the most common and critical oncogenic events. p53 function includes direct regulatory effects on mitochondrial respiration and glycolytic activity, as well as interaction with several other important metabolic mediating pathways involving a number of target genes, discussed in 1.3.2. However, contradictory findings from studies on the role of p53 in metabolic regulation in different types of cancers indicate that p53 does not function in the same manner in all tissues or cancers that arise from them (see section 1.3.2.). This suggests that p53-mediated metabolic regulation is tissue-specific, which emphasise the importance of the cancer-specific study of metabolic perturbations.

As demonstrated in 3.1, loss of function of wild type p53 contributes to the acquisition of a glycolytic "Warburg" phenotype at the expense of mitochondrial respiration in SCCHN. However, the exact mechanisms of action by which p53 regulates the balance between mitochondrial respiration and glycolytic activity, as well as how the loss of function of the wild type p53 may promote the switch toward glycolysis in SCCHN tumour cells, are still not fully understood. To investigate the mechanisms through

which p53 influences the metabolic balance, a strategy involving the identification of candidate mediators, from the literature, that could subsequently be manipulated by either RNAi or ectopic expression was employed. The hypothesis being that in so doing, it might be possible to identify p53 target genes responsible for the p53-mediated regulation of metabolism. The goal being to gain insights into the role of p53 function and loss of function in regulating the Warburg effect.

As mentioned in 1.3.3., the role of TIGAR in SCCHN tumorigenesis has not received much attention despite the close regulatory relationship between p53 and TIGAR and the number of studies that have reported TIGAR-mediated p53 regulation of metabolic reprogramming in several types of cancer (265). This makes the relationship between p53 and TIGAR in SCCHN an area that looks promising for further investigation.

In our study, a functional genetic approach (RNAi and plasmid expression vector transfection) was used to study the potential role that TIGAR, as a p53 target gene, plays in the metabolic regulation of SCCHN. These techniques have been developed to study the function of genes in cells, providing an opportunity to elucidate the roles of target genes in a specific cellular pathway. RNAi is a rapid method for specifically repressing gene expression, thereby mimicking to some extent the phenotypic effects of a loss-of-function mutation. This provides a useful mean for investigating the critical components of the cellular pathway. Plasmid DNA transfection is a commonly used method for studying gene function in which a plasmid encoding the desired gene is efficiently delivered to the respective cells. Upon delivery to cells, the plasmid DNA reaches the nucleus during cell division, where the respective gene is transcribed and the transient increase in expression of the gene is achieved (327).

3.2.2. Investigation of the metabolic profile of TIGAR-knockdown SCCHN cells

To investigate the potential role of TIGAR in the metabolic regulation of SCCHN, an RNAi technique combined with XF metabolic profiling was used to explore the changes in the mitochondrial and glycolytic function and changes in the metabolic parameters following an efficient transient knockdown of TIGAR in a panel of SCCHN cells, as detailed in 2.4.

Knockdown of TIGAR expression was performed and optimised first using a "smartpool" (Dharmacon) of four siRNAs specific to TIGAR, as detailed in 2.4., before

the two most efficient siRNAs were selected for subsequent experiments. Non-targeting siRNA (siCONT) and siRNA specific to p53, previously used and published by our laboratory (328), were used as negative and positive controls, respectively, in all experiments. Details for all siRNAs used in this study are shown in Table 2.6.

3.2.2.1. TIGAR siRNA optimisation

In brief, cells were seeded at previously optimised densities and incubated at 37°C and 5% CO_2 for 24 hours before being transiently transfected with siRNA using a transfection reagent. First, the duration of transfection was examined to identify the time required to achieve the most efficient inhibition of protein expression of TIGAR. Due to the stability of TIGAR expression (329), SCCHN cells were tested for transfection with a smartpool of four siRNAs specific to TIGAR for 24 and 48 hours. While no marked difference was observed in the efficiency of p53 knockdown (the positive control) after 24 or 48 hours of incubation, western blotting analysis showed that TIGAR knockdown was clearly more efficient after 48 hours of incubation in comparison with 24 hours (Figure 3.17. A1 and A2).

Next, the four siRNA oligonucleotides included in the smartpool of siRNAs were tested separately to identify the two most efficient TIGAR siRNA oligonucleotides after 48 hours of transfection. Western blotting analysis showed that TIGAR knockdown with siRNA oligonucleotides 2 and 3, detailed in Table 2.6., was slightly more efficient than with the other two oligonucleotides, and thus these were selected to be used in subsequent experiments (Figure 3.17. B1 and B2).

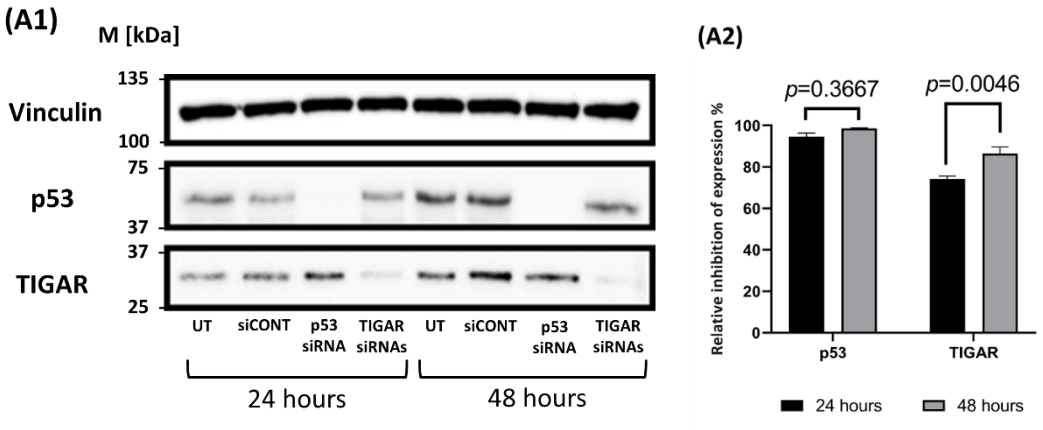

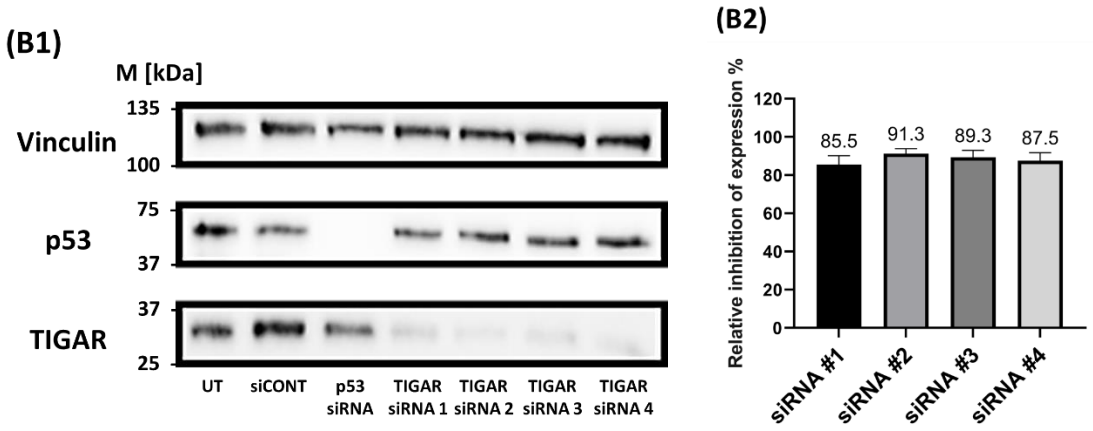

Figure 3.17.: TIGAR knockdown optimisation in SCCHN cells. Western blotting analyses of p53 and TIGAR expression levels in the wild type *TP53* cell line, UMS-CC-11A. Cells were harvested and lysed as described in section 2.8.3. Protein samples were prepared and loaded into gels, and specific antibodies were used for detection as detailed in section 2.1.9. Vinculin was used as a loading control. The migration of protein standards of the indicated approximate molecular weights is shown in kDa. **(A1)** To optimise the duration of transfection, cells were left untransfected, or transfected with either non-target siRNA (siCONT, as a negative control), siRNA specific for p53 (as a positive control) or SMARTpool of siRNAs specific for TIGAR, as described in 2.4., in a final concentration of 25nM. Cells were harvested either 24 hours or 48 hours after transfection. Western blots showed that TIGAR knockdown was clearly more efficient after 48 hours of incubation in comparison with 24 hours. **(B1)** To select TIGAR individual siRNA, cells were left untransfected, or transfected with either non-target siRNA (siCONT, as a negative control), siRNA specific for p53 (as a positive control) or the four siRNA oligonucleotides specific for TIGAR that included in the SMARTpool used in (A1) in a final concentration of 25nM. Cells were harvested 48 hours after transfection, based on results in (A1). Densitometry was used to analyse the expression of p53 and TIGAR as described in 2.8.5. and analyses of three biological replicates is depicted. Relative inhibition of protein expression in A1 and B1, normalised to the expression of the housekeeping protein vinculin in the negative control (%), is shown in (A2) and (B2), respectively. Results in A2 show that the transient knockdown of TIGAR for 48 hours show a marked increase in inhibition of TIGAR expression in comparison with 24 hours. Results in B2 show the percentage of inhibition of each oligonucleotide included in the indicated SMARTpool of siRNAs and were used to select the two most efficient TIGAR siRNA oligonucleotides after 48 hours of transfection. Oligonucleotides are detailed in Table 2.6.

3.2.2.2. Metabolic profiling of TIGAR-knockdown SCCHN cells

To identify the metabolic phenotype of TIGAR-knockdown SCCHN cells, Seahorse XFe mitochondrial and glycolytic stress tests were performed, as described in sections 2.3.6.1. and 2.3.6.2., respectively. For each group of cell lines, the TIGAR siRNA concentration was first optimised by transfecting the cells with the specific oligonucleotides previously identified to achieve the most efficient knockdown of TIGAR, as indicated in 3.2.2.1, in final concentrations of 25, 50 or 75 nM. Densitometry

was used then to analyse the expression of TIGAR as described in 2.8.5., and the relative inhibition of TIGAR expression normalised to the expression of housekeeping protein vinculin in the negative control cells was used to identify an optimal concentration for each group of cell lines. The identified optimal concentration was then used in subsequent experiments for the cell line.

Firstly, the wild type p53 cell line UM-SCC-17A was transfected with TIGAR siRNA in final concentrations of 25, 50 or 75 nM for 48 hours, and western blotting analysis was performed to identify an optimal siRNA concentration (Figure 3.18. A1). Densitometry showed the final concentrations of 75nM to be an optimal concentration of siRNA to knockdown TIGAR in UM-SCC-17A (Figure 3.18. A2).

Next, the two oligonucleotides, previously identified to achieve the most efficient knockdown of TIGAR, were used in a final concentration of 75nM to achieve a transient inhibition of TIGAR expression before Seahorse XFe metabolic profiling was performed as previously described in sections 2.4.6.1. and 2.4.6.2. Western blotting analysis was performed to verify TIGAR knockdown (Figure 3.18. B1), and densitometry was used to measure the inhibition in TIGAR expression (Figure 3.18. B2). Although Figure 3.3. shows that stably knockdown of p53 in UMSCC-17A exhibit less levels of TIGAR expression when compared to parental wild type p53 cells, no similar effect on TIGAR expression was observed in transient knockdown of p53 (Figure 3.18.).

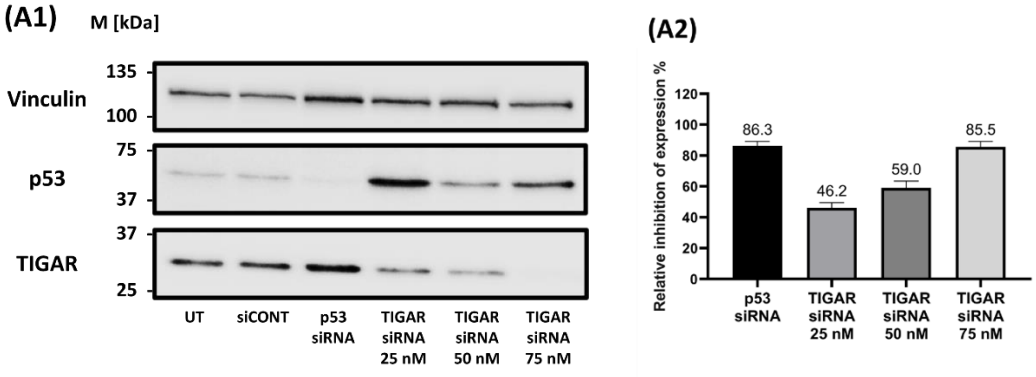

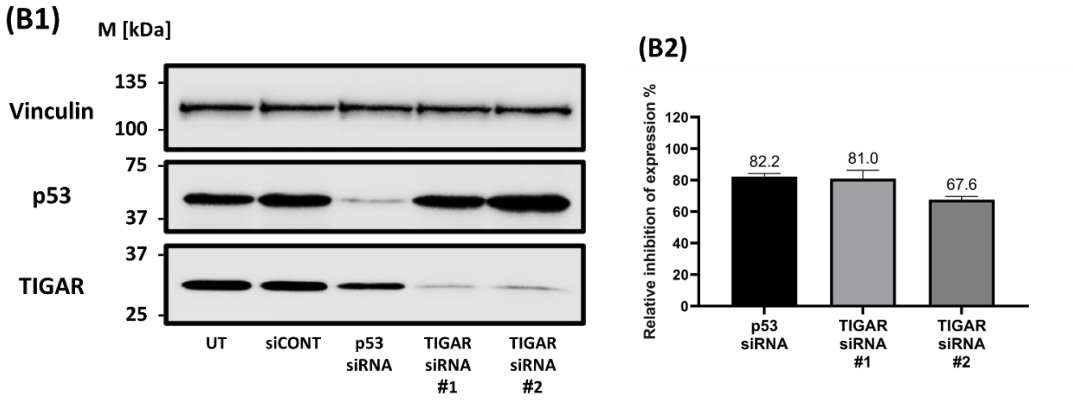

Figure 3.18.: TIGAR knockdown in UM-SCC-17A cells. Western blotting analyses of p53 and TIGAR expression levels in the wild type *TP53* cell line, UMS-CC-17A. Cells were harvested and lysed as described in section 2.8.3. Protein samples were prepared and loaded into gels, and specific antibodies were used for detection as detailed in section 2.1.9. Vinculin was used as a loading control. The migration of protein standards of the indicated approximate molecular weights is shown in kDa. **(A1)** To optimise TIGAR siRNA concentration, cells were left untransfected or transfected with either non-target siRNA (siCONT, as a negative control), siRNA specific for p53 (as a positive control) in a final concentration of 25nM or TIGAR-specific siRNA selected in 3.2.2.1. in final concentrations of 25, 50 or 75nM. Cells were harvested 48 hours after transfection. Results show that a final concentration of 75nM was an optimal concentration of siRNA to knockdown TIGAR in UM-SCC-17A. **(B1)** To verify TIGAR knockdown for metabolic studies of UM-SCC-17A, cells were left untransfected or transfected with either non-target siRNA (siCONT, as a negative control), siRNA specific for p53 (as a positive control) in a final concentration of 25nM or the two siRNA oligonucleotides specific for TIGAR in a final concentration of 75nM. The final concentration of TIGAR siRNA was selected based on results in 3.2.2.2.1. A1. Cells were harvested 48 hours after transfection. Results show significant inhibition of TIGAR expression in TIGAR siRNA 1 and TIGAR siRNA 2 groups. For both (A1) and (B1), densitometry was used to analyse the expression of p53 and TIGAR as described in 2.8.5. and analyses of three biological replicates is depicted. Relative inhibition of protein expression in A1 and B1, normalised to the expression of the housekeeping protein vinculin in the negative control cells (%), is presented in **(A2)** and **(B2)**, respectively. Oligonucleotides are detailed in Table 2.6.

To investigate the role of TIGAR in the metabolic regulation of UM-SCC-17A, the metabolic profiling of untransfected cells and cells transfected with either non-target siRNA, siRNA specific for p53 or TIGAR was performed using Seahorse XFe mitochondrial and glycolytic stress tests, as described in sections 2.3.6.1. and 2.3.6.2.. Outputs from the mitochondrial and glycolytic stress tests are presented in Figures 3.19. and 3.20.

Results of the mitochondrial stress test demonstrate a considerable reduction in the mitochondrial function in p53-knockdown cells at basal levels and following the inhibition of the ATP-linked respiration (at time point A) and uncoupling ATP synthesis

from the ETC (at time point B) when compared to the untransfected and negative control cells, while no significant changes were detected in both groups of TIGAR-knockdown UM-SCC-17A cells (Figure 3.19. panel I). The absolute normalised values of the mitochondrial parameters show a significant decrease in basal respiration, maximal and spare respiratory capacity as well as ATP production in p53-knockdown cells compared to the untransfected and negative control cells. TIGAR-knockdown UM-SCC-17A cells exhibit no significant differences in all mitochondrial parameters in comparison to the untransfected and negative control group (Figure 3.19. panel II).

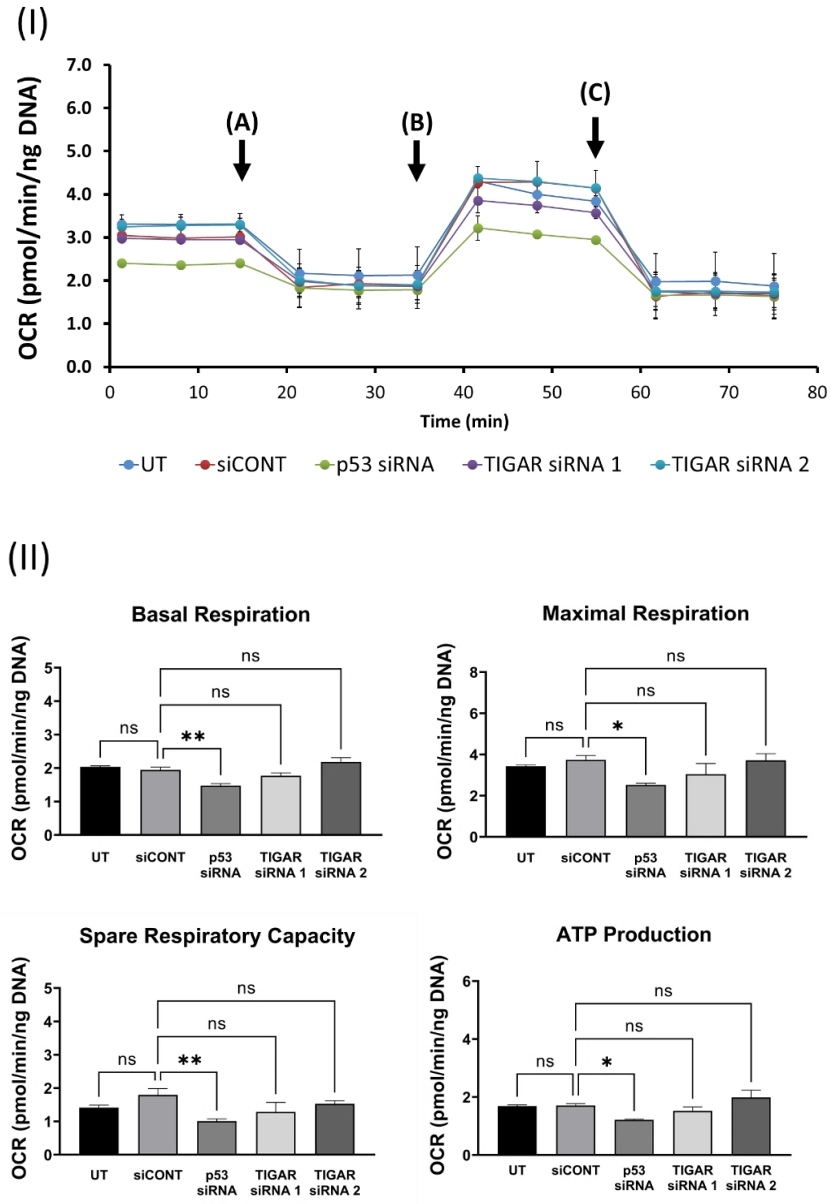

Figure 3.19.: The metabolic profile of TIGAR-knockdown UM-SCC-17A cells in the mitochondrial stress test. (I) Untransfected cells or cells transfected with either non-target siRNA (siCONT), or siRNA specific for p53 or TIGAR were subjected to mitochondrial stress test, as described in 2.3.6.1. Points A, B,

and C on the graphs refer to the injections time points of 1µM oligomycin, 0.5µM FCCP and 1µM rotenone and antimycin-A, respectively. Post-injection changes in the mitochondrial function were used to calculate the mitochondrial respiration parameters as described in Table 2.4. and are shown in Figure 2.4. p53-knockdown cells show a marked decrease in the mitochondrial function at basal levels and following the inhibition of the ATP-linked respiration (at time point A) and uncoupling ATP synthesis from the ETC (at time point B) in comparison to the untransfected or negative control cells. **(II)** Absolute data derived from mitochondrial stress tests was normalised to DNA content for all groups of cells, and the absolute values for basal respiration, maximal respiration, spare respiratory capacity and ATP production were calculated as described in section 2.3.6.1. OCR readings were obtained from three experiments (n=3), each experiment was performed in hextuplet. Data are presented as mean OCR (pmol/min), normalised to DNA content (ng DNA) as described in 2.3.8. Means of individual data were used to derive overall means. Error bars represent SEM. Statistical analysis: a one-way ANOVA with Dunnett's test. (ns) $p > 0.05$, (*) $p \leq 0.05$, (**) $p \leq 0.01$, (***) $p \leq 0.001$, (****) $p \leq 0.0001$.

Results of the glycolytic stress test demonstrate a significant increase in the glycolytic function in p53-knockdown and TIGAR-knockdown UM-SCC-17A cells following the injection of glucose (at time point A) with no marked changes following inhibiting the ATP-linked respiration (at time point B) when compared to the untransfected and negative control cells (Figure 3.20. panel I). The absolute normalised values of the glycolytic parameters show a significant increase in glycolysis in p53-knockdown and TIGAR-knockdown UM-SCC-17A cells compared to the untransfected and negative control cells. No significant differences in glycolytic capacity, glycolytic reserve and non-glycolytic acidification were detected between all groups, Figure 3.20. panel II.

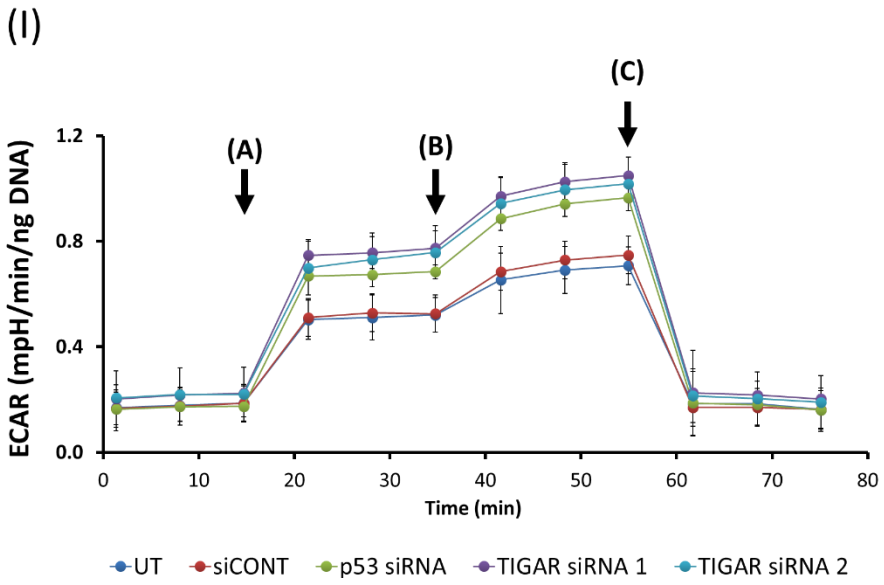

(II)

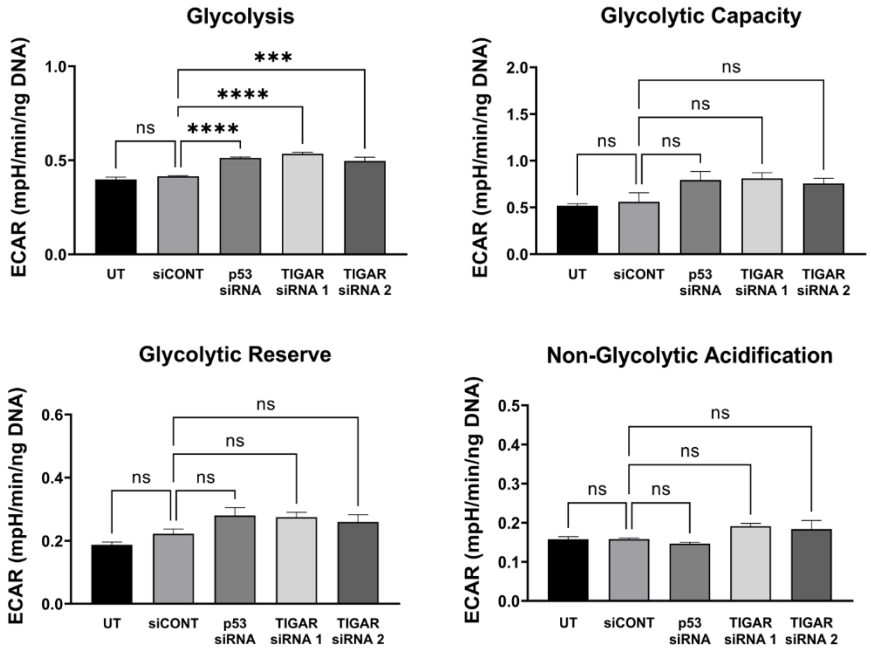

Figure 3.20.: The metabolic profile of TIGAR-knockdown UM-SCC-17A cells in the glycolytic stress test. (I) Untransfected cells or cells transfected with either non-target siRNA (siCONT), or siRNA specific for p53 or TIGAR were subjected to glycolytic stress test, as described in 2.3.6.2. Points A, B, and C on the graphs refer to the injections time points of 10mM glucose, 1μM oligomycin, and 50mM 2-DG, respectively. Post-injection changes in the glycolytic function were used to calculate the glycolytic parameters as described in Table 2.5. and are shown in Figure 2.5. p53-knockdown and TIGAR-knockdown cells show a marked increase in the glycolytic function following the injection of glucose (at time point A) with no marked increase following the inhibition of the ATP-linked respiration (at time point B) in comparison to the untransfected or negative control cells. **(II)** Absolute data derived from glycolytic stress tests was normalised to DNA content for all groups of cells, and the absolute values for glycolysis, glycolytic capacity, glycolytic reserve and non-glycolytic acidification were calculated as described in section 2.3.6.2. ECAR readings were obtained from three experiments (n=3), each experiment was performed in hextuplet. Data are presented as mean ECAR (mpH/min), normalised to DNA content (ng DNA) as described in 2.3.8. Means of individual data were used to derive overall means. Error bars represent SEM. Statistical analysis: a one-way ANOVA with Dunnett's test. (ns) $p > 0.05$, (*) $p \leq 0.05$, (**) $p \leq 0.01$, (***) $p \leq 0.001$, (****) $p \leq 0.0001$.

These results from transient p53-knockdown in UM-SCC-17A cells are consistent with the previously presented results of the stable p53-knockdown UM-SCC-17A cells, shown in Figures 3.8. and 3.9. (discussed in section 3.1.3.), which show lower respiratory activity and higher glycolytic activity than the parental cell line. Although the metabolic profiling of TIGAR-knockdown UM-SCC-17A cells exhibits similar glycolytic function to the p53-knockdown, no significant effects were observed for

TIGAR knockdown on mitochondrial function. To explore the effect of TIGAR knockdown on the balance between glycolysis and mitochondrial respiration in UM-SCC-17A, we used the same method we used previously in section 3.1.3., combining analysis of measurements of glycolysis and of respiratory activity by ascribing to each group of cells a value derived from the ratio of basal glycolysis/basal respiration. The results showed a significant increase in the ratio of basal glycolysis/basal respiration following the knockdown of p53 in wild type p53 cell line UM-SCC-17A, which is consistent with outcomes previously discussed in 3.1.3.14. However, only one group of the TIGAR-knockdown cells show a slightly significant increase in this ratio, displaying a phenotype in line with the Warburg effect, while the other group show no significant difference when compared to the untransfected or the negative control groups (Figure 3.21.). This suggests that although the knockdown of TIGAR significantly increases glycolysis in the presence of wild type p53, it has a less significant impact on the balance between glycolysis and mitochondrial respiration than, for example, does p53, which might be explained by the highly active mitochondrial function of the wild type p53 cells when compared to the less active glycolytic function.

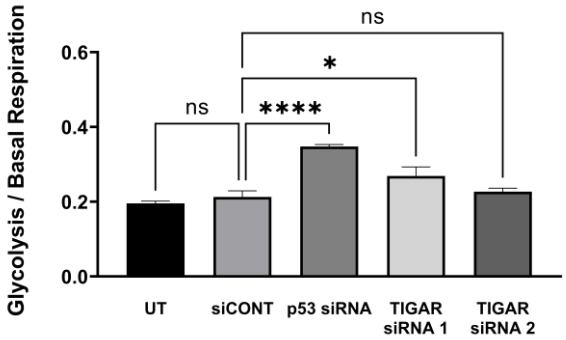

Figure 3.21.: Warburg effect in TIGAR-knockdown UM-SCC-17A cells. The Warburg effect is indicated by ascribing to each group of cells a value derived from the ratio of glycolysis/basal respiration. This ratio shows a significant effect of p53 knockdown on the balance between glycolysis and mitochondrial respiration, which indicates an increased dependence on glycolysis. Means of individual data were used to derive overall means. Error bars represent SEM. Statistical analysis: a one-way ANOVA with Dunnett's test. (ns) $p > 0.05$, (*) $p \leq 0.05$, (**) $p \leq 0.01$, (***) $p \leq 0.001$, (****) $p \leq 0.0001$.

These studies were followed up, by investigating the effects of TIGAR knockdown on the metabolic phenotype of another wild type p53 cell line UM-SCC-11A, which previously showed a distinct metabolic profile (Figure 3.11. and Figure 3.13.). This cell line has exhibited remarkably active mitochondrial function and only a limited dependence on glycolysis when compared to all SCCHN cell lines included in this study,

which may provide a clear image of the possible impacts of TIGAR knockdown on the metabolic profile of wild type p53 SCCHN cells, given the known involvement of TIGAR as a third-step regulator in the glycolytic pathway and the intrinsically low levels of glycolysis in UM-SCC-11A cells, which may make changes in the glycolytic function of UM-SCC-11A more readily detectable.

The wild type p53 cell line UM-SCC-11A was transfected with TIGAR siRNA in final concentrations of 25, 50 or 75 nM for 48 hours, and western blotting analysis was then performed to identify an optimal siRNA concentration (Figure 3.22. A1). Densitometry showed that a final concentration of 50nM is an optimal concentration of siRNA to achieve knockdown of TIGAR in UM-SCC-11A (Figure 3.22. A2).

Next, the two oligonucleotides, previously identified to achieve the most efficient knockdown of TIGAR, were used in a final concentration of 50nM to achieve a transient inhibition of TIGAR expression before Seahorse XFe metabolic profiling was performed as previously described in sections 2.3.6.1. and 2.3.6.2. Western blotting analysis was performed to verify TIGAR knockdown (Figure 3.22. B1), and densitometry was used to measure the inhibition of TIGAR expression (Figure 3.22. B2).

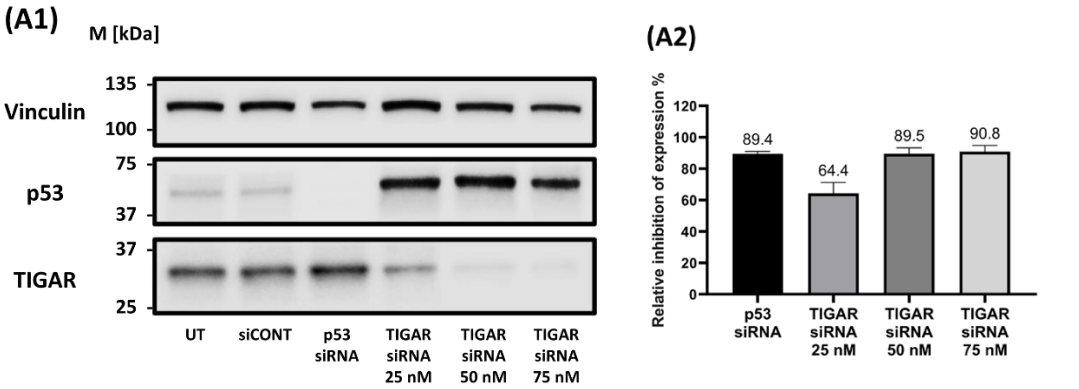

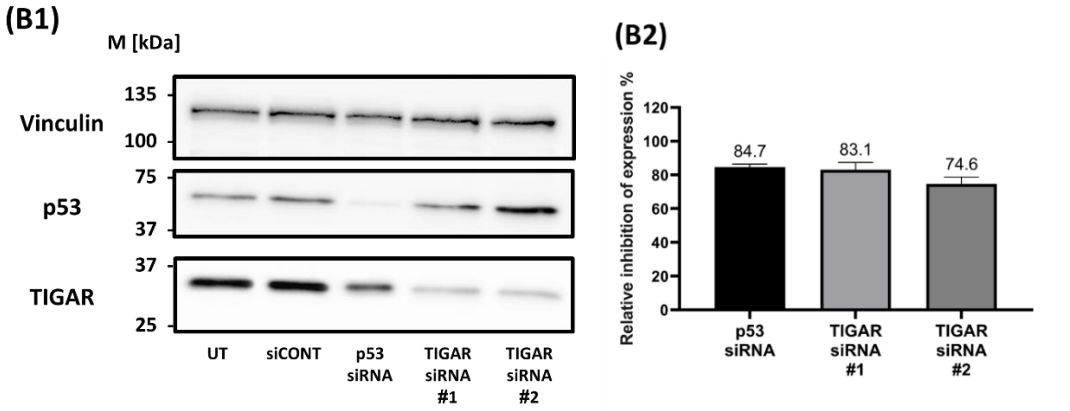

Figure 3.22.: TIGAR knockdown in UM-SCC-11A cells. Western blotting analyses of p53 and TIGAR expression levels in the wild type *TP53* cell line, UMS-CC-11A. Cells were harvested and lysed as described in section 2.8.3. Protein samples were prepared and loaded into gels, and specific antibodies were used for detection as detailed in section 2.1.9. Vinculin was used as a loading control. The migration of protein standards of the indicated approximate molecular weights is shown in kDa. **(A1)** To optimise TIGAR siRNA concentration, cells were left untransfected or transfected with either non-target siRNA (siCONT, as a negative control), siRNA specific for p53 (as a positive control) in a final concentration of 25nM or TIGAR-specific siRNA selected in 3.2.2.1. in final concentrations of 25, 50 or 75nM. Cells were harvested 48 hours after transfection. Results show that a final concentration of 50nM was an optimal concentration of siRNA to knockdown TIGAR in UM-SCC-11A. **(B1)** To verify TIGAR knockdown for metabolic studies of UM-SCC-11A, cells were left untransfected or transfected with either non-target siRNA (siCONT, as a negative control), siRNA specific for p53 (as a positive control) in a final concentration of 25nM or two siRNA oligonucleotides specific for TIGAR, in a final concentration of 50nM. The concentration of TIGAR siRNA used was selected based on results in 3.2.2.2.5 (A1). Cells were harvested 48 hours after transfection. Results show significant inhibition of TIGAR in TIGAR siRNA 1 and TIGAR siRNA 2 groups. For both (A1) and (B1), densitometry was used to analyse the expression of p53 and TIGAR as described in 2.8.5. and analyses of three biological replicates is depicted. Relative inhibition of protein expression in A1 and B1, normalised to the expression of the housekeeping protein vinculin in the negative control cells (%), is shown in **(A2)** and **(B2)**, respectively. Oligonucleotides are detailed in Table 2.6.

To investigate the role of TIGAR in the metabolic regulation of UM-SCC-11A, the metabolic profiling of untransfected cells and cells transfected with either non-target siRNA, siRNA specific for p53 or TIGAR was performed using Seahorse XFe mitochondrial and glycolytic stress tests, as described in sections 2.3.6.1. and 2.3.6.2.. Outputs from the mitochondrial stress test and glycolytic stress tests are presented in Figures 3.23. and 3.24.

Results of the mitochondrial stress test demonstrated a considerable reduction in the mitochondrial function in p53-knockdown cells at basal levels and following the inhibition of ATP-linked respiration (at time point A) and uncoupling ATP synthesis

from the ETC (at time point B) when compared to the untransfected and negative control cells, while no significant changes were detected in both groups of TIGAR-knockdown UM-SCC-11A cells (Figure 3.23. panel I). The absolute normalised values of the mitochondrial parameters show a significant decrease in basal respiration, maximal and spare respiratory capacity as well as ATP production in p53-knockdown cells compared to the untransfected and negative control group. TIGAR-knockdown UM-SCC-11A cells exhibit no significant differences in all mitochondrial parameters in comparison to the untransfected and negative control group (Figure 3.23. panel II).

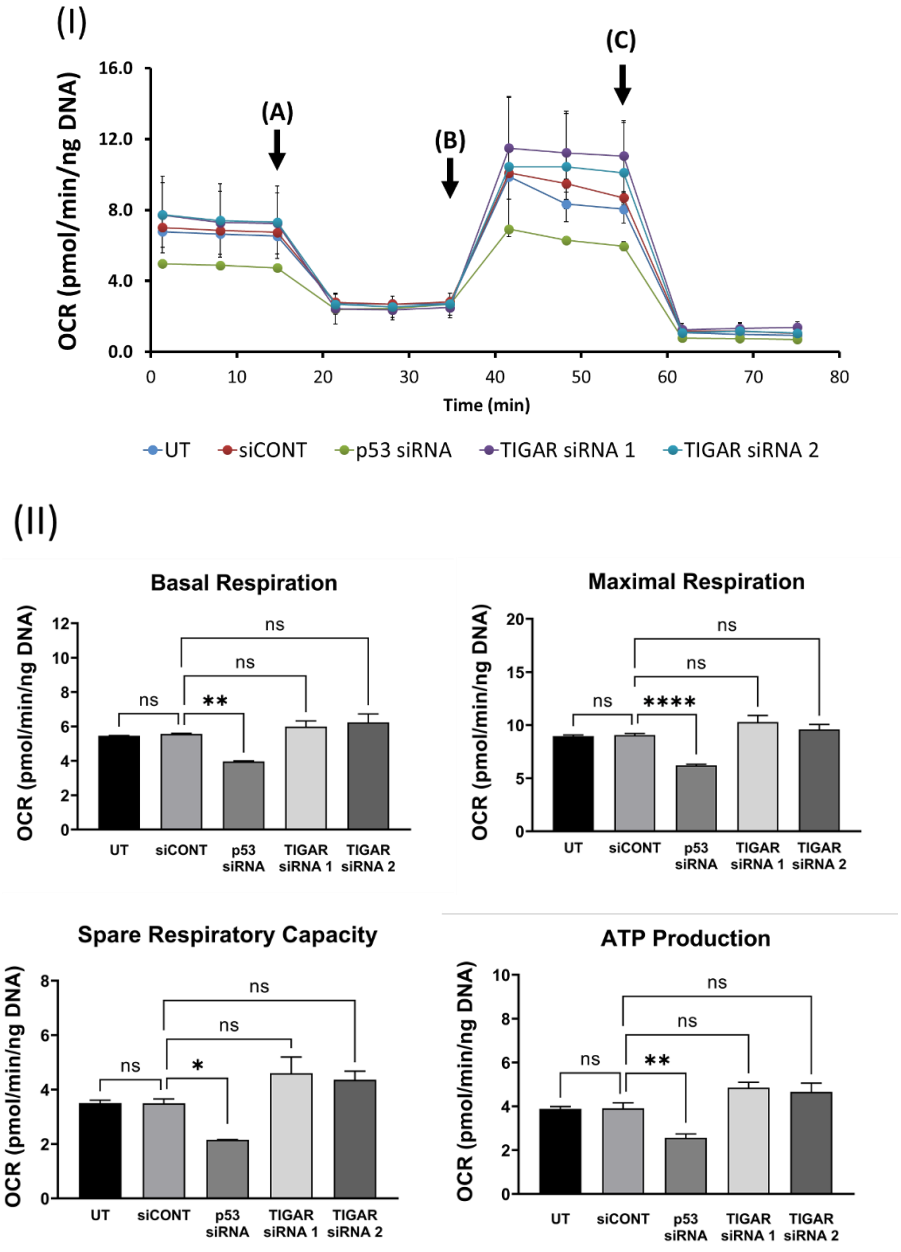

Figure 3.23.: The metabolic profile of TIGAR-knockdown UM-SCC-11A cells in the mitochondrial stress test. (I) Untransfected cells or cells transfected with either non-target siRNA (siCONT), or siRNA

specific for p53 or TIGAR were subjected to mitochondrial stress test, as described in 2.3.6.1. Points A, B, and C on the graphs refer to the injections time points of 1μM oligomycin, 0.5μM FCCP and 1μM rotenone and antimycin-A, respectively. Post-injection changes in the mitochondrial function were used to calculate the mitochondrial respiration parameters as described in Table 2.4. and are shown in Figure 2.4. p53-knockdown cells show a marked decrease in the mitochondrial function at basal levels and following the inhibition of the ATP-linked respiration (at time point A) and uncoupling ATP synthesis from the ETC (at time point B) in comparison to the untransfected or negative control cells. **(II)** Absolute data derived from mitochondrial stress tests was normalised to DNA content for all groups of cells, and the absolute values for basal respiration, maximal respiration, spare respiratory capacity and ATP production were calculated as described in section 2.3.6.1. OCR readings were obtained from three experiments (n=3), each experiment was performed in hextuplet. Data are presented as mean OCR (pmol/min), normalised to DNA content (ng DNA) as described in 2.3.8. Means of individual data were used to derive overall means. Error bars represent SEM. Statistical analysis: a one-way ANOVA with Dunnett's test. (ns) $p > 0.05$, (*) $p \leq 0.05$, (**) $p \leq 0.01$, (***) $p \leq 0.001$, (****) $p \leq 0.0001$.

Results of the glycolytic stress test demonstrated a significant increase in the glycolytic function in p53-knockdown and TIGAR-knockdown UM-SCC-11A cells following the injection of glucose (at time point A) with no marked changes following inhibition of ATP-linked respiration (at time point B) when compared to the untransfected and negative control cells (Figure 3.24. panel I). The absolute normalised values of the glycolytic parameters show a significant increase in glycolysis in p53-knockdown and TIGAR-knockdown UM-SCC-11A cells compared to the untransfected and negative control cells. No significant differences in glycolytic capacity, glycolytic reserve and non-glycolytic acidification were detected between all groups (Figure 3.24. panel II).

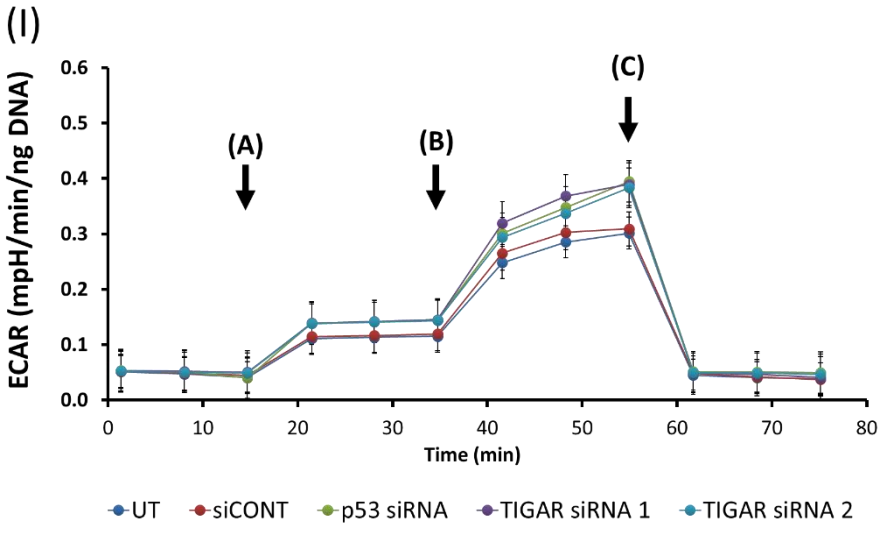

(II)

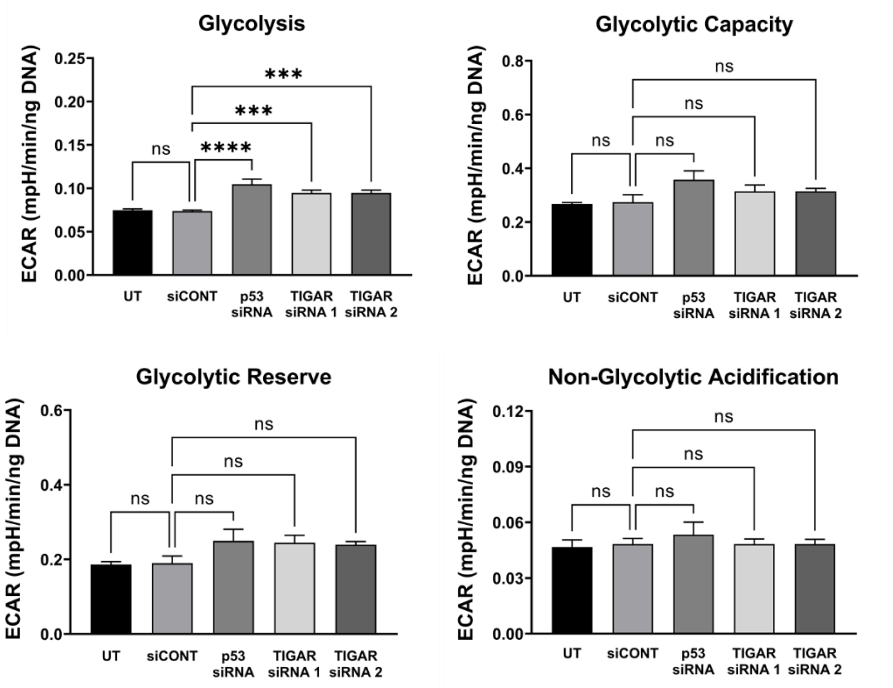

Figure 3.24.: The metabolic profile of TIGAR-knockdown UM-SCC-11A cells in the glycolytic stress test. (I) Untransfected cells or cells transfected with either non-target siRNA (siCONT), or siRNA specific for p53 or TIGAR were subjected to glycolytic stress test, as described in 2.4.6.2. Points A, B, and C on the graphs refer to the injections time points of 10mM glucose, 1μM oligomycin, and 50mM 2-DG, respectively. Post-injection changes in the glycolytic function were used to calculate the glycolytic parameters as described in Table 2.5. and are shown in Figure 2.5. p53-knockdown and TIGAR-knockdown cells show a marked increase in the glycolytic function following the injection of glucose (at time point A) with no marked increase following the inhibition of the ATP-linked respiration (at time point B) in comparison to the untransfected or negative control cells. **(II)** Absolute data derived from glycolytic stress tests was normalised to DNA content for all groups of cells, and the absolute values for glycolysis, glycolytic capacity, glycolytic reserve and non-glycolytic acidification were calculated as described in section 2.3.6.2. ECAR readings were obtained from three experiments (n=3), each experiment was performed in hextuplet. Data are presented as mean ECAR (mpH/min), normalised to DNA content (ng DNA) as described in 2.3.8. Means of individual data were used to derive overall means. Error bars represent SEM. Statistical analysis: a one-way ANOVA with Dunnett's test. (ns) $p > 0.05$, (*) $p \leq 0.05$, (**) $p \leq 0.01$, (***) $p \leq 0.001$, (****) $p \leq 0.0001$.

Results of the metabolic profiling of p53-knockdown UM-SCC-11A cells were consistent with the previously demonstrated results of the p53-knockdown and TIGAR-knockdown UM-SCC-17A cells, discussed in Figures 3.19. and 3.20., which showed lower respiratory activity and higher glycolytic activity than the untransfected and the negative control group. Although the metabolic profiling of TIGAR-knockdown UM-SCC-11A exhibits similar glycolytic function to the p53-knockdown, no significant

effects were observed for TIGAR knockdown on the mitochondrial function. In addition, TIGAR knockdown shows no significant changes in glycolytic capacity and reserves despite the low glycolytic function these cells exhibit (see Figure 3.13.), which is consistent with previous findings in UM-SCC-17A cells about a limited role for TIGAR in changing glycolytic capacity and reserves in the presence of wild type p53 (see Figure 3.20.). To explore the effect of TIGAR on the balance between glycolysis and mitochondrial respiration in UM-SCC-11A, we used the same method we used previously in section 3.1.3., combining analysis of measurements of glycolysis and of respiratory activity by ascribing to each group of cells a value derived from the ratio of basal glycolysis/basal respiration. Results showed a significant increase in the ratio of basal glycolysis/basal respiration following the knockdown of p53 in UM-SCC-11A cells, which is consistent with outcomes previously discussed in 3.1.3.11 and in 3.2.2.2.4. However, both groups of the TIGAR-knockdown cells show no significant difference in this ratio when compared to the untransfected or the negative control group (Figure 3.25.).

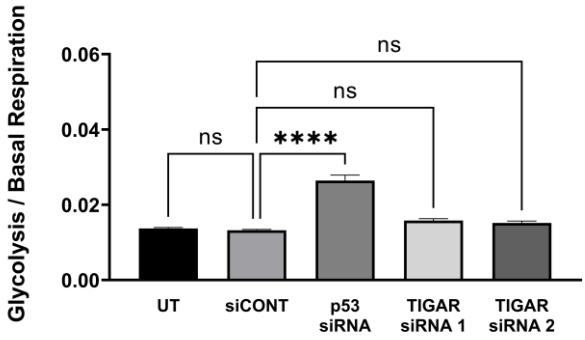

Figure 3.25.: Warburg effect in TIGAR-knockdown UM-SCC-11A cells. The Warburg effect is indicated by ascribing to each group of cells a value derived from the ratio of glycolysis/basal respiration. This ratio shows a significant effect of p53 knockdown on the balance between glycolysis and mitochondrial respiration, which indicates an increased dependence on glycolysis. Means of individual data were used to derive overall means. Error bars represent SEM. Statistical analysis: a one-way ANOVA with Dunnett's test. (ns) $p > 0.05$, (*) $p \leq 0.05$, (**) $p \leq 0.01$, (***) $p \leq 0.001$, (****) $p \leq 0.0001$.

Although these results show that TIGAR knockdown significantly increases glycolysis in the presence of wild type p53, TIGAR has less impact on the balance between glycolysis and mitochondria respiration in the presence of wild type p53. These findings do not show whether this is due to the highly active mitochondria function of the wild type p53 cells, which requires a very high increase in glycolysis function to

show a significant impact on the balance between the two functions, or due to the pivotal role that p53 plays in TIGAR regulation.

To determine whether the absence of an effect of TIGAR knockdown on the Warburg phenotype is due to the p53-promoted robust mitochondrial metabolic activity or due to the role of wild type p53 in regulating TIGAR, experiments were performed comparing the metabolic phenotype of TIGAR-knockdown UM-SCC-11A cells with another cell line UM-SCC-11B, which harbours a C242S missense mutation in the *TP53* gene that results in loss-of-function of p53 (316,330,331). Both cell lines are derived from the same patient and are thus, substantially isogenic (294,332,333). UM-SCC-11A was derived from a biopsy of primary laryngeal carcinoma, while UM-SCC-11B was cultured from a laryngectomy specimen of the same patient following chemotherapy (295). As shown previously, these two cell lines demonstrated two distinct metabolic phenotypes. UM-SCC-11A has the highest mitochondrial function and the lowest glycolytic function among the cell lines tested in this study. On the other hand, UM-SCC-11B showed a low mitochondrial function and a high glycolytic function, Figure 3.11. and Figure 3.13. This can be clearly seen through the ratio between glycolysis to mitochondrial respiration in the two cell lines, where UM-SCC-11A cells showed the lowest ratio among the cell lines used in the study (0.0112±0.003), while the UM-SCC-11B has the highest ratio (1±0.18)(Figure 3.16.).

Seahorse XFe metabolic profiling was performed as previously described in sections 2.3.6.1. and 2.3.6.2. Western blotting analysis was performed to verify TIGAR knockdown (Figure 3.26. A), and densitometry was used to measure the inhibition in TIGAR expression (Figure 3.26. B).

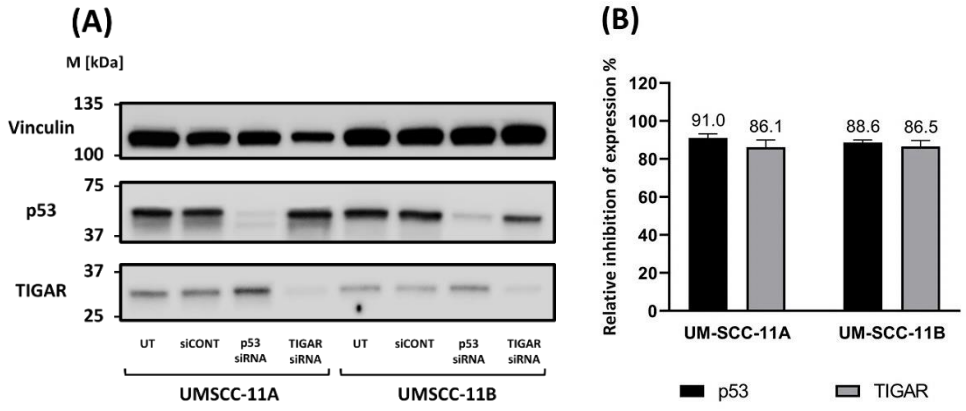

Figure 3.26.: TIGAR knockdown in UM-SCC-11A and UM-SCC-11B cells. Western blotting analyses of p53 and TIGAR expression levels in the wild type *TP53* cell line, UMS-CC-11A and the mutant *TP53* cell line,

UMS-CC-11B. Cells were harvested and lysed as described in section 2.8.3. Protein samples were prepared and loaded into gels, and specific antibodies were used for detection as detailed in section 2.1.9. Vinculin was used as a loading control. The migration of protein standards of the indicated approximate molecular weights is shown in kDa. **(A)** To verify TIGAR knockdown for metabolic studies of UM-SCC-11A and UM-SCC-11B, cells were left untransfected or transfected with either non-target siRNA (siCONT, as a negative control), siRNA specific for p53 (as a positive control) in a final concentration of 25nM or siRNA oligonucleotide specific for TIGAR in a final concentration of 50nM. Cells were harvested 48 hours after transfection. Results show marked inhibition of TIGAR in TIGAR siRNA groups. Densitometry was used to analyse the expression of p53 and TIGAR as described in 2.8.5. and analyses of three biological replicates is depicted. Relative inhibition of protein expression in (A), normalised to the expression of the housekeeping protein vinculin in the negative control cells (%), is shown in **(B)**. Oligonucleotides are detailed in Table 2.6.

Results of the mitochondrial stress test demonstrated a considerable reduction in the mitochondrial function in p53-knockdown cells at basal levels and following the inhibition of the ATP-linked respiration (at time point A) and uncoupling ATP synthesis from the ETC (at time point B) when compared to the untransfected and negative control cells, while no significant changes were detected in TIGAR-knockdown UM-SCC-11A cells, the wild type p53 cell line. No marked changes are shown between all groups in UM-SCC-11B cells, the mutant p53 cell line (Figure 3.27. panel I). The absolute normalised values of the mitochondrial parameters show a significant decrease in basal respiration, maximal and spare respiratory capacity as well as ATP production in p53-knockdown UM-SCC-11A cells in comparison to the untransfected and negative control group, while TIGAR-knockdown UM-SCC-11A cells exhibit no significant differences in all mitochondrial parameters. On the other hand, the data show no significant differences in all groups of UM-SCC-11B cells (Figure 3.27. panel II).

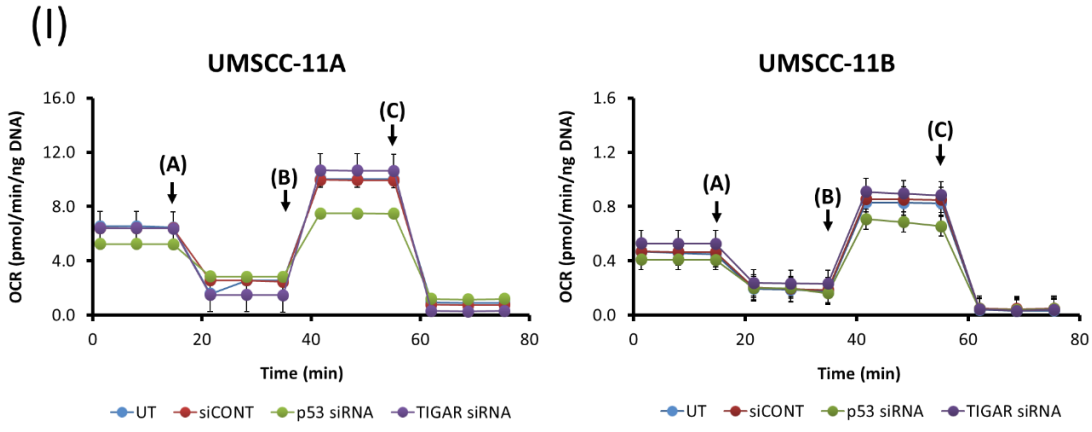

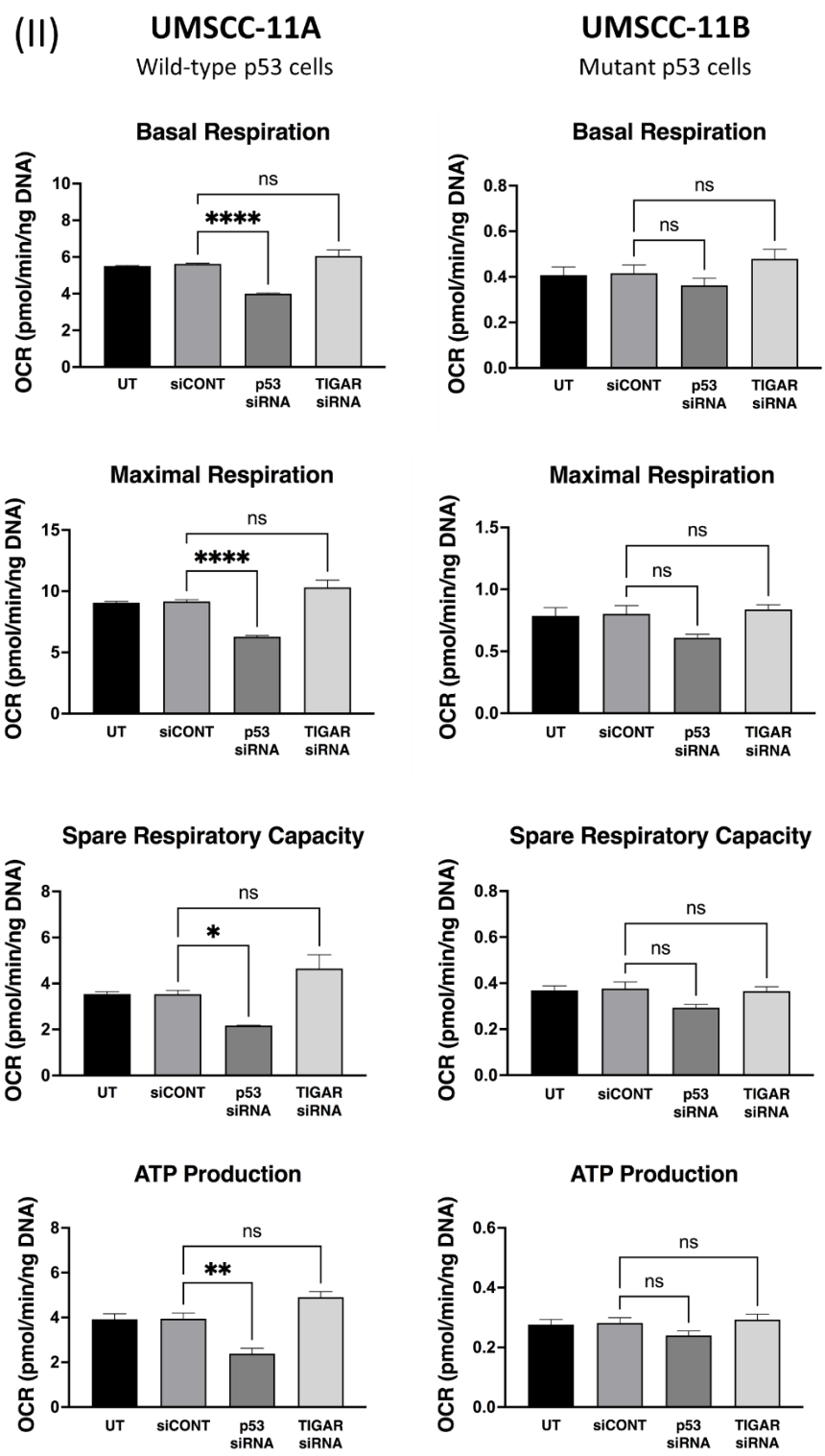

Figure 3.27.: Comparative metabolic profile of TIGAR-knockdown UM-SCC-11A and UM-SCC-11B cells in the mitochondrial stress test. (I) Untransfected cells or cells transfected with either non-target siRNA (siCONT), or siRNA specific for p53 or TIGAR were subjected to mitochondrial stress test, as described in 2.3.6.1. Points A, B, and C on the graphs refer to the injections time points of 1μM oligomycin, 0.5μM FCCP and 1μM rotenone and antimycin-A, respectively. Post-injection changes in the mitochondrial function were used to calculate the mitochondrial respiration parameters as described in Table 2.4. and are shown in Figure 2.4. p53-knockdown cells show a marked decrease in the mitochondrial function at

basal levels and following the inhibition of the ATP-linked respiration (at time point A) and uncoupling ATP synthesis from the ETC (at time point B) in comparison to the untransfected, negative control or TIGAR-knockdown cells in UM-SCC-11A, while no marked changes in the mitochondrial stress test between all groups in UM-SCC-11B. **(II)** Absolute data derived from mitochondrial stress tests was normalised to DNA content for all groups of cells, and the absolute values for basal respiration, maximal respiration, spare respiratory capacity and ATP production were calculated as described in section 2.3.6.1. OCR readings were obtained from three experiments (n=3), each experiment was performed in hextuplet. Data are presented as mean OCR (pmol/min), normalised to DNA content (ng DNA) as described in 2.3.8. Means of individual data were used to derive overall means. Error bars represent SEM. Statistical analysis: a one-way ANOVA with Dunnett's test. (ns) $p > 0.05$, (*) $p \leq 0.05$, (**) $p \leq 0.01$, (***) $p \leq 0.001$, (****) $p \leq 0.0001$.

Results of the glycolytic stress test demonstrated a significant increase in the glycolytic function in p53-knockdown and TIGAR-knockdown UM-SCC-11A cells following the injection of glucose (at time point A) with no marked changes following inhibiting the ATP-linked respiration (at time point B) when compared to the untransfected and negative control cells. Results also show no marked changes between all groups of UM-SCC-11B cells (Figure 3.28. panel I). The absolute normalised values of the glycolytic parameters show a significant increase in glycolysis in p53-knockdown and TIGAR-knockdown UM-SCC-11A cells compared to the untransfected and negative control cells, with no significant differences in glycolytic capacity, glycolytic reserve and non-glycolytic acidification were detected between all conditions. On the other hand, no significant differences were detected in all glycolytic parameters in UM-SCC-11B conditions (Figure 3.28. panel II).

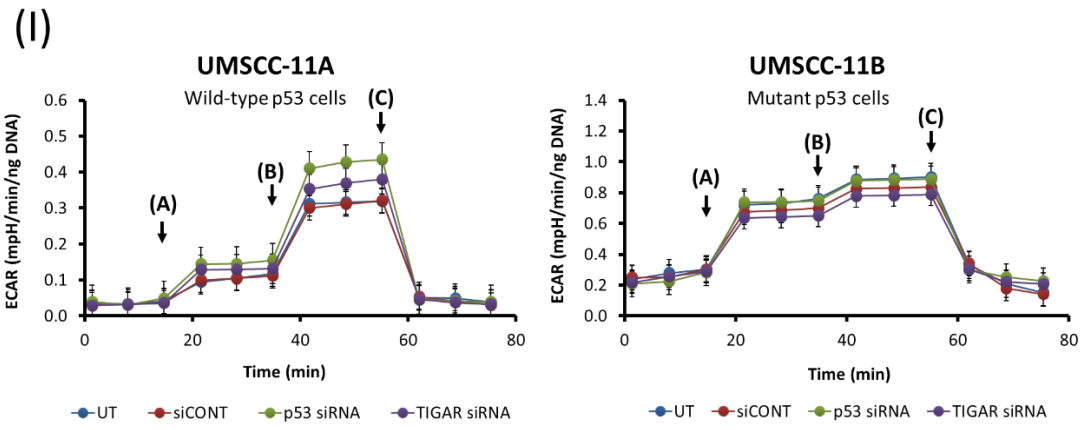

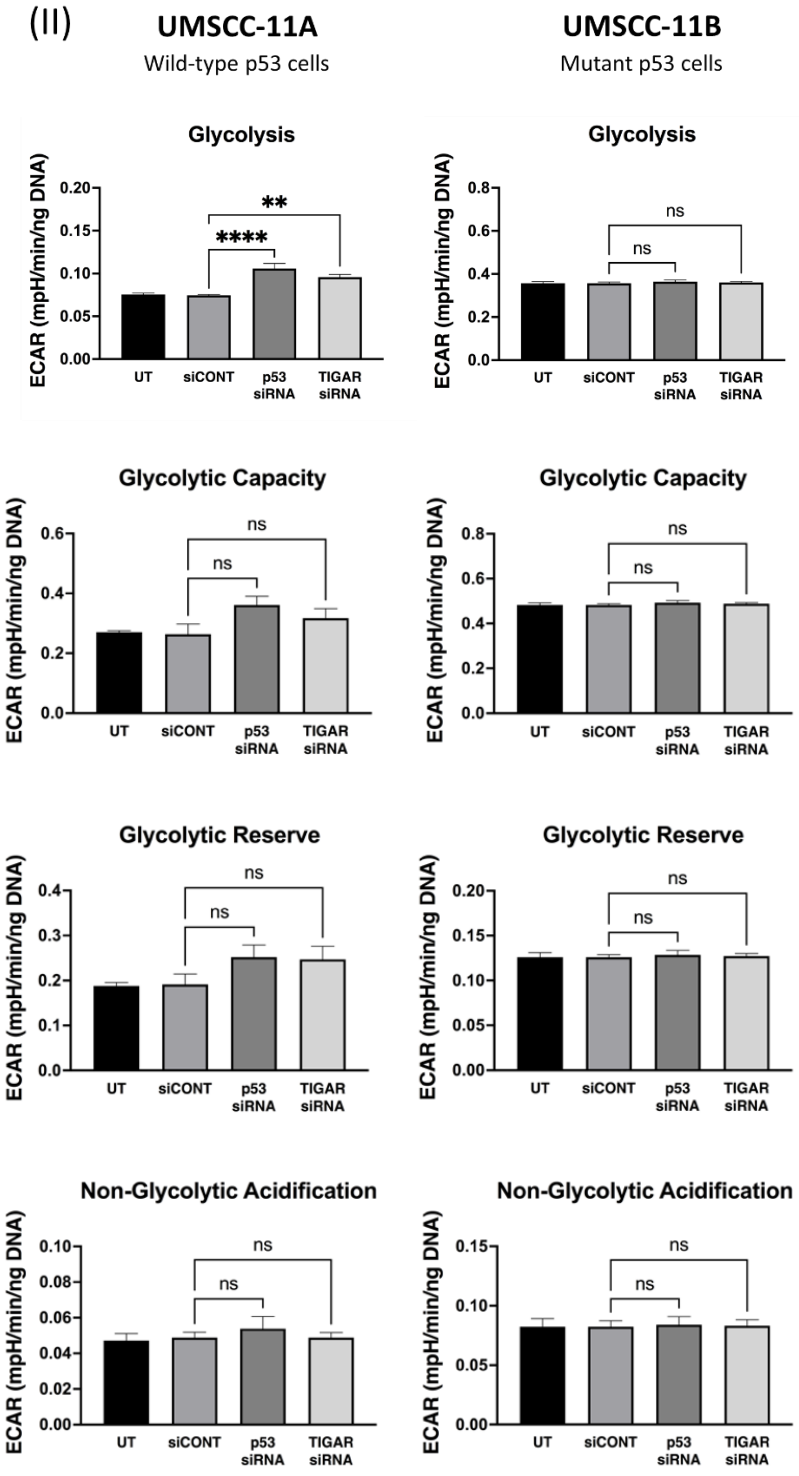

Figure 3.28.: Comparative metabolic profile of TIGAR-knockdown UM-SCC-11A and UM-SCC-11B cells in the glycolytic stress test. (I) Untransfected cells or cells transfected with either non-target siRNA (siCONT), or siRNA specific for p53 or TIGAR were subjected to glycolytic stress test, as described in 2.3.6.2. Points A, B, and C on the graphs refer to the injections time points of 10mM glucose, 1μM oligomycin, and 50mM 2-DG, respectively. Post-injection changes in the glycolytic function were used to calculate the glycolytic parameters as described in Table 2.5. and are shown in Figure 2.5. p53-knockdown and TIGAR-knockdown cells show a marked increase in the glycolytic function following the injection of glucose (at time point A) with no marked increase following the inhibition of the ATP-linked respiration

(at time point B) in comparison to the untransfected or negative control cells in UM-SCC-11A, while no marked changes in the mitochondrial stress test between all groups in UM-SCC-11B. **(II)** Absolute data derived from glycolytic stress tests was normalised to DNA content for all groups of cells, and the absolute values for glycolysis, glycolytic capacity, glycolytic reserve and non-glycolytic acidification were calculated as described in section 2.3.6.2. ECAR readings were obtained from three experiments (n=3), each experiment was performed in hextuplet. Data are presented as mean ECAR (mpH/min), normalised to DNA content (ng DNA) as described in 2.3.8. Means of individual data were used to derive overall means. Error bars represent SEM. Statistical analysis: a one-way ANOVA with Dunnett's test. (ns) $p > 0.05$, (*) $p \leq 0.05$, (**) $p \leq 0.01$, (***) $p \leq 0.001$, (****) $p \leq 0.0001$.

To explore the Warburg effect and to examine the balance between the two functions in UM-SCC-11A and UM-SCC-11B cells following the knockdown of TIGAR as previously, the ratio of basal glycolysis/basal respiration was used. The results showed a significant increase in the ratio of basal glycolysis/basal respiration following the knockdown of p53 in UM-SCC-11A cells, while TIGAR-knockdown cells show no significant difference in this ratio when compared to the untransfected or the negative control cells. On the other hand, UM-SCC-11B cells exhibit no significant differences in this ratio between all conditions (Figure 3.29.).

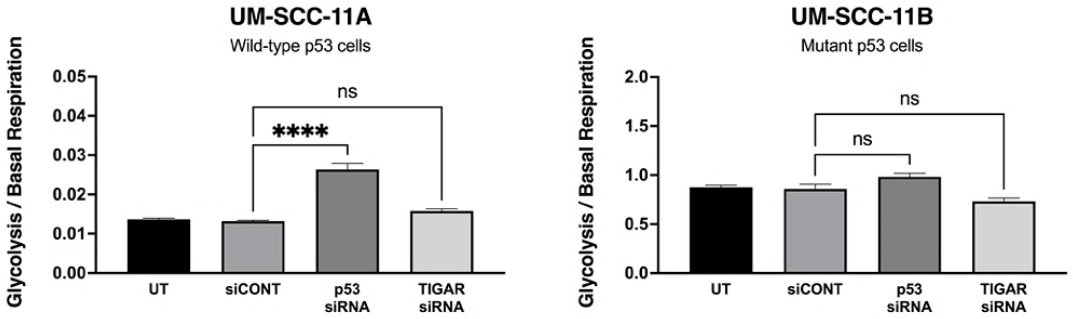

Figure 3.29.: Warburg effect in TIGAR-knockdown UM-SCC-11A and UM-SCC-11B cells. The Warburg effect is indicated by ascribing to each group of cells a value derived from the ratio of glycolysis/basal respiration. This ratio shows a significant effect of p53 knockdown on the balance between glycolysis and mitochondrial respiration, which indicates an increased dependence on glycolysis. Means of individual data were used to derive overall means. Error bars represent SEM. Statistical analysis: a one-way ANOVA with Dunnett's test. (ns) $p > 0.05$, (*) $p \leq 0.05$, (**) $p \leq 0.01$, (***) $p \leq 0.001$, (****) $p \leq 0.0001$.

These results demonstrate that transient knockdown of p53 significantly affects the metabolic profile of wild type p53 cells, while it has no impact in cells harbouring mutant *TP53*. These results also demonstrate no significant effect of TIGAR knockdown on the balance between glycolytic and mitochondrial respiration functions in the

presence of either wild type or mutant p53, supporting the notion that the absence of TIGAR knockdown effects on the balance between glycolytic function and mitochondrial respiration is not due to the high mitochondrial function, as TIGAR knockdown did not result in a significant increase in the glycolysis/mitochondrial respiration ratio in mutant p53 cells also despite the low mitochondrial respiration function in these cells. In addition, TIGAR knockdown markedly increases glycolysis in the presence of wild type p53 it does not produce a similar effect in the presence of mutant p53. this finding accords with other evidence for the pivotal role of p53 in regulating TIGAR as well as the notion that the role of TIGAR in regulating glycolysis is strongly linked to p53 regulatory function.

However, a major limitation of these studies is that they cannot identify whether TIGAR knockdown is inefficient in inducing additional glycolysis in the presence of mutant p53 due to the compromised function of p53, as a TIGAR regulator, or due to the high dependence on glycolysis as an energy source in cells with mutant p53 compared to cells with wild type p53, which makes transient inhibition of TIGAR unable to drive further glycolysis.

To further examine the role of TIGAR in the metabolic phenotype of SCCHN experiments were performed using the p53-null cell line UM-SCC-1 and a range of isogenic derivatives as detailed in section 2.2.1.1. The advantage of using this cell line lies in the complete absence of endogenous p53 function. Thus, the transient inhibition of TIGAR in these cells may provide a clearer and more detailed picture of the role that TIGAR plays in the metabolic balance between mitochondrial respiration and glycolysis in the absence of p53. The forced expression of p53 in the UM-SCC-1 WT-p53 derivative may also support the previously presented findings of the critical role of functional p53 in the regulation of TIGAR and the role TIGAR plays in glycolysis. In addition, the use of derivatives that harbour different missense mutations of *TP53* may provide a more detailed picture of a possible impact of partial retention of p53 function (UM-SCC-1 C176F-p53) and the role of p53 GOF (UM-SCC-1 R175H-p53 and R282W-p53) in the regulation of TIGAR and the role it plays in glycolysis.

Firstly, TIGAR siRNA concentration was optimised by transfecting UM-SCC-1 WT-p53 cells with TIGAR siRNA in final concentrations of 25, 50 or 75 nM for 48 hours, as well as non-target siRNA as a negative control and siRNA specific to p53 as a positive control. Western blotting analysis was performed to identify an optimal siRNA

concentration (Figure 3.30. A1). Densitometry showed that a final concentration of 25nM is an optimal concentration of siRNA to knockdown TIGAR in UM-SCC-1 cells, since neither a final concentration of 50 nor 75 nM of TIGAR siRNA resulted in additional substantial inhibition (Figure 3.30. A2).

Next, TIGAR siRNA in a final concentration of 25nM were used to achieve a transient inhibition of TIGAR expression before Seahorse XFe metabolic profiling was performed as previously described in sections 2.3.6.1. and 2.3.6.2. Western blotting analysis was performed to verify TIGAR knockdown (Figure 3.30. B1), and densitometry was used to measure the inhibition of TIGAR expression (Figure 3.30. B2).

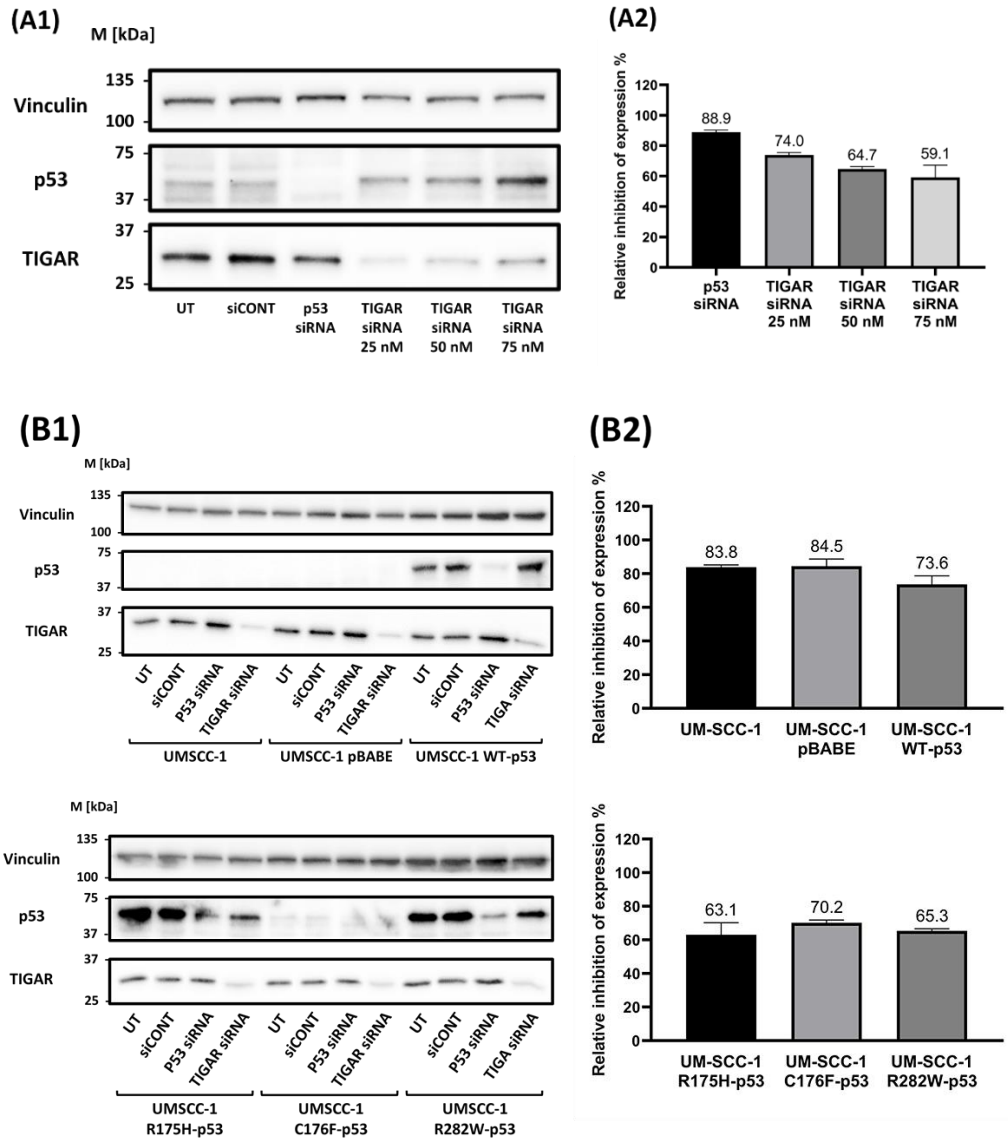

Figure 3.30.: TIGAR knockdown in UM-SCC-1 and derivative cell lines. Western blotting analyses of p53 and TIGAR expression levels in a p53-null cell line, UMS-CC-1 and derivatives. Cells were harvested

and lysed as described in section 2.8.3. Protein samples were prepared and loaded into gels, and specific antibodies were used for detection as detailed in section 2.1.9. Vinculin was used as a loading control. The migration of protein standards of the indicated approximate molecular weights is shown in kDa. **(A1)** To optimise TIGAR siRNA concentration, cells were left untransfected or transfected with either non-target siRNA (siCONT, as a negative control), siRNA specific for p53 (as a positive control) in a final concentration of 25nM or TIGAR-specific siRNA selected in 3.2.2.1. in final concentrations of 25, 50 or 75nM. Cells were harvested 48 hours after transfection. Results show that a final concentration of 25nM was an optimal concentration of siRNA to knockdown TIGAR in UM-SCC-1 cells. **(B1)** To verify TIGAR knockdown for metabolic studies of UM-SCC-1 and derivatives, cells were left untransfected or transfected with either non-target siRNA (siCONT, as a negative control), siRNA specific for p53 (as a positive control) or siRNA specific for TIGAR in a final concentration of 25nM. The concentration of TIGAR siRNA was selected based on results in 3.2.2.2.13 (A1). Cells were harvested 48 hours after transfection. Results show significant inhibition of TIGAR in TIGAR siRNA groups. For both (A1) and (B1), densitometry was used to analyse the expression of p53 and TIGAR as described in 2.8.5. and analyses of three biological replicates is depicted. Relative inhibition of TIGAR expression in A1 and B1, normalised to the expression of the housekeeping protein vinculin in the negative control cells (%), is shown in **(A2)** and **(B2)**, respectively. Oligonucleotides are detailed in Table 2.6.

Outputs from the mitochondrial stress test for TIGAR-knockdown UMSCC-1 and isogenic derivatives are shown in Figure 3.31., while outputs from glycolytic stress tests are shown in Figure 3.32. Outcomes of mitochondrial stress test from p53 knockdown were consistent with our previously discussed data, as only the derivative that harbours the wild type *TP53* shows marked inhibition in the mitochondrial function and a significant decrease in all mitochondrial parameters following the p53 knockdown. Interestingly, TIGAR knockdown results in a marked increase in the mitochondrial function in the p53-null parental cell line UM-SCC-1 as well as the derivative that harbours the empty vector (pBABE). Although TIGAR knockdown promotes a slight increase in the mitochondrial function in the derivative that harbours the wild type *TP53*, this increase was insignificant. Similarly, no significant effects were observed between all groups in the derivatives that harbour mutant *TP53* (Figure 3.31.).

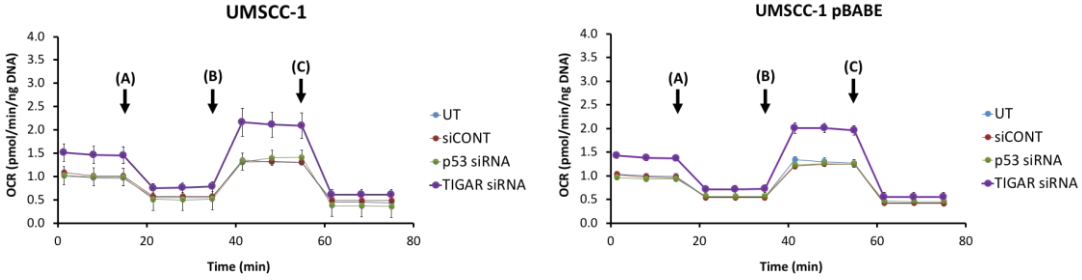

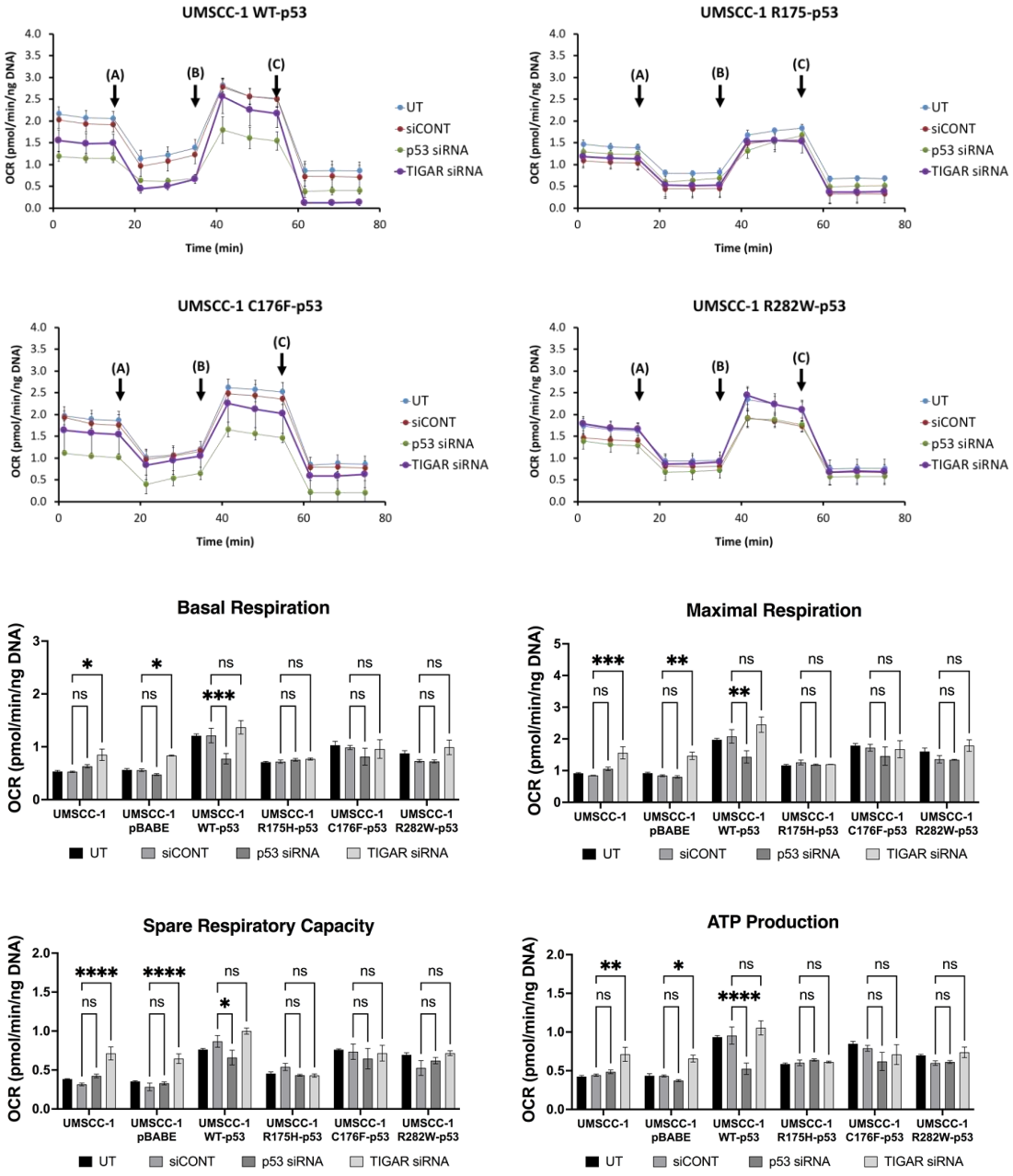

Figure 3.31.: Comparative metabolic profile of TIGAR-knockdown UM-SCC-1 and derivatives cells in the mitochondrial stress test. UM-SCC-1, UM-SCC-1 pBABE, UM-SCC-1 WT-p53, UM-SCC-1 R175H-p53, UM-SCC-1 C176F-p53, and UM-SCC-1 R282W-p53 cells, either untransfected or transfected with either non-target siRNA (siCONT), or siRNA specific for p53 or TIGAR, were subjected to mitochondrial stress test, as described in 2.3.6.1. Points A, B, and C on the graphs refer to the injections time points of 1µM oligomycin, 0.5µM FCCP and 1µM rotenone and antimycin-A, respectively. Post-injection changes in the mitochondrial function were used to calculate the mitochondrial respiration parameters as described in Table 2.4. and are shown in Figure 2.4. Absolute data derived from mitochondrial stress tests was normalised to DNA content for all groups of cells, and the absolute values for basal respiration, maximal respiration, spare respiratory capacity and ATP production were calculated as described in section 2.3.6.1. OCR readings were obtained from three experiments (n=3), each experiment was performed in triplicate. Data are presented as mean OCR (pmol/min), normalised to DNA content (ng DNA) as described in 2.3.8. Means of individual data were used to derive overall means. Error bars represent SEM. Statistical analysis:

a one-way ANOVA with Dunnett's test. (ns) $p > 0.05$, (*) $p \leq 0.05$, (**) $p \leq 0.01$, (***) $p \leq 0.001$, (****) $p \leq 0.0001$.

Outcomes of the glycolytic stress test show that TIGAR knockdown in the p53-null parental cell line, UM-SCC-1, and the derivative that harbours the empty vector (pBABE) promotes glycolytic function. This is inconsistent with the results obtained from TIGAR-knockdown-UM-SCC-11B cells in the glycolysis stress test (see Figure 3.28.). Similar to previously discussed results, TIGAR knockdown in the derivative that harbours wild type *TP53* promotes glycolytic function.

Interestingly, knockdown p53 in the force-expressed-p53 cell line, UM-SCC-1 WT-p53, results in an increase in basal glycolysis, glycolytic capacity and reserves, while the partially-functional-mutant-p53 cell line, UM-SCC-1 C176F-p53, shows increased glycolytic reserve following the p53 knockdown (Figure 3.32.).

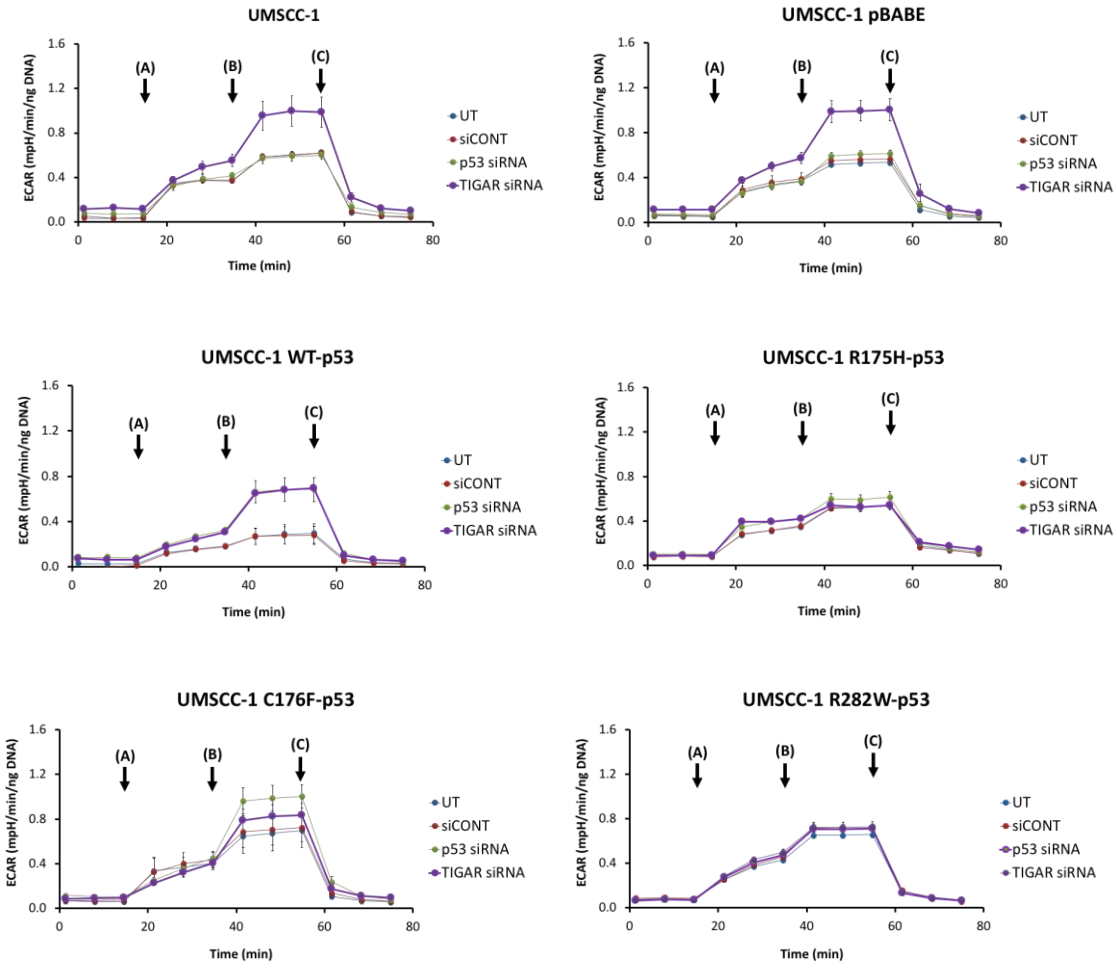

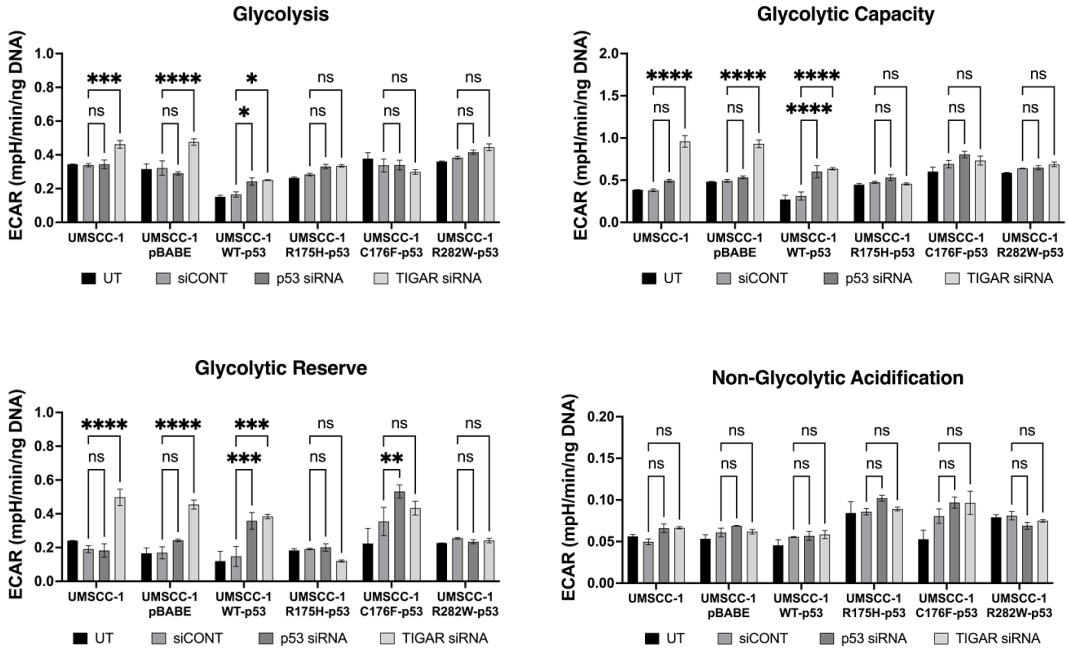

Figure 3.32.: Comparative metabolic profile of TIGAR-knockdown UM-SCC-1 and derivatives cells in the glycolytic stress test. UM-SCC-1, UM-SCC-1 pBABE, UM-SCC-1 WT-p53, UM-SCC-1 R175H-p53, UM-SCC-1 C176F-p53, and UM-SCC-1 R282W-p53 cells, either untransfected or transfected with either non-target siRNA (siCONT), or siRNA specific for p53 or TIGAR, were subjected to glycolytic stress test, as described in 2.3.6.2. Points A, B, and C on the graphs refer to the injections time points of 10mM D-glucose, 1µM oligomycin and 50mM 2-DG, respectively. Post-injection changes in the glycolytic function were used to calculate the glycolytic parameters as described in Table 2.4. and are shown in Figure 2.4. Absolute data derived from glycolytic stress tests was normalised to DNA content for all groups of cells, and the absolute values for glycolysis, glycolytic capacity, glycolytic reserve and non-glycolytic acidification were calculated as described in section 2.3.6.2. ECAR readings were obtained from three experiments (n=3), each experiment was performed in triplicate. Data are presented as mean ECAR (mpH/min), normalised to DNA content (ng DNA) as described in 2.3.8. Means of individual data were used to derive overall means. Error bars represent SEM. Statistical analysis: a one-way ANOVA with Dunnett's test. (ns) $p > 0.05$, (*) $p \leq 0.05$, (**) $p \leq 0.01$, (***) $p \leq 0.001$, (****) $p \leq 0.0001$.

To test whether these outcomes have changed the balance between mitochondrial and glycolytic functions, the ratio of basal glycolysis/basal respiration was used to explore the Warburg effect and the balance between the two functions in UM-SCC-1 and derived cell lines following the transient knockdown of TIGAR (Figure 3.33.). Results showed a significant increase in the ratio of basal glycolysis/basal respiration following the knockdown of p53 in the derivative cells that harbour the wild type *TP53* compared to the untransfected or the negative control group, while no marked differences were observed in other cell lines. On the other hand, TIGAR-knockdown in the derived cells expressing wild type p53 show a slight, but not significant, increase in the ratio of basal

glycolysis/basal respiration in comparison with untransfected or the negative control cells, while no significant differences in the ratio were shown in all other derived cell lines. These results can be explained through the marked increase in both mitochondrial and glycolytic functions following the knockdown of TIGAR in p53-null cells and the comparable differences in both functions following the knockdown of TIGAR in mutant p53 cells (Figures 3.31. and 3.32.), whereas the slight increase in glycolysis following the knockdown of TIGAR in the presence of p53, as shown in Figures 3.21., 3.25., 3.29. and 3.32., maybe not sufficient to significantly change this ratio given the previously discussed highly active mitochondrial function in wild type p53 cells.

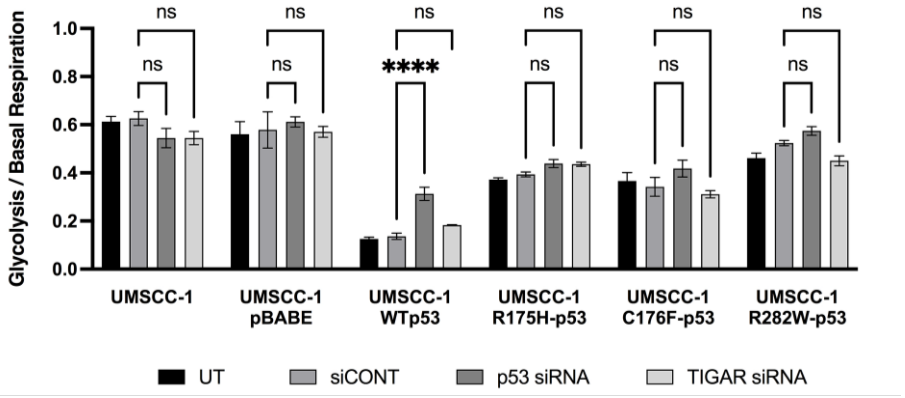

Figure 3.33.: Warburg effect in TIGAR-knockdown UM-SCC-1 and derivatives cell lines. The Warburg effect is indicated by ascribing to each cell line a value derived from the ratio of glycolysis/basal respiration in UM-SCC-1, UM-SCC-1 pBABE, UM-SCC-1 WT-p53, UM-SCC-1 R175H-p53, UM-SCC-1 C176F-p53, and UM-SCC-1 R282W-p53 cells. This ratio shows a significant tendency towards glycolysis following the knockdown of p53 in the derivative cells that harbour the wild type *TP53*, while no similar effect was shown in all other cell lines. TIGAR knockdown showed no significant effect on the ratio of glycolysis/basal respiration when compared to the untransfected or the negative control group in all cell lines. Means of individual data were used to derive overall means. Error bars represent SEM. Statistical analysis: a one-way ANOVA with Dunnett's test. (ns) $p > 0.05$, (*) $p \leq 0.05$, (**) $p \leq 0.01$, (***) $p \leq 0.001$, (****) $p \leq 0.0001$.

3.2.2.3. Conclusion

The findings presented in this section (summarised in Tables 3.2. and 3.3.) show that reducing the expression level of wild type p53 in SCCHN cells, has a significant impact on the metabolic phenotype, altering the balance between mitochondrial and glycolytic functions, with cells tending to be more dependent on glycolysis when p53 is down-regulated. No similar effects were observed in cells expressing mutant p53, which could

be explained by the greater dependence of these cells on glycolysis in comparison with wild type p53 cells, as previously discussed in 3.1.3. In addition, these cells probably do not have any suppression of glycolysis by p53 which explains why there were no differences in the metabolic profile of these cells from p53-null cells following transfection with p53 siRNA and indicates that loss of p53 function (LOH) is sufficient to lead to an increase in glycolysis (Figure 3.7.), and that GOF does not contribute further to this effect.

However, knockdown of p53 in cells expressing the partially functional mutant p53 (UM-SCC-1 C176F-p53) resulted in an increase in glycolytic reserve, which is consistent with the results presented in 3.1.3.3., where these cells showed more active mitochondrial function than non-functional mutant p53 cells (UM-SCC-1 R175H-p53 and UM-SCC-1 R282W-p53). A systematic analysis of *TP53* mutation data by Bouaoun et al has classified C176F as a partially functional p53 mutation (287) based on data obtained from the International Agency for Research on Cancer (IARC), including functional assessment of p53 variants (317), and the Next-generation sequencing (NGS) studies (287). A study by Kato et al has shown that C176F-p53 retains some wild type p53 functions, and can differentially induce *TP53* target genes like *CDKN1A, NOXA, RRM2B, GADD45 and BAX* (314), while another study by Hoffman-Luca found that C176F-p53 can form tetramers with wild type p53 that remain functionally active and can maintain the structural stability and interactions with DNA as well as the induction of p53 and p21 following treatment with MDM2 inhibitor (334). This supports the idea that the partially functional p53 maintains relatively active mitochondrial promoting function, and thus knockdown of p53 in these cells results in a small, albeit not significant, decrease in mitochondrial function parameters which could explain the comparable changes in basal values for glycolysis and then the considerable increase in glycolytic reserve following the inhibition of ATP-linked respiration.

Table 3.2.: Changes in mitochondrial parameters following knockdown of p53 or TIGAR in a panel of SCCHN cell lines.

	Cell line	*TP53* status	Gene expression manipulation	Basal reparation	Maximal respiration	Spare respiratory Capacity	ATP production
Wild type	UMSCC-17A	WT	p53 knockdown	↓	↓	↓	↓
			TIGAR knockdown	ns	ns	ns	ns
	UMSCC-11A	WT	p53 knockdown	↓	↓	↓	↓
			TIGAR knockdown	ns	ns	ns	ns
	UM-SCC-1 WTp53	WT	p53 knockdown	↓	↓	↓	↓
			TIGAR knockdown	ns	ns	ns	ns
Compromised	UM-SCC-11B	Mut	p53 knockdown	ns	ns	ns	ns
			TIGAR knockdown	ns	ns	ns	ns
	UM-SCC-1	null	p53 knockdown	ns	ns	ns	ns
			TIGAR knockdown	↓	↓	↓	↓
	UM-SCC-1 pBABE	null	p53 knockdown	ns	ns	ns	ns
			TIGAR knockdown	↓	↓	↓	↓
	UM-SCC-1 R175H-p53	Mut	p53 knockdown	ns	ns	ns	ns
			TIGAR knockdown	ns	ns	ns	ns
	UM-SCC-1 C176F-p53	Mut (partially functional)	p53 knockdown	ns	ns	ns	ns
			TIGAR knockdown	ns	ns	ns	ns
	UM-SCC-1 R282W-p53	Mut	p53 knockdown	ns	ns	ns	ns
			TIGAR knockdown	ns	ns	ns	ns

Table 3.3.: Changes in glycolytic parameters following knockdown of p53 or TIGAR in a panel of SCCHN cell lines.

	Cell line	*TP53* status	Gene expression manipulation	Basal reparation	Maximal respiration	Spare respiratory Capacity	ATP production
Wild type	UMSCC-17A	WT	p53 knockdown	↑	ns	ns	ns
			TIGAR knockdown	↑	ns	ns	ns
	UMSCC-11A	WT	p53 knockdown	↑	ns	ns	ns
			TIGAR knockdown	↑	ns	ns	ns
	UM-SCC-1 WTp53	WT	p53 knockdown	↑	↑	↑	ns
			TIGAR knockdown	↑	↑	↑	ns
Compromised	UM-SCC-11B	Mut	p53 knockdown	ns	ns	ns	ns
			TIGAR knockdown	ns	ns	ns	ns
	UM-SCC-1	null	p53 knockdown	ns	ns	ns	ns
			TIGAR knockdown	↑	↑	↑	ns
	UM-SCC-1 pBABE	null	p53 knockdown	ns	ns	ns	ns
			TIGAR knockdown	↑	↑	↑	ns
	UM-SCC-1 R175H-p53	Mut	p53 knockdown	ns	ns	ns	ns
			TIGAR knockdown	ns	ns	ns	ns
	UM-SCC-1 C176F-p53	Mut (partially functional)	p53 knockdown	ns	ns	↑	ns
			TIGAR knockdown	ns	ns	ns	ns
	UM-SCC-1 R282W-p53	Mut	p53 knockdown	ns	ns	ns	ns
			TIGAR knockdown	ns	ns	ns	ns

Consistent with this, transient inhibition of p53 in UM-SCC-1 cells that forcibly express wild type p53 also results in a significant increase in glycolytic reserve, whereas there was a small but comparable increase in other cells harbouring wild type *TP53* such (UM-SCC-11A and UM-SCC-17A). This can be explained by the higher mitochondrial function in UM-SCC-11A and UM-SCC-17A compared to UM-SCC-1 wild type (see Figure 3.11.) or C176F p53 cells (see Figure 3.5.), which results in a higher effect of p53-knockdown-mediated inhibition of mitochondrial respiration on the basal levels of glycolysis of UM-SCC-11A and UM-SCC-17A, also known as compensatory glycolysis, given the significant difference in ATP production between mitochondrial respiration and glycolysis, and thus a lower response to further increase in glycolysis reserves following the oligomycin-mediated ATP synthase inhibition of mitochondrial activity. This is clearly shown in the comparable differences in glycolysis rates between p53-knockdown cells and control cells following injection point B in UM-SCC-17A and UM-SCC-11A cells (Figure 3.20. and 3.2.2.2.7.) compared to higher and significant differences at the same injection point in p53-knockdown UM-SCC-1 WT-p53 and UM-SCC-1 C176F-p53 cells (Figure 3.27.). Figure 3.34. depicts the difference between the two patterns of response to ATP synthase inhibition following p53 knockdown, either in cells expressing fully- or partially-functional p53 with relatively higher or lower mitochondrial function. These results suggest that the effect of *TP53*-mediated metabolic regulation on glycolytic reserves may be dependent on the capacity of the respiratory function, as wild type p53 cells with relatively greater respiratory function show less stimulation of glycolytic reserves following inhibition of p53 function compared to wild type p53 cells with relatively lower respiratory capacity (Figure 3.34.). These findings are consistent with the outcomes of the stable knockdown of p53 (Figure 3.9.).

These results also indicate that UM-SCC-1 cells that forcibly express p53 may respond better to increased energy demands compared to their counterpart p53-null/mutant p53 isogenic cells, which, together with metabolic phenotypes of other wild type p53 cells, could reflect the metabolic diversity in SCCHN cells expressing wild type p53 compared to the limited diversity in loss-of-p53-function cells (Figure 3.32.). Thus, it can be argued that wild type p53 cells with greater respiratory function have relatively greater diversity to use several metabolic pathways to respond to increased energy demands following inhibition of mitochondrial function.

In the line with the aforementioned evidence, our results are consistent with the critical role of p53 as a determinant of the metabolic phenotype discussed earlier in 3.1.3.

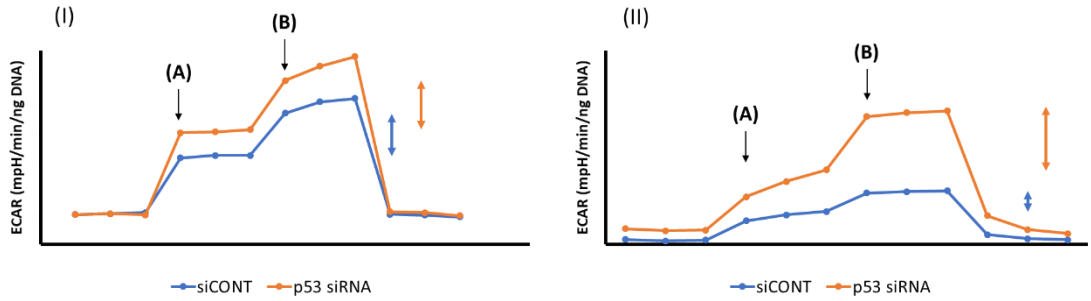

Figure 3.34.: Patterns of response to ATP synthase inhibition in SCCHN cells expressing fully- or partially-functional p53. A depiction of two different patterns of response to ATP synthase inhibition following transfection with p53 siRNA. **(I)** represents the glycolytic function of cells with relatively higher mitochondrial function, UM-SCC-11A and UM-SCC-17A, in a glycolytic stress test. p53-knockdown-mediated inhibition of mitochondrial respiration results in increased glycolysis rates (at injection point A), while no marked difference was observed in increased glycolysis following oligomycin-mediated inhibition of mitochondrial respiration (at injection point B). **(II)** represents the glycolytic function of cells with relatively lower mitochondrial function, UM-SCC-1 WT-p53 and UM-SCC-1 C176F-p53, in a glycolytic stress test. Similar to (I), p53-knockdown-mediated inhibition of mitochondrial respiration results in increased glycolysis rates (at injection point A), while a substantial difference was observed in increased glycolysis following oligomycin-mediated inhibition of mitochondrial respiration (at injection point B). The length of the arrows on the right represents the increase in ECAR readings (mpH/min/ng DNA) between injection points A and B which is calculated to represent the values for glycolytic reserves.

On the other hand, TIGAR knockdown has a less significant effect on the balance between mitochondrial and glycolytic functions in SCCHN cells having different p53 status. TIGAR knockdown in p53 wild type cells results in an increase in glycolysis (Figures 3.20., 3.24., 3.28. and 3.32.) with no marked effect on mitochondrial respiration (Figures 3.19., 3.23., 3.27. and 3.31.) and an inconsistent significant increase in the balance between the two functions given the high capacity of mitochondrial respiration in p53 wild type cells (Figures 3.21., 3.25., 3.29. and 3.33.).

Transient inhibition of TIGAR has no significant effect on the balance between glycolysis and mitochondrial respiration functions in the absence of p53 function (p53-null and mutant p53 cells). Interestingly, this balance is maintained due to the increase in baseline values of both glycolysis and mitochondrial respiration in p53-null SCCHN cells, or due to the absence of such increase in mutant SCCHN cells. This may suggest a possible alternative mechanism that regulates the role of TIGAR in the absence of p53.

Although these findings raise some questions about p53-independent regulation of TIGAR and how TIGAR knockdown promotes both mitochondrial respiration and glycolysis in p53-null cells but not in mutant p53 cells, these findings support the notion that the role of TIGAR in regulating glycolysis is inextricably linked to *TP53* regulatory function and that the effects of transient inhibition of TIGAR on the balance between mitochondrial and glycolysis functions of SCCHN is p53-dependent.

However, our results in this section do not allow us to determine whether the alternative mechanism that regulates TIGAR in the absence of p53 is related to a different metabolic regulatory role that TIGAR plays in the absence of the p53 regulatory mechanism (increased basal respiration in p53-null cells but not in wild type p53 or p53-mutant cells) or is related to p53 GOF in cells harbouring mutant *TP53* that abrogate or reverse the effect of TIGAR inhibition on glycolytic function (increased glycolysis in p53-null and wild type p53 cells but not in p53-mutant cells)(Figure 3.35.)

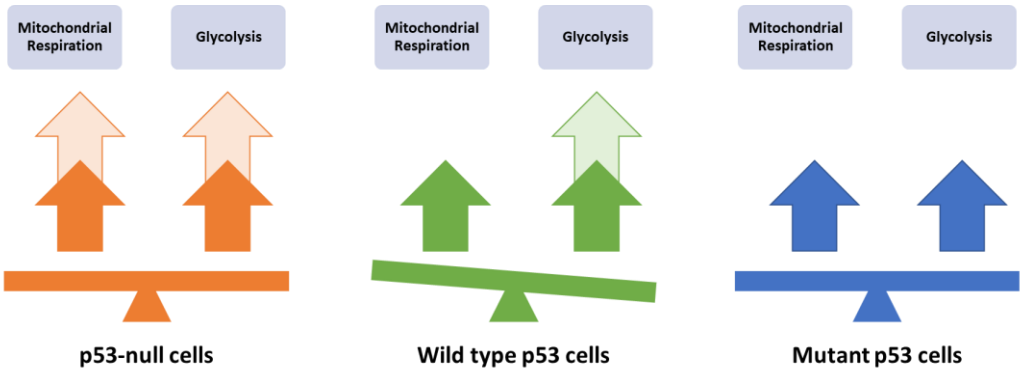

Figure 3.35.: Effect of TIGAR knockdown on the balance between mitochondrial respiration and glycolysis in SCCHN cells with different p53 status. p53-null cells show an increase (arrows in a lighter colour) in both mitochondrial and glycolysis functions following TIGAR knockdown, while mutant p53 cells show no significant differences from the basal levels (arrows in a darker colour) in both functions. This results in no marked effect on the balance between the two functions in both p53-null and mutant p53 cells. On the other hand, wild type p53 show an increase in glycolysis function only following TIGAR knockdown, which may result in switching the balance between the two functions towards glycolysis despite the inconsistent effect of this increase on the ratio between glycolysis and mitochondrial respiration due to higher mitochondrial function of wild type p53 cells.

3.2.3. Investigation of the potential effect of p53-independent TIGAR expression using TIGAR-overexpressed SCCHN cells

In addition to studying the function of TIGAR by down-regulating endogenous protein levels with RNAi, experiments were performed in which TIGAR was overexpressed following transient transfection of a TIGAR expression vector. The goal of these studies was to investigate the potential effect of any p53-independent TIGAR expression. Following transient expression of TIGAR, Seahorse XFe metabolic profiling was performed as described previously in 2.3.6.1. and 2.3.6.2. to explore the changes in the mitochondrial and glycolytic functions and changes in the metabolic parameters in the TIGAR-overexpressed SCCHN cells, either in the presence of wild type or mutant p53, as well as in the absence of p53.

Briefly, cells were cultured at optimised densities 24 hours before plasmid transfection was performed. Cells were left either untransfected or transfected to introduce either an empty vector control plasmid DNA or myc-tagged TIGAR expressing DNA constructs. MDM2-expressing DNA constructs previously used and published by our laboratory (335) were also used as a control to facilitate the analysis of western blot data. Cells were co-transfected with a GFP-expressing plasmid to monitor transfection efficiency. 48 hours after transfection, cell uptake of the GFP-expressing plasmid was examined and imaged by fluorescence microscopy and overexpression efficiency was confirmed by analysing protein expression using western blotting, as detailed in 2.5.4.

3.2.3.1. Metabolic profiling of TIGAR-overexpressed SCCHN cells

For each group of cell lines, the plasmid concentration was optimised by transfecting the cells with plasmid in a final concentration of 0.1, 0.2, 0.3, or 0.5 μg/ml of media (10 ml in 10 cm dishes) using different volumes of the transfection reagent and regularly checking cells after 24 and 48 hours using a light microscope to detect cell death.

Firstly, the wild type p53 cell line UM-SCC-17A was transfected with 0.5 μg/ml plasmid for 48 hours, fluorescence microscopy was used to monitor the transfection and images of transfected cells were taken one hour before Seahorse XFe metabolic profiling was performed. The Transfection Efficiency (TE) of GFP plasmid DNA was measured as described in 2.5.4. (Figure 3.36.), and western blotting analysis was performed to determine the protein expression levels of MDM2, p53 and TIGAR (Figure 3.39. B1).

Densitometry was used to calculate the relative expression of MDM2, p53 and TIGAR compared to expression of the relevant protein in empty vector condition normalised to the expression of housekeeping protein vinculin in the empty-vector-transfected cells (Figure 3.36. B2). We have previously shown before that transient knockdown of TIGAR show an increase in levels of p53 expression in a dose-independent manner (Figure 3.18.). Consistent with this regulatory relationship between p53 and TIGAR, expression of TIGAR decreases levels of p53 expression (Figure 3.36.).

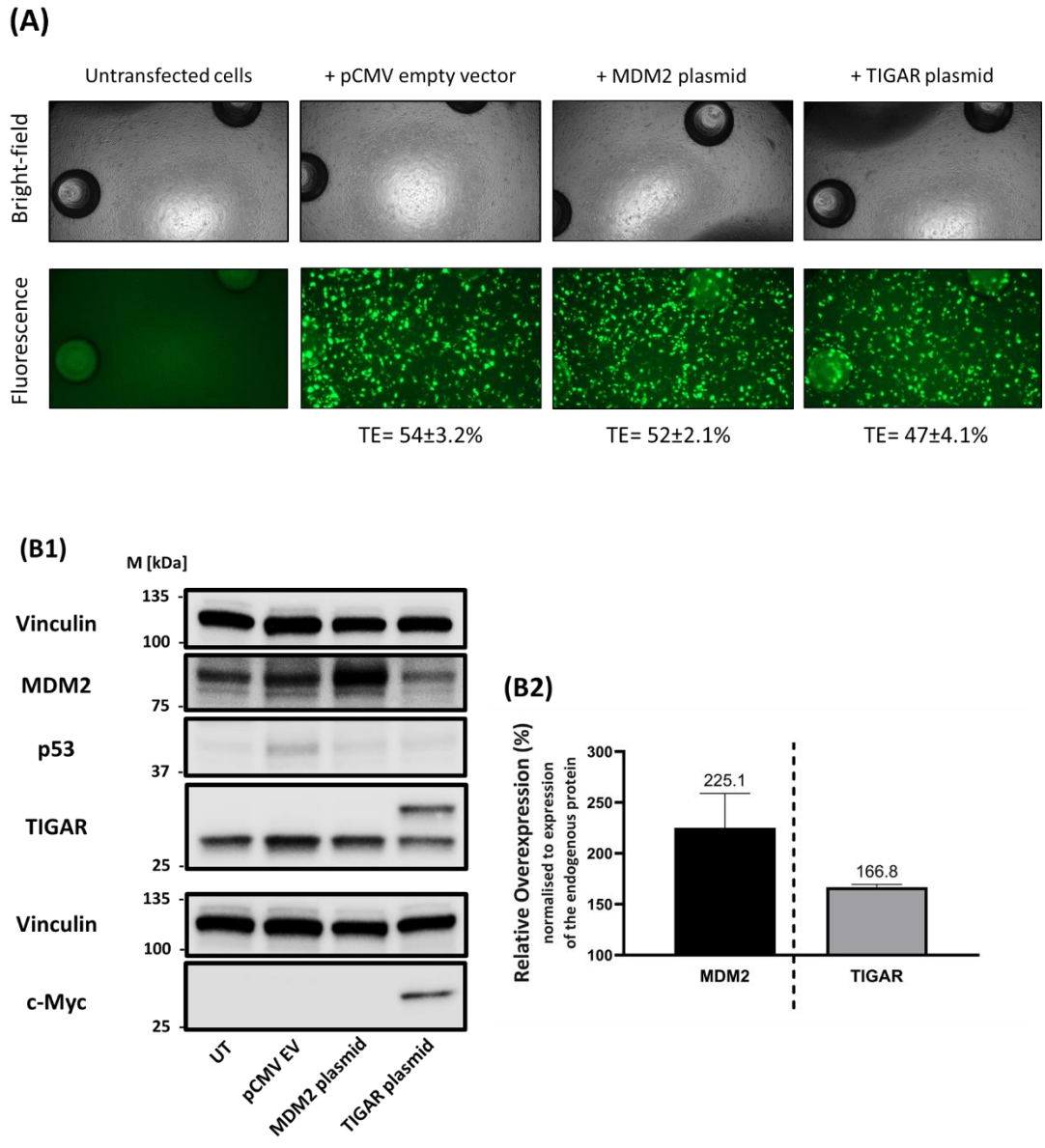

Figure 3.36.: TIGAR overexpression in a wild type *TP53* cell line, UM-SCC-17A. (A) Bright-field and fluorescence microscopy images (AMG EVOS, 10X objective) of GFP plasmid-transfected UM-SCC-17A cells after 48 hours of transfection, taken in Seahorse XFe96 plate wells one hour before metabolic profiling test was performed. Transfection efficiency (TE) is presented as a mean percentage of three wells for each condition. **(B1)** Western blotting analyses of MDM2, p53, TIGAR (endogenous and Myc-DDK-tagged

protein) and c-Myc expression levels in UMS-CC-17A cells. Cells were harvested and lysed as described in section 2.8.3. Protein samples were prepared and loaded into gels, and specific antibodies were used for detection as detailed in section 2.1.9. Vinculin was used as a loading control. The migration of protein standards of the indicated approximate molecular weights is shown in kDa. Transfection with Myc-DDK-tagged TIGAR plasmid resulted in the detection of two bands: a top band at ~32kD represents the expression of Myc-DDK-tagged TIGAR and a bottom band at ~30kD represents the expression of endogenous TIGAR. **(B2)** Densitometry analysis of the expression of MDM2 and TIGAR in plasmid-DNA-transfected cells as described in 2.8.5. Relative elevation in protein expression of three biological replicates compared to the endogenous expression of the relevant protein in empty vector group normalised to the expression of the housekeeping protein vinculin (%), as shown in (B1). Plasmids used are detailed in 2.1.7..

Results of mitochondrial stress test showed no marked differences in mitochondrial function between untransfected, empty vector-, MDM2-plasmid- and TIGAR-plasmid-transfected cells and values for all mitochondrial parameters were comparable between all experimental conditions (Figure 3.7.). Although basal glycolysis levels in TIGAR-overexpressing UM-SCC-17A cells were unaffected, values for glycolytic capacity and reserves were significantly decreased in comparison with other groups of cells (Figure 3.38.). These results are consistent with the notion we discussed in results obtained from TIGAR-knockdown UM-SCC-17A cells, as alteration in TIGAR expression (both knockdown and overexpression) has no significant impact on the mitochondrial function in the presence of wild type p53 (Figures 3.19. and 3.37.), while altered expression of TIGAR has a significant effect on the glycolytic function as TIGAR knockdown promotes glycolysis (Figure 3.20.) and TIGAR overexpression decreases the glycolytic capacity and reserves (Figure 3.38.). In addition, given that TIGAR knockdown results in increased basal glycolysis in the presence of wild type p53, overexpressing TIGAR has no effect on basal glycolysis, which, together with the decreased levels of glycolytic capacity and reserves, may suggest saturation of glycolytic activity.

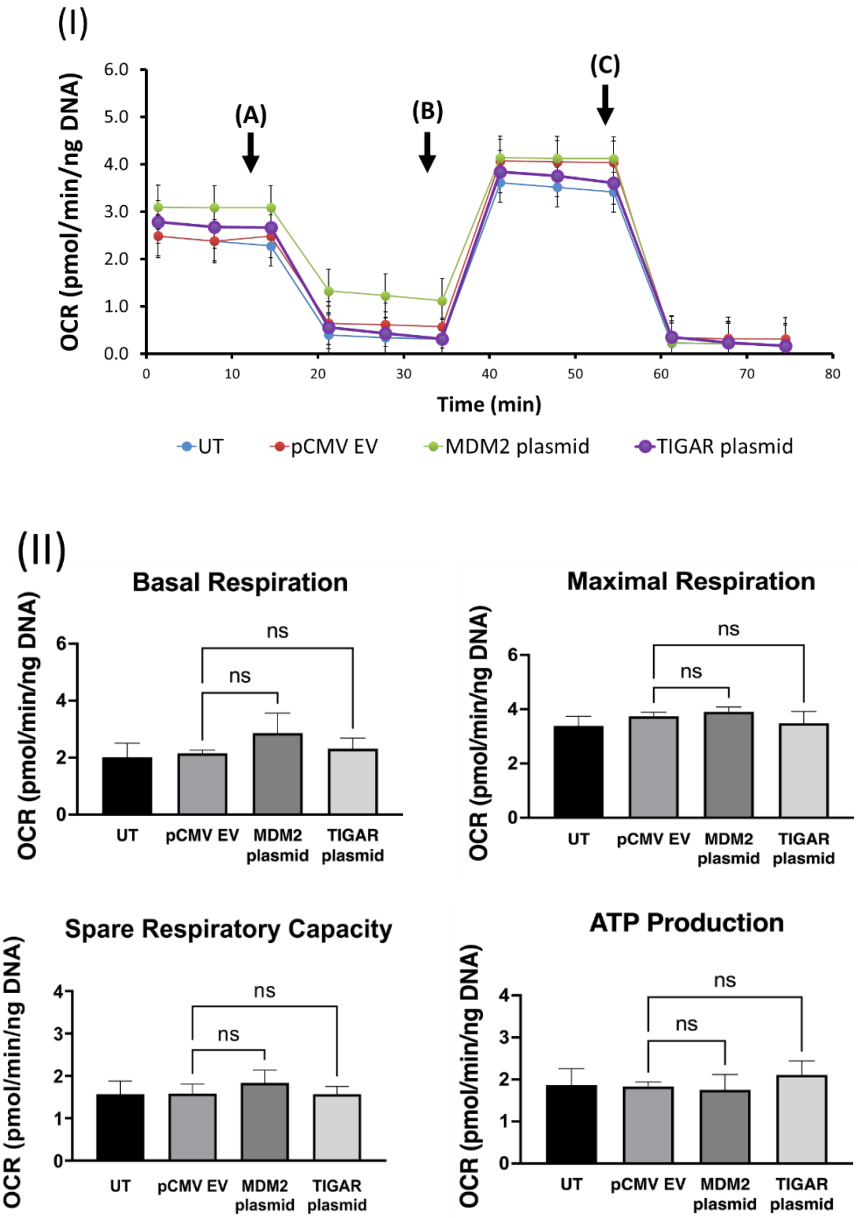

Figure 3.37.: The metabolic profile of TIGAR-overexpressing UM-SCC-17A cells analysed using a mitochondrial stress test. Untransfected cells (UT) or cells transfected with either empty vector plasmid, MDM2 or TIGAR DNA constructs were subjected to mitochondrial stress test, as described in 2.3.6.1. Points A, B, and C on the graphs refer to the injections time points of 1µM oligomycin, 0.5µM FCCP and 1µM rotenone and antimycin-A, respectively. Post-injection changes in the mitochondrial function were used to calculate the mitochondrial respiration parameters as described in Table 2.4. and are shown in Figure 2.4. **(I)** TIGAR-and MDM2-overexpressed cells show non-marked changes in the mitochondrial function at basal levels and following the inhibition of the ATP-linked respiration (at time point A) and uncoupling ATP synthesis from the ETC (at time point B) in comparison to the untransfected or empty vector cells groups. **(II)** Absolute data derived from mitochondrial stress tests was normalised to DNA content for all groups of cells, and the absolute values for basal respiration, maximal respiration, spare respiratory capacity and ATP production were calculated as described in section 2.3.6.1. No significant differences were shown in values for basal respiration, maximal respiration, spare respiratory capacity and ATP production between all groups. OCR readings were obtained from three experiments (n=3), each

experiment was performed in hextuplet. Data are presented as mean OCR (pmol/min), normalised to DNA content (ng DNA) as described in 2.3.8. Means of individual data were used to derive overall means. Error bars represent SEM. Statistical analysis: a one-way ANOVA with Dunnett's test. (ns) $p > 0.05$, (*) $p \leq 0.05$, (**) $p \leq 0.01$, (***) $p \leq 0.001$, (****) $p \leq 0.0001$.

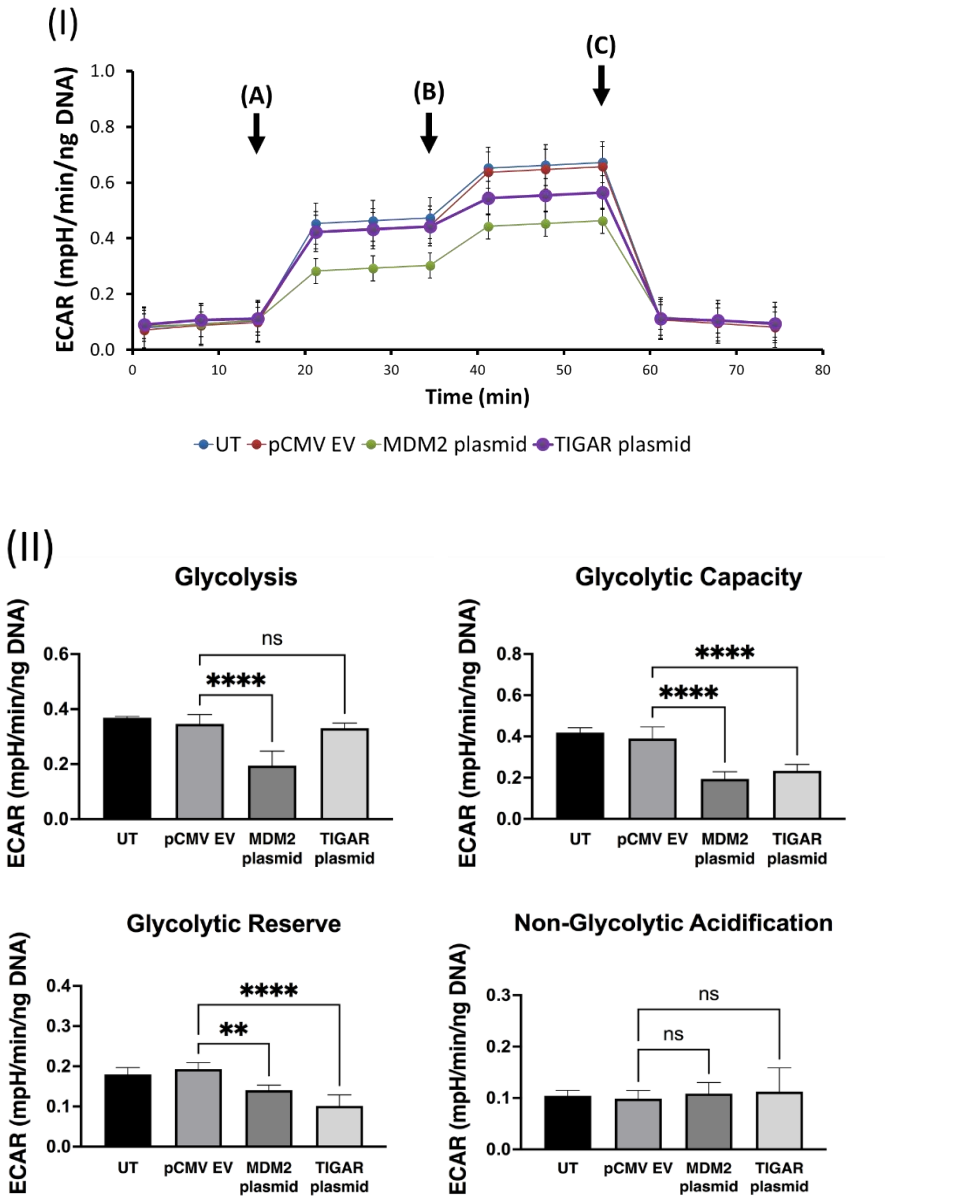

Figure 3.38.: The metabolic profile of TIGAR-overexpressed UM-SCC-17A cells in the glycolytic stress test. Untransfected cells (UT) or cells transfected with either empty vector, MDM2 or TIGAR DNA construct were subjected to glycolytic stress test, as described in 2.3.6.2. Points A, B, and C on the graphs refer to the injections time points of 10mM glucose, 1µM oligomycin, and 50mM 2-DG, respectively. Post-injection changes in the glycolytic function were used to calculate the glycolytic parameters as described in Table 2.5. and are shown in Figure 2.5. **(I)** TIGAR-overexpressed cells show non-marked changes in the glycolytic function following the injection of glucose (at time point A), but show marked inhibition following the inhibition of the ATP-linked respiration (at time point B) in comparison with the untransfected or empty vector cells. MDM2-overexpressed cells show marked inhibition in the glycolytic

function following the injection of glucose (at time point A), with less marked change following the inhibition of the ATP-linked respiration (at time point B) in comparison to the untransfected or empty vector cells. **(II)** Absolute data derived from glycolytic stress tests was normalised to DNA content for all groups of cells, and the absolute values for glycolysis, glycolytic capacity, glycolytic reserve and non-glycolytic acidification were calculated as described in section 2.3.6.2. ECAR readings were obtained from three experiments (n=3), each experiment was performed in hextuplet. Data are presented as mean ECAR (mpH/min), normalised to DNA content (ng DNA) as described in 2.3.8. Means of individual data were used to derive overall means. Error bars represent SEM. Statistical analysis: a one-way ANOVA with Dunnett's test. (ns) $p > 0.05$, (*) $p \leq 0.05$, (**) $p \leq 0.01$, (***) $p \leq 0.001$, (****) $p \leq 0.0001$.

Interestingly, the glycolytic stress test showed a marked decrease in glycolysis, glycolytic capacity and reserve in MDM2-overexpressing UM-SCC-17A cells. The role that MDM2 plays in suppressing glycolytic function has recently been reported elsewhere and investigated (336–339). Data shown for the glycolytic function of MDM2-overexpressed UM-SCC-17A cells (Figure 3.38.) may indicate a p53-independent function for MDM2 in regulating metabolism. However, our findings need to be further explored using cells with different p53 status to identify the role of overexpressing MDM2 and TIGAR in p53-dependent metabolic regulation.

We previously used a matched pair of cell lines, derived from a single patient, harbouring p53 wild type or a p53 mutation (UM-SCC-11A and 11B respectively) to examine the dependence of metabolic phenotypes on p53 status. We, therefore, used the same experimental design to examine the metabolic phenotype of TIGAR-overexpression in SCCHN in these cells. As stated before, UM-SCC-11A is a wild type p53 SCCHN cell line with the highest mitochondrial function and the lowest glycolytic function among the cell lines tested in this study, while UM-SCC-11B cells harbour the loss-of-function C242S missense mutation in the *TP53* gene and exhibit high glycolytic function and a low mitochondrial function (Figures 3.11. and 3.13.).

As previously, UM-SCC-11A and UM-SCC-11B cells were transfected with 0.3 µg/ml plasmid for 48 hours, fluorescence microscopy was used to check transfection and images of transfected cells were taken only one hour before Seahorse XFe metabolic profiling was performed. The transfection efficiency of GFP plasmid DNA was measured as described in 2.5.4. (Figure 3.39. A), and western blotting analysis was performed to check the protein expression of MDM2, p53 and TIGAR (Figure 3.39. B1). Densitometry was used to calculate the relative expression of MDM2, p53 and TIGAR normalised to

the expression of housekeeping protein vinculin in the empty-vector-transfected cells (Figure 3.39. B2.).

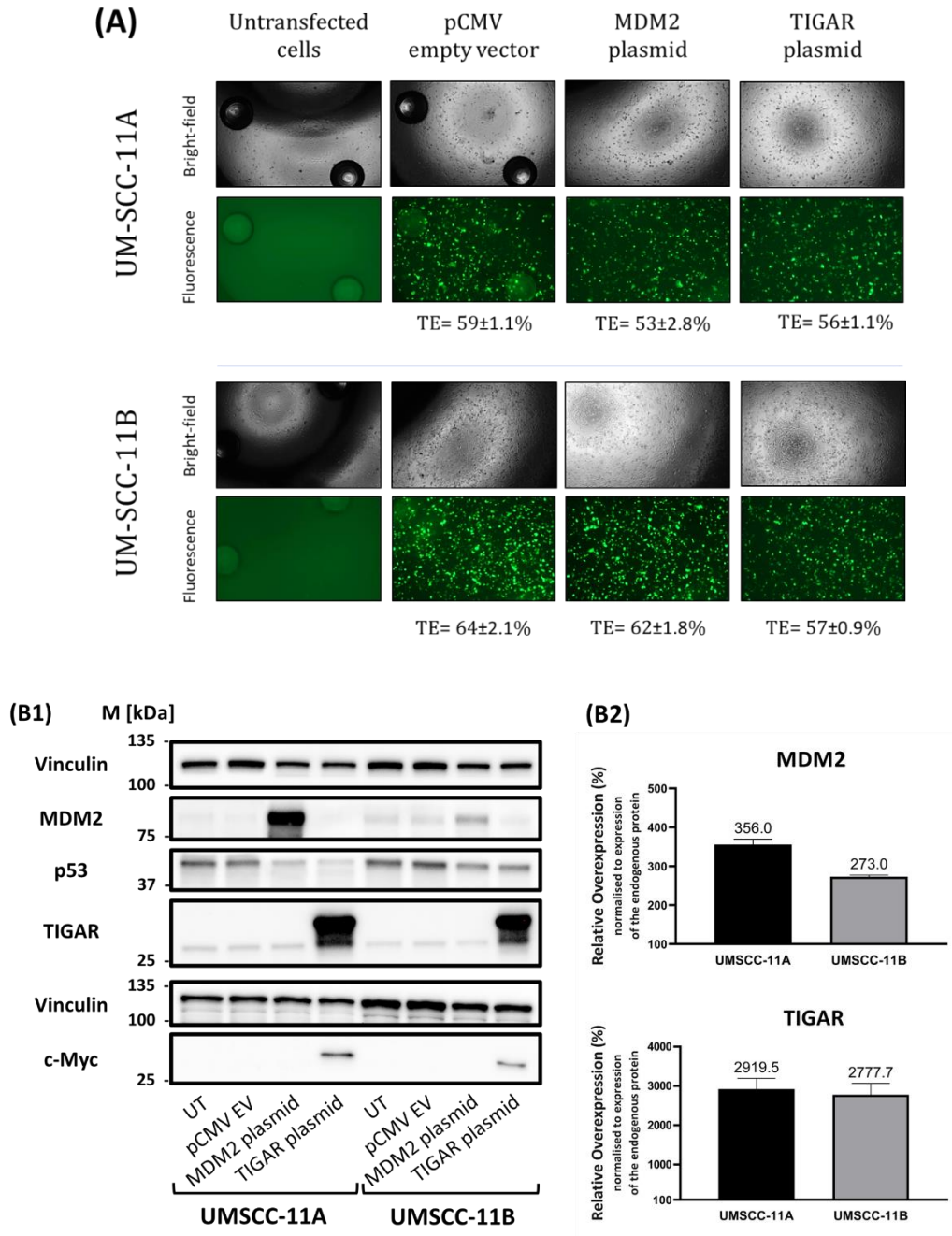

Figure 3.39.: TIGAR overexpression in the wild type *TP53* cell line, UM-SCC-11A and the mutant *TP53* cell line UM-SCC-11B. (A) Bright-field and fluorescence microscopy images (AMG EVOS, 10X objective) of GFP plasmid-transfected UM-SCC-11A and UM-SCC-11B cells after 48 hours of transfection, taken in Seahorse XFe96 plate wells one hour before metabolic profiling test was performed. Transfection efficiency is presented as a mean percentage of three wells for each condition. **(B1)** Western blotting analyses of MDM2, p53, TIGAR (endogenous and Myc-DDK-tagged protein) and c-Myc expression levels in UMS-CC-11A and UM-SCC-11B cells. Cells were harvested and lysed as described in section 2.8.3. Protein samples were prepared and loaded into gels, and specific antibodies were used for detection as detailed in section 2.1.9. Vinculin was used as a loading control. The migration of protein standards of the indicated

approximate molecular weights is shown in kDa. Transfection with Myc-DDK-tagged TIGAR plasmid resulted in the detection of two bands: a top band at ~32kD represents the expression of Myc-DDK-tagged TIGAR and a bottom band at ~30kD represents the expression of endogenous TIGAR. **(B2)** Densitometry analysis of the expression of MDM2 and TIGAR in plasmid-DNA-transfected cells as described in 2.8.5. Relative elevation in protein expression of three biological replicates compared to the endogenous expression of the relevant protein in empty vector group, normalised to the expression of the housekeeping protein vinculin (%), as shown in [B1]. Plasmids used are detailed in 2.6.

Results of the mitochondrial stress test showed no marked differences in the mitochondrial function between untransfected, empty vector-, MDM2-plasmid- and TIGAR-plasmid-transfected cells and values for all mitochondrial parameters were comparable for all groups in both cell lines (Figure 3.40. A and B). Although basal glycolysis levels in TIGAR-overexpressed UM-SCC-11A cells were unaffected, values for glycolytic capacity and glycolytic reserve were significantly decreased in comparison with the untransfected and the empty vector cells groups. In addition, the glycolytic stress test showed a marked decrease in glycolysis, glycolytic capacity and reserve in MDM2-overexpressed UM-SCC-11A cells. On the other hand, the glycolytic function of MDM2-plasmid- and TIGAR-plasmid-transfected UM-SCC-11B were comparable with those of untransfected and the empty vector cells groups (Figure 3.41. A and B).

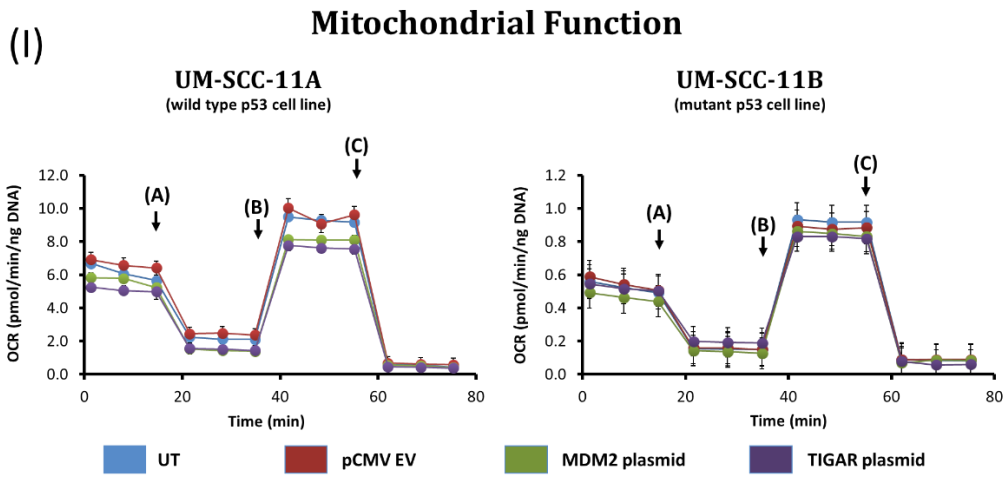

(II)

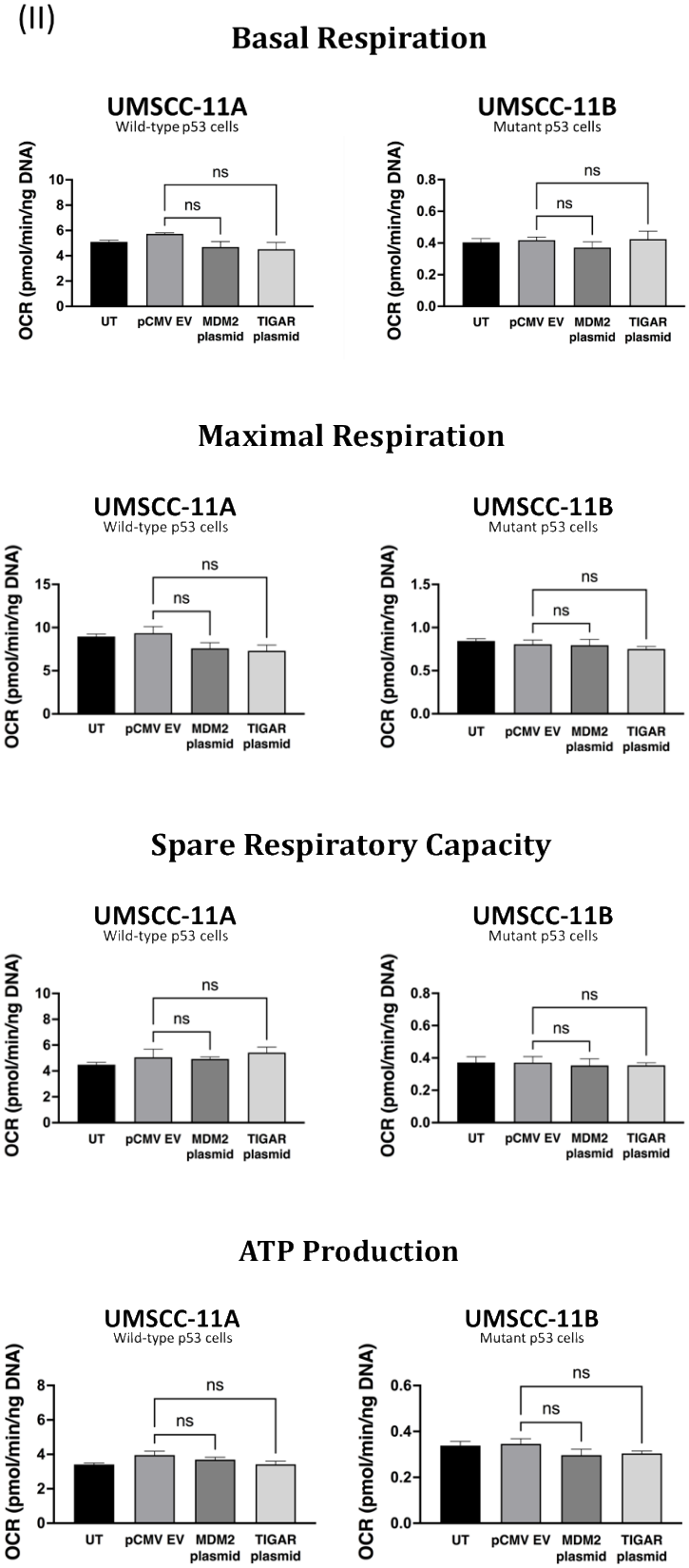

Figure 3.40.: Comparative metabolic profile of TIGAR-overexpressed UM-SCC-11A and UM-SCC-11B cells in the mitochondrial stress test. Untransfected cells (UT) or cells transfected with either empty vector, MDM2 or TIGAR DNA constructs were subjected to mitochondrial stress test, as described in

2.3.6.1. Points A, B, and C on the graphs refer to the injections time points of 1µM oligomycin, 0.5µM FCCP and 1µM rotenone and antimycin-A, respectively. Post-injection changes in the mitochondrial function were used to calculate the mitochondrial respiration parameters as described in Table 2.4. and are shown in Figure 2.4. (I) TIGAR-and MDM-overexpressed cells show non-marked changes in the mitochondrial function at basal levels and following the inhibition of the ATP-linked respiration (at time point A) and uncoupling ATP synthesis from the ETC (at time point B) in comparison to the untransfected or empty vector group in both cell lines. (II) Absolute data derived from mitochondrial stress tests was normalised to DNA content for all groups of cells, and the absolute values for basal respiration, maximal respiration, spare respiratory capacity and ATP production were calculated as described in section 2.3.6.1. OCR readings were obtained from three experiments (n=3), each experiment was performed in hextuplet. Data are presented as mean OCR (pmol/min), normalised to DNA content (ng DNA) as described in 2.3.8. Means of individual data were used to derive overall means. Error bars represent SEM. Statistical analysis: a one-way ANOVA with Dunnett's test. (ns) $p > 0.05$, (*) $p \leq 0.05$, (**) $p \leq 0.01$, (***) $p \leq 0.001$, (****) $p \leq 0.0001$.

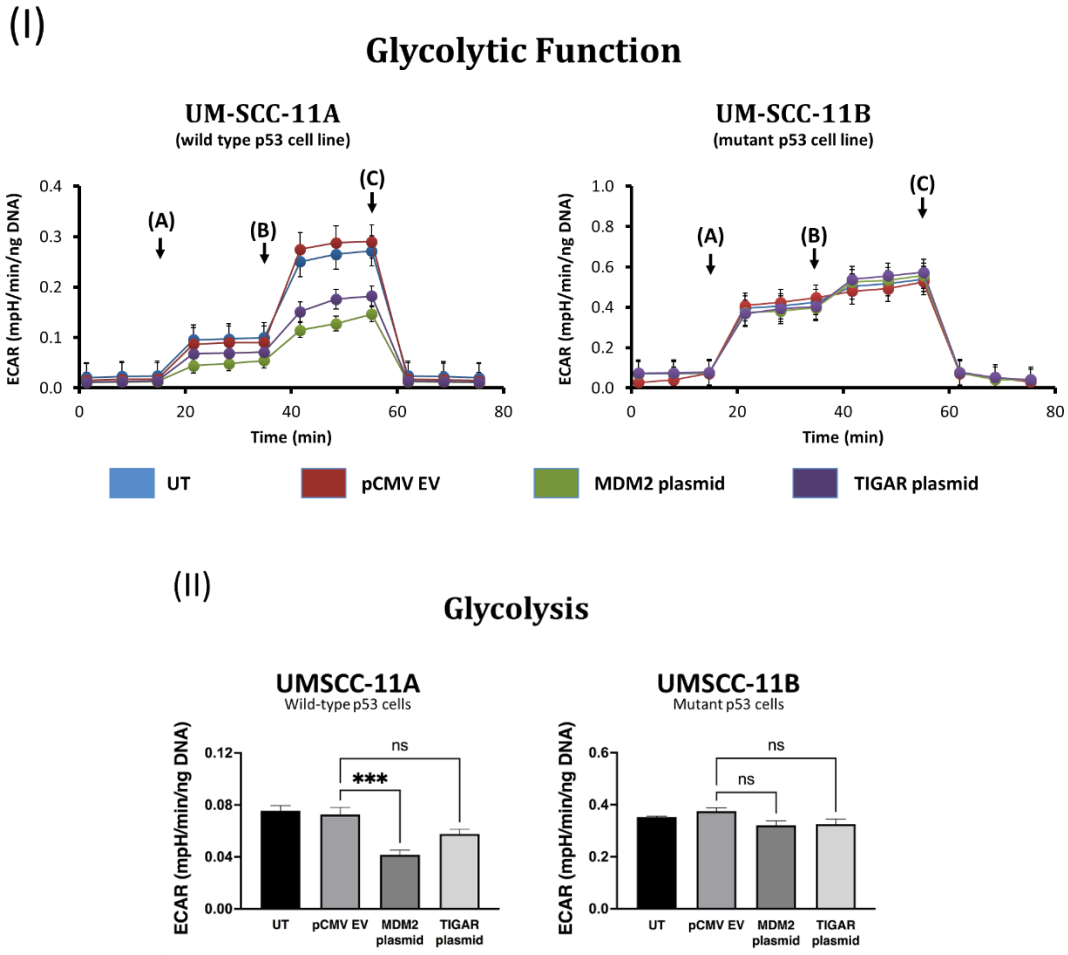

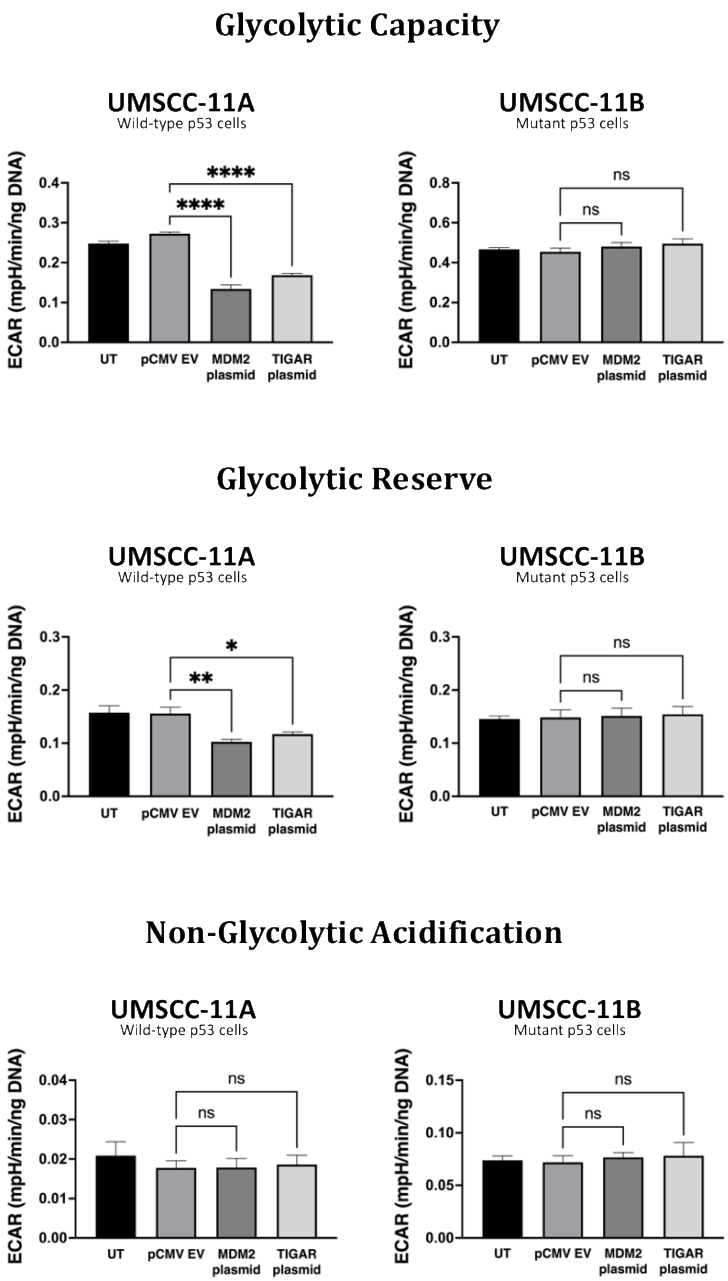

Figure 3.41.: Comparative metabolic profile of TIGAR-overexpressed UM-SCC-11A and UM-SCC-11B cells in the glycolytic stress test. Untransfected cells (UT) or cells transfected with either empty vector, MDM2 or TIGAR DNA constructs were subjected to glycolytic stress test, as described in 2.3.6.2. Points A, B, and C on the graphs refer to the injections time points of 10mM glucose, 1µM oligomycin, and 50mM 2-DG, respectively. Post-injection changes in the glycolytic function were used to calculate the glycolytic parameters as described in Table 2.5. and are shown in Figure 2.5. **(I)** TIGAR-overexpressed cells show non-marked changes in the glycolytic function following the injection of glucose (at time point A), but show marked inhibition following the inhibition of the ATP-linked respiration (at time point B) in comparison with the untransfected or empty vector groups in UM-SCC-11A. MDM2-overexpressed cells UM-SCC-11A show marked inhibition in the glycolytic function following the injection of glucose (at time point A), and the inhibition of the ATP-linked respiration (at time point B) in comparison to the untransfected or empty vector cells. No marked changes are observed between all groups in UM-SCC-11B cells. **(II)** Absolute data derived from glycolytic stress tests was normalised to DNA content for all groups of cells, and the absolute

values for glycolysis, glycolytic capacity, glycolytic reserve and non-glycolytic acidification were calculated as described in section 2.3.6.2. Although TIGAR-overexpressed UM-SCC-11A cells show no significant differences in values for basal glycolysis, values for glycolytic capacity and reserve were significantly lower in comparison with the untransfected or empty vector cells. Values for glycolysis, glycolytic capacity and glycolytic reserve were considerably lower in the MDM2-overexpressed UM-SCC-11A cells (left). ECAR readings were obtained from three experiments (n=3), each experiment was performed in hextuplet. Data are presented as mean ECAR (mpH/min), normalised to DNA content (ng DNA) as described in 2.3.8. Means of individual data were used to derive overall means. Error bars represent SEM. Statistical analysis: a one-way ANOVA with Dunnett's test. (ns) $p > 0.05$, (*) $p \leq 0.05$, (**) $p \leq 0.01$, (***) $p \leq 0.001$, (****) $p \leq 0.0001$.

With respect to TIGAR, these results are consistent with results obtained from TIGAR-knockdown UM-SCC-11A and UM-SCC-11B cells. The alteration in TIGAR expression (both knockdown and overexpression) show a comparable impact on the mitochondrial function in the presence of wild type p53 (Figures 3.23. and 3.40.), while altered expression of TIGAR has a significant effect on the glycolytic function as TIGAR knockdown promotes glycolysis (Figure 3.24.) and TIGAR overexpression decreases the glycolytic capacity and reserves (Figure 3.41.) in the presence of wild type p53. In addition, the alteration in TIGAR expression (both knockdown and overexpression) show a comparable impact on both the mitochondrial (Figures 3.23. and 3.40.) and glycolytic functions (Figures 3.24. and 3.41.) in the presence of mutant p53. Although overexpressing TIGAR has no effect on basal glycolysis in the presence or absence of functional p53, it significantly increases glycolytic capacity and reserve in wild type p53 cells but not in the mutant p53 cells. In addition, our data show that overexpressing MDM2 in the presence of wild type function of p53 inhibits the glycolytic function, with no similar impact on cells that harbour mutant *TP53*.

Together, alterations in the glycolytic profile following the overexpressing of MDM2 or TIGAR appears likely to be linked to the wild type function of p53, since overexpressing MDM2 or TIGAR in the presence of mutant p53 has no significant impact on the metabolic phenotype, either mitochondrial or glycolytic. These findings are consistent with the pivotal role of p53 in regulating TIGAR and support our notion that the role of TIGAR in regulating glycolysis in SCCHN is strongly linked to the p53 regulatory function, whilst raising questions about the function of MDM2 in metabolic regulation.

However, these results cannot determine whether TIGAR overexpression fails to impact the glycolytic function in the presence of mutant p53 due to the compromised

function of p53, as a TIGAR regulator, or whether this is due to GOF properties in mutant p53 cells (C242S, in this instance).

To expand on the above analysis, similar experiments were performed in UM-SCC-1 cells and isogenic derivatives. Since the parental line lacks any p53 protein, the transient overexpression of TIGAR in these cells can be used to determine the p53 dependence of any effects of TIGAR overexpression. In addition, the comparing null and WT-p53 expressing cells with an isogenic background permits us to examine whether previous data suggesting that p53 is required for TIGAR-mediated regulation of glycolysis are correct. In addition, the use of derivatives that harbour different missense mutations of *TP53* may provide a more detailed picture of a possible impact of partial retention of p53 function (UM-SCC-1 C176F-p53) and the role of p53 GOF (UM-SCC-1 C176F-p53 and R282W-p53) in the regulation of TIGAR role in glycolysis.

UM-SCC-1 and isogenic derivative cells were transfected with 0.1 μg/ml plasmid for 48 hours, fluorescence microscopy was used to check transfection and images of transfected cells were taken only one hour before Seahorse XFe metabolic profiling was performed. The transfection efficiency of GFP plasmid DNA was measured as described in 2.5.4. (Figure 3.42. A), and western blotting analysis was performed to check the protein expression of MDM2, p53 and TIGAR (Figure 3.42. B1). Densitometry was used to calculate the relative expression of MDM2, p53 and TIGAR normalised to the expression of housekeeping protein vinculin in the empty-vector-transfected cells (Figure 3.42. B2.). Interestingly, overexpression of MDM2 in UM-SCC-1 cells expressing mutant p53 (R175H, C176F and R282W) shows a decrease in levels of p53 expression (Figure 3.42.), which support ample literature which indicates that show that MDM2 retains the ability to ubiquitinate and degrade mutant p53 (340–342).

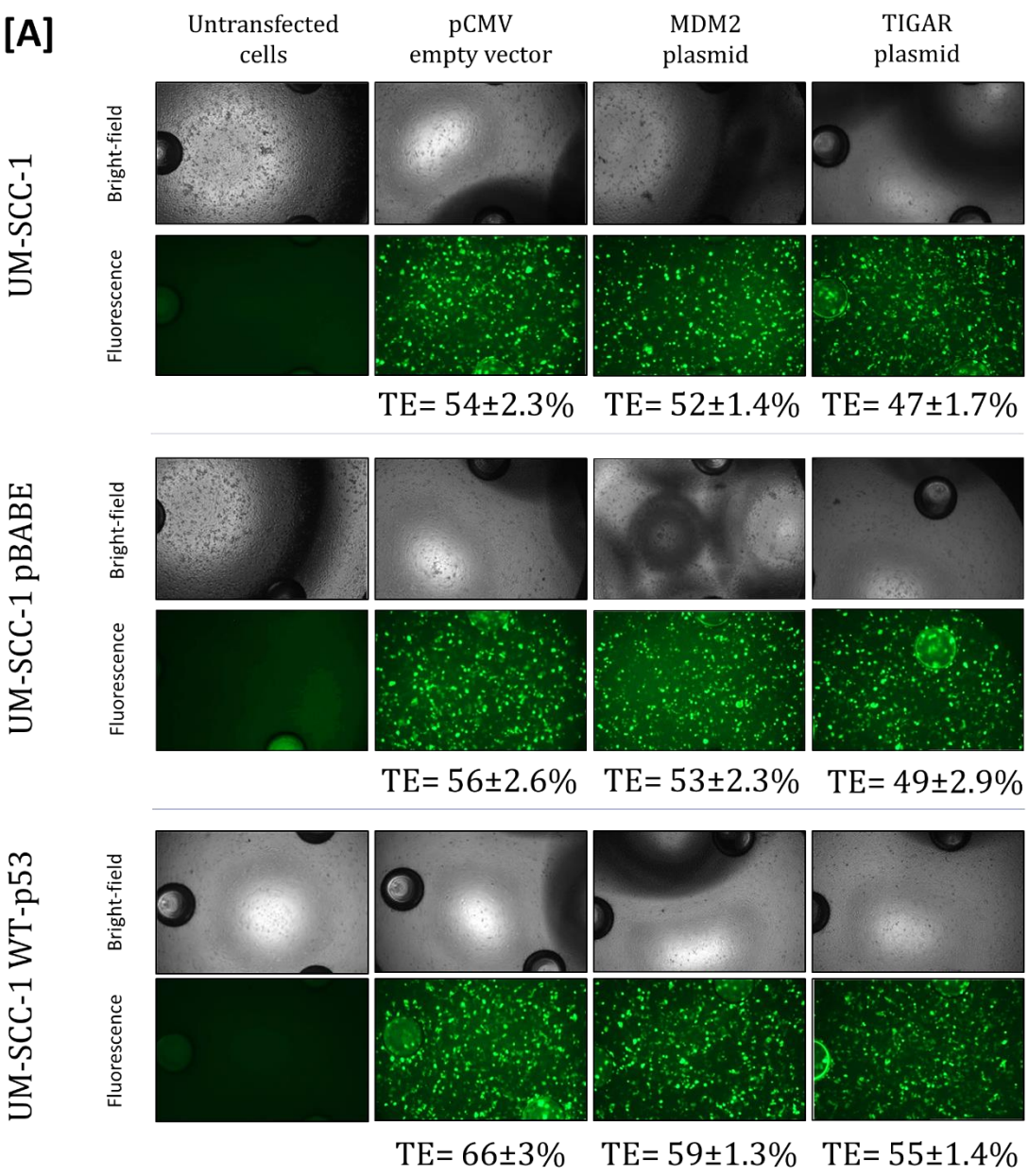
[A]
Untransfected cells
pCMV empty vector
MDM2 plasmid
TIGAR plasmid
UM-SCC-1
Bright-field
Fluorescence
TE= 54±2.3%
TE= 52±1.4%
TE= 47±1.7%
UM-SCC-1 pBABE
Bright-field
Fluorescence
TE= 56±2.6%
TE= 53±2.3%
TE= 49±2.9%
UM-SCC-1 WT-p53
Bright-field
Fluorescence
TE= 66±3%
TE= 59±1.3%
TE= 55±1.4%

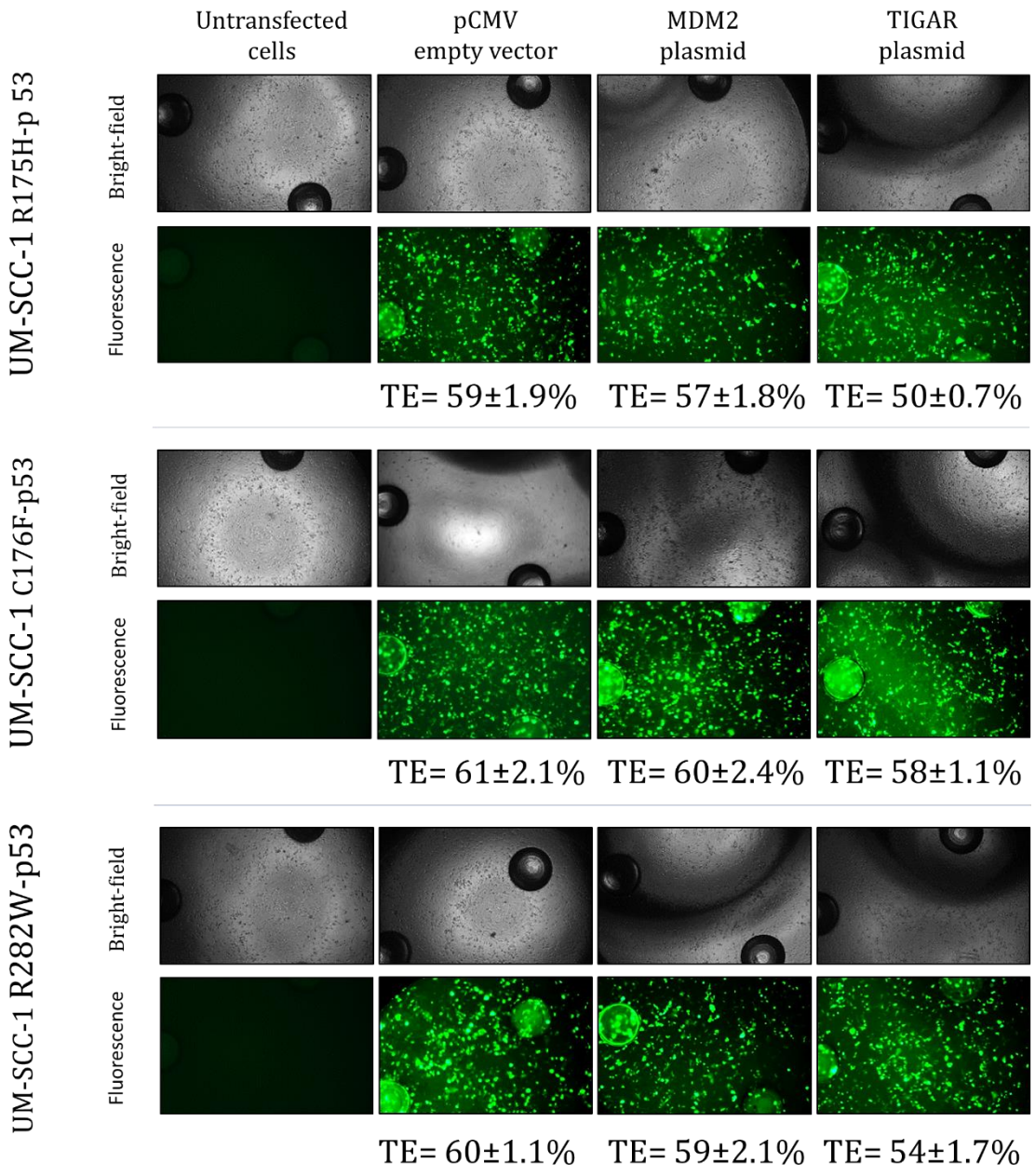
Untransfected cells
pCMV empty vector
MDM2 plasmid
TIGAR plasmid
UM-SCC-1 R175H-p 53
Bright-field
Fluorescence
TE= 59±1.9%
TE= 57±1.8%
TE= 50±0.7%
UM-SCC-1 C176F-p53
Bright-field
Fluorescence
TE= 61±2.1%
TE= 60±2.4%
TE= 58±1.1%
UM-SCC-1 R282W-p53
Bright-field
Fluorescence
TE= 60±1.1%
TE= 59±2.1%
TE= 54±1.7%

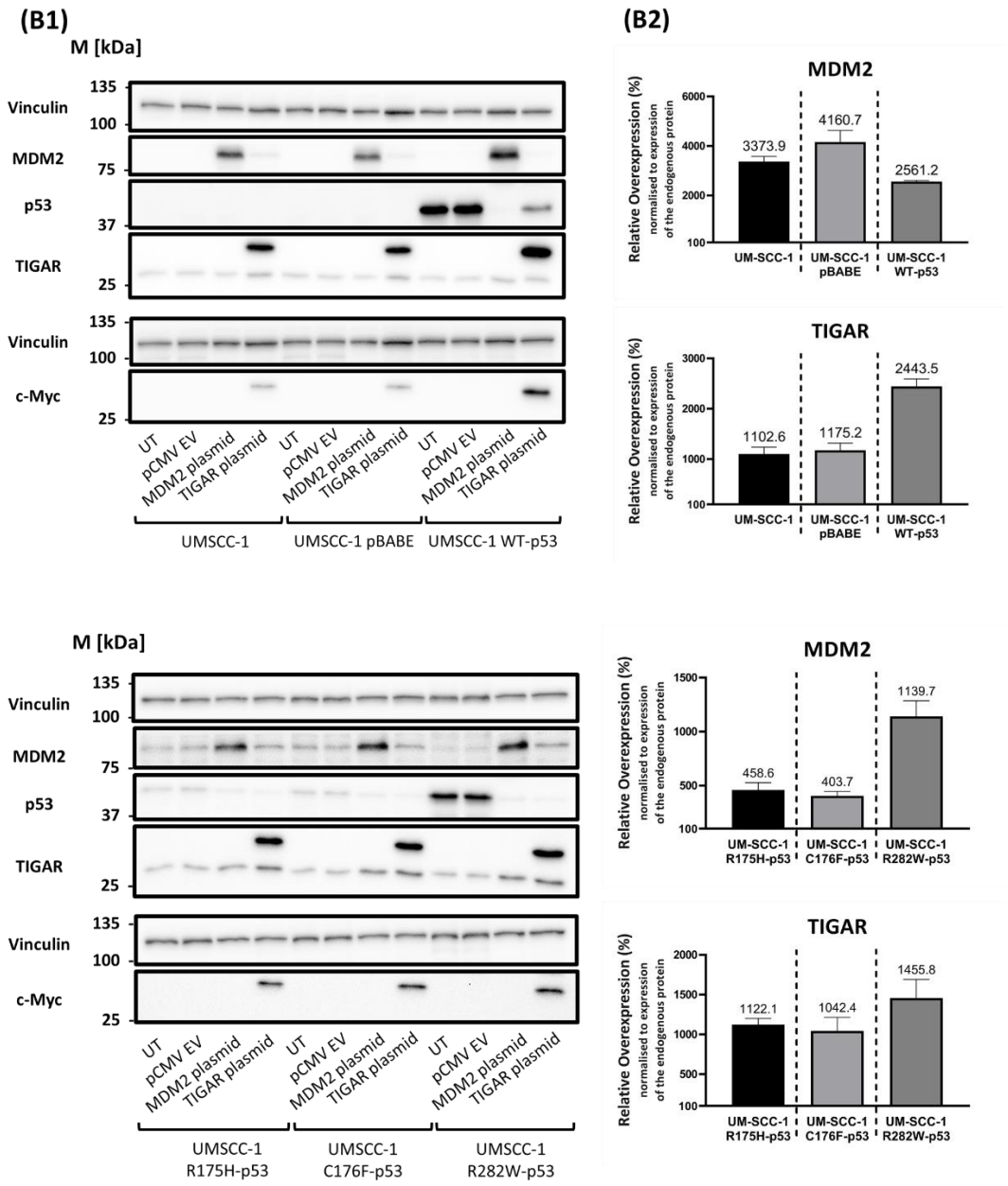

Figure 3.42.: TIGAR overexpression in UM-SCC-1 and derivatives cell lines. [A] Bright-field and fluorescence microscopy images (AMG EVOS, 10X objective) of GFP plasmid-transfected UM-UM-SCC-1 and derivatives cells after 48 hours of transfection, taken in Seahorse XFe96 plate wells one hour before metabolic profiling test was performed. Transfection efficiency is presented as a mean percentage of three wells for each condition. **[B1]** Western blotting analyses of MDM2, p53, TIGAR and c-Myc expression levels in UM-SCC-1 and derivatives cells. Cells were harvested and lysed as described in section 2.8.3. Protein samples were prepared and loaded into gels, and specific antibodies were used for detection as detailed in section 2.1.9. Vinculin was used as a loading control. The migration of protein standards of the indicated approximate molecular weights is shown in kDa. Transfection with Myc-DDK-tagged TIGAR plasmid resulted in the detection of two bands: a top band at ~32kD represents the expression of Myc-DDK-tagged TIGAR and a bottom band at ~30kD represents the expression of endogenous TIGAR. **[B2]** Densitometry analysis of the expression of MDM2 and TIGAR in plasmid-DNA-transfected cells as described in 2.8.5. Relative elevation in protein expression of three biological replicates compared to the endogenous

expression of the relevant protein in empty vector group normalised to the expression of the housekeeping protein vinculin (%), as shown in [B1]. Plasmids used are detailed in 2.6.

Outputs from the mitochondrial stress test for TIGAR-overexpressed UMSCC-1 and isogenic derivatives are shown in Figure 3.43., while outputs from glycolytic stress tests are shown in Figure 3.44.

Outcomes of mitochondrial stress test from MDM2- and TIGAR-overexpressed UM-SCC-1 and derivatives cells were consistent with previously discussed data. Overexpressing MDM2 or TIGAR results in no marked alteration in mitochondrial function in the absence or presence of functional p53 (Figure 3.43.). The results also show that only the derivative that harbours the wild type *TP53* exhibits marked inhibition of glycolytic function following the overexpression of either MDM2 or TIGAR. Consistent with the results previously discussed in this section, overexpressing TIGAR in wild type p53 cells has no significant impact on basal glycolysis, but it shows a considerable reduction in glycolytic capacity and reserve. MDM2-overexpressed cells show a significant decrease in basal glycolysis, glycolytic capacity and reserve in the wild type p53 derivative, while no significant effects were observed between all groups in the derivatives that harbour mutant *TP53* (Figure 3.44.). No considerable differences are shown between the p53-null and mutant p53 cells, which weakens the possibility that the negligible effect of overexpression of MDM2 and TIGAR on the mitochondrial phenotype can be attributed to p53 GOF properties in SCCHN and support the notion that the wild type function of p53 is the main determinant of the metabolic phenotype in SCCHN.

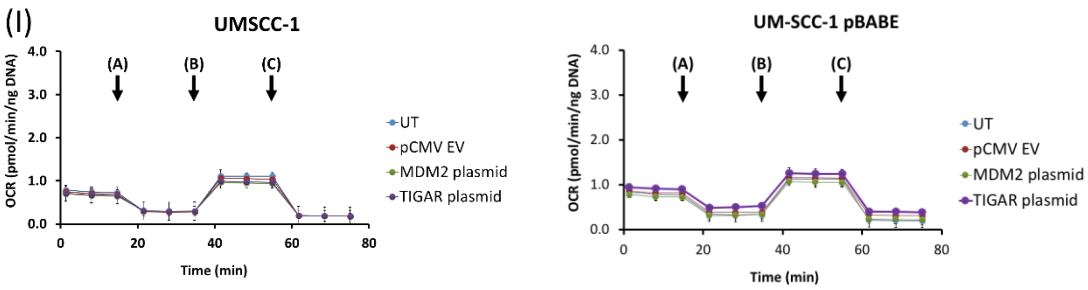

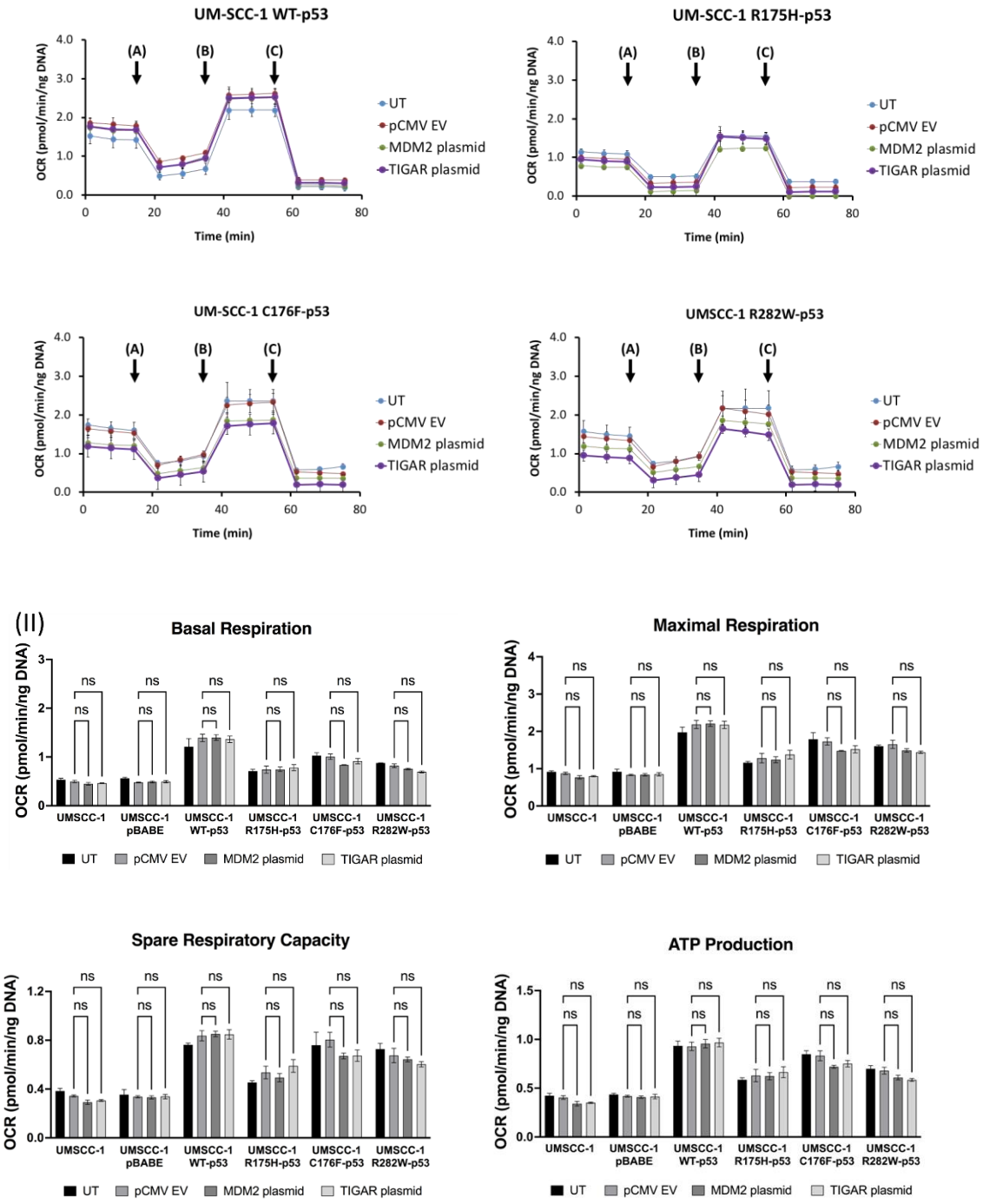

Figure 3.43.: Comparative metabolic profile of TIGAR-overexpressed UM-SCC-1 and derivative cell lines in the mitochondrial stress test. Untransfected cells (UT) or cells transfected with either empty vector, MDM2 or TIGAR DNA constructs were subjected to mitochondrial stress test, as described in 2.3.6.1. Points A, B, and C on the graphs refer to the injections time points of 1µM oligomycin, 0.5µM FCCP and 1µM rotenone and antimycin-A, respectively. Post-injection changes in the mitochondrial function were used to calculate the mitochondrial respiration parameters as described in Table 2.4. and are shown in Figure 2.4. **(I)** TIGAR-and MDM-overexpressed cells show non-marked changes in the mitochondrial function at basal levels and following the inhibition of the ATP-linked respiration (at time point A) and uncoupling ATP synthesis from the ETC (at time point B) in comparison to the untransfected or empty vector group in all cell lines. **(II)** Absolute data derived from mitochondrial stress tests was normalised to

DNA content for all groups of cells, and the absolute values for basal respiration, maximal respiration, spare respiratory capacity and ATP production were calculated as described in section 2.3.6.1. OCR readings were obtained from three experiments (n=3), each experiment was performed in hextuplet. Data are presented as mean OCR (pmol/min), normalised to DNA content (ng DNA) as described in 2.3.8. Means of individual data were used to derive overall means. Error bars represent SEM. Statistical analysis: a one-way ANOVA with Dunnett's test. (ns) $p > 0.05$, (*) $p \leq 0.05$, (**) $p \leq 0.01$, (***) $p \leq 0.001$, (****) $p \leq 0.0001$.

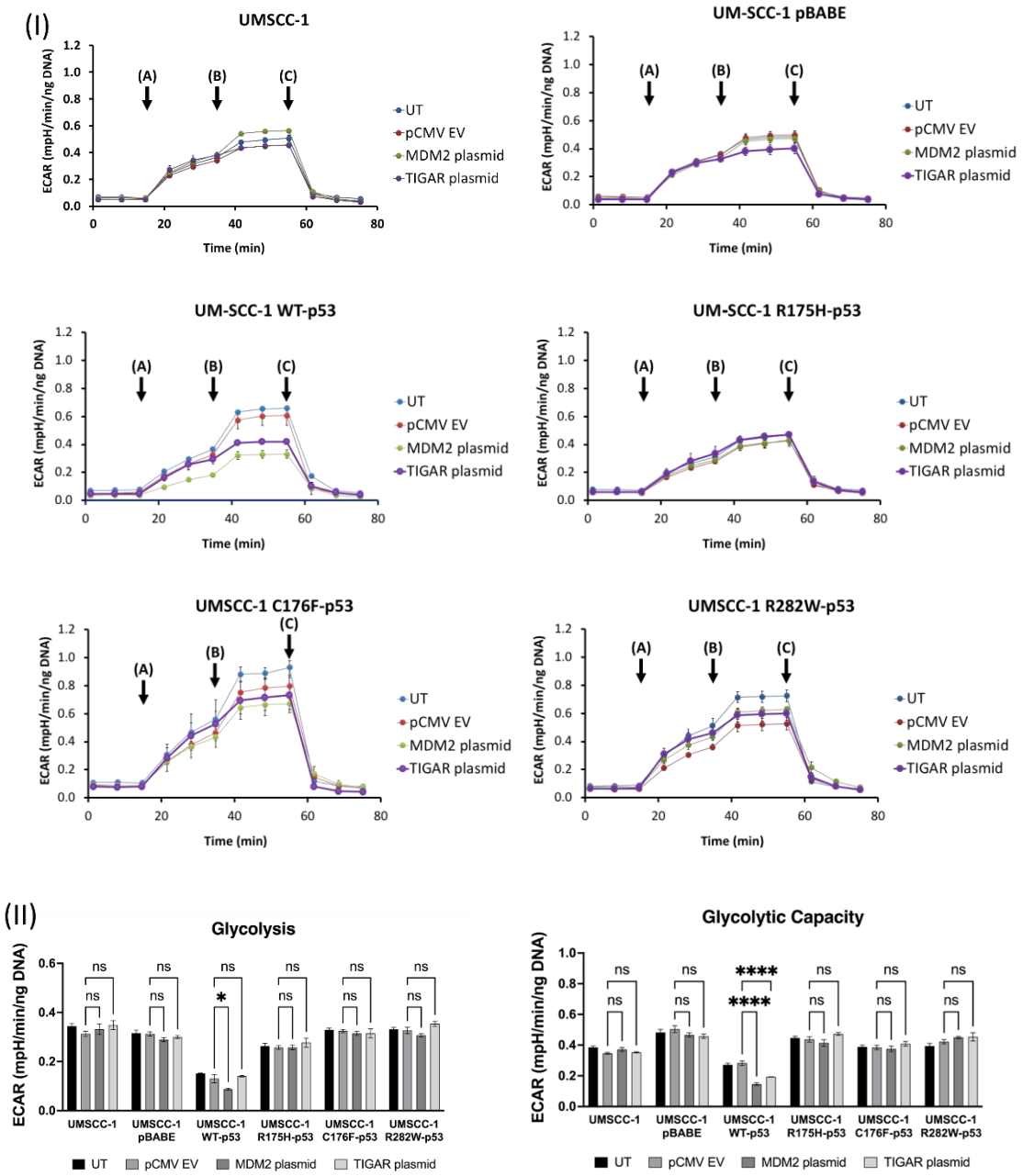

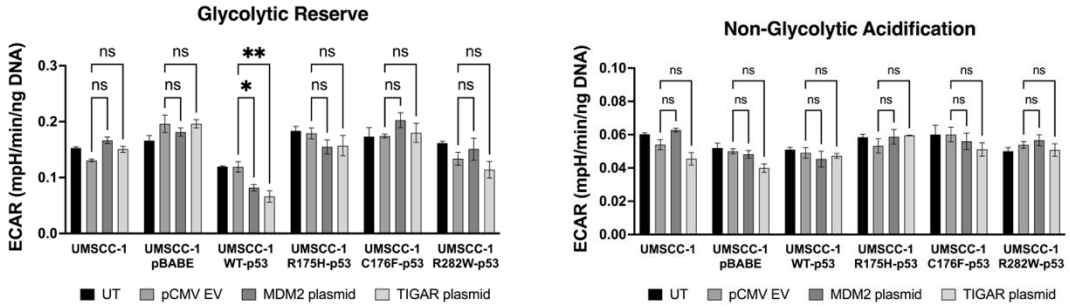

Figure 3.44.: Comparative metabolic profile of TIGAR-overexpressed UM-SCC-1 and derivatives cells in the glycolytic stress test. Untransfected cells (UT) or cells transfected with either empty vector, MDM2 or TIGAR DNA constructs were subjected to glycolytic stress test, as described in 2.3.6.2. Points A, B, and C on the graphs refer to the injections time points of 10mM glucose, 1μM oligomycin, and 50mM 2-DG, respectively. Post-injection changes in the glycolytic function were used to calculate the glycolytic parameters as described in Table 2.5. and are shown in Figure 2.5. **(I)** TIGAR-overexpressed cells show non-marked changes in the glycolytic function following the injection of glucose (at time point A), but show marked inhibition following the inhibition of the ATP-linked respiration (at time point B) in comparison with the untransfected or empty vector groups in the derivative that harbour the wild type *TP53*. Overexpressing MDM2 in the same derivative cell line show marked inhibition in the glycolytic function following the injection of glucose (at time point A), and the inhibition of the ATP-linked respiration (at time point B) in comparison to the untransfected or empty vector cells. No marked changes are observed between all groups in all other cell lines. **(II)** Absolute data derived from glycolytic stress tests was normalised to DNA content for all groups of cells, and the absolute values for glycolysis, glycolytic capacity, glycolytic reserve and non-glycolytic acidification were calculated as described in section 2.3.6.2. ECAR readings were obtained from three experiments (n=3), each experiment was performed in hextuplet. Data are presented as mean ECAR (mpH/min), normalised to DNA content (ng DNA) as described in 2.3.8. Means of individual data were used to derive overall means. Error bars represent SEM. Statistical analysis: a one-way ANOVA with Dunnett's test. (ns) $p > 0.05$, (*) $p \leq 0.05$, (**) $p \leq 0.01$, (***) $p \leq 0.001$, (****) $p \leq 0.0001$.

These experiments demonstrate that exogenous expression of MDM2 inhibits glycolytic function, and hence the Warburg effect, in a p53 dependent manner. This observation is surprising, since the well-documented role of MDM2 as a ubiquitin ligase that targets p53 for degradation, together with the role of p53 in suppressing glycolysis, would predict the opposite effect (343,344). An explanation for this observed effect of MDM2 overexpression may come from the published role of MDM2 as a PGAM ubiquitin ligase, which could also provide some support of earlier evidence of potential tumour suppressing activities of MDM2 reported *in vitro* (336,345,346). PGAM catalyses the conversion of 3-phosphoglycerate (3-PG) to 2-phosphoglycerate (2-PG)(251), and its activity is increased in several malignancies compared to normal tissues (347,348). *TP53* negatively regulates the expression of PGAM, which controls a unique step in

glycolysis, as many glycolytic intermediates that are employed as anabolic biosynthesis precursors are found upstream of this step (200). The loss of *TP53* in cancer cells has been shown to upregulate PGAM gene expression (204,251,349,350). Thus, MDM2 may have functionally opposing effects on two distinct substrates, p53 and PGAM, that regulate glycolysis (351). A study by Mikawa et al found that MDM2 attenuates the Warburg effect by ubiquitinating and degrading PGAM in the presence of functional p53 (336). However, these opposing effects of MDM2-mediated regulation of p53 and PGAM need further investigation. In addition, one study has found that increased expression of MDM2 in p53 null H1299 cells resulted in a marked decrease in the levels of extracellular lactic acid (204), which also accords with the data presented here in this section and might be explained by the reported activity of MDM2 promoting degradation of PGAM.

3.2.3.2. Conclusion

Considered as a whole, the results presented in this section (summarised in Tables 3.4. and 3.5.) demonstrate that exogenous overexpression of TIGAR has no impact on the basal metabolic activity of wild type p53 cells, which exhibit low glycolytic activity and high mitochondrial respiration activity (Figures 3.37., 3.38., 3.40., 3.41., 3.43. and 3.44.). Results presented in this section also demonstrate that overexpression of TIGAR can decrease glycolytic capacity and reserves following ATP synthase inhibition in wild type p53 cells (Figures 3.38., 3.41., and 3.44.) but not in p53-null cells or cells expressing mutant p53 (Figures 3.41., and 3.44.). These results: increased glycolytic capacity and reserves following TIGAR knockdown/decreased glycolytic capacity and reserves following overexpression of TIGAR in cells expressing wild type p53 and the absence of this effect in cells lacking p53 function (null/mutants) supports the notion that the TIGAR-mediated regulatory mechanism of glycolytic function is p53-dependent, and adds to our understanding of the role that TIGAR plays in the regulation of glycolysis in SCCHN cells.

Table 3.4. : Changes in mitochondrial parameters following overexpression of MDM2 or TIGAR in a panel of SCCHN cell lines.

	Cell line	*TP53* status	Gene expression manipulation	Basal reparation	Maximal respiration	Spare respiratory Capacity	ATP production
Wild type	UMSCC-17A	WT	MDM2 overexpression	ns	ns	ns	ns
			TIGAR overexpression	ns	ns	ns	ns
	UMSCC-11A	WT	MDM2 overexpression	ns	ns	ns	ns
			TIGAR overexpression	ns	ns	ns	ns
	UM-SCC-1 WTp53	WT	MDM2 overexpression	ns	ns	ns	ns
			TIGAR overexpression	ns	ns	ns	ns
Compromised	UM-SCC-11B	Mut	MDM2 overexpression	ns	ns	ns	ns
			TIGAR overexpression	ns	ns	ns	ns
	UM-SCC-1	null	MDM2 overexpression	ns	ns	ns	ns
			TIGAR overexpression	ns	ns	ns	ns
	UM-SCC-1 pBABE	null	MDM2 overexpression	ns	ns	ns	ns
			TIGAR overexpression	ns	ns	ns	ns
	UM-SCC-1 R175H-p53	Mut	MDM2 overexpression	ns	ns	ns	ns
			TIGAR overexpression	ns	ns	ns	ns
	UM-SCC-1 C176F-p53	Mut (partially functional)	MDM2 overexpression	ns	ns	ns	ns
			TIGAR overexpression	ns	ns	ns	ns
	UM-SCC-1 R282W-p53	Mut	MDM2 overexpression	ns	ns	ns	ns
			TIGAR overexpression	ns	ns	ns	ns

Table 3.5.: Changes in glycolytic parameters following overexpression of MDM2 or TIGAR in a panel of SCCHN cell lines.

	Cell line	*TP53* status	Gene expression manipulation	Basal reparation	Maximal respiration	Spare respiratory Capacity	ATP production
Wild type	UMSCC-17A	WT	MDM2 overexpression	↓	↓	↓	ns
			TIGAR overexpression	ns	↓	↓	ns
	UMSCC-11A	WT	MDM2 overexpression	↓	↓	↓	ns
			TIGAR overexpression	ns	↓	↓	ns
	UM-SCC-1 WTp53	WT	MDM2 overexpression	↓	↓	↓	ns
			TIGAR overexpression	ns	↓	↓	ns
Compromised	UM-SCC-11B	Mut	MDM2 overexpression	ns	ns	ns	ns
			TIGAR overexpression	ns	ns	ns	ns
	UM-SCC-1	null	MDM2 overexpression	ns	ns	ns	ns
			TIGAR overexpression	ns	ns	ns	ns
	UM-SCC-1 pBABE	null	MDM2 overexpression	ns	ns	ns	ns
			TIGAR overexpression	ns	ns	ns	ns
	UM-SCC-1 R175H-p53	Mut	MDM2 overexpression	ns	ns	ns	ns
			TIGAR overexpression	ns	ns	ns	ns
	UM-SCC-1 C176F-p53	Mut (partially functional)	MDM2 overexpression	ns	ns	ns	ns
			TIGAR overexpression	ns	ns	ns	ns
	UM-SCC-1 R282W-p53	Mut	MDM2 overexpression	ns	ns	ns	ns
			TIGAR overexpression	ns	ns	ns	ns

In addition, although TIGAR knockdown results in increased basal metabolic activity in p53-null cells, with no similar impact on the metabolic profile of cells harbouring mutant p53 (Figure 3.32.), the results presented in 3.44. show that TIGAR overexpression has no significant impact on the metabolic profile of both p53-null or mutant p53 cells. These findings suggest that any effects of a possible p53-independent regulation mechanism of TIGAR (discussed in 3.2.2.3.) are not related to a different regulatory role that TIGAR plays in the absence of p53 function. In addition, the increased basal glycolysis in p53-null and wild type p53 cells following TIGAR knockdown with no significant impact on basal glycolysis in mutant p53 cells (discussed in 3.2.2.3.) may be due to GOF properties in cells expressing mutant p53 that abrogate or reverse the effect of TIGAR knockdown on glycolytic function.

Given the apparently important role of the switch toward aerobic glycolysis as a hallmark of cancer (discussed in detail in 1.3.1.) and the critical role of p53 function as a determinant of this switch as demonstrated by our results in section 3.1.3., the results presented in 3.2. indicate that the highly active glycolytic function and the limited metabolic diversity in p53-null or mutant p53 SCCHN cells could constitute a therapeutic target for anti-metabolic agents in these cells but one that may be appropriate in the p53 wild type cells which show greater metabolic diversity and less dependence on glycolysis. Interestingly, the results presented in 3.2. show that inhibiting TIGAR expression in cells harbouring wild type p53 results in a significant increase in glycolytic function comparable to that resulting from inhibiting p53 in these cells (Figure 3.32.). Thus, TIGAR-inhibition-mediated increases in glycolytic function could also represent a therapeutic target for anti-metabolic agents in SCCHN cells harbouring wild type p53. These results suggest further investigation of the response of SCCHN cells harbouring different p53 status to treatment with anti-metabolic agents, with or without TIGAR inhibition, is warranted. The aim being to examine the potential impact of such on the sensitivity of cells to IR, and this is the focus of the next chapter.

3.3. Investigating the potential role of p53 and TIGAR in determining response to anti-metabolic agents

Our study primarily aimed to learn more about the mechanisms that influence cell life and death in SCCHN, and how this knowledge can help us find new therapeutic approaches that improve therapeutic response, survival, and other clinically relevant

factors. Thus, and in line with our findings in sections 3.1. and 3.2., the final section of our study aims to investigate the potential role of p53 and TIGAR in determining the efficacy of drugs targeting the glycolysis pathway in improving response to IR in SCCHN. In this section, three isogenic derivatives of the parental cell line UM-SCC-1: UM-SCC-1 pBABE, a p53-null derivative that harbour empty vector pBABE, UM-SCC-1 WT-p53, a wild type p53 derivative, and UM-SCC-1 R175H-p53, a mutant p53 derivative that harbour the most common *TP53* mutation. These three derivatives were used in our study to investigates the metabolic profile of SCCHN cells and the potential role of TIGAR in p53-mediate metabolic regulation of SCCHN, and the use of these isogenic derivatives in the subsequent study (transfected with either non-targeting siRNA (siCONT) or siRNA specific to TIGAR) will provide a comprehensive insight into the potential effects of therapeutic inhibition of the glycolytic pathway in SCCHN cells expressing different status of p53 (null, wild type and mutant) with or without inhibition of TIGAR, which can help to develop novel therapeutic approaches that target the glycolytic pathway in SCCHN cells based on p53 status.

Since the half-maximal inhibitory concentration (IC_{50}) is the most commonly used metric for the on-target effectiveness of a drug in inhibiting a specific biological or biochemical function (352), we determined this empirically and applied the candidate inhibitors at their IC_{50} to investigate the cellular responses, including changes in cell viability, metabolic profile, as well as altering the radiosensitivity of SCCHN.

In our study, we used five candidate drugs that affect different parts of the glycolysis pathway. These specific inhibitors were chosen based on their effects on several mechanisms in the glycolytic function, upstream and downstream the third step of the glycolysis pathway which is regulated by TIGAR (Figure 3.45.), and are all discussed below:

2-Deoxy-D-glucose (2-DG) is a glucose analogue that inhibits the first step of glycolysis (353). 2-DG is phosphorylated by hexokinase, a mediator of one of the three rate-limiting steps of glycolysis, to 2-DG-P which cannot be further metabolised by phosphoglucose isomerase in the second step of the glycolysis pathway. This leads to the accumulation of 2-DG-P in the cell and the depletion of cellular ATP. *In vitro*, 2-DG has been shown to induce autophagy, increase ROS production, and activate AMPK (353). A number of studies have shown that 2-DG can radisosensitise SCCHN cells (246,354). It is expected that inhibiting the first step of glycolysis pathway would lead

to significant decrease in the glycolytic flux and the subsidiary routes (for instance: PPP and pyruvate fate).

6-aminonicotinamide (6-AN) is a monocarboxylic acid amide that is converted into 6-amino-NADP+ by NAD-glycohydrolase, a NADP analogue that inhibits NADP+-dependent enzymes of the pentose phosphate pathway: 6-phosphogluconate dehydrogenase (6-PGD), glutathione reductase and glucose 6-phosphate dehydrogenase (G6PD)(355,356), which result in ROS-mediated apoptosis (357–359). Studies have shown that 6-AN can sensitise cancer cells to cisplatin (258), and to radiation (257,360). 6-AN-mediated inhibition of PPP is expected to inhibit the cell viability by inhibiting the anti-oxidant activity of PPP and the biosynthesis of nucleotides and nucleic acids

3PO (3-(3-pyridinyl)-1-(4-pyridinyl)-2-propen-1-one) is a potent and selective inhibitor of PFKFB3 that reduces glycolytic flux and suppresses glucose uptake (248), depriving SCCHN of the dominant source of energy (245). 3PO decreases the intracellular concentration of F2,6BP, lactate, ATP, NAD+, and NADH, and markedly attenuates the proliferation of several human tumours *in vitro* (248). Although the effect of 3PO on PPP is yet to be known, it is expected that inhibiting the glycolysis pathway at the third step, unlike targeting the first step of the pathway, would increase the PPP flux and NADPH levels and enhance the ability to regulate cellular levels of ROS and oxidative stress.

UK-5099 [α-cyano-β-(2-phenylindol-3-yl)acrylate] is a potent inhibitor of MPC (361), and hence inhibits pyruvate-dependent oxygen consumption and induces lactate generation. UK-5099 was found to show some conflicting effects on cancer cells *in vitro*. UK-5099 has been shown to inhibit mitochondrial respiration, increase glycolysis and sensitise cells to radiation in hypopharyngeal tumour cells (362). Although similar effects on glycolysis, mitochondrial respiration and lactate levels were found in oesophageal squamous cell carcinomas cell lines following treatment with UK-5099, it was found that UK-5099 has increased radioresistance in these cells (363). The inhibition of pyruvate transport to mitochondria by UK-5099 is expected to inhibit mitochondrial respiration and increase extracellular acidification.

Sodium dichloroacetate (DCA) is a specific inhibitor of pyruvate dehydrogenase kinase (PDK)(364). It increases reactive oxygen species (ROS) generation and triggers

apoptosis in cancer cells. Several studies have found that DCA radisosensitises cancer cells *in vitro* (365–367). DCA treatment is likely to increase the absolute values of mitochondrial respiration parameters and increase oxidative stress.

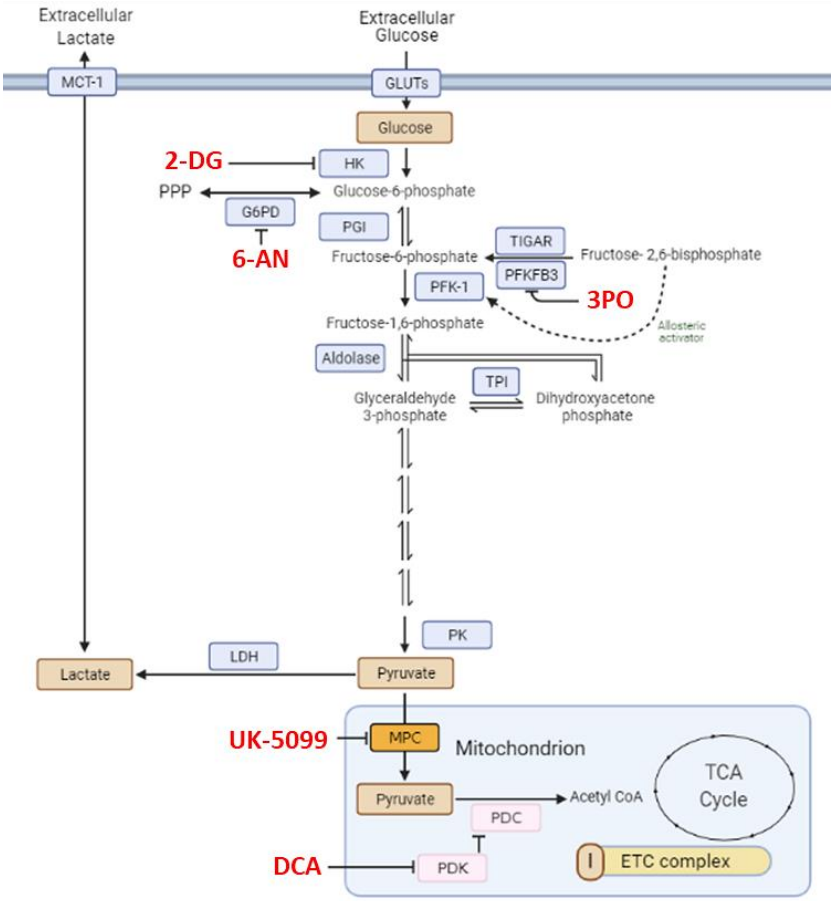

Figure 3.45.: Action of the candidate anti-metabolic agents used in the study. 2-DG is a glucose analogue that inhibits the first step of glycolysis, which is one of the three rate-limiting steps of the pathway. 6-AN is an indirect inhibitor of PPP enzymes, 6-PGD and G6PD. 3PO is a potent and selective inhibitor of PFKFB3 that reduces glycolytic flux and suppresses glucose uptake at the third step of the pathway. UK-5099 is a potent inhibitor of MPC that inhibits pyruvate-dependent oxygen consumption and induces lactate generation. DCA is a specific inhibitor of PDK.

3.3.1. Determining the IC_{50} of the candidate anti-metabolic agents

Since as stated above, the half-maximal inhibitory concentration (IC_{50}) is the most commonly used metric for the on-target effectiveness of a drug in inhibiting a specific biological or biochemical function, determining the IC_{50} of the candidate drugs was the first step in these experiments. The IC_{50} value represents the drug concentration that reduces a biological process by 50% in comparison with a control. To identify the IC_{50}

of the potential drugs, MTT assays were performed as described in section 2.7. for each cell line and a range of drug concentrations in complete medium (see section 2.2.2.) applied for 24, 48 or 72 hours on a pre-determined number of cells (as detailed in 2.7.1.).

The results presented in Figure 3.46. demonstrate that there is no significant difference in inhibition of cell viability between the three time points for all drugs with the exception of DCA, which showed a decrease in the ability to suppress cell viability after 48 and 72 hours of treatment, most likely due to the short half-life of the drug (368)(Figure 3.46.). In subsequent experiments, all drugs were applied at their IC_{50}, as follows: 2-DG at 9mM, 6-AN at 13µM, 3PO at 44µM, UK-5099 at 45µM and DCA at 0.3 mM, for 24 hours.

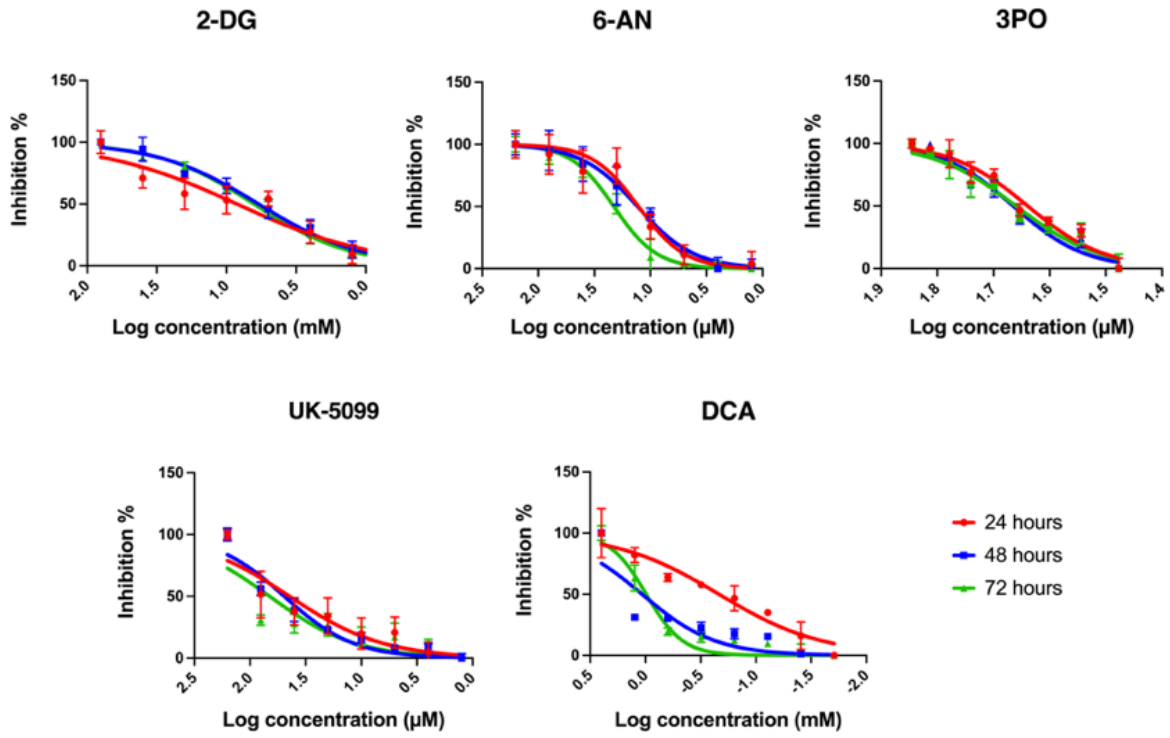

Figure 3.46.: Determination of IC_{50} values for the inhibitors used in this study. The half-maximal inhibitory concentration (IC_{50}) values were measured after 24, 48 and 72 hours of applying seven different concentrations of 2-DG, 6-AN, 3PO, UK-5099 and DCA on pre-determined cell number of the three cell derivatives cell lines used in this section. At the end of the incubation period, cell viability was detected using an MTT-based assay. IC_{50} values were calculated from the dose-response curves by nonlinear regression using Prism GraphPad. Means of individual data were used to derive overall means. Error bars represent SEM.

3.3.2. Investigating the role of p53 status in altering the response to treatment with anti-metabolic agents in SCCHN cells

Results presented in section 3.1. demonstrate that p53 status is an important determinant of the metabolic phenotype of SCCHN, and thus alterations in p53 status lead to marked changes in mitochondrial function and glycolysis in SCCHN cells. Given the importance of changes in the metabolic phenotype as a hallmark of cancer, it is reasonable to consider metabolic pathways as potential targets for cancer therapy. As mentioned in section 1.3.2., contradictory findings from studies on the role of p53 in regulating metabolism in different types of cancer indicate that p53 does not function in the same way in all tissues or the cancers from which it arises (207). Thus, studies of the therapeutic response to drugs targeting p53-regulated metabolic pathways should be performed in cancer-specific systems.

3.3.2.1. The role of p53 status in altering the metabolic profile of SCCHN cells in response to treatment with anti-metabolic agents

To investigate the role of p53 status as a determinant of responses to metabolic inhibitors, the Seahorse XFe mitochondrial stress test and glycolytic stress test were used 24 hours after applying the IC_{50} of each drug individually, as described in 2.3.6.1 and 2.3.6.2. This technique allows for identifying subtle changes in the metabolic profile in response to inhibition of different parts of the glycolytic pathway in the presence or absence of functional p53 and also including p53 GOF mutants. To correct for the expected decrease in oxygen consumption rates (OCR) and extracellular acidification rate (ECAR) caused by cell death and growth arrest anticipated by using drugs, all data were normalised to DNA content.

Results presented in Figure 3.47. show that inhibiting the first step of glycolysis using 2-DG or inhibiting the pentose phosphate pathway using 6-AN results in promoting basal respiration in the absence of wild type p53 (both p53-null and mutant cells) but not in cells that express wild type p53. Although inhibiting MPC using UK-5099 results in a decrease in the mitochondrial respiration (basal, maximal and spare) in a p53-independent, it significantly decreases the mitochondrial-linked ATP production in wild type p53 cells only, mostly due to the highly active mitochondrial function and the greater dependence on mitochondrial respiration to produce ATP in these cells. However, inhibiting PFKFB3 using 3PO or inhibiting PDK using DCA displays no

significant effect on the mitochondrial function in all groups. Results also show that all indicated metabolic inhibitors alter the spare respiratory capacity in wild type p53, as treatment with 2-DG, 6-AN and UK-5099 decrease this, whereas treatment with 3PO and DCA increase it.

Data obtained from the glycolytic stress test show significant inhibition of glycolytic function in the absence of functional p53 following treatment with the indicated metabolic inhibitors. In addition, our results showed that inhibiting the core pathway of glycolysis, either at the first step using 2-DG or at the third step using 3PO, inhibits basal glycolysis and glycolytic capacity in a p53-independent manner, while targeting subsidiary routes, PPP (using 6-AN) and pyruvate fate (using UK-5099 and DCA), has no significant effect on basal glycolysis and glycolytic capacity of wild type p53 cells, which may reflect the greater metabolic diversity these cells show, in contrast to non-functional p53 (null/mutant) mutant cells which show significant changes in basal glycolysis and glycolytic capacity in response to the mono treatment with all glycolysis inhibitors used (with the exception of the mono treatment of mutant p53 cells with DCA). Furthermore, the data show that treatments targeting the glycolytic pathway do not change non-glycolytic acidification in the wild type p53 but show marked alterations in the absence of functional p53.

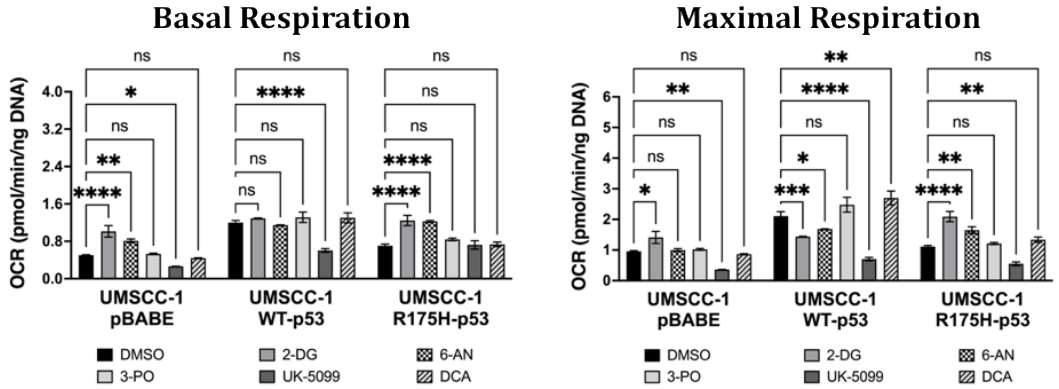

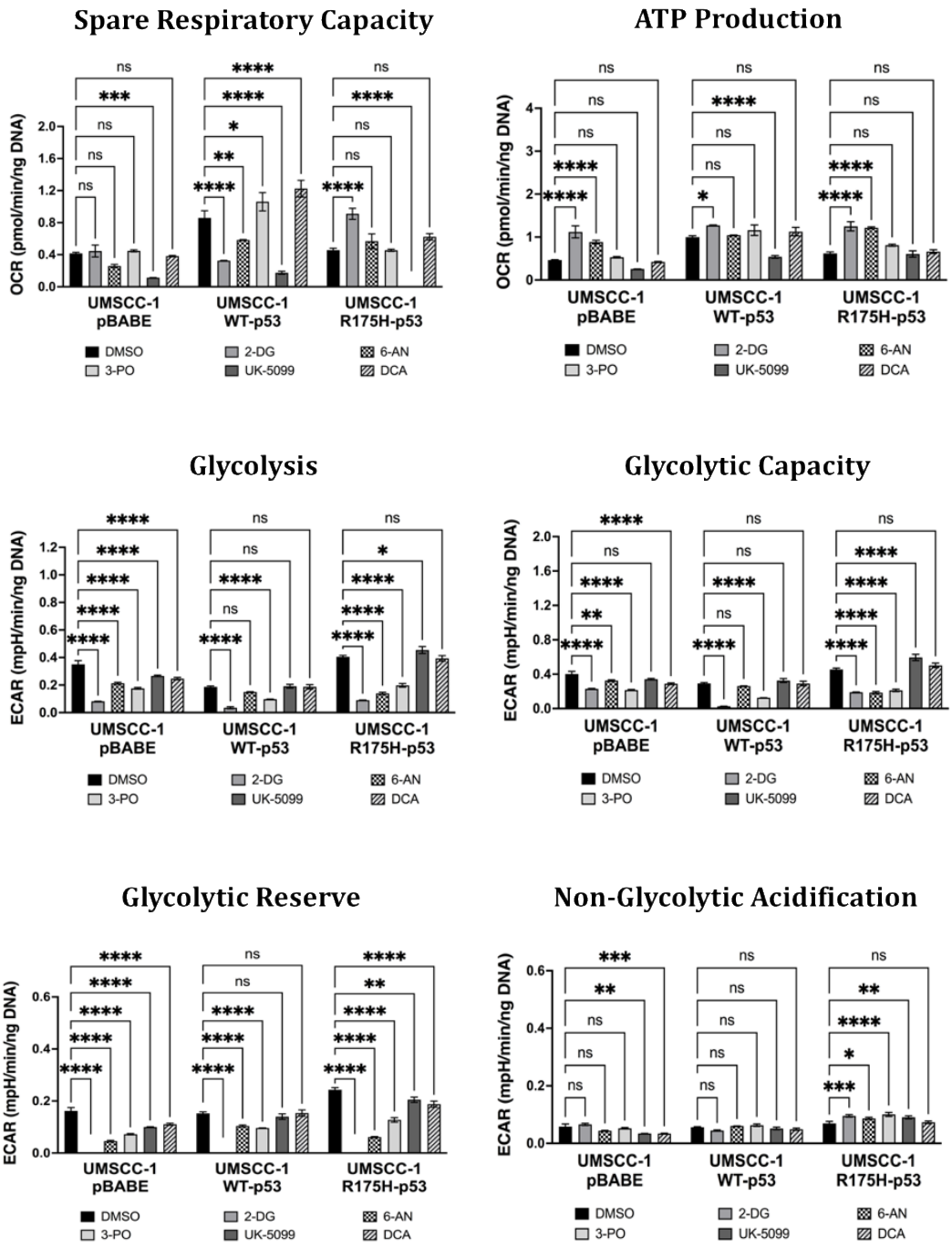

Figure 3.47.: Post-treatment metabolic profile of UM-SCC-1 isogenic derivative cell lines. Cells were subjected to the indicated drugs for 24 hours, before mitochondrial stress test and glycolytic stress test were performed, as described in 2.3.6.1 and 2.3.6.2.. Absolute data derived from mitochondrial stress and glycolytic stress tests were normalised to DNA content for all groups of cells, and the absolute values for basal respiration, maximal respiration, spare respiratory capacity, ATP production, glycolysis, glycolytic capacity, glycolytic reserve and non-glycolytic acidification as described in section 2.3.6.1. and 2.3.6.2.. OCR and ECAR readings were obtained from three experiments (n=3), each experiment was performed in triplicate. Data are presented as mean OCR (pmol/min) and ECAR (mpH/min), respectively, normalised to DNA content (ng DNA) as described in 2.3.8. Means of individual data were used to derive overall means. Error bars represent SEM. Statistical analysis: a one-way ANOVA with Dunnett's test. (ns) $p > 0.05$, (*) $p \leq 0.05$, (**) $p \leq 0.01$, (***) $p \leq 0.001$, (****) $p \leq 0.0001$.

Summarising results presented in this section show that inhibiting the first step of the glycolytic pathway increases basal respiration in the absence of functional p53 with no significant effect in the wild type p53 cells. In the absence of functional p53, this inhibition increases the maximal respiration and in wild type p53 cells it decreases it. One possible explanation for this increase in mitochondrial respiration following 2-DG mediated glycolysis inhibition is the opposing of the Crabtree effect. In this phenomenon, which was named after the English biochemist Herbert Grace Crabtree (369), the presence of glucose in sufficient concentrations causes cells to use glycolysis to produce energy even in the presence of sufficient amounts of oxygen. This increase in glucose concentrations promotes more glycolysis and, therefore, less oxygen consumption to fulfil the demand for ATP, resulting in less mitochondrial respiration. Results have shown that 2DG-mediated inhibition of glycolysis opposed the Crabtree effect, as evidenced by an increase in the absolute values of mitochondrial respiration, only in the absence of p53 function, with no discernible effect in wild-type cells. This supports the findings discussed in section 3.1., in which wild type p53 SCCHN cells demonstrated greater metabolic flexibility and greater use of mitochondrial respiration for energy production, resulting in less effect of 2DG-mediated inhibition of glycolysis on mitochondrial-linked ATP production in these cells. These findings are consistent with the results shown in 3.1. that the cellular decision to use aerobic glycolysis is determined by the presence or absence of functional p53, since inhibiting the first step of glycolysis in the absence of p53 promotes mitochondrial respiration in these cells with no similar effect in wild type p53 cells. Moreover, uncoupling ATP synthesis from the ETC following inhibition of the first step of glycolysis induces a significant increase in maximal respiration in the absence of p53 as these cells rely on mitochondrial respiration to respond to the high energy demand that results from inhibition of glycolysis.

The results also show that 6-AN-mediated inhibition of the PPP, and indirectly DNA synthesis, increases basal respiration and ATP production and decreases basal glycolysis and glycolytic capacity in the absence of p53 function, with no significant effect detected in wild type p53 cells. It was also observed that inhibiting glycolysis at the third step using 3PO increases the spare respiratory capacity of wild type p53 cells with no effect in the absence of p53 function. In addition, UK-5099-mediated inhibition of MPC which blocks the entrance of pyruvate into the TCA cycle decreases ATP production only in p53 wild type cells, while uncoupling ATP synthesis from the ETC following MPC inhibition results in decreasing glycolytic reserves in the absence of p53

function, but not in p53wild type cells, which can be explained by the increased conversion of pyruvate to lactate and the limited metabolic diversity in the absence of functional p53. These data also show that DCA-mediated inhibition of PDK increases maximal respiration and spare respiratory capacity only in wild type cells and decreases glycolytic reserves in the absence of functional p53 but not in p53wild type cells.

These data provide evidence of a link between the expression of functional p53 and differential response to glucose deprivation following treatment with anti-metabolic agents that target different parts of the glycolytic pathway. Interestingly, studies have reported ed that depriving cells of glucose can lead to an increase in p53 levels (370,371). However, no study has investigated the alteration in p53 protein expression following inhibition of glycolysis in SCCHNs.

3.3.2.2. Changes in protein expression of p53 in response to treatment with anti-metabolic agents in SCCHNs

Given the indicated correlation between the expression of functional p53 and alterations in the metabolic profile in response to anti-metabolic agents, as shown in 3.3.3.1., and the intimate connection between p53, MDM2 and steady-state protein levels determined by the autoregulatory feedback loop (see section 1.2.4.), and the role of p53 in regulating TIGAR expression as well as the role of p53 in the balance between mitochondrial respiration and glycolysis in SCCHN, as discussed in 3.1.3., it seems likely that p53, MDM2 and TIGAR protein levels will impact glucose metabolism and that examining the steady-state protein levels would be informative to examine the potential changes in protein expression in the state of the metabolic imbalance following the inhibition of glycolysis using the candidate drugs.

In addition, given that TIGAR inhibition in the presence of functional p53 showed a similar effect on the glycolytic profile to that of the inhibited functional p53 cells (see Figure 3.32.), it would also be informative to examine whether potential changes in p53 protein expression following inhibition of glycolysis using anti-metabolic agents can be reversed by inducing glycolysis using TIGAR knockdown.

Protein expression analysis was performed using western blotting as described in 2.8. Cells were transfected with control siRNA or siRNA specific for TIGAR for 48 hours

before being treated with the indicated drug for 24 hours and then harvesting cells and preparing protein samples for gel electrophoresis and western blotting (Figure 3.48.).

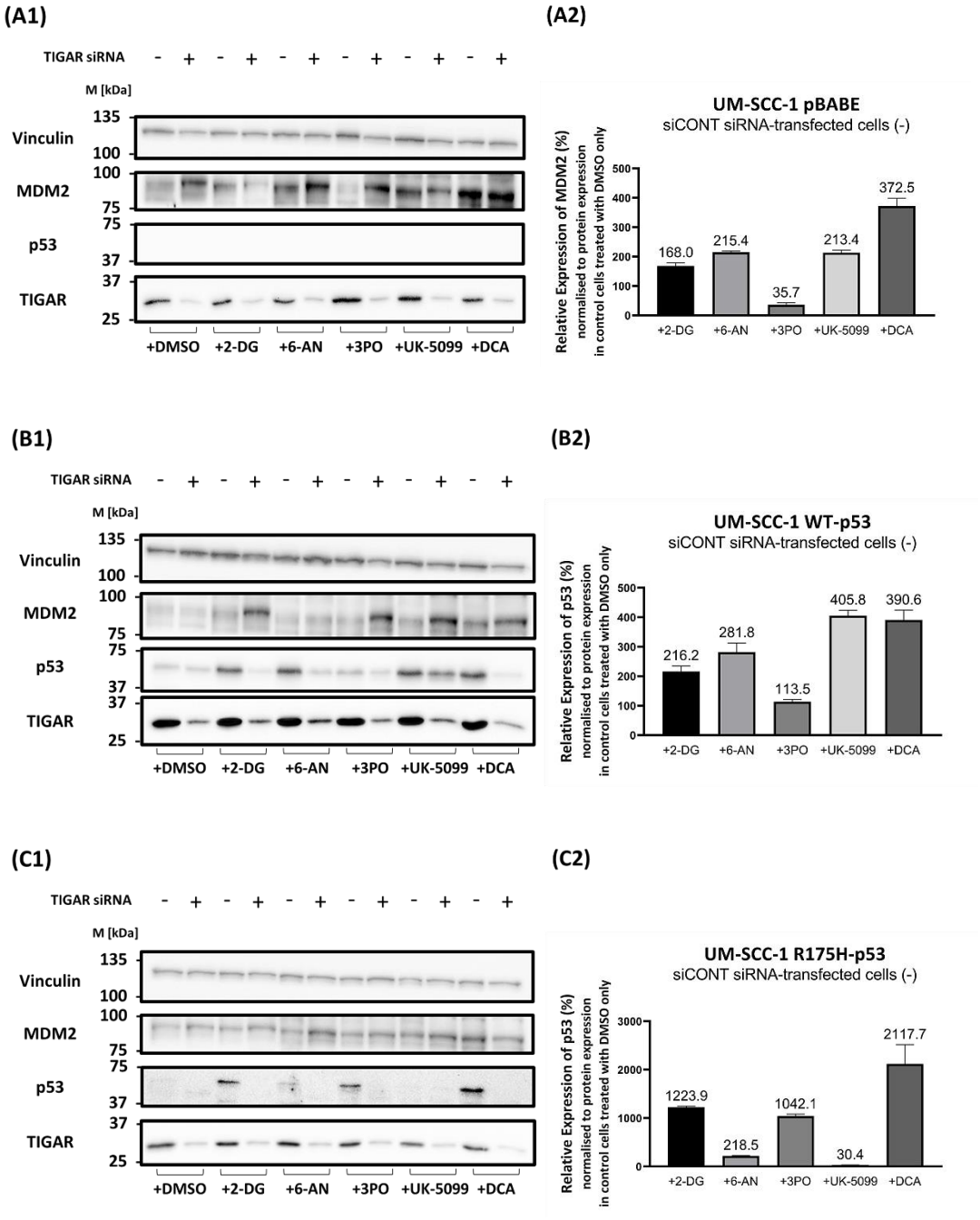

Figure 3.48.: Protein expression of MDM2, p53 and TIGAR in TIGAR-knockdown UM-SCC-1 isogenic derivatives following treatment with anti-metabolic drugs. Western blotting analyses of MDM2, p53 and TIGAR expression levels in **(A1)** UMS-CC-1 pBABE (a p53-null cell line), **(B1)** a UM-SCC-1 wild type p53 (a wild type p53 cell line) and **(C1)** UM-SCC-1 R175H-p53 (a mutant p53 cell line). Cells were left untransfected or transfected with either non-target siRNA (siCONT, as a negative control, indicated as **[-]**) or TIGAR-specific siRNA (indicated as **[+]**) in a final concentration of 25nM. 48 hours after transfection, cells were treated with the indicated drugs for 24 hours. Cells were harvested and lysed as described in

section 2.8.3. Protein samples were prepared and loaded into gels, and specific antibodies were used for detection as detailed in section 2.1.9. Vinculin was used as a loading control. The migration of protein standards of the indicated approximate molecular weights is shown in kDa. Results show that treatment with anti-metabolic drugs induced a significant increase in p53 levels in wild type or R175H-p53 mutant p53 cells, with the exception of the treatment with UK-5099 in mutant cells. No similar increase was observed in the TIGAR-knockdown group of each treatment. Densitometry was used to analyse the expression of MDM2 in UM-SCC-1 pBABE **(A2)** and p53 in UM-SCC-1 WT-p53 **(B2)** and UM-SCC-1 R175H-p53 **(C2)**, as described in 2.8.5. and analyses of three biological replicates is depicted. Relative protein expression normalised to the expression of the housekeeping protein vinculin in the negative control (%), is shown next to the indicated blot. Oligonucleotides are detailed in Table 2.6.

Western blot analysis of control-siRNA-transfected cells showed a considerable increase in p53 levels in SCCHN cells expressing wild type or R175H-mutant p53 after 24 hours of treatment with anti-metabolic agents, with the exception of the treatment with UK-5099 in cells expressing R175H-mutant p53. This increase in p53 expression, however, was not observed in the TIGAR-knockdown group of each treatment. Given that no similar effect was observed in DMSO-only-treated cells (see Figure 3.48.), it is unlikely that these changes are due to the known transcriptional regulation of TIGAR expression by p53. It was found that glucose deprivation promotes the phosphorylation of AMP-activated protein kinase catalytic subunit α (AMPKα), which is associated with significant transcriptional induction of p53. AMPK monitors cellular energy levels and works as an intracellular energy sensor that down-regulates the ATP consuming metabolic pathways and activates the energy-generating processes through phosphorylating the key targets involved in energy metabolism (372). It is activated in response to energy-depleting stresses such as glucose deprivation, hypoxia, and oxidative stress (373–375). It has been shown recently that cells treated with low glucose were arrested in the G1 phase of the cell cycle, which was associated with significant activation of AMPK. The activated AMPK phosphorylates p53 at Ser-15, which disrupts the p53-MDM2 interaction, and thus stabilises p53 (376–378).

These results suggest that the TIGAR-inhibition-mediated increase of glycolysis reverses the increase in p53 expression following treatment with anti-metabolic agents. Thus, further investigation is needed into the role of TIGAR inhibition in attenuating the role of p53 in determining the response to anti-metabolic treatment.

3.3.3. Investigating the relevance of TIGAR status of SCCHN cells in altering the response to treatment with potential drugs

The results presented thus far show that TIGAR inhibition in the presence of p53 function produces an effect on the glycolytic profile similar to that of p53 inhibition and that promoting glycolysis by the inhibition of TIGAR reverses the increased expression of p53 in response to glycolysis inhibition by candidate drugs. Thus, TIGAR inhibition appears to be of importance in determining the response to inhibition of glycolysis in SCCHN cells. In this section, we explore the effects of TIGAR inhibition on metabolic-linked cell viability, radiosensitivity, and metabolic phenotype of SCCHNs with different p53 status following treatment with anti-metabolic candidate drugs.

3.3.3.1. Cell viability

Since cancer cells preferentially use an inefficient pathway for generating ATP (glycolysis), it seems likely that this is an adaptive response to provide other essentials for cell proliferation and survival. For example, we can envisage that this might provide increased reducing and macromolecular biosynthesis capacities through the PPP. It must also increase or promote viability (perhaps as a consequence of increased reducing capacity). Given the dual role that TIGAR plays in cancer cells through inhibiting glycolysis and suppressing both autophagy and apoptosis (see section 1.4.3.), our next goal was to determine whether TIGAR inhibition has an effect on metabolically-linked cell viability and the response to anti-metabolic agents and whether this effect is related to p53 status given the role we previously demonstrated for p53 in determining the metabolic switch (see section 3.1.).

To determine the impact of TIGAR inhibition on the metabolically-linked cell viability of UM-SCC-1 isogenic derivatives, cells were transfected with either control siRNA or siRNA specific for TIGAR for 24 hours before treatment with the indicated anti-metabolic agents for another 24 hours. MTT assay was then performed as described in 2.6. This assay relies on mitochondrial function as a surrogate indicator of cell viability.

Figure 3.49. shows cell viability data from the isogenic derivative cell lines of UM-SCC-1 treated with anti-metabolic agents. p53-null cells show no marked alterations in cell viability between cells transfected with TIGAR siRNA and the control group in response to treatment. However, cells expressing wild type p53 showed a significant decrease in

the inhibitory effect of 3PO in cells transfected with TIGAR siRNA in comparison with the control group. This slight decrease in 3PO-mediated inhibition of cell viability may be due to the mechanism through which 3PO inhibits glycolysis, as TIGAR inhibition promotes more glycolysis in wild type p53 cells which may attenuate the anti-glycolytic effect of 3PO at the same step of the pathway.

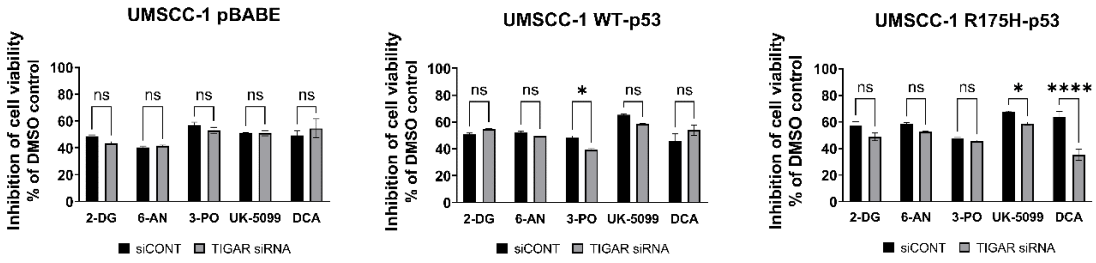

Figure 3.49.: Cell viability of post-treatment TIGAR-knockdown UM-SCC-1 isogenic derivatives as measured by MTT assay. Viability was assessed in TIGAR-knockdown UM-SCC-1 isogenic derivatives following the treatment with the indicated drugs: 2-DG at 9mM, 6-AN at 13μM, 3PO at 44μM, UK-5099 at 45μM and DCA at 0.3 mM, for 24 hours. Values represent the mean of the relative decrease in cell viability from three separate experiments. Means of individual data were used to derive overall means. Error bars represent SEM. Statistical analysis: Student's t-test. (ns) $p > 0.05$, (*) $p \leq 0.05$, (**) $p \leq 0.01$, (***) $p \leq 0.001$, (****) $p \leq 0.0001$.

Transient inhibition of TIGAR in R175H-p53 cells results in a significant increase in cell viability following treatment with UK-5099 and DCA in comparison with the control group which is surprising since TIGAR inhibition has a little detectable impact on glycolytic activity in mutant cells (Figure 3.32.). These differences in cell viability in response to UK-5099 and DCA between p53-null and mutant p53 cells following inhibition of TIGAR, together with the differences shown in the metabolic profile between the two groups (see Figure 3.32.), may suggest a role for GOF properties. Since both UK-5099 and DCA target the glycolytic pathway through mechanisms that involve mitochondrial pyruvate (see section 3.3.), the proposed GOF properties based on these results may be involved in determining the fate of mitochondrial pyruvate. These data suggest further investigation as to whether these differences in mitochondrial-linked cell viability between p53-null and mutant p53 cells, and any possible GOF properties, have effects on the metabolic profile or influence any potential effect of anti-metabolic agents on the sensitivity of cells to IR, as an indicator to response to therapy.

3.3.3.2. Colony formation

As discussed in 3.3.3.1., TIGAR knockdown had no marked effect in altering the cell viability in p53-null and wild type p53 cells following treatment with anti-metabolic agents, with the exception of wild type p53 cells treated with 3PO. On the other hand, the results presented in 3.3.3.1. suggest GOF properties that increase survival of R175H-p53 cells in response to UK-5099 and DCA, two metabolic inhibitors that target pyruvate fate. However, these differences in response to treatment with anti-metabolic in TIGAR-transfected UM-SCC-1 isogenic derivatives cells, together with the effect of TIGAR inhibition on the metabolic profile of these cells (discussed in 3.2.), may necessitate further investigation into the long-term effects of treatment with drugs that target different parts of the glycolysis pathway and whether the inhibition of TIGAR in these cells may affect the radiosensitivity of these cells in response to these drugs.

To assess the long-term cell survival and proliferation following treatment with the candidate drugs and/or exposure to IR, clonogenic assays were utilised as described in 2.7. In brief, cells were transfected with either 25nM of non-target siRNA (siCONT, as a negative control) or TIGAR-specific siRNA. 48 hours after transfection, cells were treated with either DMSO (as a vehicle only control) or the IC_{50} of 2-DG; 6-AN; 3PO; UK-5099 and DCA for one hour. Cells were then irradiated at doses of 0Gy, 2Gy, 4Gy, or 6Gy at room temperature. Cells were then washed, harvested, counted and seeded at two different cell densities in triplicate for each treatment condition and incubated at 37°C, 5% CO_2 for 15 days to enable colony visualisation. Following 15 days of incubation, cells were washed, fixed and stained for 1 hour at room temperature before being counted and imaged (Figure 3.50.). Survival parameters were calculated as described in section 2.7.

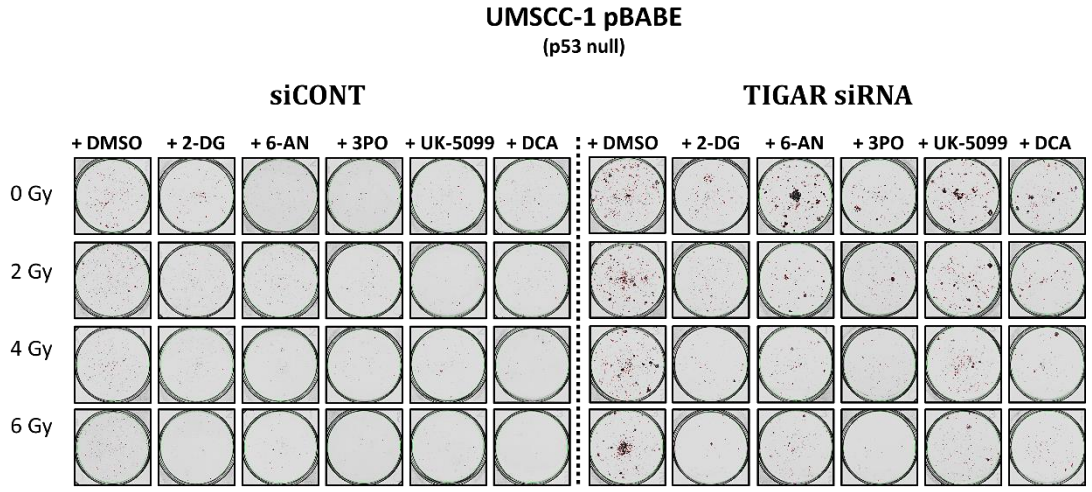

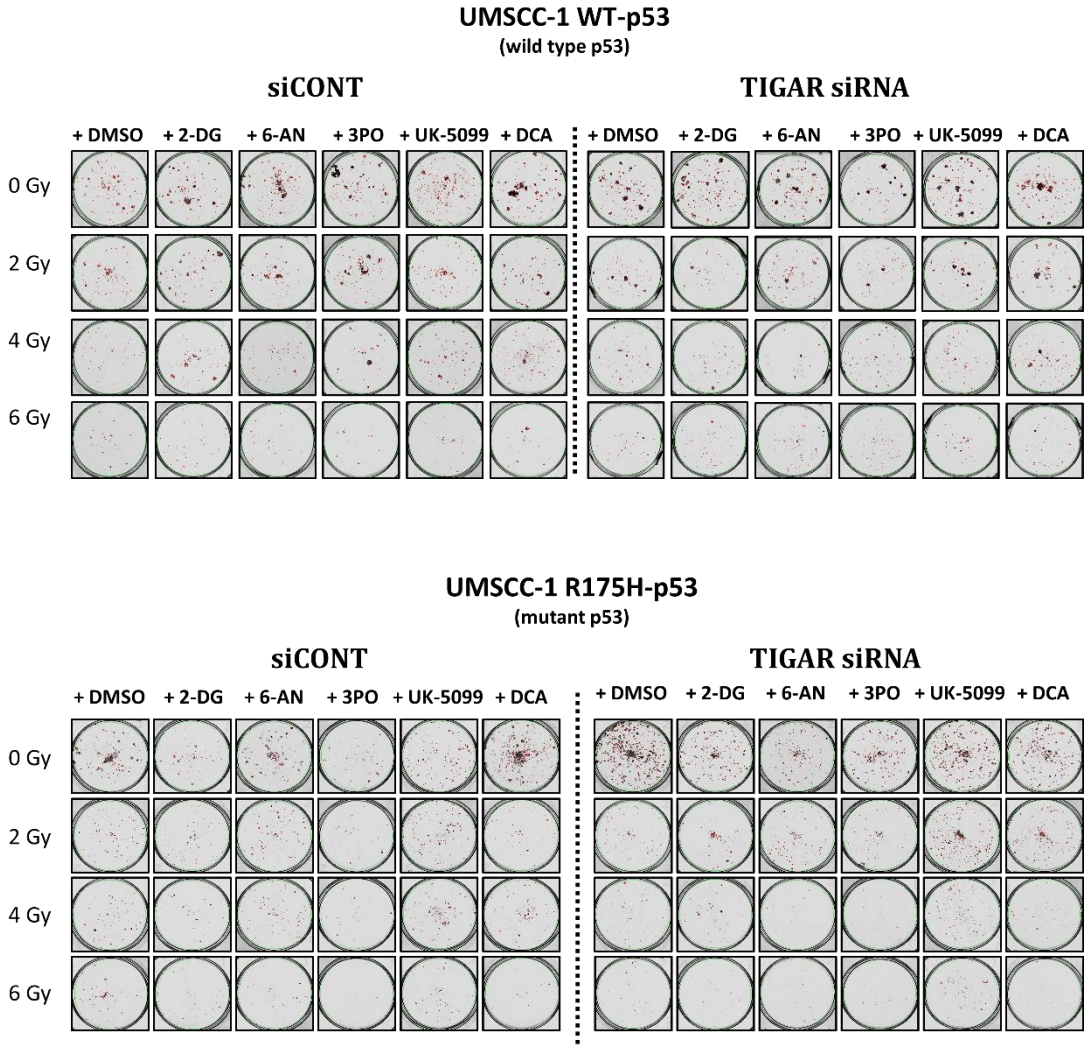

Figure 3.50.: Colony formation in response to increasing dose of ionising radiation in pre-treated TIGAR-knockdown UM-SCC-1 isogenic cell lines. Cells were transfected with non-targeting control siRNA or siRNA specific for TIGAR for 48 hours before clonogenic assays were performed as detailed in 2.7.. Representative images of colony formation in cells treated with the indicated drugs for one hour before being exposed to a radiation dose of 0 (control), 2, 4 and 6Gy. Representative images of 0Gy clearly show that TIGAR knockdown increases colony formation in the absence of functional p53 (p53-null and mutant p53 groups) but not in the presence of wild type p53 cells. This alteration affects the plating efficiency and thus Survival parameters.

Generally, the images obtained from clonogenic assay experiments clearly show that TIGAR knockdown increases colony formation in p53-null and p53-mutant cells but not in the wild type p53 cells, as shown in comparing the 0Gy+DMSO control group in siCONT and TIGAR siRNA group in all three cell lines (Figure 3.50.), and in comparing the plating efficiency between the control and TIGAR knockdown groups (Table 2.8.).

The surviving fraction (SF) was calculated for each treatment condition based on the number of colonies formed after treatment and the plating efficiency, as detailed in 2.7. Figures 3.51-53. present clonogenic survival curves for TIGAR-knockdown UM-SCC-1 isogenic cell lines with or without administration of either 2-DG, 6-AN or 3PO.

Results show that inhibition of glycolysis using these drugs significantly increases radiosensitivity in the absence of functional p53 (p53-null and mutant p53), but not in the wild type p53. Interestingly, promoting glycolysis by TIGAR knockdown discernibly potentiates the efficacy of the anti-metabolic agents 2-DG, 6-AN and 3PO in radiosensitising wild type p53 cells.

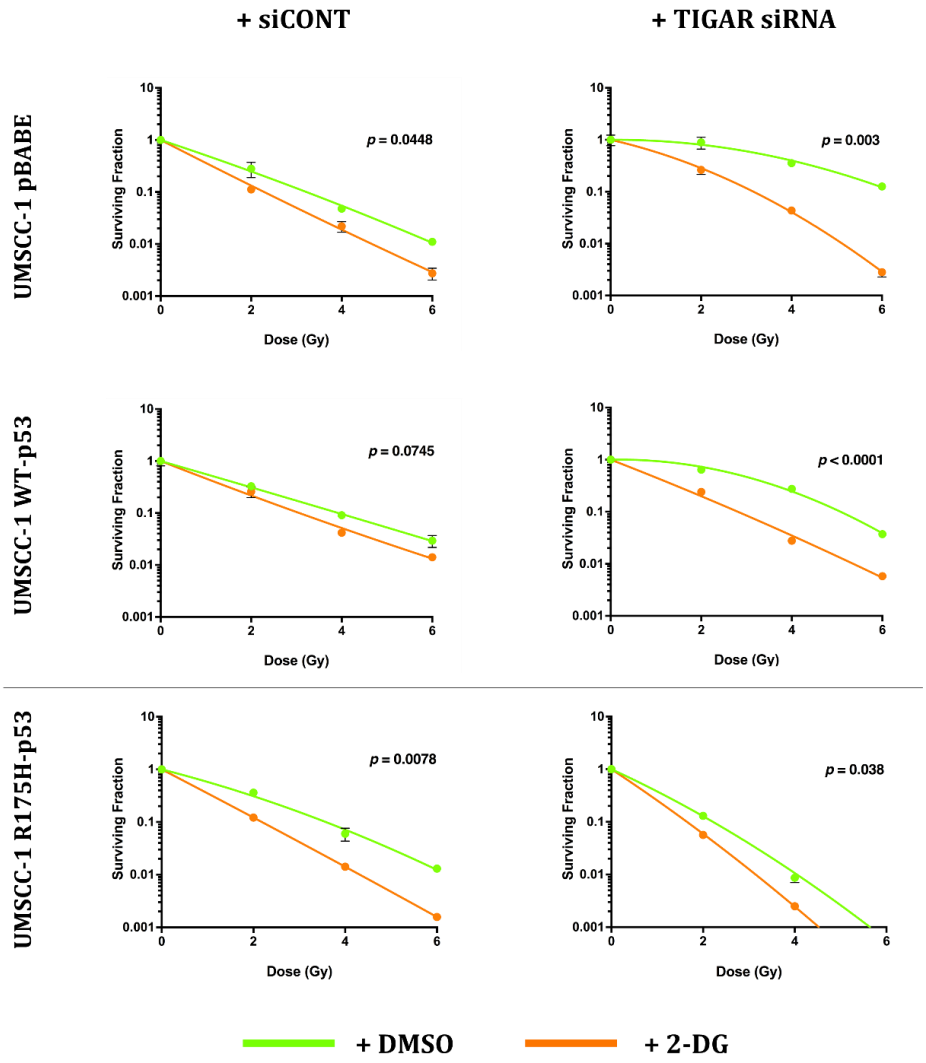

Figure 3.51. Clonogenic survival curves for TIGAR-knockdown UM-SCC-1 isogenic cell lines with or without administration of 2-DG. The results shown represent the mean values obtained from three biologically independent experiments. Data was normalised against the 0Gy of each cell line, which was

set to 1 on Y-axis. Means of individual data were used to derive overall means. Error bars represent the SEMs. p- values are shown where there is a statistically significant difference between the clonogenic survival curves (<0.05), or not (≥0.05).

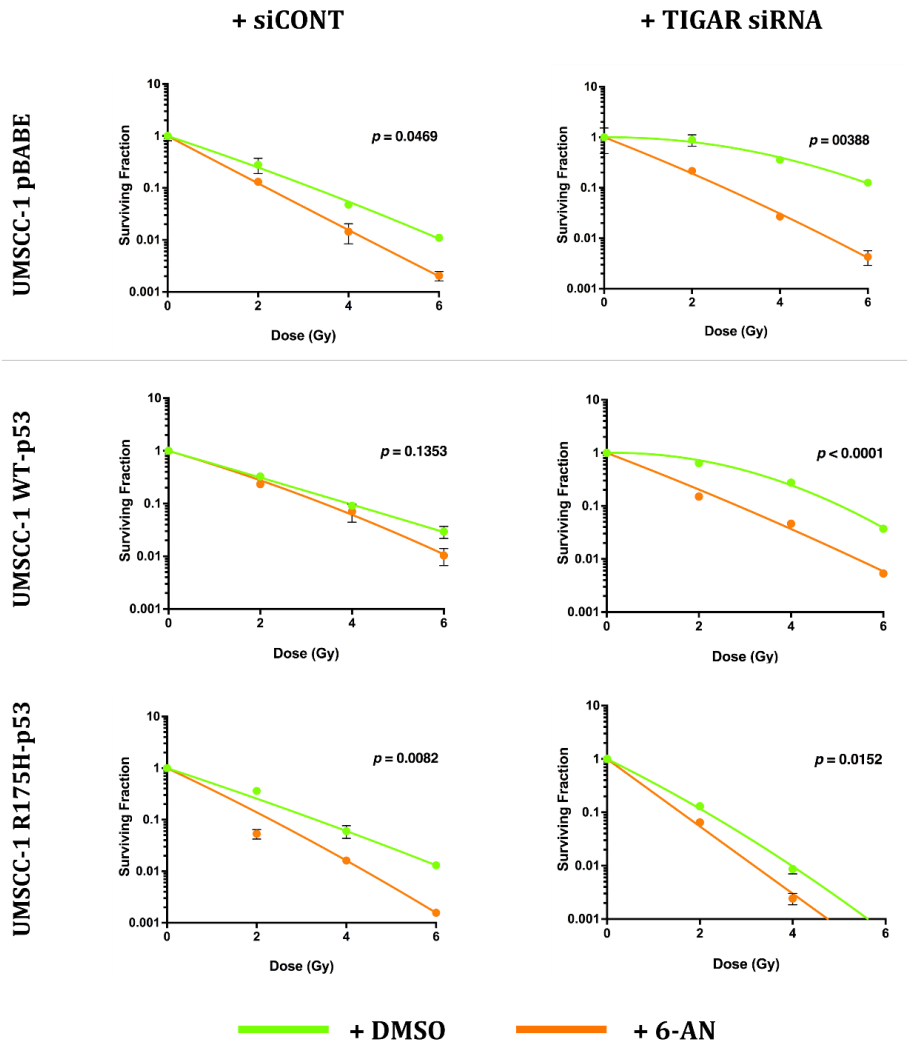

Figure 3.52.: Clonogenic survival curves for TIGAR-knockdown UM-SCC-1 isogenic cell lines with or without administration of 6-AN. The results shown represent the mean values obtained from three biologically independent experiments. Data was normalised against the 0Gy of each cell line, which was set to 1 on Y-axis. Means of individual data were used to derive overall means. Error bars represent the SEMs. p- values are shown where there is a statistically significant difference between the clonogenic survival curves (<0.05), or not (≥0.05).

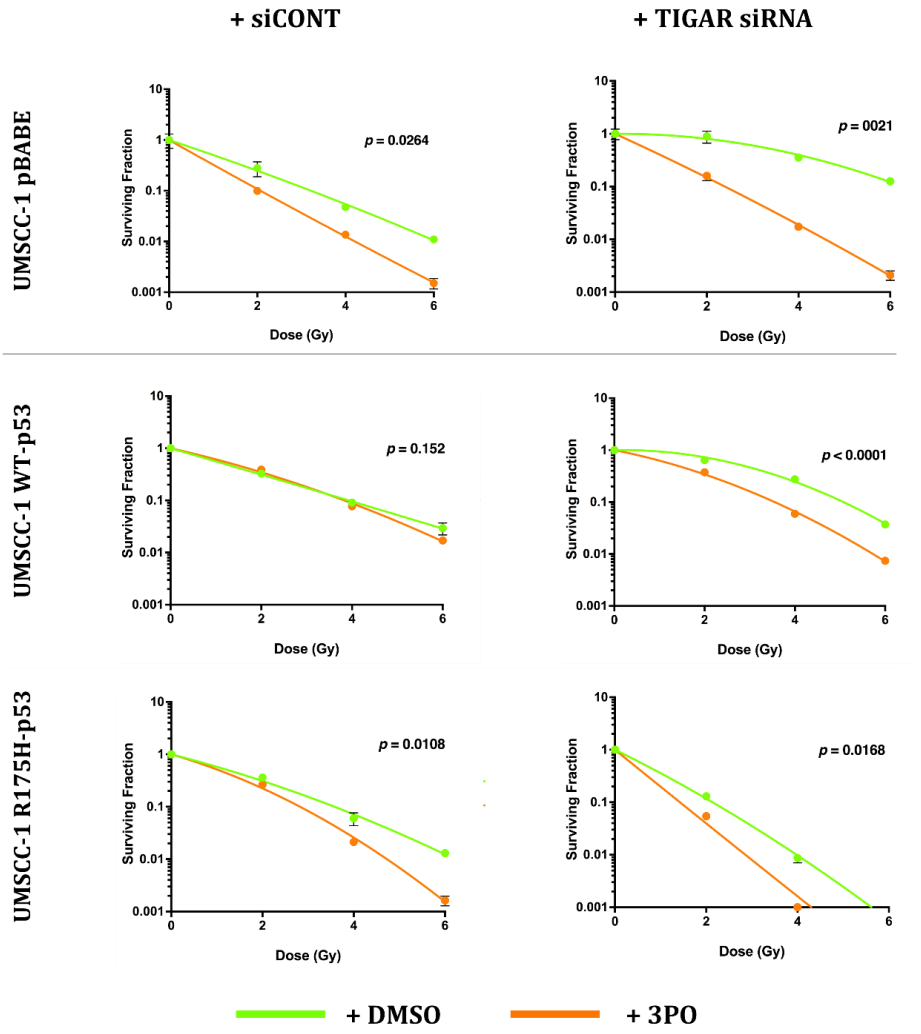

Figure 3.53.: Clonogenic survival curves for TIGAR-knockdown UM-SCC-1 isogenic cell lines with or without administration of 3PO. The results shown represent the mean values obtained from three biologically independent experiments. Data was normalised against the 0Gy of each cell line, which was set to 1 on Y-axis. Means of individual data were used to derive overall means. Error bars represent the SEMs. p- values are shown where there is a statistically significant difference between the clonogenic survival curves (<0.05), or not (≥0.05).

Studies show that mitochondrial dysfunction in SCCHN, as measured by low expression of oxidative phosphorylation genes, is associated with poor clinical outcomes (379,380). It is reasonable to suggest that the poor clinical outcomes of mutant *TP53* SCCHNs (174,381–384) can also be linked to mitochondrial dysfunction. The loss of p53 activity has been shown to disrupt cell cycle arrest and death in response to DNA damage, resulting in resistance to genotoxic agents' treatment. We can explain the relationship between *TP53* mutation in SCCHN cells and the increased potentiating effects of glycolysis inhibitors on radiosensitivity through the metabolic switch toward

aerobic glycolysis (discussed in 1.3.1.). As discussed in 3.1., the loss of functional *TP53* was found to promote a metabolic switch away from mitochondrial respiration toward aerobic conversion of pyruvate to lactate. This effect increases the cell dependence on glycolysis as the dominant source of ATP production, and this suggests an explanation for the increased radiosensitivity in the presence of glycolysis inhibitors being due to depriving cells of the predominant energy source on which they depend. This accords with data from a study by Sandulache et al in which the authors explained that the resistance of wild type p53 SCCHN cells to the effect of the glycolytic inhibitors in potentiating radiosensitivity is due to the diverse metabolic profile of these cells, which reduces the possibility of cell death by inhibiting a specific metabolic pathway. Mutant p53 SCCHN cells, in contrast, exhibit a strong dependence on a major dominant pathway, glycolysis, which explains their apparent sensitivity to inhibition of this pathway and their increased likelihood of death in response to radiotherapy (246).

In addition, our results show that transient inhibition of TIGAR further potentiates the effects of 2-DG, 6-AN and 3PO in sensitising SCCHN cells harbouring wild type *TP53* to IR, with a significant reduction in IR dose required to achieve the same inhibition. No additional potentiating effects were observed in cells that harbour compromised *TP53*. These findings represent the first indication of the role that TIGAR inhibition may play in the efficacy of treatment with glycolysis inhibitors sensitising wild type p53 SCCHN cells to IR.

We can understand these results in light of the outcomes of the metabolic profiling performed on SCCHN cells following TIGAR knockdown as shown in section 3.2.2. In the presence of wild type p53, transient inhibition of TIGAR increases glycolysis with no marked effect on mitochondrial respiration. Thus, increased glycolysis in wild type *TP53* cells, as a direct result of TIGAR inhibition, potentiated the efficacy of glycolysis inhibitors in sensitising cells harbouring wild type *TP53* to IR in a manner comparable to the effect of increased glycolysis in cells with loss of *TP53* function. Furthermore, a number of studies have indicated that depriving cells of glucose or treatment with glycolysis inhibitors can lead to an increase in p53 levels (53,54). As discussed in 3.3.3.2., our results show a considerable increase in p53 levels both in wild type and mutant p53 SCCHN cells after 24 hours of treatment with metabolic inhibitors. This increase supports the potential role of p53 in regulating the response to inhibition of glycolysis in these cells. Interestingly, this increase in p53 expression after 24 hours of treatment with metabolic inhibitors was not observed in TIGAR-knockdown cells,

which means that pre-stimulation of glycolysis by TIGAR inhibition counteracts the increased expression of p53 induced by metabolic inhibitors. This result is remarkably consistent with the effect of TIGAR inhibition which increases the efficacy of metabolic inhibitors in promoting radiosensitivity in wild type-expressing SCCHN cells, as well as the lack of significant differences in outcomes of such treatment in response to IR in the absence of functional p53 with or without TIGAR inhibition. These results demonstrate that the role of TIGAR in the Warburg effect is linked to *TP53* function, and that any potential role of TIGAR inhibition in increasing anti-glycolytic-mediated radiosensitisation remains determined by p53 status, even in the presence of a putative p53-independent mechanism that regulates TIGAR in the absence of p53 function. The observed increase in p53 levels of mutant p53 SCCHN cells in response to treatment with glycolytic inhibitors may be due to the increased p53 transcription and the prolonged half-life of the mutant p53 protein compared to that of the wild type p53 protein (385,386), which may be partially attributed to the inefficient degradation exerted by MDM2, which is a direct transcriptional target of wild type p53 (343,344). However, the effect of TIGAR inhibition on levels of mutant p53 following treatment with glycolysis inhibitors raises some questions and needs further investigation.

Our study also shows that the mitochondrial pyruvate transporter (MPC) inhibitor, UK-5099 cannot radiosensitise mutant *TP53* SCCHN cells but can radiosensitise p53 null and wild type cells (Figure 3.54.). The MPC transports pyruvate from the cytosol to the mitochondrial matrix to fuel the TCA cycle whereby pyruvate can be metabolised to either oxaloacetic acid by pyruvate carboxylase or to acetyl-CoA by pyruvate dehydrogenase (387). UK-5099 inhibits the MPC and prevents the transfer of pyruvate from glycolysis to mitochondria, thus limiting mitochondrial respiration and promoting pyruvate conversion to lactate (388). A number of studies have shown decreased expression of MPC in many cancers, a defect that can be rescued by exogenous expression (389).

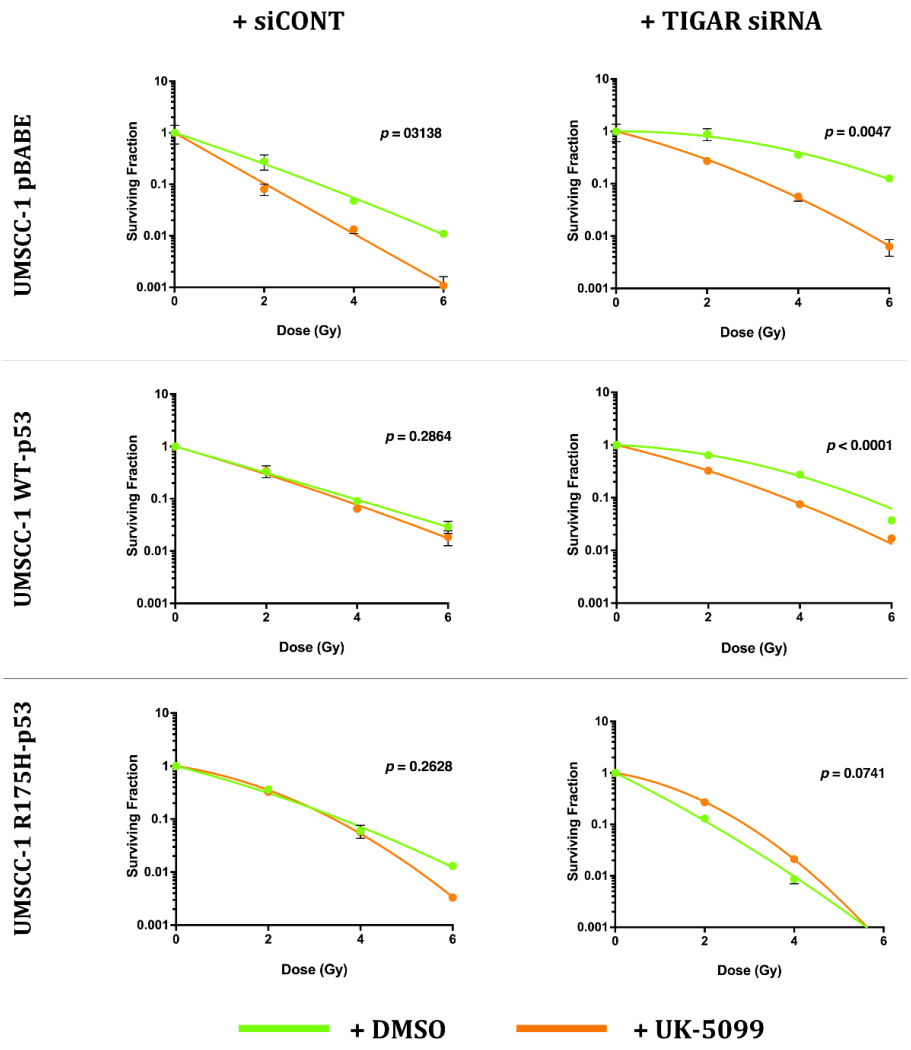

Figure 3.54.: Clonogenic survival curves for TIGAR-knockdown UM-SCC-1 isogenic cell lines with or without administration of UK-5099. The results shown represent the mean values obtained from three biologically independent experiments. Data was normalised against the 0Gy of each cell line, which was set to 1 on Y axis. Means of individual data were used to derive overall means. Error bars represent the SEMs. p- values are shown where there is a statistically significant difference between the clonogenic survival curves (<0.05), or not (≥0.05).

The import of pyruvate into mitochondria is a crucial metabolic decision because it links glycolysis, a process that does not require oxygen, with the oxygen-dependent process of mitochondrial oxidative phosphorylation (390). Inhibition of the MPC leads to inhibition of pyruvate oxidation in mitochondria and hence inhibition of ROS production through the electron transport chain. Although it is critical for cancer cells to avoid an excessive production of ROS in order to survive, cancer cells have been shown to also require mitochondrial TCA activity, intact ETC function, and mitochondrial metabolism-dependent biosynthetic pathways (391,392). For these

reasons, it is not surprising that the MPC plays a key role in proliferation in cancer (389,393,394). Two studies have shown a decrease in the MPC function in Ehrlich hyperdiploid ascites tumour cells and Morris hepatoma tumours, resulting in a lower ability to oxidise pyruvate (395,396). This may indicate that although the role of MPC is important in proliferation and enhancing biosynthetic functions in cancer, it may be less active than in normal cells.

Two of our findings support the conclusion that stimulation of glycolysis may be a key determinant of radioresistance in SCCHNs. First, the ineffectiveness of UK-5099 in sensitising cells harbouring mutant *TP53* to IR, which can simply be explained by the enhanced glycolysis and reduced mitochondrial respiration resulting from inhibition of the MPC (397). Second, the considerable increase in radiosensitivity to glycolysis inhibitors in wild type p53 cells, which are less dependent on glycolysis, after increasing glycolysis by transient knockdown of TIGAR. Wild type p53 cells have greater metabolic diversity, being less dependent on glycolysis they are able to produce acetyl-CoA through β-oxidation of fatty acids and may thus exhibit resistance to MPC inhibition by UK-5099. This can also provide an explanation for the increased radiosensitivity following transient inhibition of TIGAR, resulting in increased glycolytic flux, and a reduction in antioxidant synthesis from the PPP. However, the different response of p53-null cells to treatment with UK-5099 in comparison with mutant p53 cells, raises some questions about any possible role for GOF properties in the response of GOF mutant p53 cells to the UK-5099-mediated inhibition of MPC and needs further investigation.

Given the observed impact of pyruvate levels on metabolism and radiosensitivity, it is interesting to consider other ways to examine the role of pyruvate in these processes. For example, the fate of pyruvate can also be controlled pharmacologically through the inhibition of pyruvate dehydrogenase kinase (PDK) by DCA. This enzyme inhibits the pyruvate dehydrogenase complex (PDC), which mediates the conversion of mitochondrial pyruvate into acetyl-CoA (Figure 1.8.). Inhibition of this enzyme by DCA increases the production of acetyl-CoA required for the TCA cycle, leading to a reduction in the steady-state levels of pyruvate and thus less conversion of pyruvate to lactate. In many cell types including SCCHN derived cells, lactate has been investigated as a final by-product of glycolysis and thus as a surrogate indicator of glycolytic activity. Moreover, high levels of lactate in SCCHN tumours have been inferred to indicate high levels of glycolytic flux, and these have been found to be associated with poorer survival

outcomes before (227) and after irradiation (228), as well as being associated with higher resistance to radiotherapy *in vivo* (229,230).

Treatment of SCCHN cells with DCA sensitises R175H-p53 mutant cells to IR with no similar effects in p53-null or wild type p53 SCCHN cells. Inhibition of TIGAR, however, enhanced DCA-mediated radiosensitivity in p53-null or wild type p53 cells, with no further impact on mutant p53 cells (Figure 3.55.). Inhibition of TIGAR, as observed previously for the MPC inhibitor UK-5099, has little effect on mutant p53 cells presumably because these cells are preferentially utilising, and more dependent upon, glucose as an energy source. Wild type p53 cells retain a significant capacity to increase glycolysis in response to TIGAR inhibition (Figure 3.32.), which may explain the increased radiosensitivity following treatment with UK-5099 or DCA in TIGAR-knockdown wild type p53 cells. However, the effect of TIGAR inhibition on the response of p53-null cells to IR following treatment with DCA, despite their high levels of basal glycolysis, remains more difficult to explain.

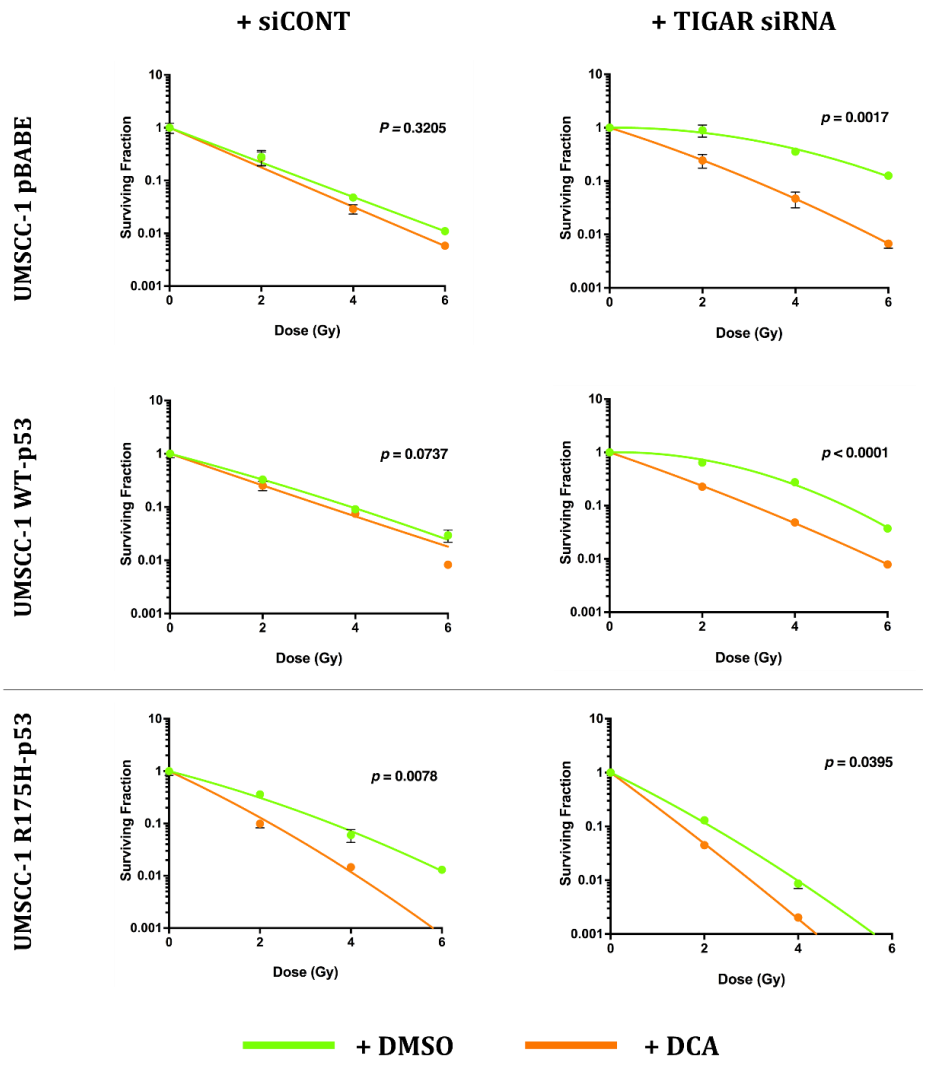

Figure 3.55.: Clonogenic survival curves for TIGAR-knockdown UM-SCC-1 isogenic cell lines with or without administration of DCA. The results shown represent the mean values obtained from three biologically independent experiments. Data was normalised against the 0Gy of each cell line, which was set to 1 on Y axis. Means of individual data were used to derive overall means. Error bars represent the SEMs. p- values are shown where there is a statistically significant difference between the clonogenic survival curves (<0.05), or not (≥0.05).

It is likely that differences in plating efficiency of cells caused by the treatment conditions have a major effect on these differences between p53-null and mutant p53 cells. Although significant inhibition of glycolysis (Figure 3.47.) and marked inhibition of colony formation in the control group (0Gy), and thus PE (Table 2.8.), were observed in p53-null cells following mono treatment with all metabolic inhibitors, it is interesting that only treatment with DCA has no significant effect on radiosensitivity in p53 null cells. Table 2.8. shows that mono treatment with DCA does not induce marked changes

in PE in mutant p53 when compared 0 Gy conditions in DMSO- and DCA-treated groups (PE was 10.8±1.6 for cells treated with DMSO only compared with 11.9±0.8 for cells treated with DCA). In contrast, mono treatment with DCA induced marked reduction in PE in p53-null cells (PE was 7.7±0.3 for cells treated with DMSO only compared with 2.4±1.1 for cells treated with DCA). These differences in plating efficiency following treatment with DCA, may explain to some extent the differences in response to IR following treatment with DCA between p53-null cells and those expressing mutant p53 cells.

Inhibition of PDK, using DCA, promotes the entry of pyruvate metabolites into the TCA cycle and thus increases the cells ability to perform mitochondrial respiration, with the result being a decrease in the Warburg effect. As pyruvate levels are depleted following DCA treatment, the cell viability in response to IR diminishes. At this point, we do not know why this is, but a link with ROS production seems plausible. Several studies have indicated an increased level of ROS following treatment of cells with DCA (364,398–400), and this likely explains the increased sensitivity to IR. It is interesting to note that p53-null cells and those expressing wild type p53 showed a distinct pattern of response to DCA than that of cells expressing mutant p53. As previously shown in Figure 3.32., p53-null and wild type p53 cells showed a significant increase in glycolysis following siRNA-mediated transient inhibition of TIGAR while cells harbouring mutant p53 did not show a similar response. This distinct pattern of response to TIGAR inhibition that distinguishes the metabolic profile of p53-null and wild type p53 cells from those harbouring mutant p53 have similarities to the patterns of response these cells show to DCA-mediated radiosensitivity. Therefore, in order to better understand the mechanisms through which these candidate drugs sensitise cells to IR, with or without TIGAR inhibition, we investigated the changes in the metabolic profile of the indicated cells following transfection with either control or TIGAR siRNA and treatment with the anti-metabolic drugs.

3.3.3.3. Metabolic phenotype

Seahorse XFe metabolic studies were performed to investigate the changes in the metabolic phenotype of SCCHN cells in response to metabolic inhibitors and the role of TIGAR in determining radiosensitivity, (results discussed in 3.3.3.3.). UM-SCC-1 and isogenic derivatives cells were transfected with either control siRNA or siRNA specific

for TIGAR before treatment with drugs for 24 hours followed by mitochondrial and glycolytic stress tests as described 2.3.6.1 and 2.3.6.2..

Results obtained from mitochondrial stress test show that TIGAR knockdown significantly promotes an increase in mitochondrial respiration following treatment with UK-5099 and DCA in p53-null and wild type p53 cells, but not in R175H-p53 mutant cells. (Figure 3.56.).

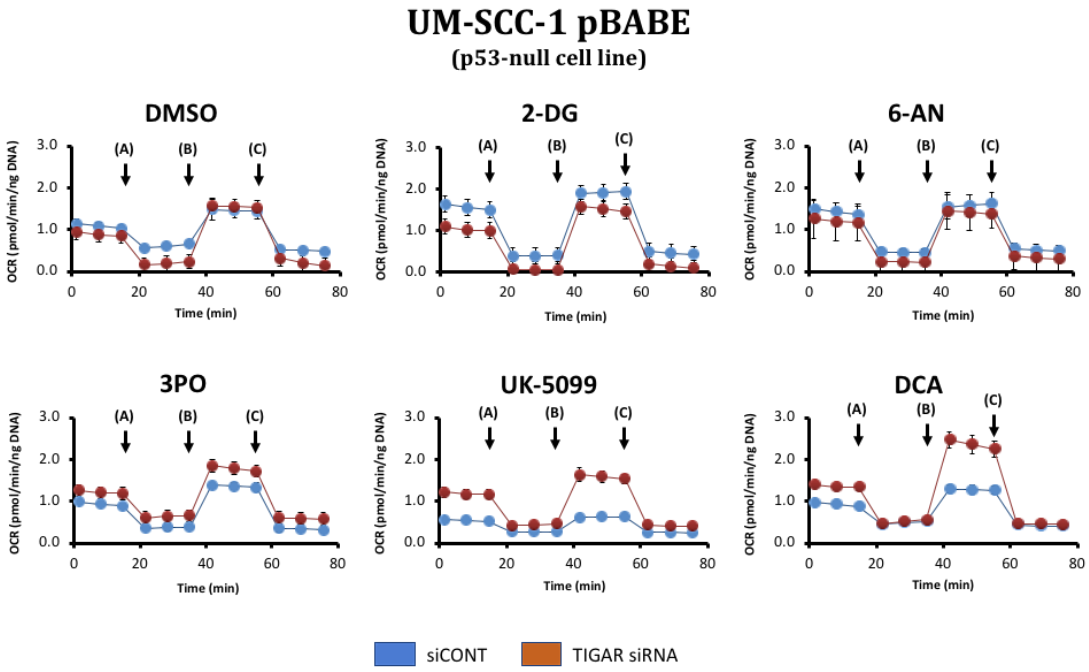

UM-SCC-1 WT-p53
(wild type p53 cell line)

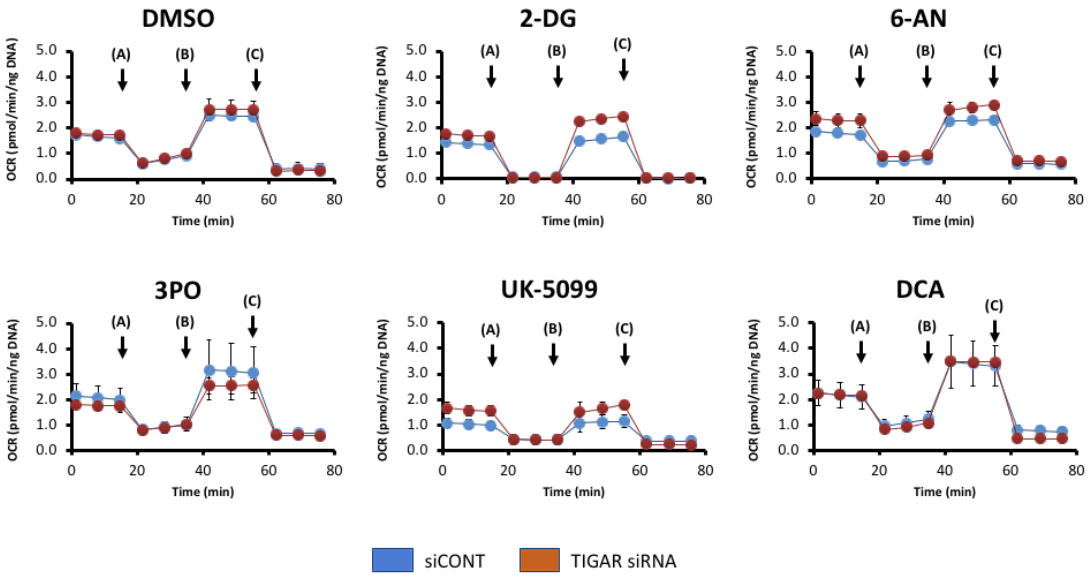

UM-SCC-1 R175H-p53
(mutant p53 cell line)

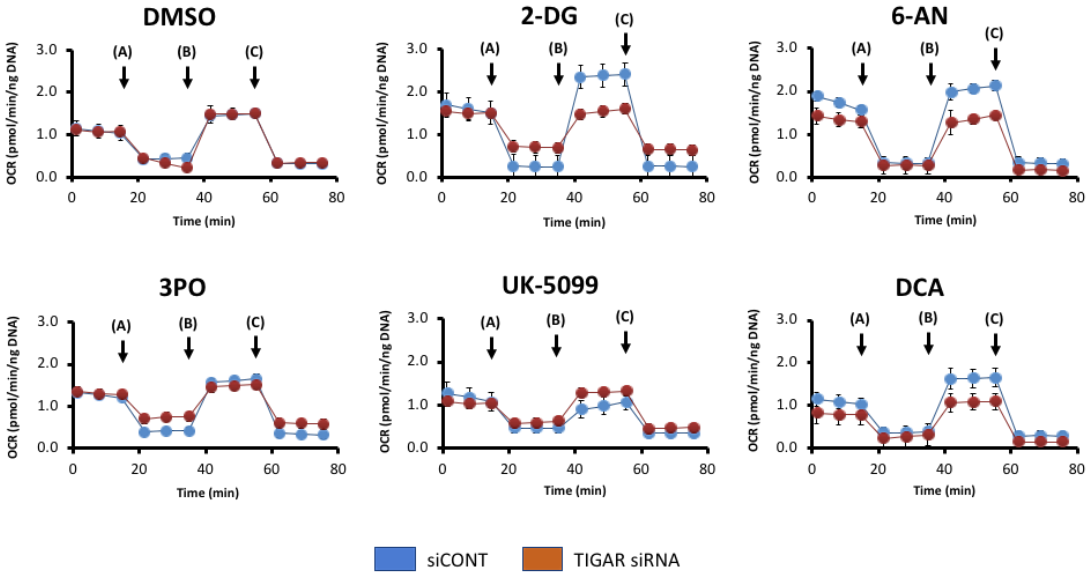

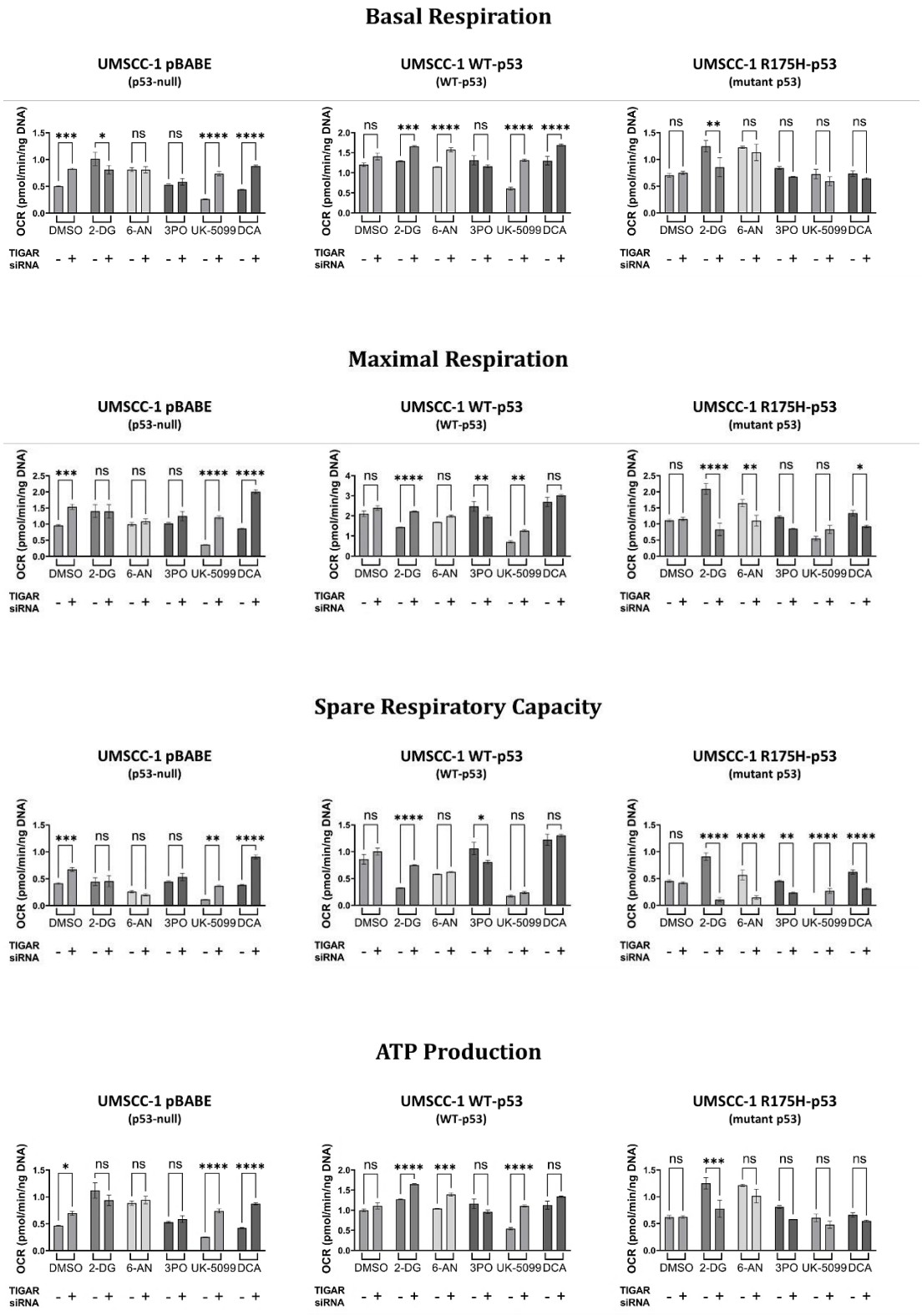

Figure 3.56.: Changes in the mitochondrial profile of TIGAR-knockdown UM-SCC-1 isogenic derivatives following treatment with anti-metabolic drugs. UM-SCC-1 pBABE, UM-SCC-1 WT-p53 and UM-SCC-1 R175H-p53 cells transfected with either non-target siRNA (siCONT, indicated as **[-]**) or siRNA specific for TIGAR (indicated as **[+]**) were treated with the indicated drugs for 24 hours before being subjected to mitochondrial stress test, as described in 2.3.6.1. Points A, B, and C on the graphs refer to the

injections time points of 1µM oligomycin, 0.5µM FCCP and 1µM rotenone and antimycin-A, respectively. Post-injection changes in the mitochondrial function were used to calculate the mitochondrial respiration parameters as described in Table 2.4. and are shown as normalised absolute values for basal respiration, maximal respiration, spare respiratory capacity and ATP production. OCR readings were obtained from three experiments (n=3), each experiment was performed in triplicate. Data are presented as mean OCR (pmol/min), normalised to DNA content (ng DNA) as described in 2.3.8. Means of individual data were used to derive overall means. Error bars represent SEM. Statistical analysis: a Student's t-test. (ns) $p > 0.05$, (*) $p \leq 0.05$, (**) $p \leq 0.01$, (***) $p \leq 0.001$, (****) $p \leq 0.0001$.

Results from glycolytic stress test shows that TIGAR knockdown significantly increase basal glycolysis following treatment with UK-5099 and DCA in p53-null and wild type p53 cells but only following treatment with DCA in p53 mutant cells (Figure 3.57.).

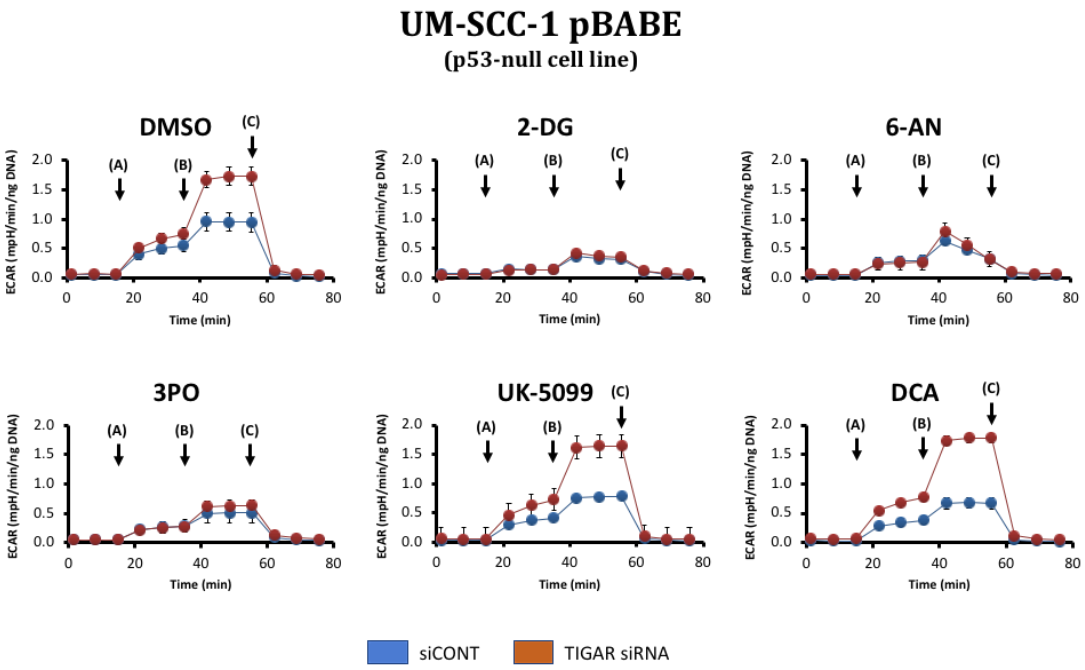

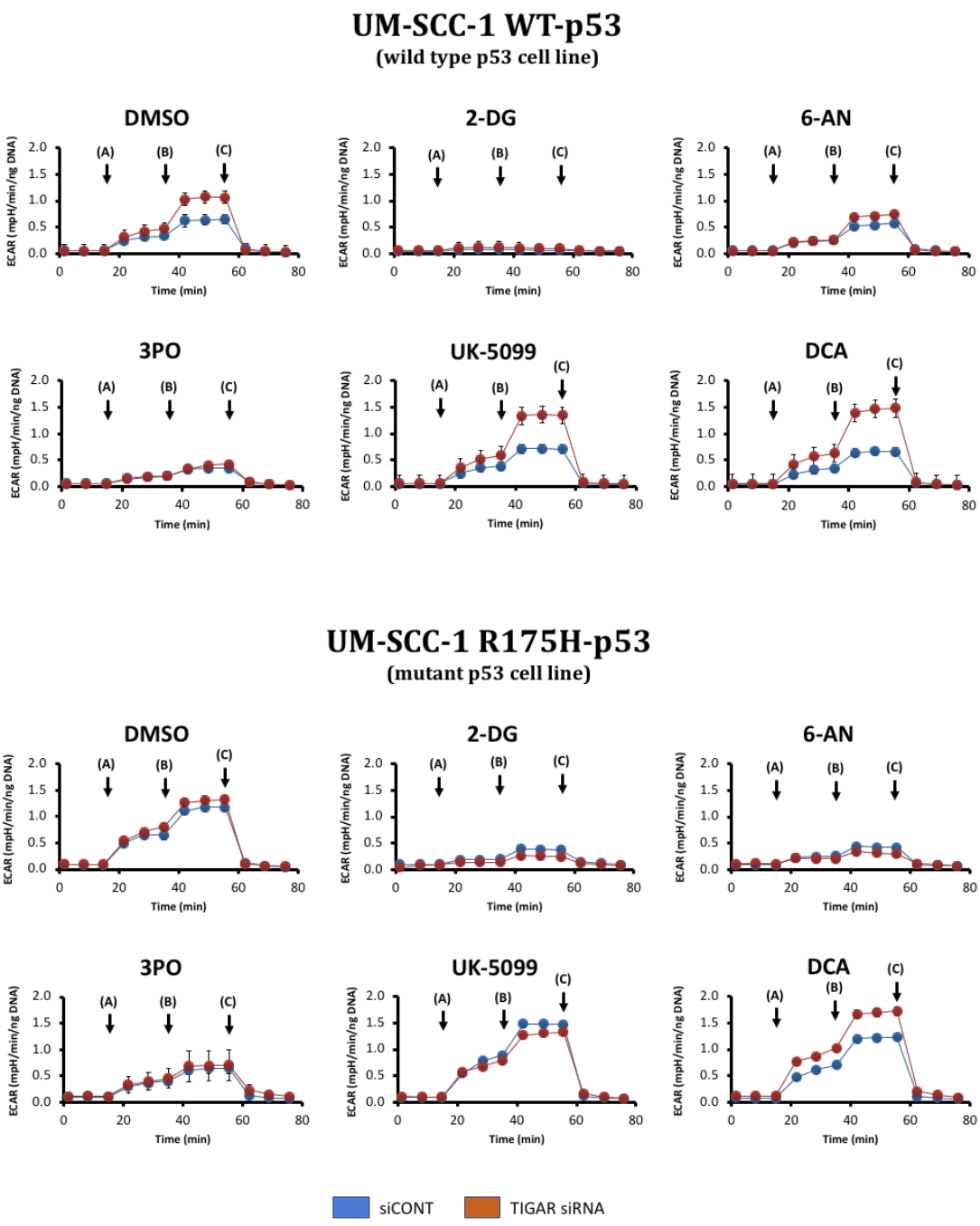
UM-SCC-1 WT-p53
(wild type p53 cell line)
DMSO
2-DG
6-AN
3PO
UK-5099
DCA
ECAR (mpH/min/ng DNA)
Time (min)
(A)
(B)
(C)
UM-SCC-1 R175H-p53
(mutant p53 cell line)
siCONT
TIGAR siRNA

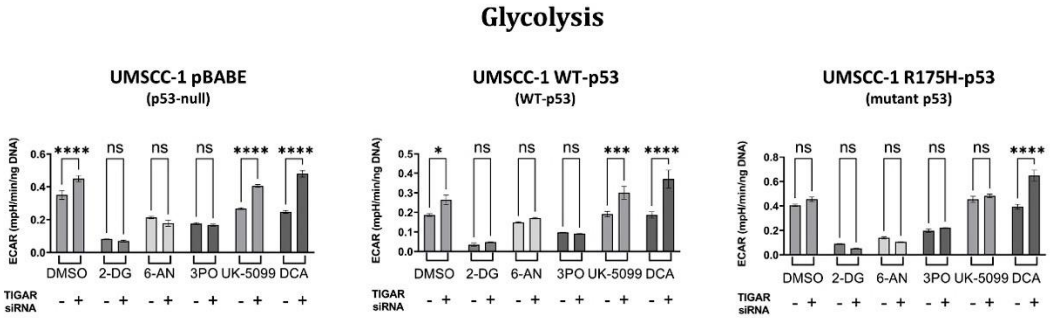
Glycolysis
UMSCC-1 pBABE
(p53-null)
UMSCC-1 WT-p53
(WT-p53)
UMSCC-1 R175H-p53
(mutant p53)
ECAR (mpH/min/ng DNA)
DMSO
2-DG
6-AN
3PO
UK-5099
DCA
TIGAR siRNA

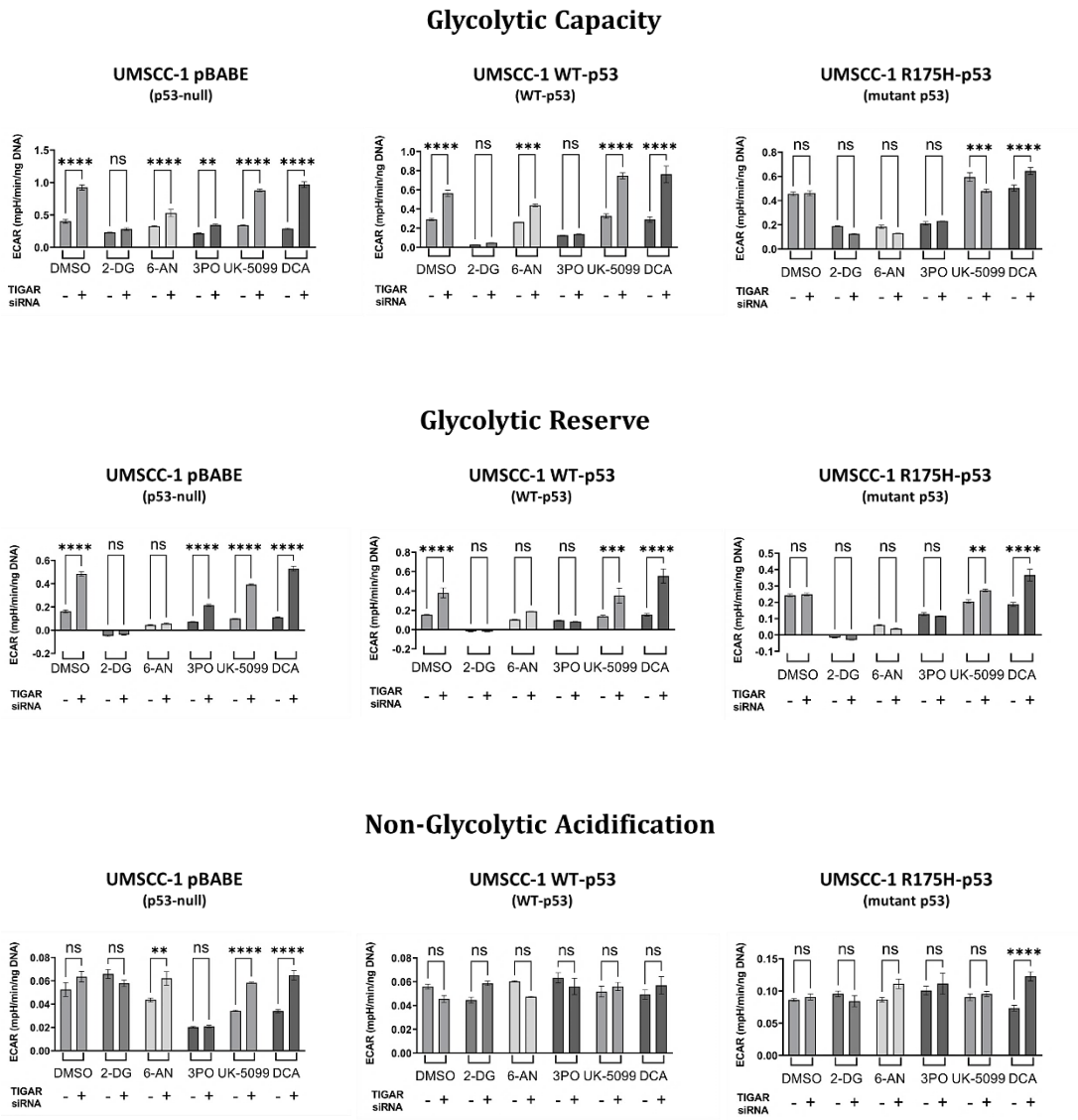

Figure 3.57.: Changes in the glycolytic profile of TIGAR-knockdown UM-SCC-1 isogenic derivatives following treatment with anti-metabolic drugs. UM-SCC-1 pBABE, UM-SCC-1 WT-p53 and UM-SCC-1 R175H-p53 cells transfected with either non-target siRNA (siCONT, indicated as [-]) or siRNA specific for TIGAR (indicated as [+]) were treated with the indicated drugs for 24 hours before being subjected to glycolytic stress test, as described in 2.3.6.2. Points A, B, and C on the graphs refer to the injections time points of 10mM D-glucose, 1μM oligomycin and 50mM 2-DG, respectively. Post-injection changes in the glycolytic function were used to calculate the glycolytic parameters as described in Table 2.5. and are shown as normalised absolute values for glycolysis, glycolytic capacity, glycolytic reserve and non-glycolytic acidification. ECAR readings were obtained from three experiments (n=3), each experiment was performed in triplicate. Data are presented as mean ECAR (mpH/min), normalised to DNA content (ng DNA) as described in 2.3.8. Means of individual data were used to derive overall means. Error bars represent SEM. Statistical analysis: a Student's t-test. (ns) $p > 0.05$, (*) $p \leq 0.05$, (**) $p \leq 0.01$, (***) $p \leq 0.001$, (****) $p \leq 0.0001$.

The results presented in Figures 3.56. and 3.57., together with results presented in section 3.3., show significant differences in cell viability, colony formation and metabolic profiling between p53-null and mutant p53 cells following treatment with UK-5099 and DCA. For instance, we showed in Figure 3.47. that treatment with UK-5099 inhibits mitochondrial respiration in p53-null cells with no similar effect observed in mutant p53 cells. This treatment also inhibits glycolysis in p53-null cells and increases glycolysis in mutant p53 cells. Figure 3.47. also show that oligomycin-mediated inhibition of ATP-synthase, and consequently of mitochondrial respiration, led to a compensatory increase in glycolytic capacity in cells harbouring mutant p53 following UK-5099-mediated inhibition of pyruvate transport to mitochondria with no similar response in p53-null cells. In addition, we also showed in Figure 3.49. that TIGAR knockdown has no effect on the mitochondrial-linked cell viability in response to treatment with both UK-5099 and DCA in p53-null cells, while it results in increased cell viability in mutant p53 cells. Moreover, treatment with UK-5099 radiosensitises p53-null cells to IR with or without TIGAR inhibition, whereas no similar effect was detected in cells expressing mutant p53 (Figure 3.54.). On the other hand, treatment with DCA increases radiosensitivity in mutant p53 cells with no similar effects were shown in p53-null cells (Figure 3.55.). Results in Figure 3.48. also showed that UK-5099-mediated inhibition of pyruvate entry into mitochondria has no effect on the expression of mutated p53, in contrast to the observed increase in p53 expression following treatment with other anti-metabolic agents. These differences, summarised in Table 3.6., between the metabolic profiling and radiosensitivity outcomes of p53-null cells and those harbouring mutant p53 suggest GOF properties of cells harbouring mutant p53 (reviewed in 1.2.5.) whereby mutant p53 can promote the acquisition of aggressive tumour cell phenotypes, different from those of cells harbouring wild type *TP53*. These GOF p53 mutations have been shown to increase resistance to radiation and chemotherapy through multiple mechanisms (401–403). Given that the mechanism of both UK-5099 and DCA targets the fate of pyruvate, it is reasonable to consider that the GOF properties we propose here are related to the fate of pyruvate. However, because the molecular mechanisms underlying p53 GOF are poorly understood, it is difficult to explain some responses that cells with these mutations exhibit to different therapeutic strategies, which warrants further investigation in order to better understand these mechanisms.

Table 3.6.: Major differences in effects of UK-5099 and DCA on basal respiration, glycolysis and radiosensitivity between p53-null and mutant p53 SCCHN cells.

	+ UK-5099				+ DCA			
	UM-SCC-1 pBABE (p53-null)		UM-SCC-1 R175H-p53 (mutant p53)		UM-SCC-1 pBABE (p53-null)		UM-SCC-1 R175H-p53 (mutant p53)	
	+siCONT	+TIGAR siRNA	+siCONT	+TIGAR siRNA	+siCONT	+TIGAR siRNA	+siCONT	+TIGAR siRNA
Basal Respiration	↓	↑	ns	ns	ns	↑	ns	ns
Basal Glycolysis	↓	↑	↑	ns	↓	↑	ns	↑
Radiosensitivity	↑	↑	ns	ns	ns	↑	↑	↑

3.3.3.4. Investigation of potential anti-metabolic combination treatments

In the final section of this study, the effects of TIGAR inhibition on cell viability and associated metabolic phenotype of SCCHNs in response to a variety of combinations of the indicated anti-metabolic drugs were investigated. The aim of this section is to explore drug combinations that may achieve additional inhibitory activity by targeting different parts of the glycolysis pathway to try to find better ways to sensitise cells to radiotherapy in future studies, with the ultimate aim of achieving improved control with lower doses of radiation, to avoid the co-morbidities/toxicities of the RT.

The mitochondrial-linked viability of cells was monitored following transfection with control siRNA or TIGAR siRNA and then treatment with a panel of anti-metabolic drugs applied in paired combinations (Figure 3.58.).

The results showed that inhibition of TIGAR in wild type p53 cells results in a significant decrease in the inhibitory effect on the mitochondrial-linked for all groups of anti-metabolic drugs, except for the combination of 3PO and UK-5099.

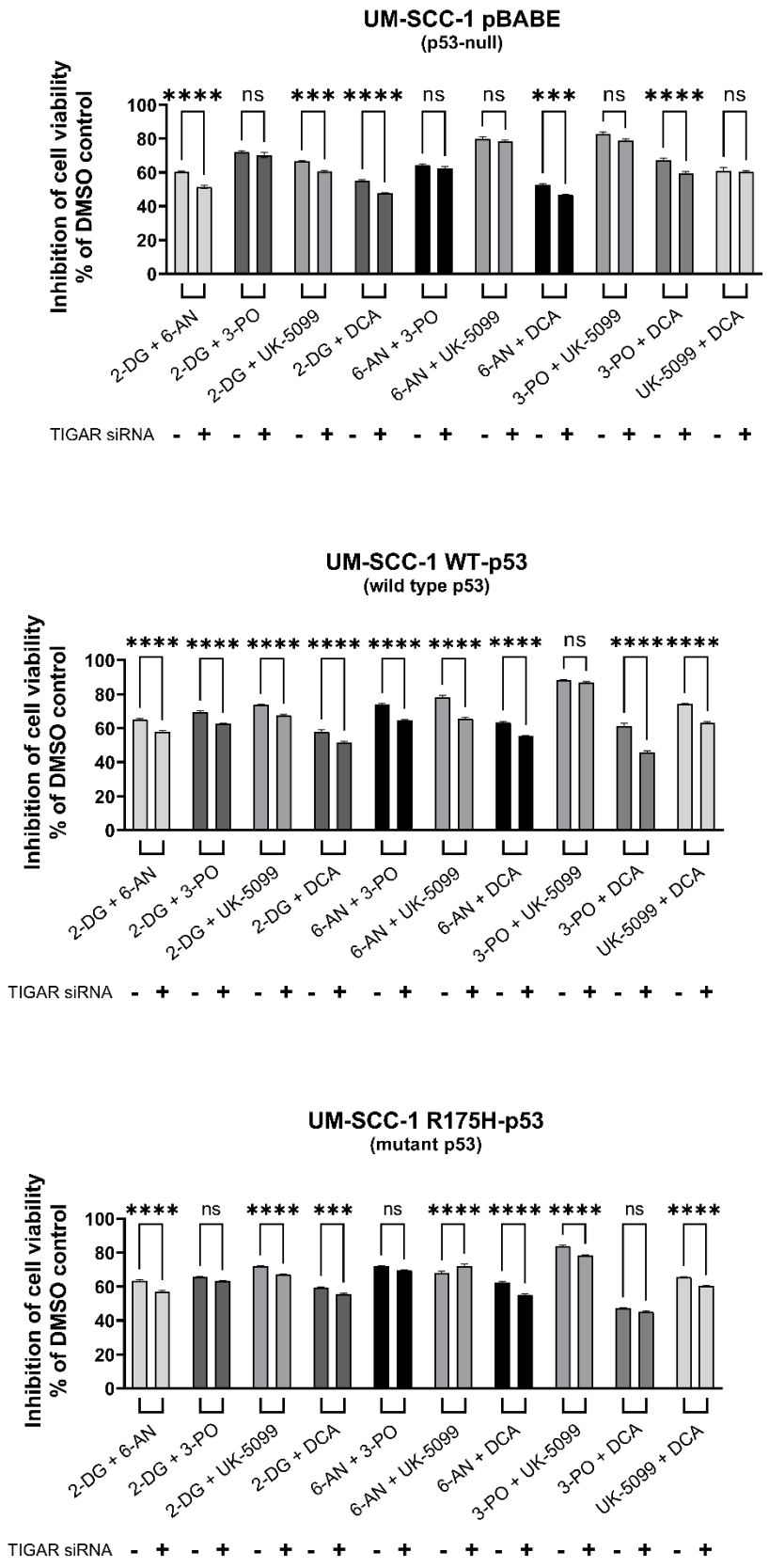

Figure 3.58.: Cell viability of TIGAR-knockdown UM-SCC-1 isogenic derivatives post-treatment with combinations of anti-metabolic agents. Viability was assessed in TIGAR-knockdown UM-SCC-1 isogenic derivatives following the treatment with different combinations of the indicated drugs, in pairs, as follow:

2-DG at 9mM, 6-AN at 13μM, 3PO at 44μM, UK-5099 at 45μM and DCA at 0.3 mM, for 24 hours. Values represent the mean from three separate experiments. Statistical analysis: Student's t-test. Means of individual data were used to derive overall means. Error bars represent SEM. (ns) $p > 0.05$, (*) $p \leq 0.05$, (**) $p \leq 0.01$, (***) $p \leq 0.001$, (****) $p \leq 0.0001$.

Investigating the effects of combining anti-metabolic drugs on the metabolic profile of SCCHN cells generated some interesting results (Figure 3.59.), which are summarised in Table 3.7.. In p53-null and mutant-p53 cells, the combination of hexokinase inhibitor, 2-DG, and other glycolysis inhibitors, in pairs, did not show an additional inhibition of basal values for mitochondrial respiration and glycolysis in comparison with using 2-DG alone, whereas, in the wild type p53 cells, these combinations showed significant inhibition of basal values for mitochondrial respiration. These results support the benefits of inhibiting the first step of glycolysis as a therapeutic approach to cells expressing non-functional p53, thus abolishing any additional metabolic capacity that could be inhibited by drug combinations given that glycolysis is the predominant pathway for energy production in these cells. In wild type p53 cells, which are less dependent on glycolysis, co-administration of anti-metabolic agents did not result in significant additional inhibition in basal values for glycolysis but produced a considerable decrease in basal respiration levels (Figure 3.59.). This could be explained through the possible decrease in pyruvate levels prior to entry into the TCA, which would have a major impact on the basal values for mitochondrial respiration, given the high dependence of these cells on mitochondrial respiration.

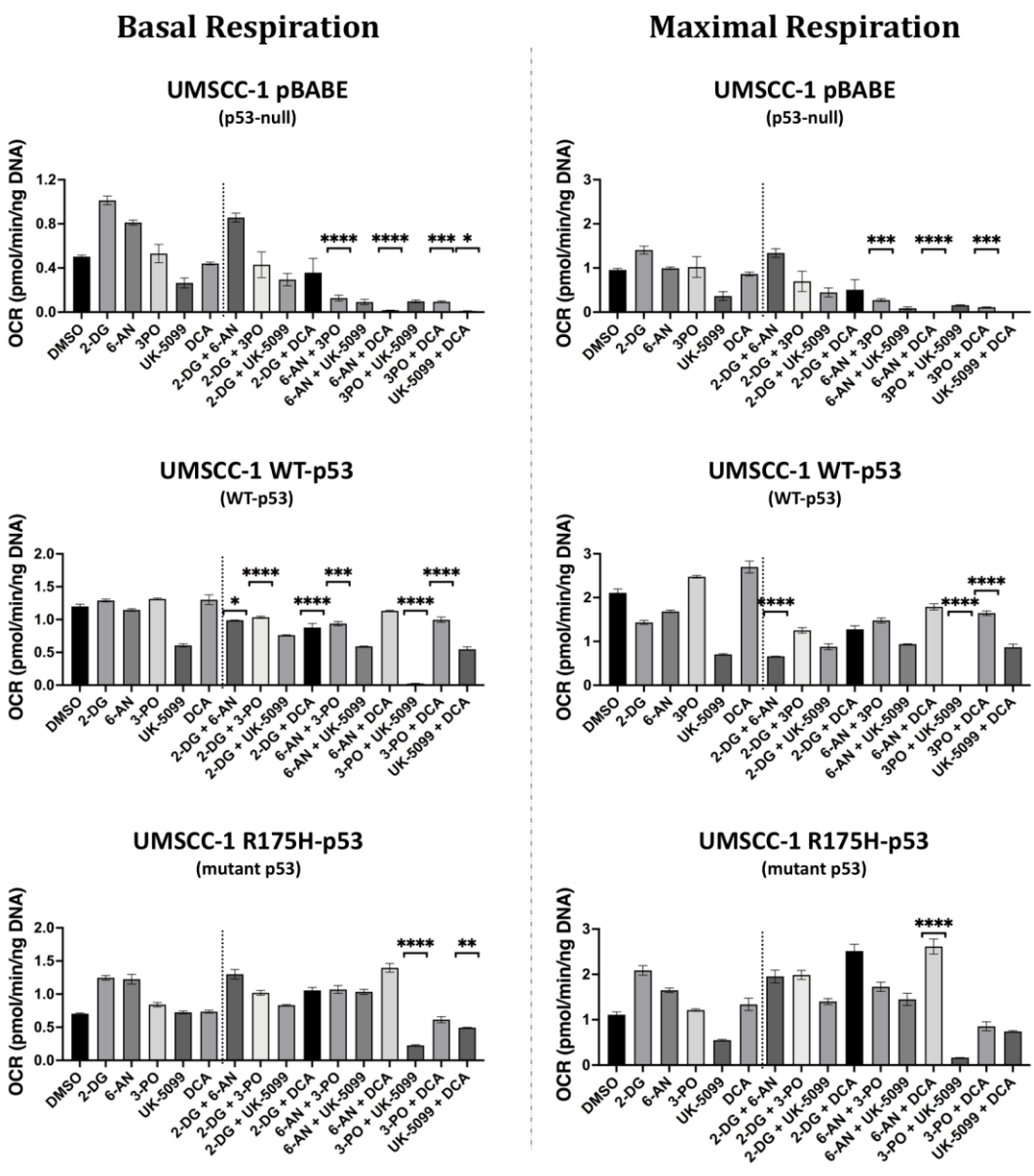
Basal Respiration
Maximal Respiration
UMSCC-1 pBABE
(p53-null)
UMSCC-1 WT-p53
(WT-p53)
UMSCC-1 R175H-p53
(mutant p53)
OCR (pmol/min/ng DNA)
DMSO
2-DG
6-AN
3PO
UK-5099
DCA
2-DG + 6-AN
2-DG + 3PO
2-DG + UK-5099
2-DG + DCA
6-AN + 3PO
6-AN + UK-5099
6-AN + DCA
3PO + UK-5099
3PO + DCA
UK-5099 + DCA

Spare Respiratory Capacity

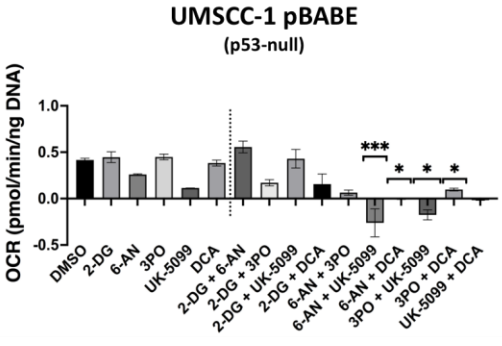

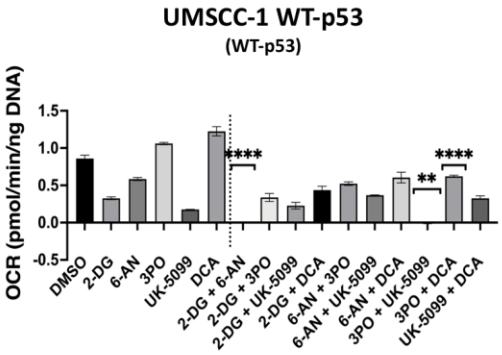

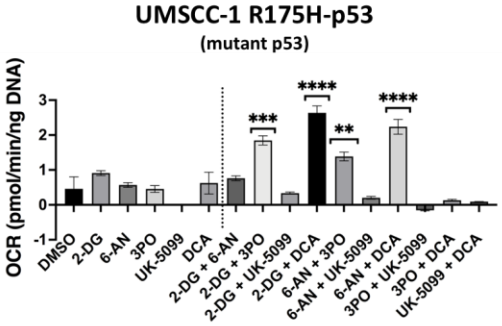

ATP Production

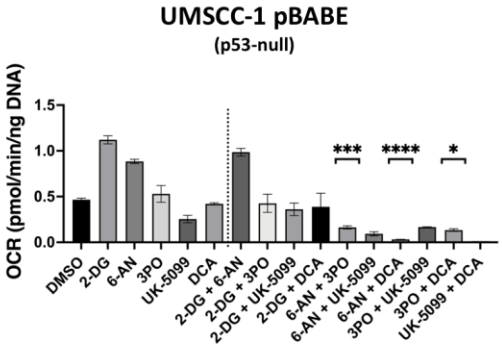

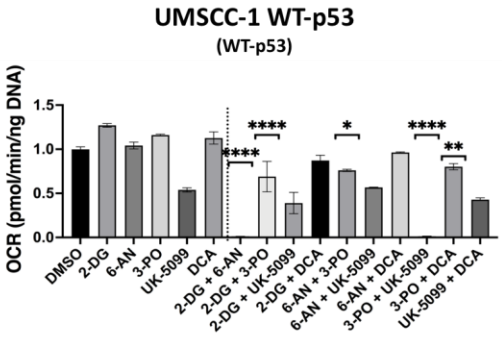

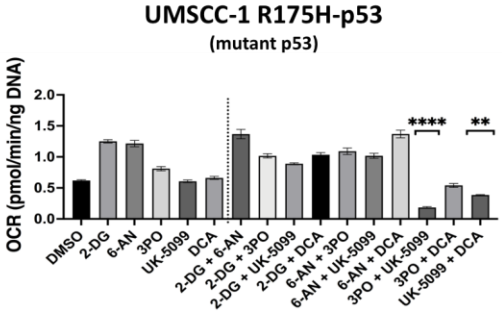

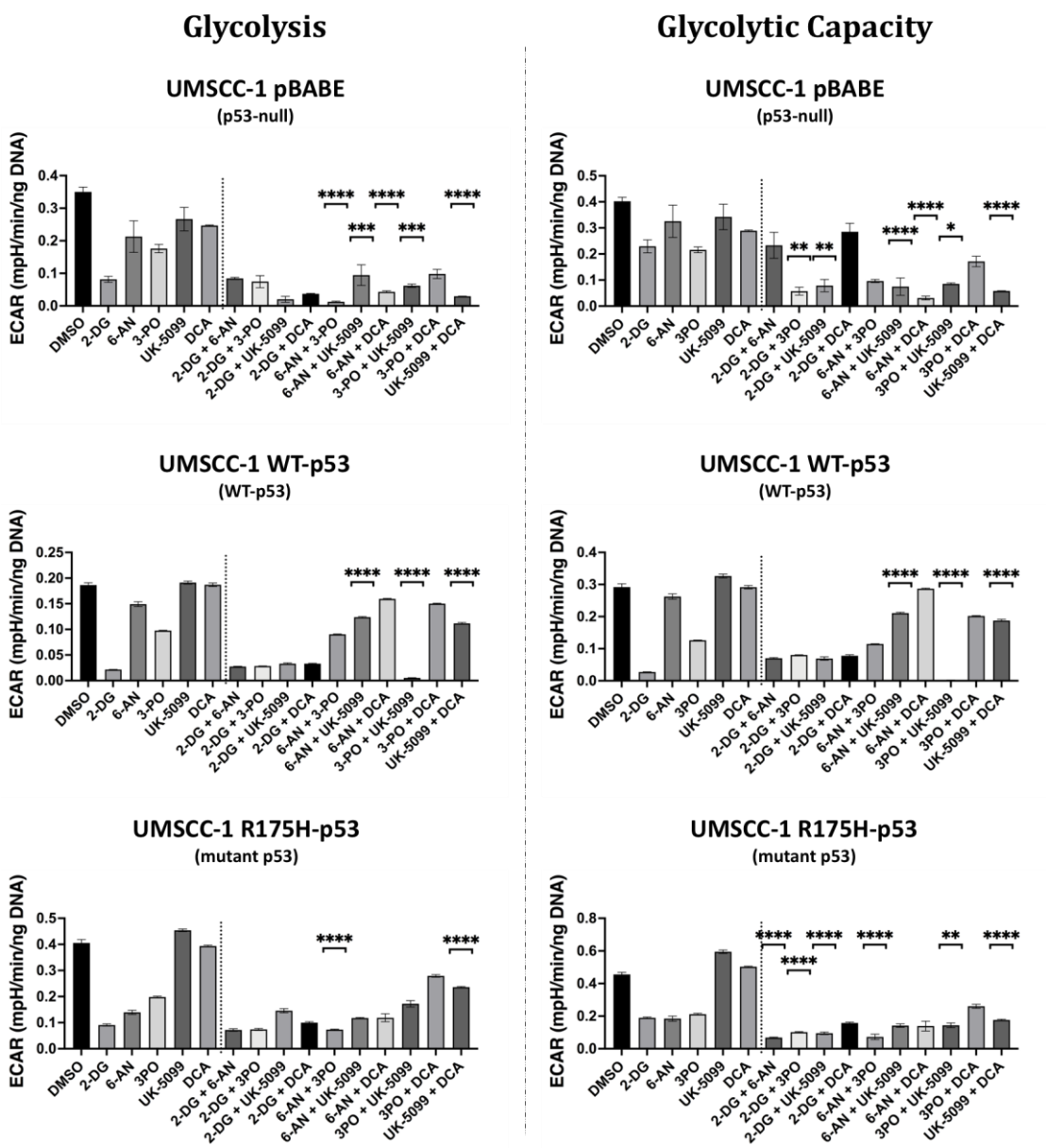
Glycolysis
Glycolytic Capacity
UMSCC-1 pBABE
(p53-null)
UMSCC-1 WT-p53
(WT-p53)
UMSCC-1 R175H-p53
(mutant p53)
ECAR (mpH/min/ng DNA)
DMSO
2-DG
6-AN
3-PO
UK-5099
DCA
2-DG + 6-AN
2-DG + 3-PO
2-DG + UK-5099
2-DG + DCA
6-AN + 3-PO
6-AN + UK-5099
6-AN + DCA
3-PO + UK-5099
3-PO + DCA
UK-5099 + DCA

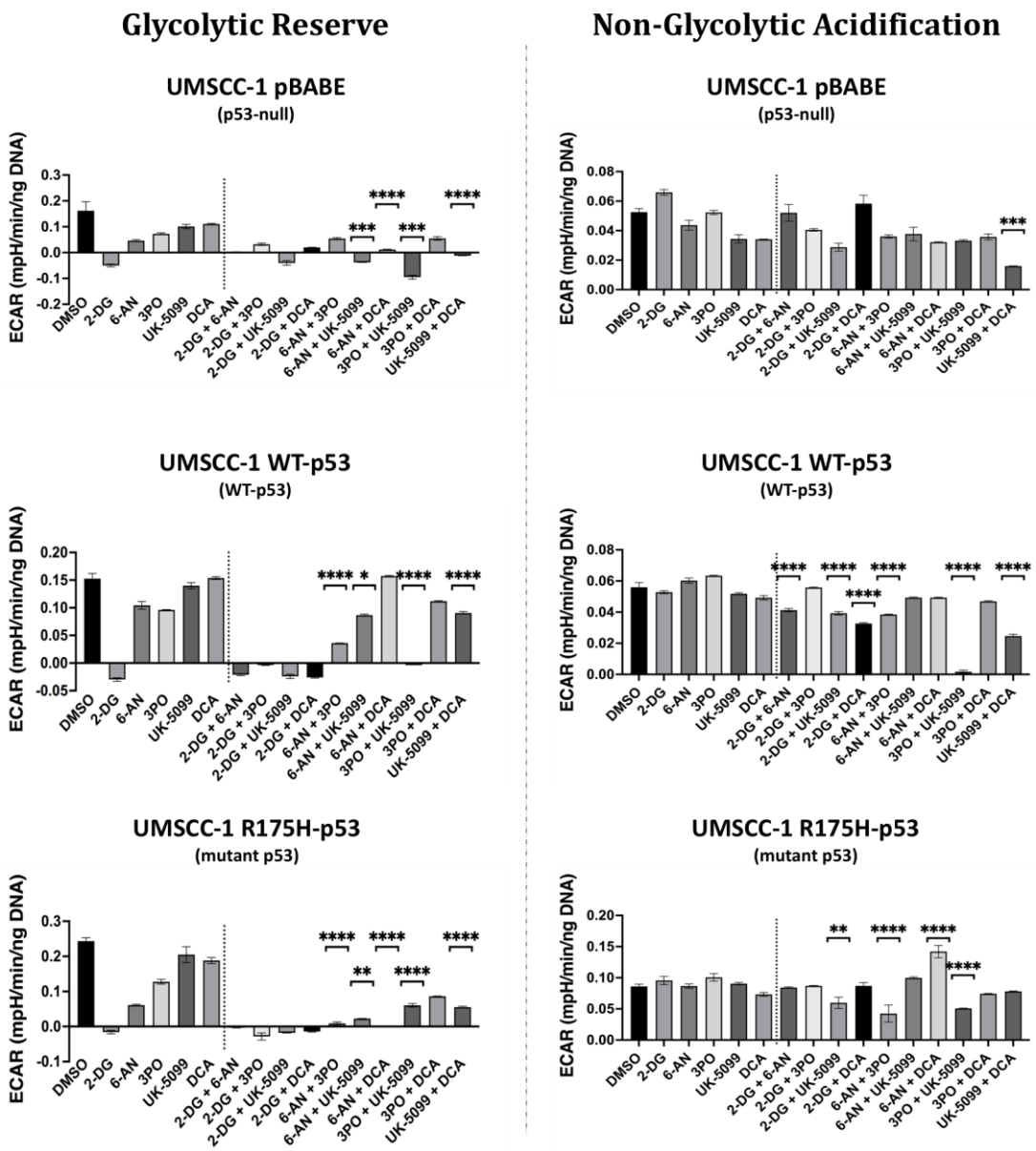

Figure 3.59.: Comparative metabolic profile of UM-SCC-1 isogenic derivatives following treatment with a variety of anti-metabolic combinations compared with monotherapy. Cells were subjected to combinations of the indicated drugs for 24 hours, before mitochondrial stress test and glycolytic stress test were performed, as described in 2.4.6.1 and 2.4.6.2., respectively. Absolute data derived from mitochondrial stress and glycolytic stress tests were normalised to DNA content for all groups of cells, and the absolute values for basal respiration, maximal respiration, spare respiratory capacity, ATP production, glycolysis, glycolytic capacity, glycolytic reserve and non-glycolytic acidification as described in section 2.4.6.1. and 2.4.6.2, respectively. To facilitate the comparison, the dotted lines used to separate the results from monotherapy (left) and from combinations (right). OCR and ECAR readings were obtained from three experiments (n=3), each experiment was performed in triplicate. Data are presented as mean OCR (pmol/min) and ECAR (mpH/min), respectively, normalised to DNA content (ng DNA) as described in 2.3.8. Means of individual data were used to derive overall means. Error bars represent SEM. Statistical analysis: a one-way ANOVA with Dunnett's test. (ns) $p > 0.05$, (*) $p \leq 0.05$, (**) $p \leq 0.01$, (***) $p \leq 0.001$, (****) $p \leq 0.0001$.

Table 3.7.: Changes in the metabolic profile parameters of UM-SCC-1 isogenic derivatives (p53 null, wild type and mutant) following treatment with a variety of combinations of anti-metabolic agents

UM-SCC-1 pBABE (p53-null)				
Mitochondrial Function				
	Basal Respiration	Maximal Respiration	Spare Respiratory Capacity	ATP Production
2DG + 6AN	ns	ns	ns	ns
2DG + 3PO	ns	ns	ns	ns
2DG + UK5099	ns	ns	ns	ns
2DG + DCA	ns	ns	ns	ns
6AN + 3PO	↓	↓	ns	↓
6AN + UK5099	ns	ns	↓	ns
6AN + DCA	↓	↓	↓	↓
3PO + UK5099	ns	ns	↓	ns
3PO + DCA	↓	↓	↓	↓
UK5099 + DCA	↓	ns	ns	ns
Glycolytic Function				
	Glycolysis	Glycolytic Capacity	Glycolytic Reserve	Non-glycolytic Acidification
2DG + 6AN	ns	↓	ns	ns
2DG + 3PO	ns	↓	ns	ns
2DG + UK5099	ns	ns	ns	ns
2DG + DCA	ns	ns	ns	ns
6AN + 3PO	↓	ns	ns	ns
6AN + UK5099	↓	↓	↓	ns
6AN + DCA	↓	↓	↓	ns
3PO + UK5099	↓	↓	↓	ns
3PO + DCA	ns	ns	ns	ns
UK5099 + DCA	↓	↓	↓	↓

UM-SCC-1 WT-p53 (WT p53)				
Mitochondrial Function				
	Basal Respiration	Maximal Respiration	Spare Respiratory Capacity	ATP Production
2DG + 6AN	↓	↓	↓	↓
2DG + 3PO	↓	ns	ns	↓
2DG + UK5099	ns	ns	ns	ns
2DG + DCA	↓	ns	ns	ns
6AN + 3PO	↓	ns	ns	↓
6AN + UK5099	ns	ns	ns	ns
6AN + DCA	ns	ns	ns	ns
3PO + UK5099	↓	↓	↓	↓
3PO + DCA	↓	↓	↓	↓
UK5099 + DCA	ns	ns	ns	ns
Glycolytic Function				
	Glycolysis	Glycolytic Capacity	Glycolytic Reserve	Non-glycolytic Acidification
2DG + 6AN	ns	ns	ns	↓
2DG + 3PO	ns	ns	ns	ns
2DG + UK5099	ns	ns	ns	↓
2DG + DCA	ns	ns	ns	↓
6AN + 3PO	ns	ns	↓	↓
6AN + UK5099	↓	↓	↓	ns
6AN + DCA	ns	ns	ns	ns
3PO + UK5099	↓	↓	↓	↓
3PO + DCA	ns	ns	ns	ns
UK5099 + DCA	↓	↓	↓	↓

UM-SCC-1 R175H-p53 (mutant p53)				
Mitochondrial Function				
	Basal Respiration	Maximal Respiration	Spare Respiratory Capacity	ATP Production
2DG + 6AN	ns	ns	ns	ns
2DG + 3PO	ns	ns	↑	ns
2DG + UK5099	ns	ns	ns	ns
2DG + DCA	ns	ns	↑	ns
6AN + 3PO	ns	ns	↑	ns
6AN + UK5099	ns	ns	ns	ns
6AN + DCA	ns	↑	↑	ns
3PO + UK5099	↓	ns	ns	↓
3PO + DCA	ns	ns	ns	ns
UK5099 + DCA	↓	ns	ns	↓
Glycolytic Function				
	Glycolysis	Glycolytic Capacity	Glycolytic Reserve	Non-glycolytic Acidification
2DG + 6AN	ns	↓	ns	ns
2DG + 3PO	ns	↓	ns	ns
2DG + UK5099	ns	↓	ns	↓
2DG + DCA	ns	ns	ns	ns
6AN + 3PO	↓	↓	↓	↓
6AN + UK5099	ns	ns	↓	ns
6AN + DCA	ns		↓	↑
3PO + UK5099	ns	↓	↓	↓
3PO + DCA	ns	ns	ns	ns
UK5099 + DCA	↓	↓	↓	ns

Although there was a negligible effect of DCA and UK-5099 independently on basal values for glycolysis in wild type p53 cells (Figure 3.47.), a combination of these drugs results in an additional reduction in glycolytic function in these cells with no effect observed on basal mitochondrial respiration. On the other hand, this combination results in additional inhibitory effects on baseline values of both mitochondrial respiration and glycolysis in cells with non-functional p53. These p53-status-linked differences could be attributed to the opposing actions of the two drugs on the fate of pyruvate in mitochondria and the highly active mitochondrial function of wild type p53.

Consistent with data shown in 3.3.3.2. and 3.3.3.3., drug combination treatments using UK-5099 or DCA, in pairs with other anti-metabolic drugs, showed inconsistent results between p53-null cells and those expressing R175H mutant p53, which may again suggest GOF properties that interfere with the response to UK-5099-mediated inhibition of pyruvate transport to mitochondria and DCA-mediated increase in pyruvate conversion to acetyl-CoA. Further research is needed to investigate the GOF properties that interfere with the fate of pyruvate and its effect on enhancing drug resistance in mutant p53 SCCNs.

Moreover, the metabolic profile of cells treated with a combination of 3PO and DCA shows no significant impact on the glycolytic function when compared to treatment with 3PO or DCA only in all p53 status, which excludes any possible significance of this combination in anti-glycolytic treatment.

Although the drug combination of 3PO and UK-5099 resulted in >80% inhibition in cell viability in mutant p53 cells, it was interesting that a comparable inhibition was observed in cells harbouring wild type *TP53* (Figure 3.58.). By looking at the metabolic profile of wild type p53 cells following this treatment, this is the only drug combination that induced a marked decrease in the values of all respiratory and glycolytic parameters. This combination produced a significant increase in inhibitory effect on metabolic functions when compared to treatment with 3PO or UK-5099 only, through 3PO-mediated inhibition of the third step of the glycolysis and UK-5099-mediated inhibition of the mitochondrial respiration by inhibition of MPC. This combination showed similar inhibitory effects to that reported following the combination between 2-DG and Metformin in a number of metabolic studies which found that the 2-DG-mediated inhibition of glycolysis pathway accompanied by the metformin-mediated inhibitory effects on mitochondrial function may provide a promising therapeutic strategy to target SCCHN (245,246,312,404).

Together, the finding presented in this section support several observations previously shown in this thesis about the critical role of p53 function in determining response to treatment with anti-metabolic agents in SCCHN. This is also consistent with the results of protein expression presented in 3.3.3.2.1., as treatment with anti-metabolic agents induces expression of p53 which is reversed by transient inhibition of TIGAR that increases glycolysis. Given that multiple studies have shown that loss of p53 function is associated with poorer overall survival outcomes in SCCHN, our results support the

notion that drug resistance and cell survival are substantially linked to the acquisition of glycolic phenotype which is found to be determined by p53 status, as we demonstrated in 3.1., making the p53 status a determinant of the therapeutic response of SCCHNs to anti-metabolic inhibitors.

4. Discussion

As stated in section 1.5., the main aims of this thesis were to investigate the potential role of *TP53* status in determining the metabolic phenotype in SCCHN, and to investigate the possible mechanisms through which *TP53*-mediated metabolic regulation functions, particularly focusing on the potential contribution of TIGAR, given the recent increased interest of TIGAR function as a regulator of glycolysis. In addition, I wanted to investigate whether anti-metabolic therapy approaches might have potential, based on their *in vitro* activities, as therapeutic strategies for SCCHNs, as well as to evaluate the significance of *TP53* and TIGAR status in determining the role of anti-metabolic therapeutic agents in modulating the response to IR.

These research objectives were rationally determined based upon a number of pieces of evidence. The first is the fact that survival rates for HPV-negative SCCHN have not improved significantly over the past 20-30 years, mostly because of the failure of current treatment regimens to stimulate a response in advanced-stage patients, who account for nearly two-thirds of SCCHN patients (8) and have overall survival rates of less than 35% (405,406). Thus, more effective and tailored treatment strategies are urgently needed to try to improve upon this situation. In nearly three-quarters of SCCHN cases, radiation is administered as a monotherapy or in combination with other treatments. However, resistance to radiotherapy continues to be a serious concern, especially since increasing the dose of radiotherapy is not an option due to its marked toxicity in normal tissues. Second, the increased interest that metabolic reprogramming has begun to receive as a hallmark of cancer, as well as the large number of recently published studies that have remarkably linked metabolic changes with the phenotype of cancer, have led to the creation of a major research focus to exploit metabolic reprogramming as a target for cancer therapy (407–410). There has been a significant increase in research into this topic, such as the growing evidence that switching the glucose metabolism of cancer cells from the glycolytic phenotype characteristic of metabolic reprogramming to the more normal reliance in normoxia on oxidative phosphorylation leads to the induction of apoptosis (233,411), and the promising outcomes of *in vitro* studies that have suggested new therapeutic strategies targeting cancer cells metabolism such as targeting enzymes of the glycolysis pathway or enhancing mitochondrial oxidative phosphorylation (reviewed in 1.3.4.). In SCCHN, however, this subject remains relatively unstudied and thus there is a great need for

more work investigating this area. Third, recent work to which I have contributed (412,413) and from others (245,246) has supported the idea that *TP53* is a critical determinant of metabolic programming in SCCHN cells. Combining this with the fact that loss of functional p53 is the most common oncogenic event in SCCHN (reviewed in 1.2.) makes targeting metabolic reprogramming a highly compelling potential therapeutic strategy for improving clinical outcomes in SCCHN. Fourth, given the complexity of the metabolic regulating mechanisms through which p53 functions (reviewed in (414)), it is essential to investigate the role that these mechanisms play in altering the metabolic phenotype in SCCHN in order to better understand how these complex mechanisms can be manipulated and whether this might lead to improved responses and/or strategies for radiotherapy in SCCHN. Among these mechanisms, several studies have recently focused on the role of the p53-responsive gene *TIGAR* in regulating glycolysis and the metabolic consequences of manipulating *TIGAR* gene expression (265,278,415–417). However, to date, no published work has investigated the potential role of TIGAR in the metabolic phenotype of SCCHN, nor the effect of manipulating TIGAR gene expression on the efficacy of anti-metabolic agents in improving the response to radiotherapy. It is also important to understand how p53 status may modulate the effect of manipulating TIGAR activity/function.

The data presented in this thesis provides a clear picture of the functional link between p53 status and the metabolic phenotype of SCCHN, and shows that the loss of p53 function determines the metabolic switch towards aerobic glycolysis. Our study also looks in more detail than previous studies in SCCHN at the consequences of manipulating TIGAR expression levels, on the metabolic phenotype of SCCHN. Furthermore, our work provides data on the effects of inhibiting TIGAR gene expression on cell viability, metabolic phenotype and colony formation following anti-metabolic treatment in SCCHN cells, and this, together with proposals for future work, will be the focus of discussion in this section.

4.1. *TP53* is a determinant of metabolic reprogramming in SCCHNs

Recent work has shown that Warburg's original observation that cancer cells tend to utilise fermentation to metabolise glucose and produce more lactate rather than rely solely on respiration even in oxygen-rich environments is the most characteristic metabolic disturbance in tumour metabolism (reviewed in 1.3.1.). We now know that this switch toward lactate production is accompanied by an increase in glucose uptake

and glycolytic flux, so considering the fact that aerobic glycolysis is substantially less efficient than oxidative phosphorylation in terms of ATP synthesis, and this raises the question of why tumour cells do this. Studies have demonstrated that Warburg's explanation of the switch toward aerobic glycolysis as a compensation for an energy shortfall caused by a defect in (mitochondrial) respiration is not correct (181). In addition, the switch of some bronchogenic tumours and leukemic cells, which exist in oxygen-rich environments, to aerobic glycolysis (418–421) provides further evidence that the Warburg effect is not an adaptive response to hypoxic conditions during the early stages of avascular tumour development (422). There is increasing evidence to support the notion that metabolic reprogramming is a dynamic process adopted by cancer cells to meet the complex demands of continuous cell proliferation, which is supported by studies that have reported a similar tendency in highly proliferating normal tissues, such as embryonic stem cells and activated lymphocytes. This has prompted researchers to investigate the link between the major oncogenic events that underlie ongoing cellular proliferation, such as the loss of *TP53* function, and the metabolic reprogramming in cancer cells. This is especially relevant to SCCHN given the high frequency of loss of p53 function occurring in 84% of HPV-negative SCCHNs (6).

In the first section of the results 3.1., the metabolic phenotype in SCCHN was investigated through the use of the highly sensitive microplate-based XF extracellular flux assays. These allow reliable quantitative metabolic analysis to be performed and can provide information on the metabolic phenotype in real-time (as detailed in 2.4.). In order to evaluate the potential role of *TP53* status as a determinant of the metabolic phenotype of SCCHN, a panel of SCCHN cell lines as well as two sets of isogenic derivative cell lines were used (as detailed in 2.2.1.). Results presented in section 3.1. clearly linked the function of p53 to the maintenance of metabolic diversity and robust mitochondrial function, with levels of glycolytic reserves comparable to those shown in cells with compromised p53 function that show a greater dependence on glycolysis (Figure 4.1.).

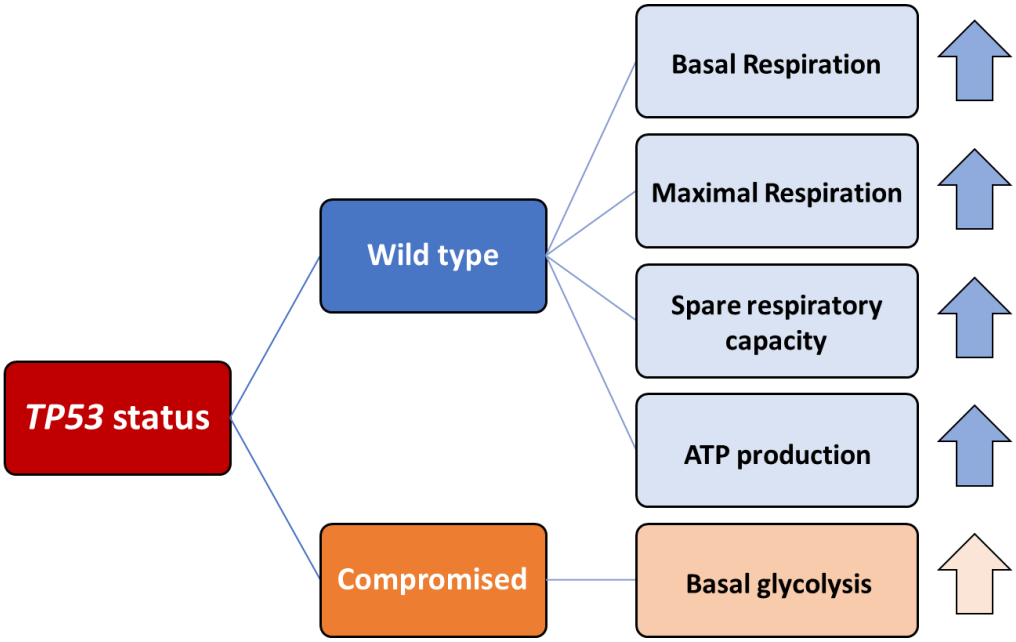

Figure 4.1. TP53 is a determinant of metabolic reprogramming in SCCHNs. A diagram shows the primary outcomes of the first chapter of the current study (3.1.). In cell lines expressing wild type p53, there was an increase in basal respiration, maximal respiration, spare respiratory capacity, and ATP production, indicating a highly active mitochondrial function. Cells expressing compromised p53 function (p53-null, mutant, or wild type p53 knockdown) consistently exhibited a distinct metabolic phenotype (which clearly resembles that described by Warburg), with lower active mitochondrial function and higher levels of basal glycolysis, with no significant differences in glycolytic capacity and reserves based on p53 status.

Two studies from Sandulache et al have suggested a link between the Warburg-like metabolic phenotype of SCCHN and *TP53* status (245,246). The authors reported a significant difference in the metabolic profile between the cell lines used which correlated with *TP53* status. The first paper, published in January 2011, showed that cells expressing wild type p53 exhibited relatively higher resistance to glucose deprivation and treatment with glycolysis inhibitors when compared to cells expressing mutant p53 (245).

Subsequently, the follow-up study, which was published in June 2011 and used a similar extracellular XF analysis to that used in this study, showed a considerably lower respiratory capacity in cells expressing mutant p53 compared to those expressing wild type p53 (246). The results also showed that wild type p53 SCCHN cells have a large spare respiratory capacity compared to cells expressing mutant p53, with no significant difference in the basal levels of respiration. Based on these findings, the authors suggested that cells expressing mutant p53 functioned at the maximal capacity of

mitochondria which would be contradictory to the hypothesis that cells expressing mutant p53 convert pyruvate to lactate to avoid mitochondrial respiration and to decrease ROS production (423). Mitochondria are the major site of intracellular ROS production, and thus excessive production of ROS can damage mitochondrial DNA and oxidise proteins and lipids, with numerous resulting effects, including lowering the efficiency of the electron transport chain. Therefore, cells that display high mitochondrial activity often protect the electron transport machinery by balancing ROS through enhanced antioxidant capacity (424–426). The Sandaluche et al study also showed attenuated compensatory glycolysis following inhibition of mitochondrial activity in mutant p53 cells when compared to wild type p53 cells. The authors described this as a globalised loss of metabolic flexibility due to the maximum use of (available) pathways.

The present study not only shows remarkable consistency with the general findings of Sandulache et al, but is also supported by stronger functional genetic evidence using isogenic derived cell lines expressing a variety of p53 statuses (p53-null cells, forcibly or endogenously expressed p53, knockdown of *TP53*, partially functional or GOF *TP53* mutations) demonstrating a clearly deterministic role for p53 in the regulation of cellular metabolic profile. Although the results presented in this thesis showed a large reserve respiratory capacity in SCCHN cells expressing wild type p53 compared to cells expressing mutant p53, the basal respiration level was also significantly higher in the wild type group, which suggests that the robust respiratory function in SCCHN cells expressing wild type p53 could be the simplest explanation for the large spare respiratory capacity of these cells. Furthermore, the results presented in this thesis showed no marked differences based on *TP53* status in levels of glycolytic compensation after mitochondrial inhibition, thus contradicting the hypothesis of a globalised loss of metabolic flexibility and maximal use of the glycolytic pathway in the absence of functional p53. Given that derivatives cell lines with compromised p53 (null, mutant or knockdown) showed a decrease in levels of mitochondrial function parameters and increase in levels of basal glycolysis without a significant change in the values for glycolytic capacity and reserves, the results presented here suggest that compromised p53 cells are not driven to maximal use of the glycolytic pathway due to the (availability) of this pathway, as suggested by Sandulache et al, but instead adapt to the demands of rapid proliferation with minimal products of mitochondrial respiration.

The Sandulache et al studies used only the percentage of changes in the oxygen consumption and extracellular acidification rates, whereas the present study used the absolute quantification of metabolic activity levels by normalising the data to DNA content allowing us to compare even relatively subtle differences in levels of mitochondrial ETC /respiratory activity between different cell lines. In addition, we not only compared the absolute values of the parameters of mitochondrial respiration and glycolysis, but also paid more attention to the metabolic switch from mitochondrial respiration to aerobic glycolysis. This switch can be assessed by analysis of the ratio of the absolute values of glycolysis to the absolute values of mitochondrial respiration as an indicator of the switch to the Warburg phenotype. This ratio was first utilised in Warburg's studies as an indicator of rapid tumour progression and proliferation in the presence of oxygen by comparing the values of this ratio between a number of benign and malignant rat tumours, where malignant tumours showed high values for this ratio compared to those obtained in benign tumours (318) and it has since been used in a number of studies as an indicator of metabolic reprogramming (319–322). In our study, the results of using this ratio in metabolic profiling of SCCHN results in clear dichotomisation of cells into p53 wild type and p53 compromised groups (see Figure 3.16.), with results consistently following the pattern in the isogenic cell lines demonstrating the deterministic function of p53 in regulating this metabolic balance.

My results are also consistent with a study by Eriksson et al 2017, which used derivatives of the p53-null human non-small-cell lung carcinoma cell line H1299 that had been genetically modified to stably express nine point mutations of *TP53* (427). The parental cell line used has a homozygous partial deletion of the *TP53* gene and was chosen to exclude the possibility that mutant p53 would act through dominant-negative effects on any endogenous wild type p53. The expression of wild type or mutant p53 was induced using doxycycline before metabolic studies were performed, and thus clonal selection of compensatory mutations or epigenetic effects was minimised. The study also used transient siRNA and plasmid transfection to alter the expression of p53 in a number of cell lines: colon cancer (HCT116), ovarian cancer (ES-2), breast cancer (MDA-MB-231) and the normal epithelial breast (MCF-10A)(427). All of the H1299 mutant p53 lines studied exhibited increased basal glycolysis with the exception of derivatives expressing H179R (LOF) and D281G (GOF) mutant p53. Also, with the exception of one derivative (expressing the GOF R273H mutant p53), all other mutant p53 cell lines showed no significant increase in maximal glycolytic capacity when compared to the parental cell line. However, these results were not consistent

with the metabolic profiling of HCT116 cells, as inducing mutant p53 expression in these cells increased both glycolysis and maximal glycolytic capacity, similar to the effects of stable expression of these mutations in HCT116 cells. In addition, Eriksson et al found that basal mitochondrial and ATP-linked respiration were both suppressed for the majority of mutant p53 cells, with varying levels of respiratory capacity. This is consistent with the results presented in this thesis, as cells harbouring mutant p53 showed low levels of basal respiration and ATP- linked respiration. The study by Eriksson et al also described siRNA-mediated transient inhibition of p53 in cells endogenously expressing wild type or mutant p53, which showed a significant decrease in both basal values of glycolysis and mitochondrial respiration, as well as ATP-linked respiration in a number of mutant derivatives without similar effects in cells expressing wild type p53. The authors attributed these differences in the metabolic profile between loss of p53 function (siRNA-mediated transient inhibition of p53) cells and mutant p53 cells to the effects of p53 GOFs, indicating that the acquisition of a glycolic metabolic phenotype results from the p53 GOFs rather than the absence of functional p53. However, the authors also indicated that these proposed effects of GOFs may be cell type-specific and not a general response given that they were not observed in all mutant derivatives used in the study. It is noteworthy that this study did not refer to the impact of siRNA-mediated transient inhibition of p53 on cell viability, as tiny changes in cell viability could substantially change OCR and ECAR values, and thus the absolute values of glycolytic and mitochondrial parameters. As mentioned above. This was avoided in our study by normalising the absolute values of metabolic parameters to the cellular DNA content, which exhibited no significant differences in the mitochondrial and glycolytic parameters following the transient inhibition of mutant p53 (following siRNA knockdown), except for an increase in glycolytic reserves in cells expressing a partially functional mutant C176F p53. Our findings do not agree with those of Eriksen et al regarding the role of p53 GOF mutants in metabolic reprogramming. We found no significant differences between the metabolic profile of p53 mutant cells and siRNA-mediated knockdown p53 cells, both groups of cells show increased basal glycolysis and decreased mitochondrial respiration when compared to wild type p53, indicating that the role of p53 as a determinant of metabolic reprogramming is a result of loss of wild type p53 function rather than any oncogenic GOF properties possessed by a specific *TP53* mutation.

The results presented in section 3.1. provide clear evidence for the role of p53 function as a determinant of metabolic reprogramming in SCCHNs. p53 function is associated

with high respiratory activity whereas the loss of p53 function is correlated with higher levels of aerobic glycolysis without significant p53-status-related differences in glycolytic reserves. It is necessary to point out that our findings are based on measurements taken at baseline or following exposure to acute metabolic stress, and although this provides data regarding the metabolic phenotype of SCCHN cells and the impact of p53-status-related variants, it is important to consider the potential for cells to adapt through the upregulation of glycolysis as may occur during chronic conditions of metabolic stress, such as hypoxia.

4.2. The role of TIGAR in the metabolic regulation of SCCHNs is p53-dependant

The data presented in section 3.1. demonstrate that loss of wild type p53 function in SCCHN contributes to the acquisition of a glycolytic phenotype at the expense of mitochondrial respiration. However, the precise mechanism of action by which p53 regulates the balance between mitochondrial respiration and glycolytic activity, as well as how the loss of function of wild type p53 may promote a switch toward glycolysis in SCCHN cells, is not well understood. In the second part of our study, we aimed to begin to investigate potential mechanisms of *TP53*-mediated metabolic regulation and the role these might play in the switch towards aerobic glycolysis, focusing for several reasons on TIGAR in the first instance. The function of p53 includes direct regulatory effects on mitochondrial respiration and glycolytic activity, as well as interaction with several other key metabolic pathways involving a number of target genes, which are discussed in 1.3.2. and illustrated in Figure 1.7. Thus, manipulating the expression of potential target genes of the cellular p53-responsive machinery that regulate different parts of glucose metabolism may be valuable in elucidating these mechanisms of action and in determining key elements of the Warburg effect in SCCHN. One of these potential target mediators of the p53-responsive cellular machinery that regulates glucose metabolism is TIGAR, which has recently gained importance in cancer research due to the dual role it plays in cancer development (discussed in 1.4.3.). However, only a few studies have investigated the role of TIGAR in SCCHN. RNAi and plasmid transfection were used to manipulate the expression of TIGAR to try to determine its contribution to the Warburg phenotype with respect to changes in metabolic profile and sensitivity to potential therapeutic agents.

In section 3.2., the role that TIGAR plays in the metabolic regulation of SCCHN was investigated and the consequences of manipulating the expression of this protein on

the metabolic phenotype. According to the literature, TIGAR functions by indirectly reducing PFK-1 activity and thus decreasing glycolytic flux in the third step of the pathway. This inhibition promotes the pentose phosphate (PPP) pathway, resulting in enhanced production of NADPH, which contributes to an increase in GSH levels and thus enhances the scavenging of reactive oxygen species (ROS).

Results obtained from our panel of SCCHN cells as detailed in section 3.2.2., showed an increase in absolute values for basal glycolysis with no significant effect on absolute values for basal respiration following siRNA-mediated transient inhibition of TIGAR in cells expressing wild type p53, whereas an increase in absolute values for both functions were demonstrated in p53-null cells. Although these results may be due to lower mitochondrial respiration capacity in p53-null cells as any increase in glycolytic flux due to TIGAR inhibition would make a significant increase in basal respiration levels, these results may also suggest a possible role for an alternative p53-independent mechanism that regulates TIGAR in the absence of p53 (259,269,428–430). However, no significant effect of siRNA-mediated transient inhibition of TIGAR was observed in cells expressing mutant p53, which might suggest GOF properties of p53 mutants that counteract this alternative regulatory mechanism and thus limit the effect of TIGAR transient inhibition on basal glycolysis and mitochondrial respiration values in the absence of functional p53. It is not unexpected that mutant p53 might elicit GOF properties that alter cellular metabolism. Indeed, many studies have reported that metabolic regulation in mutant p53 cells could involve distinct GOF mechanisms (32–36). These GOF effects include increased cell proliferation, cell migration and invasion, as well as increased resistance to chemotherapy and also increased anti-apoptotic functions (reviewed in 1.2.5.1.).

Results also showed that whilst TIGAR overexpression did not affect baseline glycolysis values, it did, as might be expected, markedly inhibit glycolytic capacity and reserves in wild type p53 cells (Figure 4.2.). Although these findings demonstrate the important role that TIGAR plays in regulating glycolysis, any potential effect of TIGAR in regulating the balance between glycolysis and mitochondrial respiration as well as the Warburg effect appears to be p53-dependant. It is significant that these results clearly demonstrate that wild type cells exhibit a glycolytic phenotype following TIGAR inhibition similar to that exhibited by loss-of-function p53 cells, and therefore TIGAR inhibition may have importance in future therapeutic studies targeting metabolic reprogramming in cells expressing wild type p53, but not in cells with mutated *TP53*.

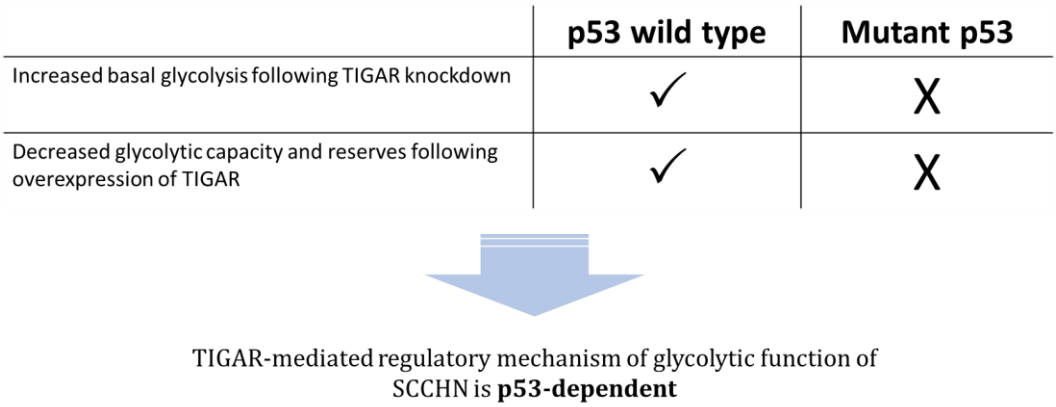

Figure 4.2. The role of TIGAR in the metabolic regulation of SCCHNs is p53-dependant. Results from the current study showed an increase in absolute values for basal glycolysis following siRNA-mediated transient inhibition of TIGAR in cells expressing wild type p53, whereas no similar effect was observed in cells expressing mutant p53. Results also showed that whilst TIGAR overexpression had no effect on baseline glycolysis values, it markedly inhibits glycolytic capacity and reserves in wild type p53 cells, with no similar effect in mutant p53 cells. Although these findings show that TIGAR plays an important role in glycolysis regulation, any potential effect of TIGAR in regulating the balance of glycolysis and mitochondrial respiration, as well as the Warburg effect, appears to be p53-dependent.

4.3. A p53-status-based model for sensitising SCCHNs to IR

In the final chapter of this thesis, the role of *TP53* and *TIGAR* and their interaction in regulating cell viability, metabolic phenotype, and colony formation following treatment with a variety of metabolic inhibitors were investigated (discussed in section 3.3). Given the accumulating evidence that metabolism is dramatically altered and exhibits a complex relationship with malignant transformation, it is not surprising that it has been identified as a potential therapeutic target for more than a decade. Metabolic treatments aim to target metabolites or the enzymes that generate them and which are involved in energy production in several metabolic pathways. As stated previously, a number of preclinical and/or clinical trials are being conducted utilizing different agents that act on these pathways (240,242,248,431–433)(discussed in detail 1.3.4.).

The most significant observation to arise from the present study is that it demonstrates clearly the efficacy of using inhibitors of various steps in glycolysis to increase the sensitivity of SCCHN cells harbouring compromised *TP53* to ionising radiation. This works selectively for mutant p53 since no comparable effects are observed in cells harbouring wild type *TP53*. This is potentially important because it supports previous observations that loss of *TP53* function leads to metabolic reprogramming and

promotes the switch towards aerobic glycolysis, making cells more dependent or "addicted" to glycolysis even in normoxic conditions, and resulting in a higher sensitivity to radiation following the inhibition of glycolysis. Our results are consistent with the findings of a number of studies that have found that the use of glycolysis inhibitors increases the sensitivity of cells to radiation in the absence of p53 function (243,245,246,434).

Given the need for a broader anti-metabolic approach to increase the radiosensitivity of SCCHN tumours expressing wild type *TP53*, the current study has also provided evidence that a radiosensitising effect of glycolysis inhibitors can be achieved in the presence of wild type p53 by inhibiting TIGAR. Studies have shown that TIGAR suppresses senescence (265), autophagy (364), apoptosis (278,279) and chemotherapy sensitivity (435–437), and in addition, reduced radiosensitivity was observed when TIGAR is overexpressed (438).

Our results suggest a treatment model that is directly related to p53 status, and which by the additional option of inhibiting TIGAR, could provide a new stratified therapeutic approach for both aggressive disease typical of mutant *TP53* and also for those patients with tumours harbouring wild type p53. This proposed therapeutic strategy would be based on the use of glycolysis inhibitors as sensitisers for radiotherapy for SCCHN patients with mutant *TP53* disease, thus targeting the limited metabolic flexibility of these cells and depriving them of their predominant source of energy. In addition, our therapeutic strategy demonstrates the efficacy of inhibiting TIGAR expression followed by administration of glycolysis inhibitors as a potentially promising therapeutic combination for SCCHN patients with wild type *TP53*-associated disease that has greater metabolic flexibility.

Thus, the work presented here identifies two means to radiosensitise SCCHN cells that could become part of a therapeutic strategy for patients stratified by their *TP53* status, one that works for mutant p53, including p53 null cells, and one that works for wild type p53 cells (Figure 4.3.). Given the importance of RT in the treatment for the vast majority of SCCHNs, such strategies clearly need further investigation to determine their potential to enhance RT outcomes for patients with SCCHN. The proposed therapeutic approach also provides a strong basis for future research to study the efficacy and safety of compounds that inhibit the expression of TIGAR as a promising therapeutic approach to target the metabolic diversity in SCCHN cases harbouring wild

type *TP53* in combination with glycolysis inhibitors. One study in leukaemia has already demonstrated the efficacy of treatment with glycolysis inhibitor 2-DG following TIGAR knockdown in inducing apoptosis in patients with cytogenetically normal acute myeloid leukaemia associated with poor prognosis (439).

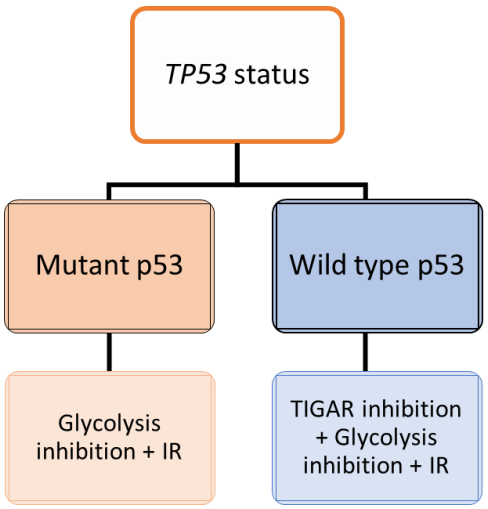

Figure 4.3.: A schematic diagram p53-status-based model for sensitising SCCHNs to IR. The current study clearly demonstrated the efficacy of using inhibitors of various steps in glycolysis pathway to increase the sensitivity of SCCHN cells harbouring compromised *TP53* to IR. This study has also provided evidence that a radiosensitising effect of glycolysis inhibitors can be achieved in the presence of wild type p53 by inhibiting TIGAR.

From a therapeutic perspective, although the proposed combination of TIGAR inhibition and glycolysis inhibitors shows some promise, producing increased radiosensitivity in wild type *TP53* SCCHNs, and potentially expanding the therapeutic approach to these cells, there is an obvious risk that in so doing. This approach increases toxicity to normal cells, and thus loses the advantage predicted in mutant cells of an enhanced therapeutic index. It would be anticipated that this would particularly affect cells that have high proliferation rates, and therefore an in-depth study into the potential adverse effects of such combinations in normal cells and in preclinical models would be essential. Nevertheless, since the therapeutic benefits of this approach stem primarily from the fact that tumour cells, are characterized by rapid cellular proliferation and exhibit a higher influx of glucose may display a much greater response to this therapeutic approach compared to normal tissues.

4.4. The potential mechanism of the role of targeting glycolysis in radiosensetising SCCHNs

Although one of the fundamental goals of improving radiological cancer treatment is to increase tumour cell sensitivity to radiotherapy, and the fact that we understand much of how radiation interacts with cells, the mechanisms through which such sensitisation might be successfully accomplished are unclear. Cells exposed to IR dissipate energy through water radiolysis, resulting in the formation of (ROS)(440). ROS are also the natural by-products of mitochondrial respiration (265). ROS oxidise fatty acids, causing lipid peroxidation chain reactions, that alter the structure and function of the cell (441). One lipid peroxidation by-product is malondialdehyde which has been demonstrated to form direct DNA adducts of purine and pyrimidine bases, increasing the risk of mutations. Such increased DNA damage may also induce cell death when not repaired (441). Cancer cells appear to control the high levels of ROS by decreasing dependence on mitochondrial respiration and increasing glycolysis and perhaps by inducing the expression of enzymatic antioxidants, like superoxide dismutase and catalase, or by boosting the levels of non-enzymatic antioxidants, such as GSH or NADPH, as the latter is over-produced during typical carcinogenic metabolic reprogramming, mainly through activation of the PPP (440,442). A recent unpublished study in our laboratory found that the expression of two of the key PPP enzymes, G6PD and 6-PGD and the NADPH/NADP ratios were higher in mutant *TP53* SCCHN cells when compared to wild type p53 cells (312). Similarly, a published study by Mims et al, 2015 found that radioresistant SCCHN cells exhibit a marked increase in the expression of PPP enzymes and an increase in NADPH production, which was linked to the increased dependence of these cells on glycolysis (232). Given that the current study has demonstrated a significant increase in glycolysis in mutant p53 cells compared to wild type p53 cells, the correlation of this with an expected increase in PPP activity in mutant p53 cells may provide an additional explanation for the efficacy of glycolysis inhibitors in radiosensitising mutant p53 cells. Not only does inhibition of glycolysis deprive the mutant p53 cells of their dominant energy source, but it will also inhibit the PPP, resulting in restricting NADPH production and down-regulating the production of antioxidants and consequently increased ROS and oxidative stress. We also expect that the efficacy of inhibiting TIGAR in radiosensitising wild type p53 cells following treatment with glycolysis inhibitors is consistent with this idea. Given that wild type p53 cells are less dependent on glycolysis as an energy source compared to mutant p53 cells, this is likely to be part of the explanation for the relative resistance of these cells

to IR following glycolysis inhibition. Given that cells require PPP activity for DNA synthesis and antioxidant activity, inhibiting TIGAR drives the glycolytic pathway away from accumulating metabolites that can enter the PPP, increasing the exposure to ROS and oxidative stress. This also explains the increased radiosensitivity of wild type p53 cells following combined TIGAR and glycolytic inhibition.

Further evidence of the importance of the role of redox in determining cell fate in response to IR is derived from studies involving the antioxidant N-acetyl cysteine (NAC) in combination with a glycolytic inhibitor (241,245,246). Treatment with NAC results in a complete reversal of the effects of 2-DG on radiosensitivity, and was associated with lower cellular reducing potential (245), a decreased ratio of reduced glutathione/glutathione disulphide (241), and a marked increase in ROS levels (246).

In addition to the expected role of inhibiting PPP and antioxidant activity following treatment with glycolysis inhibitors, the significant energy required to activate repair pathways after treatment-induced DNA damage is another plausible explanation for the sensitivity of mutant p53 cells to glycolysis inhibitors, given that these cells are more dependent on glycolysis, which can only less efficiently generate the required energy.

4.5. Limitations

The results presented in this study and the proposed therapeutic approaches, have a number of limitations. As with most of the limited number of previous studies that have addressed metabolic reprogramming as a potential therapeutic target in SCCHN, the data presented are from *in vitro* cell culture studies, and have used solely homotypic, monolayer cell cultures of a panel of immortalised cell lines derived from a variety of SCCHN tumours. Whilst these represent the most extensively used model systems for SCCHN and have provided the foundation of much biological research, their clinical relevance has been called into question due to several factors (443). Among these is the resulting heterogeneity in tumours *in vivo* due to clonal evolution (444), as well as the difference in the reduced level of oxygen supply in the centre of a 3-dimensional solid tumour compared to those growing in a single layer in cell culture, and thus the subsequent stimulation adaptive responses such as HIF-1-induced glycolysis (445). In addition, the lack of cell-to-cell interactions typical of tumours *in vivo*, as well as the potentially complex interactions between the tumour and surrounding stroma on the

one hand, and the tumour and invoked immune responses on the other, are clearly factors that cannot be addressed through studies of simple monolayer cell cultures (284). Spheroids could be a useful model in this regard. This model has an outer layer of proliferating cells, an inner layer of quiescent cells and a core of necrotic cells, which mimics the growth pattern of solid tumours *in vivo*. The use of spheroids models has shown close similarity of genetic and molecular cytogenetic between *in vitro* and *in vivo* (26,284).

4.6. Future perspectives

Recently, the therapeutic use of different inhibitors of glycolysis in the treatment of cancer had received increased attention, with promising outcomes *in vitro* (241–246,354,360,446) and *in vivo* (242,248,431). Although clinical research on the therapeutic targeting of glycolysis is limited, some past results are promising (240,432,433), but it is clear that which inhibitor is used (for example 2-DG or DCA) makes a significant difference. In 1994, two clinical studies evaluated the role of metabolic targeting in SCCHN, and both were based on the oral administration of lonidamine, a hexokinase inhibitor (432,433). The first trial was a phase II randomised control trial that examined a combination of lonidamine and methotrexate in 89 patients with recurrent or metastatic SCCHN (433), while the second was a stage III, randomized, double-blind, placebo-controlled trial that examined a combination of lonidamine and IR in 96 patients with primary advanced SCCHN (432). The use of lonidamine improved clinical outcomes in both trials (432,433), with a substantial decrease in the rate of subsequent treatment failure following initial disease clearance, as well as enhanced locoregional control and disease-free survival at three and five years in the phase III study (432). Similar positive results were shown in smaller phase II trials in other cancers (447,448). However, two randomised phase III trials of lonidamine in combination with chemotherapy on 371 and 326 metastatic breast cancer patients respectively showed negative outcomes as no significant differences were observed in time to progression, response rate or overall survival as well as side effects (449,450). No further clinical trials were conducted using this glycolysis inhibitor after the last study in 2002. Phase I/II clinical trials using 2-DG in combination with RT in 20 patients of supratentorial glioma have demonstrated that this combination is well tolerated without any acute toxicity or late radiation damage to the normal brain tissue with a moderate increase in survival (451). Another phase I clinical trial used a combination of 2-DG and docetaxel in 34 patients with advanced solid

tumours to evaluate the safety, pharmacokinetics and maximum tolerated dose in this combination. Outcomes showed tolerable adverse effects with common hypoglycaemic symptoms (240). A phase I clinical trial in one stage IV patient with breast cancer and six previously treated stage IIIB/IV patients with NSCLC was conducted with oral administration of DCA. The study was terminated due to serious adverse events, including quick progression in the brain after eight weeks of stable disease in the only breast cancer patient, disease progression prior to the first scheduled scans in two NSCLC patients, sudden death of one patient within one week of DCA administration and a fatal pulmonary embolism was experienced by another patient (452). However, two phase I clinical trials in 15 patients with stage III – IV recurrent malignant brain tumours (453) and 24 patients with solid tumours (454) showed that chronic, oral administration of DCA is feasible and well-tolerated, with adverse events include fatigue, neuropathy and nausea. In 2010, a phase I clinical trial was started with a primary aim of determining the maximum tolerated dose of DCA in 17 patients with recurrent SCCHN who had failed first-line therapy. The results of this trial have yet to be published (455).

In general, it is well known that translating *in vivo* findings to clinical trials has limitations, as indicated by the lack of progress in clinical studies with metabolic inhibitors to date. Despite some promising results in clinical studies, further investigation is needed in glycolysis inhibitors dose tolerance, induced toxicity, and the degree of tumour radiosensitisation (456), particularly given the metabolic diversity found in different cancers, which results in varied responses to inhibition of glycolysis.

Given the importance of radiotherapy in treatment of SCCHN, it would be useful to study highly radio-resistant cells in a more relevant preclinical setting, specifically to assess the response to radiotherapy in oxygen levels similar to those found in the tumour environment, to improve the ability to predict the outcome of cancer patients undergoing RT. Because oxygen reacts with ROS radicals and protects against DNA damage, low levels of oxygen in tumours limit the effectiveness of RT and chemotherapy (457,458). Therefore, achieving oxygen levels in preclinical settings that are equivalent to those seen in the tumour environment could provide accurate predictive information about the outcomes of treatment in patients. One potentially useful preclinical system that could be used would be three-dimensional spheroidal cultures (459), since these can mimic the organisation of patient tumours more faithfully, with the outer layer typically exhibiting more highly proliferative cells, then

more quiescent cells as one moves away from the surface, and finally necrotic cells predominantly in the core (460,461). Despite the difficulty in establishing cell lines that can associate into spherical clusters (284), these systems, will undoubtedly be useful since they can provide information based on a more irregular tumour structure and behaviour due to differences in growth, distribution of nutrients and oxygen availability as occurs *in vivo* (460,461). Another useful system will be to use *in vivo* xenograft models, typically these have been based upon human cell lines xenografted into immunocompromised mice, in order to further test the proposed therapeutic approaches described in this thesis. A number of SCCHN cell lines have been successfully used to generate xenografts in athymic nude mice, and this model can be considered as one of the more appropriate and widely used in studies of SCCHN among the immunodeficient mouse models used in research (reviewed in (284)). Better still would be to use patient-derived mouse xenograft (PDX) models. These preclinical models allow for the examination of patient tumour tissue in an *in vivo* setting that more accurately recapitulates the heterogeneity and microenvironment of human tumours without dramatically affecting the cellular complexity, genomics and stromal structure of the tumours (462), and thus probably represents the most reliable and clinically relevant experimental platforms to predict the activity of anti-cancer agents on solid tumours (463–465).

Whilst the efficacy of the treatment clearly needs evaluating in a more relevant model system, one of the biggest challenges to the strategy being developed successfully is uncertainty about the therapeutic window in targeting the glucose pathway, due to the common characteristics of the metabolic phenotype of cancer cells that are found in normal, highly proliferating cells and other normal cells that depend primarily on glycolysis, such as red blood cells, neurons and activated lymphocytes. However, previously mentioned clinical studies do suggest that some of these obstacles might be managed.

Another possible challenge in studying the proposed therapeutic approaches in SCCHN cells expressing mutant p53 is intratumor genetic heterogeneity, which is caused by the persistent acquisition of mutations (466). Genetic heterogeneity in SCCHN is significantly associated with tumour progression and adverse treatment outcomes (467,468), with higher levels of heterogeneity being linked to worse clinical outcomes including therapeutic resistance (468–472). *TP53* mutations have been found to be remarkably prevalent and concordant in both initial and recurrent SCCHN tumours

(473). However, one of the great strengths of the proposed therapeutic approaches in this thesis is that the glycolytic phenotype, not the p53 mutation, is the treatment target. Given that the glycolytic phenotype is a (consequence) of p53 mutation, and the approach used is broadly not mutation-specific, the future selection of different or additional p53 mutations would not be expected to lead to resistance to such a therapeutic strategy.

Because it remains unclear how TIGAR is regulated differentially in the absence of functional p53, future work to investigate the mechanism of TIGAR regulation in the absence of p53 function in SCCHN should focus on studying the relationship of TIGAR to the genes that are likely to mediate this mechanism. One approach to investigating this would be to perform a broad functional genomic screen to identify genes that mediate or regulate TIGAR function in p53-null or mutant p53 SCCHN cells. One strategy would be to use RNAi or CRISPR/Cas9 libraries to enable the modulation of thousands of genes in a single experiment designed to identify genetic pathways that interact with a specific gene (reviewed in detail in reference (474).

Further work is clearly needed to investigate the mechanism underlying the effect of TIGAR inhibition in the increased radiosensitisation of wild type p53 cells following treatment with glycolysis inhibitors. For example, is this primarily attributable to increased dependence of these cells on glycolysis mediated by TIGAR inhibition and then deprivation of glycolysis using glycolysis inhibitors, or to inhibition of PPP, which results in decreased glutathione levels, increased ROS, and consequently increased cell sensitivity to radiation.

Since there is no known chemical inhibitor of TIGAR, there is growing interest in identifying such inhibitors, which appears likely to be fruitful. A recent study by Chandel et al (2021) used a library of 105 FDA approved anti-cancer compounds and a molecular docking approach screening to identify anti-cancer inhibitors against TIGAR. This study found that Trabectedin forms a very stable complex with TIGAR, suggesting this drug to might be a promising candidate as an anti-cancer agent that acts by binding to TIGAR (475). Another study by Boyya et al (2021) examined the ability of more than 67,000 natural products to compete with F2,6BP, the TIGAR substrate, for binding to the active site of TIGAR using docking point systems, with Trabectedin identified in Chandel et al study as a reference, and using the molecular mechanics/generalised Born surface area (MMGBSA) for molecular dynamics simulation studies. This study

identified 2-(2-(3,4-dihydroxy phenyl)-3,5-dihydroxy-8-(4-hydroxyphenyl)-4-oxo-4H-furo[2,3-h]chromen-9-yl) acetic acid (DDFA) as the lead compound in both docking and molecular dynamics studies with high structural stability achieved in TIGAR protein binding to this compound, which suggests DDFA might form the basis for TIGAR binding agents (476). In addition to docking and molecular dynamics studies, the use of the High Throughput Screening (HTS) techniques to explore pharmacological options potentially possessing inhibitory effects on TIGAR activity *in vitro* and *in vivo* could be utilised. This technology allows for rapidly performing millions of chemical, genetic or pharmacological tests, enabling the rapid identification of active compounds that alter a specific biomolecular pathway (477). Analysis of phosphatase activity of recombinant human TIGAR protein on a series of physiological phosphate ester substrates has already identified ed that an excellent substrate for TIGAR is 2,3-bisphosphoglycerate (23BPG), followed by 2-phosphoglycerate (2PG), 2-phosphoglycolate, and phosphoenolpyruvate (PEP) and thus targeting these substrates through a HTS strategy could be used to identify potential useful TIGAR inhibitors suitable for further testing *in vitro* and *in vivo* (262).

One interesting drug combination identified in this research combines 3PO with UK-5099 and showed promising outcomes in radiosensitising wild type p53 SCCHNs through inhibition of both mitochondrial and glycolytic functions. A number of studies, including one from our laboratory (312,478–480), have discussed the efficacy of targeting both glycolysis and mitochondrial respiration as a potential therapeutic strategy to enhance radiotherapy in SCCHN cells that maintain high rates of glycolytic activity and robust mitochondrial respiration, such as cells harbouring wild type *TP53*.

Although not a central focus of this work, one of the curious findings of the current study was the discovery that MDM2 expression indirectly enhances the negative regulatory role of p53 in suppressing glycolysis, independently of the well-established MDM2 direct regulatory role in p53 ubiquitination and degradation. Metabolic profiling results presented in this thesis (Figure 3.43. and 3.44.) showed that overexpression of MDM2 has no effect on the mitochondrial profile of SCCHN cells in the presence or absence of functional p53, whereas it results in inhibition of glycolytic function in cells expressing wild type p53 only. These results indicate that MDM2 exerts a p53-dependant inhibitory effect on glycolytic function with no similar effects on mitochondrial function. Given the negative regulatory role of MDM2 on p53 function (see section 1.2.4.) and since the metabolic profiling in this study has also shown low

glycolytic function in cells expressing functional p53, the results obtained from the glycolytic profiling of MDM2-overexpressed cells are counter-intuitive and unexpected. One possible explanation for these results is the role that MDM2 plays as a ubiquitin ligase for PGAM (336,345,346). PGAM controls an important step in the glycolysis pathway and is frequently overexpressed in cancer cells. A study by Mikawa et al found that MDM2 attenuates the Warburg effect by ubiquitinating and degrading PGAM in the presence of functional p53 (336). It is reasonable to think that negative regulation of PGAM activity by both p53 and MDM2 induces inhibition in glycolytic function in MDM2-overexpressed wild type p53 cells. Further investigation of this role of MDM2 in opposing the acquisition of the glycolytic phenotype in SCCHNs is needed as it is conceivable that this role and the well-studied regulatory relationship between MDM2 and PGAM may be a potential therapeutic target in SCCHN.

4.7. Conclusion

The major findings of the current study can be summarised in the following points:

- TP53 is a determinant of metabolic reprogramming in SCCHNs, and this role is a result of loss of wild type p53 function rather than any oncogenic GOF properties possessed by a specific TP53 mutation.
- The role of TIGAR in the metabolic regulation of SCCHNs is p53-dependant.
- Inhibiting glycolysis increase the sensitivity of SCCHN cells harbouring compromised TP53 to IR, and this radiosensitising effect of glycolysis inhibitors can be achieved in the presence of wild type p53 by inhibiting TIGAR.

In light of the results of metabolic profiling of SCCHN cells presented in this study, it is appealing to propose developing stratification and treatment approaches that would include *TP53* status as part of the treatment decisions for SCCHN patients. These decisions are currently based primarily on the TNM and UICC/AJCC staging systems incorporating clinical and radiological findings (481). These systems lack predictive value despite their consistency and ease of use (482). On the other hand, the identification of tumour factors, such as *TP53* status, that could more reliably predict which patients would benefit from a certain treatment might be envisaged as discussed here, and permit the successful development of more personalised therapies for SCCHN patients. A recent study by Kobayashi et al using formalin-fixed paraffin-embedded

samples showed that All-exon *TP53* sequencing and p53 protein phenotype analysis can accurately predict clinical outcomes of SCCHN (483). Thus, *TP53* status may provide an important prognostic marker for determining the therapeutic strategy of SCCHN patients. There are some major challenges ahead, to date, chronic lymphocytic leukaemia (CLL) remains the only cancer for which *TP53* status is used as a stratification for clinically available treatment strategies (484), despite considerable recent interest in the high predictive value of this type of dichotomisation of patients in a number of cancers (485–488). Hopefully, the strategies identified in this thesis, focusing on p53 status as a potential stratification tool, show sufficient promise to encourage future studies that will evaluate these in improved model systems and determine whether such approaches might be applied for the benefit of patients.

References

1. Mehanna H, Paleri V, West CML, Nutting C. Head and neck cancer - Part 1: Epidemiology, presentation, and prevention. BMJ. 2010;341(7774):663–6.
2. Sung H, Ferlay J, Siegel RL, Laversanne M, Soerjomataram I, Jemal A, et al. Global Cancer Statistics 2020: GLOBOCAN Estimates of Incidence and Mortality Worldwide for 36 Cancers in 185 Countries. CA Cancer J Clin. 2021 May 4;71(3):209–49.
3. Oral Cavity and Pharynx Cancer — Cancer Stat Facts. [cited 2022 Jan 21].
4. Capote-Moreno A, Brabyn P, Muñoz-Guerra MF, Sastre-Pérez J, Escorial-Hernandez V, Rodríguez-Campo FJ, et al. Oral squamous cell carcinoma: epidemiological study and risk factor assessment based on a 39-year series. Int J Oral Maxillofac Surg. 2020 Dec;49(12):1525–34.
5. Gatta G, Botta L, Sánchez MJ, Anderson LA, Pierannunzio D, Licitra L, et al. Prognoses and improvement for head and neck cancers diagnosed in Europe in early 2000s: The EUROCARE-5 population-based study. Eur J Cancer. 2015 Oct;51(15):2130–43.
6. Lawrence MS, Sougnez C, Lichtenstein L, Cibulskis K, Lander E, Gabriel SB, et al. Comprehensive genomic characterization of head and neck squamous cell carcinomas. Nature. 2015 Jan 29;517(7536):576–82.
7. Wilkie MD, Lau AS, Vlatkovic N, Jones TM, Boyd MT. Metabolic signature of squamous cell carcinoma of the head and neck: Consequences of TP53 mutation and therapeutic perspectives. Oral Oncol. 2018 Aug;83:1–10.
8. Argiris A, Karamouzis M V., Raben D, Ferris RL. Head and neck cancer. Vol. 371, The Lancet. Elsevier; 2008. p. 1695–709.
9. Argiris A, Eng C. Epidemiology, staging, and screening of head and neck cancer. Vol. 114, Cancer treatment and research. Springer, Boston, MA; 2003. p. 15–60.
10. Cardesa A, Slootweg PJ. Pathology of the head and neck. Pathology of the Head and Neck. 2006. 1–316 p.
11. Lo K-W, Chung GT-Y, To K-F. Deciphering the molecular genetic basis of NPC through molecular, cytogenetic, and epigenetic approaches. Semin Cancer Biol. 2012 Apr;22(2):79–86.
12. Chang ET, Adami H-O. The Enigmatic Epidemiology of Nasopharyngeal Carcinoma. Cancer Epidemiol Biomarkers Prev. 2006 Oct 1;15(10):1765–77.
13. Lee T-F, Liou M-H, Huang Y-J, Chao P-J, Ting H-M, Lee H-Y, et al. LASSO NTCP predictors for the incidence of xerostomia in patients with head and neck squamous cell carcinoma and nasopharyngeal carcinoma. Sci Rep. 2015 May 28;4(1):6217.
14. Blanchard P, Biau J, Huguet F, Racadot S, Berthold C, Wong-Hee-Kam S, et al. Radiotherapy for nasopharyngeal cancer. Cancer/Radiothérapie. 2021 Dec;
15. Cramer JD, Burtness B, Le QT, Ferris RL. The changing therapeutic landscape of head and neck cancer. Nat Rev Clin Oncol. 2019;16(11):669–83.
16. Bray F, Ferlay J, Soerjomataram I, Siegel RL, Torre LA, Jemal A. Global cancer statistics 2018: GLOBOCAN estimates of incidence and mortality worldwide for 36 cancers in 185 countries. CA Cancer J Clin. 2018;68(6):394–424.
17. Shibuya K, Mathers CD, Boschi-Pinto C, Lopez AD, Murray CJL. Global and regional estimates of cancer mortality and incidence by site: II. Results for the global burden of disease 2000. BMC Cancer. 2002;2:1–26.

18. Cancer Research UK. Head and neck cancers statistics. 2016.
19. Johnson NW, Gupta BH, Speicher DJ, Ray C, Shaikh MH, Al-Hebshi NE GP. Etiology and risk factors. In: Oral and Oropharyngeal Cancer. 2nd ed. 2018.
20. Dwivedi RC, Chisholm E KN. Epidemiology, aetiology and natural history of head and neck cancer. In: Staffieri A, Sebastian P KM, editor. Essentials of Head and Neck Cancer. 2012. p. 1–7.
21. Nocini R, Molteni G, Mattiuzzi C, Lippi G. Updates on larynx cancer epidemiology. Chinese J Cancer Res. 2020;32(1):18–25.
22. Landry D, Glastonbury CM. Squamous Cell Carcinoma of the Upper Aerodigestive Tract. A Review. Radiol Clin North Am. 2015;53(1):81–97.
23. Hashibe M, Brennan P, Benhamou S, Castellsague X, Chen C, Curado MP, et al. Alcohol drinking in never users of tobacco, cigarette smoking in never drinkers, and the risk of head and neck cancer: Pooled analysis in the international head and neck cancer epidemiology consortium. J Natl Cancer Inst. 2007;99(10):777–89.
24. Kreimer AR, Clifford GM, Boyle P, Franceschi S. Human papillomavirus types in head and neck squamous cell carcinomas worldwide: A systemic review. Cancer Epidemiol Biomarkers Prev. 2005 Feb 1;14(2):467–75.
25. Marur S, D'Souza G, Westra WH, Forastiere AA. HPV-associated head and neck cancer: a virus-related cancer epidemic. Lancet Oncol. 2010 Aug;11(8):781–9.
26. Sutherland RM. Cell and Environment Interactions in Tumor Microregions: The Multicell Spheroid Model. Science (80-). 1988 Apr 8;240(4849):177–84.
27. Ries LAG, Melbert D KM. SEER Cancer Statistics Review, 1975–2004. Bethesda, MD; 2006.
28. Grégoire V, Lefebvre J-L, Licitra L, Felip E. Squamous cell carcinoma of the head and neck: EHNS–ESMO–ESTRO Clinical Practice Guidelines for diagnosis, treatment and follow-up. Ann Oncol. 2010 May;21:v184–6.
29. Molinolo AA, Amornphimoltham P, Squarize CH, Castilho RM, Patel V, Gutkind JS. Dysregulated molecular networks in head and neck carcinogenesis. Oral Oncol. 2009;45(4–5):324–34.
30. Nagao T, Warnakulasuriya S. Envoi—An Appraisal of Targeted Therapies for Head and Neck Cancer. In: Squamous cell Carcinoma. Dordrecht: Springer Netherlands; 2017. p. 217–78.
31. Lechner M, Frampton GM, Fenton T, Feber A, Palmer G, Jay A, et al. Targeted next-generation sequencing of head and neck squamous cell carcinoma identifies novel genetic alterations in HPV+ and HPV- tumors. Genome Med. 2013;5(5):49.
32. Kim MM, Califano JA. Molecular pathology of head-and-neck cancer. Int J Cancer. 2004 Nov 20;112(4):545–53.
33. Niazi S, Purohit M, Niazi JH. Role of p53 circuitry in tumorigenesis: A brief review. Eur J Med Chem. 2018 Oct;158:7–24.
34. Erber R, Conradt C, Homann N, Enders C, Finckh M, Dietz A, et al. TP53 DNA contact mutations are selectively associated with allelic loss and have a strong clinical impact in head and neck cancer. Oncogene. 1998 Apr 23 [cited 2021 Apr 20];16(13):1671–9.
35. Giacinti C, Giordano A. RB and cell cycle progression. Oncogene. 2006 Aug 28;25(38):5220–7.
36. Pande P, Mathur M, Shukla NK, Ralhan R. pRB and p16 protein alterations in human oral tumorigenesis. Oral Oncol. 1998 Sep;34(5):396–403.
37. Ambrosch P, Schlott T, Hilmes D, Ruschenburg I. p16 Alterations and retinoblastoma protein expression in squamous cell carcinoma and neighboring dysplasia from the upper aerodigestive tract. Virchows Arch. 2001 Apr 30;438(4):343–9.

38. Squarize CH, Castilho RM, Sriuranpong V, Pinto DS, Gutkind JS. Molecular cross-talk between the NFκB and STAT3 signaling pathways in head and neck squamous cell carcinoma. Neoplasia. 2006;8(9):733–46.
39. Wieckowski E, Atarashi Y, Stanson J, Sato T-A, Whiteside TL. FAP-1-mediated activation of NF-κB induces resistance of head and neck cancer to fas-induced apoptosis. J Cell Biochem. 2007 Jan 1;100(1):16–28.
40. Freudlsperger C, Bian Y, Wise SC, Burnett J, Coupar J, Yang X, et al. TGF- b and NF- k B signal pathway cross-talk is mediated through TAK1 and SMAD7 in a subset of head and neck cancers. Oncogene. 2013;(April 2012):1549–59.
41. Tweardy DJ. Elevated Levels of Transforming Growth Factor a and Epidermal Growth Factor Receptor Messenger RNA Are Early Markers of Carcinogenesis in Head and Neck Cancer. Cancer Res. 1993;53(15):3579–84.
42. Lemmon MA, Schlessinger J. Cell Signaling by Receptor Tyrosine Kinases. Cell. 2010 Jun;141(7):1117–34.
43. Temam S, Kawaguchi H, El-Naggar AK, Jelinek J, Tang H, Liu DD, et al. Epidermal Growth Factor Receptor Copy Number Alterations Correlate With Poor Clinical Outcome in Patients With Head and Neck Squamous Cancer. J Clin Oncol . 2007 Jun 1;25(16):2164–70.
44. Iglesias-Bartolome R, Martin D, Silvio Gutkind J. Exploiting the head and neck cancer oncogenome: Widespread PI3K-mTOR pathway alterations and novel molecular targets. Cancer Discov. 2013;3(7):722–5.
45. Scully C, Field JK, Tanzawa H. Genetic aberrations in oral or head and neck squamous cell carcinoma (SCCHN): 1. Carcinogen metabolism, DNA repair and cell cycle control. Oral Oncol. 2000;36(3):256–63.
46. Olshan AF, Weissler MC, Pei H, Conway K, Anderson S, Fried DB, et al. Alterations of the p16 gene in head and neck cancer: frequency and association with p53, PRAD-1 and HPV. Oncogene . 1997 Feb 18;14(7):811–8.
47. Cairns P, Polascik TJ, Eby Y, Tokino K, Califano J, Merlo A, et al. Frequency of homozygous deletion at p16/CDKN2 in primary human tumours. Nat Genet . 1995 Oct;11(2):210–2.
48. Lydiatt WM, Murty VVVS, Davidson BJ, Xu L, Dyomina K, Sacks PG, et al. Homozygous Deletions and Loss of Expression of theCDKN2 gene occur frequently in head and neck squamous cell carcinoma cell lines but infrequently in primary tumors. Genes, Chromosom Cancer . 1995 Jun;13(2):94–8.
49. Mountzios G, Rampias T, Psyrri A. The mutational spectrum of squamous-cell carcinoma of the head and neck: targetable genetic events and clinical impact. Ann Oncol . 2014 Oct;25(10):1889–900.
50. Leeman RJ, Lui VWY, Grandis JR. STAT3 as a therapeutic target in head and neck cancer. Expert Opin Biol Ther . 2006 Mar 27;6(3):231–41.
51. Boguski MS, McCormick F. Proteins regulating Ras and its relatives. Nature . 1993 Dec;366(6456):643–54.
52. Barbacid M. ras Genes. Annu Rev Biochem . 1987 Jun;56(1):779–827.
53. Johnson DE, Burtness B, Leemans CR, Lui VWY, Bauman JE, Grandis JR. Head and neck squamous cell carcinoma. Nat Rev Dis Prim . 2020 Dec 26;6(1):92.
54. Field JK, Spandidos DA. The role of ras and myc oncogenes in human solid tumours and their relevance in diagnosis and prognosis (review). Anticancer Res . 10(1):1–22.
55. Lee JI, Soria JC, Hassan KA, El-Naggar AK, Tang X, Liu DD, et al. Loss of PTEN expression as a prognostic marker for tongue cancer. Arch Otolaryngol - Head Neck Surg. 2001;127(12):1441–5.

56. Massarelli E, Liu DD, Lee JJ, El-Naggar AK, Muzio L Lo, Staibano S, et al. Akt activation correlates with adverse outcome in tongue cancer. Cancer. 2005;104(11):2430–6.
57. Amornphimoltham P, Sriuranpong V, Patel V, Benavides F, Conti CJ, Sauk J, et al. Persistent activation of the Akt pathway in head and neck squamous cell carcinoma: A potential target for UCN-01. Clin Cancer Res. 2004;10(12 I):4029–37.
58. Nathan CAO, Amirghahari N, Abreo F, Rong X, Caldito G, Jones ML, et al. Overexpressed eIF4E is functionally active in surgical margins of head and neck cancer patients via activation of the Akt/mammalian target of rapamycin pathway. Clin Cancer Res. 2004;10(17):5820–7.
59. Nathan CAO, Amirghahri N, Rice C, Abreo FW, Shi R, Stucker FJ. Molecular analysis of surgical margins in head and neck squamous cell carcinoma patients. Laryngoscope. 2002;112(12):2129–40.
60. Patel SG, Shah JP. TNM Staging of Cancers of the Head and Neck: Striving for Uniformity Among Diversity. CA Cancer J Clin. 2005;55(4):242–58.
61. Takes RP, Rinaldo A, Silver CE, Haigentz M, Woolgar JA, Triantafyllou A, et al. Distant metastases from head and neck squamous cell carcinoma. Part I. Basic aspects. Oral Oncol . 2012;48(9):775–9.
62. Schmalbach CE, Miller FR. Occult primary head and neck carcinoma. Curr Oncol Rep. 2007;9(2):139–46.
63. Lajer CB, Buchwald C Von. The role of human papillomavirus in head and neck cancer. Apmis . 2010 Jun 15;118(6–7):510–9.
64. Delaney G, Jacob S, Barton M. Estimation of an optimal external beam radiotherapy utilization rate for head and neck carcinoma. Cancer. 2005;103(11):2216–27.
65. Chow LQM. Head and neck cancer. N Engl J Med. 2020;382(1):60–72.
66. Adelstein D, Gillison ML, Pfister DG, Spencer S, Adkins D, Brizel DM, et al. NCCN Guidelines Insights: Head and Neck Cancers, Version 2.2017. J Natl Compr Canc Netw. 2017;15(6):761–70.
67. Vitti ET, Parsons JL. The Radiobiological Effects of Proton Beam Therapy: Impact on DNA Damage and Repair. Cancers (Basel) . 2019 Jul 5;11(7):946.
68. Leeman JE, Romesser PB, Zhou Y, McBride S, Riaz N, Sherman E, et al. Proton therapy for head and neck cancer: expanding the therapeutic window. Lancet Oncol . 2017 May;18(5):e254–65.
69. Kim JK, Leeman JE, Riaz N, McBride S, Tsai CJ, Lee NY. Proton Therapy for Head and Neck Cancer. Curr Treat Options Oncol . 2018 Jun 9;19(6):28.
70. Brana I, Siu LL. Locally advanced head and neck squamous cell cancer : treatment choice based on risk factors and optimizing drug prescription. Educ B 37th ESMO Congr Vienna, Austria, 28 Sept – 2 Oct 2012 . 2012;23(Supplement 10):x178–85.
71. Braakhuis BJM, Brakenhoff RH, Leemans CR. Treatment choice for locally advanced head and neck cancers on the basis of risk factors : biological risk factors. Educ B 37th ESMO Congr Vienna, Austria, 28 Sept – 2 Oct 2012 . 2012;23(Supplement 10):x173–7.
72. Le Tourneau C, Siu LL. Molecular-targeted therapies in the treatment of squamous cell carcinomas of the head and neck. Curr Opin Oncol . 2008 May;20(3):256–63.
73. Levine AJ, Hu W, Feng Z. The P53 pathway: What questions remain to be explored? Cell Death Differ. 2006;13(6):1027–36.
74. Khan SA, Thomas HC, Toledano MB, Cox IJ, Taylor-Robinson SD. p53 mutations in human cholangiocarcinoma: a review. Liver Int . 2005 Aug;25(4):704–16.
75. Yao H, Feng Y, Zhou T, Wang J, Wang Z-X. NMR Studies of the Interaction between Human Programmed Cell Death 5 and Human p53. Biochemistry . 2012 Apr 3;51(13):2684–93.
76. Joerger AC, Fersht AR. Structural Biology of the Tumor Suppressor p53. Annu Rev Biochem . 2008

Jun;77(1):557–82.

77. Toledo F, Lee CJ, Krummel KA, Rodewald L-W, Liu C-W, Wahl GM. Mouse Mutants Reveal that Putative Protein Interaction Sites in the p53 Proline-Rich Domain Are Dispensable for Tumor Suppression. Mol Cell Biol. 2007;27(4):1425–32.
78. Jurneczko E, Cruickshank F, Porrini M, Clarke DJ, Campuzano IDG, Morris M, et al. Probing the Conformational Diversity of Cancer-Associated Mutations in p53 with Ion-Mobility Mass Spectrometry. Angew Chemie . 2013 Apr 15;125(16):4466–70.
79. Laptenko O, Prives C. Transcriptional regulation by p53: One protein, many possibilities. Cell Death Differ. 2006;13(6):951–61.
80. Poyurovsky M V, Katz C, Laptenko O, Beckerman R, Lokshin M, Ahn J, et al. The C terminus of p53 binds the N-terminal domain of MDM2. Nat Struct Mol Biol . 2010 Aug 18;17(8):982–9.
81. Aubrey BJ, Kelly GL, Janic A, Herold MJ, Strasser A. How does p53 induce apoptosis and how does this relate to p53-mediated tumour suppression? Cell Death Differ . 2018;25(1):104–13.
82. Lu X. p53: A heavily dictated dictator of life and death. Curr Opin Genet Dev. 2005;15(1):27–33.
83. Riley T, Sontag E, Chen P, Levine A. Transcriptional control of human p53-regulated genes. Nat Rev Mol Cell Biol. 2008;9(5):402–12.
84. Kruiswijk F, Labuschagne CF, Vousden KH. p53 in survival, death and metabolic health: a lifeguard with a licence to kill. Nat Rev Mol Cell Biol . 2015 Jul 23;16(7):393–405.
85. Ryan KM, Phillips AC, Vousden KH. Regulation and function of the p53 tumor suppressor protein. Curr Opin Cell Biol. 2001;13(3):332–7.
86. Vousden KH. Outcomes of p53 activation - Spoilt for choice. J Cell Sci. 2006;119(24):5015–20.
87. Collavin L, Lunardi A, Del Sal G. p53-family proteins and their regulators: hubs and spokes in tumor suppression. Cell Death Differ . 2010 Jun 9;17(6):901–11.
88. Maddocks ODK, Vousden KH. Metabolic regulation by p53. J Mol Med. 2011;89(3):237–45.
89. Lodish H, Berk A, Kaiser C, Krieger M, Bretscher A, Ploegh H, Amon A MK. Molecular Cell Biology. 8th ed. WH Freeman; 2016. 873–919 p.
90. Pines J, Hunter T. Cyclin-dependent kinases: a new cell cycle motif? Trends Cell Biol. 1991;1(5):117–21.
91. Cayrol C, Knibiehler M, Ducommun B. p21 binding to PCNA causes G1 and G2 cell cycle arrest in p53-deficient cells. Oncogene. 1998;16(3):311–20.
92. Zhan Q, Antinore MJ, Wang XW, Carrier F, Smith ML, Harris CC, et al. Association with Cdc2 and inhibition of Cdc2/Cyclin B1 kinase activity by the p53-regulated protein Gadd45. Oncogene. 1999;18(18):2892–900.
93. Ohki R, Nemoto J, Murasawa H, Oda E, Inazawa J, Tanaka N, et al. Reprimo, a New Candidate Mediator of the p53-mediated Cell Cycle Arrest at the G2 Phase. J Biol Chem . 2000 Jul;275(30):22627–30.
94. Elmore S. Apoptosis: A Review of Programmed Cell Death. Toxicol Pathol. 2007;35(4):495–516.
95. Hanahan D, Weinberg RA. Hallmarks of cancer: The next generation. Cell . 2011;144(5):646–74.
96. Ashkenazi A, Dixit VM. Death receptors: Signaling and modulation. Science (80-). 1998;281(5381):1305–8.
97. Haupt S, Berger M, Goldberg Z, Haupt Y. Apoptosis - The p53 network. J Cell Sci. 2003;116(20):4077–85.
98. Krepela. Granzyme B-induced apoptosis in cancer cells and its regulation (Review). Int J Oncol . 2010 Oct 22;37(6).
99. Vogelstein B, Lane D, Levine AJ. Surfing the p53 network. Nature. 2000;408(6810):307–10.

100. Vogt Sionov R, Haupt Y. The cellular response to p53: The decision between life and death. Oncogene. 1999;18(45):6145–57.
101. Brown JM, Attardi LD. The role of apoptosis in cancer development and treatment response. Nat Rev Cancer . 2005 Mar;5(3):231–7.
102. Yerlikaya A, Okur E, Ulukaya E. The p53-independent induction of apoptosis in breast cancer cells in response to proteasome inhibitor bortezomib. Tumor Biol. 2012;33(5):1385–92.
103. Maria Cuervo A. Autophagy: in sickness and in health. Trends Cell Biol . 2004 Feb;14(2):70–7.
104. Mathiassen SG, De Zio D, Cecconi F. Autophagy and the Cell Cycle: A Complex Landscape. Front Oncol . 2017 Mar 31;7.
105. Thorburn A. Apoptosis and autophagy: regulatory connections between two supposedly different processes. Apoptosis . 2008 Jan 8;13(1):1–9.
106. Maiuri MC, Galluzzi L, Morselli E, Kepp O, Malik SA, Kroemer G. Autophagy regulation by p53. Curr Opin Cell Biol . 2010 Apr;22(2):181–5.
107. Herranz N, Gil J. Mechanisms and functions of cellular senescence. J Clin Invest . 2018 Apr 2;128(4):1238–46.
108. Mijit M, Caracciolo V, Melillo A, Amicarelli F, Giordano A. Role of p53 in the Regulation of Cellular Senescence. Biomolecules . 2020 Mar 8;10(3):420.
109. Childs BG, Baker DJ, Kirkland JL, Campisi J, Deursen JM. Senescence and apoptosis: dueling or complementary cell fates? EMBO Rep . 2014 Nov 13;15(11):1139–53.
110. Valentine JM, Kumar S, Moumen A. A p53-independent role for the MDM2 antagonist Nutlin-3 in DNA damage response initiation. BMC Cancer . 2011 Dec 21;11(1):79.
111. Spallarossa P, Altieri P, Aloi C, Garibaldi S, Barisione C, Ghigliotti G, et al. Doxorubicin induces senescence or apoptosis in rat neonatal cardiomyocytes by regulating the expression levels of the telomere binding factors 1 and 2. Am J Physiol Circ Physiol . 2009 Dec;297(6):H2169–81.
112. Itahana K, Dimri G, Campisi J. Regulation of cellular senescence by p53. Eur J Biochem . 2001 May 15;268(10):2784–91.
113. Ventura A, Kirsch DG, McLaughlin ME, Tuveson DA, Grimm J, Lintault L, et al. Restoration of p53 function leads to tumour regression in vivo. Nature . 2007 Feb 24;445(7128):661–5.
114. Schuler M, Green DR. Transcription, apoptosis and p53: Catch-22. Trends Genet. 2005;21(3):182–7.
115. Wade M, Li Y-C, Wahl GM. MDM2, MDMX and p53 in oncogenesis and cancer therapy. Nat Rev Cancer . 2013 Feb 10;13(2):83–96.
116. Brooks CL, Gu W. p53 ubiquitination: Mdm2 and beyond. Mol Cell. 2006;21(3):307–15.
117. Meek DW. The p53 response to DNA damage. DNA Repair (Amst) . 2004 Aug;3(8–9):1049–56.
118. Mayo LD, Donner DB. The PTEN, Mdm2, p53 tumor suppressor–oncoprotein network. Trends Biochem Sci . 2002 Sep;27(9):462–7.
119. Teufel DP, Bycroft M, Fersht AR. Regulation by phosphorylation of the relative affinities of the N-terminal transactivation domains of p53 for p300 domains and Mdm2. Oncogene . 2009 May 13;28(20):2112–8.
120. Shieh S-Y, Ikeda M, Taya Y, Prives C. DNA Damage-Induced Phosphorylation of p53 Alleviates Inhibition by MDM2. Cell . 1997 Oct;91(3):325–34.
121. Kruse J-P, Gu W. Modes of p53 Regulation. Cell . 2009 May;137(4):609–22.
122. Appella E, Anderson CW. Post-translational modifications and activation of p53 by genotoxic stresses. Eur J Biochem . 2001 May 15;268(10):2764–72.
123. Wu Z, Earle J, Saito S, Anderson CW, Appella E, Xu Y. Mutation of Mouse p53 Ser23 and the Response

to DNA Damage. Mol Cell Biol . 2002 Apr 15;22(8):2441–9.

124. MacPherson D, Kim J, Kim T, Rhee BK, van Oostrom CTM, DiTullio RA, et al. Defective apoptosis and B-cell lymphomas in mice with p53 point mutation at Ser 23. EMBO J . 2004 Sep 15;23(18):3689–99.
125. Chao C, Herr D, Chun J, Xu Y. Ser18 and 23 phosphorylation is required for p53-dependent apoptosis and tumor suppression. EMBO J . 2006 Jun 1;
126. Sluss HK, Armata H, Gallant J, Jones SN. Phosphorylation of Serine 18 Regulates Distinct p53 Functions in Mice. Mol Cell Biol . 2004 Feb;24(3):976–84.
127. Chao C, Hergenhahn M, Kaeser MD, Wu Z, Saito S, Iggo R, et al. Cell Type- and Promoter-specific Roles of Ser18 Phosphorylation in Regulating p53 Responses. J Biol Chem . 2003 Oct;278(42):41028–33.
128. Blattner C, Tobiasch E, Litfen M, Rahmsdorf HJ, Herrlich P. DNA damage induced p53 stabilization: no indication for an involvement of p53 phosphorylation. Oncogene . 1999 Mar 15;18(9):1723–32.
129. Ashcroft M, Taya Y, Vousden KH. Stress Signals Utilize Multiple Pathways To Stabilize p53. Mol Cell Biol . 2000 May;20(9):3224–33.
130. Ashcroft M, Kubbutat MHG, Vousden KH. Regulation of p53 Function and Stability by Phosphorylation. Mol Cell Biol . 1999 Mar;19(3):1751–8.
131. Wang X, Taplick J, Geva N, Oren M. Inhibition of p53 degradation by Mdm2 acetylation. FEBS Lett . 2004 Mar 12;561(1–3):195–201.
132. Li M, Luo J, Brooks CL, Gu W. Acetylation of p53 Inhibits Its Ubiquitination by Mdm2. J Biol Chem . 2002 Dec;277(52):50607–11.
133. Ito A, Lai C-H, Zhao X, Saito S, Hamilton MH, Appella E, et al. p300/CBP-mediated p53 acetylation is commonly induced by p53-activating agents and inhibited by MDM2. EMBO J . 2001 Mar 15;20(6):1331–40.
134. Weber JD, Taylor LJ, Roussel MF, Sherr CJ, Bar-Sagi D. Nucleolar Arf sequesters Mdm2 and activates p53. Nat Cell Biol . 1999 May;1(1):20–6.
135. Sherr CJ. Divorcing ARF and p53: an unsettled case. Nat Rev Cancer . 2006 Sep 17;6(9):663–73.
136. Lowe SW, Sherr CJ. Tumor suppression by Ink4a–Arf: progress and puzzles. Curr Opin Genet Dev . 2003 Feb;13(1):77–83.
137. Llanos S, Clark PA, Rowe J, Peters G. Stabilization of p53 by p14ARF without relocation of MDM2 to the nucleolus. Nat Cell Biol . 2001 May 5;3(5):445–52.
138. Honda R, Yasuda H. Association of p19(ARF) with Mdm2 inhibits ubiquitin ligase activity of Mdm2 for tumor suppressor p53. EMBO J . 1999 Jan 4;18(1):22–7.
139. Itahana K, Mao H, Jin A, Itahana Y, Clegg H V., Lindström MS, et al. Targeted Inactivation of Mdm2 RING Finger E3 Ubiquitin Ligase Activity in the Mouse Reveals Mechanistic Insights into p53 Regulation. Cancer Cell . 2007 Oct;12(4):355–66.
140. Fang S, Jensen JP, Ludwig RL, Vousden KH, Weissman AM. Mdm2 Is a RING Finger-dependent Ubiquitin Protein Ligase for Itself and p53. J Biol Chem . 2000 Mar;275(12):8945–51.
141. Brooks CL, Li M, Hu M, Shi Y, Gu W. The p53–Mdm2–HAUSP complex is involved in p53 stabilization by HAUSP. Oncogene . 2007 Nov 21;26(51):7262–6.
142. Hu M, Gu L, Li M, Jeffrey PD, Gu W, Shi Y. Structural Basis of Competitive Recognition of p53 and MDM2 by HAUSP/USP7: Implications for the Regulation of the p53–MDM2 Pathway. Petsko G, editor. PLoS Biol . 2006 Jan 17;4(2):e27.
143. Tang J, Qu L-K, Zhang J, Wang W, Michaelson JS, Degenhardt YY, et al. Critical role for Daxx in regulating Mdm2. Nat Cell Biol . 2006 Aug 16;8(8):855–62.
144. Song MS, Song SJ, Kim SY, Oh HJ, Lim D-S. The tumour suppressor RASSF1A promotes MDM2 self-

ubiquitination by disrupting the MDM2–DAXX–HAUSP complex. EMBO J . 2008 Jul 9;27(13):1863–74.
145. Marine J-C, Lozano G. Mdm2-mediated ubiquitylation: p53 and beyond. Cell Death Differ . 2010 Jan 5;17(1):93–102.
146. Lahav G, Rosenfeld N, Sigal A, Geva-Zatorsky N, Levine AJ, Elowitz MB, et al. Dynamics of the p53-Mdm2 feedback loop in individual cells. Nat Genet . 2004 Feb 18;36(2):147–50.
147. Stad R, Little NA, Xirodimas DP, Frenk R, van der Eb AJ, Lane DP, et al. Mdmx stabilizes p53 and Mdm2 via two distinct mechanisms. EMBO Rep . 2001 Nov;2(11):1029–34.
148. Chène P. Inhibiting the p53-MDM2 interaction: An important target for cancer therapy. Nat Rev Cancer . 2003 Feb;3(2):102–9.
149. Vousden KH, Lu X. Live or let die: the cell's response to p53. Nat Rev Cancer . 2002 Aug;2(8):594–604.
150. Soussi T, Lozano G. p53 mutation heterogeneity in cancer. Biochem Biophys Res Commun . 2005 Jun;331(3):834–42.
151. Olivier M, Hollstein M, Hainaut P. TP53 Mutations in Human Cancers: Origins, Consequences, and Clinical Use. Cold Spring Harb Perspect Biol . 2010 Jan 1;2(1):a001008–a001008.
152. Petitjean A, Mathe E, Kato S, Ishioka C, Tavtigian S V., Hainaut P, et al. Impact of mutant p53 functional properties on TP53 mutation patterns and tumor phenotype: lessons from recent developments in the IARC TP53 database. Hum Mutat . 2007 Jun;28(6):622–9.
153. Goh AM, Coffill CR, Lane DP. The role of mutant p53 in human cancer. J Pathol . 2011 Jan;223(2):116–26.
154. Oren M, Rotter V. Mutant p53 Gain-of-Function in Cancer. Cold Spring Harb Perspect Biol . 2010 Feb 1;2(2):a001107–a001107.
155. Mantovani F, Collavin L, Del Sal G. Mutant p53 as a guardian of the cancer cell. Cell Death Differ . 2019 Feb 11;26(2):199–212.
156. Bergamaschi D, Gasco M, Hiller L, Sullivan A, Syed N, Trigiante G, et al. p53 polymorphism influences response in cancer chemotherapy via modulation of p73-dependent apoptosis. Cancer Cell . 2003 Apr;3(4):387–402.
157. Vikhanskaya F, Lee MK, Mazzoletti M, Broggini M, Sabapathy K. Cancer-derived p53 mutants suppress p53-target gene expression--potential mechanism for gain of function of mutant p53. Nucleic Acids Res . 2007 Mar 1;35(6):2093–104.
158. Lu Q, Tan Y-H, Luo R. Molecular Dynamics Simulations of p53 DNA-Binding Domain. J Phys Chem B . 2007 Oct;111(39):11538–45.
159. Bossi G, Lapi E, Strano S, Rinaldo C, Blandino G, Sacchi A. Mutant p53 gain of function: reduction of tumor malignancy of human cancer cell lines through abrogation of mutant p53 expression. Oncogene . 2006 Jan 19;25(2):304–9.
160. Pirollo KF, Bouker KB, Chang EH. Does p53 status influence tumor response to anticancer therapies? Anticancer Drugs . 2000 Jul;11(6):419–32.
161. Lowe S, Bodis S, McClatchey A, Remington L, Ruley H, Fisher D, et al. p53 status and the efficacy of cancer therapy in vivo. Science (80-) . 1994 Nov 4;266(5186):807–10.
162. O'Connor PM, Jackman J, Bae I, Myers TG, Fan S, Mutoh M, et al. Characterization of the p53 tumor suppressor pathway in cell lines of the National Cancer Institute anticancer drug screen and correlations with the growth-inhibitory potency of 123 anticancer agents. Cancer Res . 1997 Oct 1;57(19):4285–300.
163. Houldsworth J, Xiao H, Murty V, Chen W, Ray B, Reuter VE, et al. Human male germ cell tumor resistance to cisplatin is linked to TP53 gene mutation. Oncogene . 1998 May 26;16(18):2345–9.

164. Bunz F, Hwang PM, Torrance C, Waldman T, Zhang Y, Dillehay L, et al. Disruption of p53 in human cancer cells alters the responses to therapeutic agents. J Clin Invest . 1999 Aug;104(3):263–9.
165. Fan S, Smith ML, Rivet DJ, Duba D, Zhan Q, Kohn KW, et al. Disruption of p53 function sensitizes breast cancer MCF-7 cells to cisplatin and pentoxifylline. Cancer Res . 1995 Apr 15;55(8):1649–54.
166. van der Zee AG, Hollema H, Suurmeijer AJ, Krans M, Sluiter WJ, Willemse PH, et al. Value of P-glycoprotein, glutathione S-transferase pi, c-erbB-2, and p53 as prognostic factors in ovarian carcinomas. J Clin Oncol . 1995 Jan;13(1):70–8.
167. Righetti SC, Della Torre G, Pilotti S, Ménard S, Ottone F, Colnaghi MI, et al. A comparative study of p53 gene mutations, protein accumulation, and response to cisplatin-based chemotherapy in advanced ovarian carcinoma. Cancer Res . 1996 Feb 15;56(4):689–93.
168. Bristow RG, Benchimol S, Hill RP. The p53 gene as a modifier of intrinsic radiosensitivity: implications for radiotherapy. Radiother Oncol . 1996 Sep;40(3):197–223.
169. Lowe SW, Bodis S, Mcclatchey A, Remington L, Ruley HE, Fisher DE, et al. p53 status and the efficacy of cancer therapy in vivo. Science (80-) . 1994 Nov 4;266(5186):807–10.
170. Lee JM, Bernstein A. p53 Mutations increase resistance to ionizing radiation. Proc Natl Acad Sci U S A . 1993 Jun 15;90(12):5742–6.
171. Koch WM, Brennan JA, Zahurak M, Goodman SN, Westra WH, Schwab D, et al. p53 Mutation and Locoregional Treatment Failure in Head and Neck Squamous Cell Carcinoma. JNCI J Natl Cancer Inst . 1996 Nov 6;88(21):1580–6.
172. Hamada M, Fujiwara T, Hizuta A, Gochi A, Naomoto Y, Takakura N, et al. Thep53 gene is a potent determinant of chemosensitivity and radiosensitivity in gastric and colorectal cancers. J Cancer Res Clin Oncol . 1996 Jun;122(6):360–5.
173. Bergh J, Norberg T, Sjögren S, Lindgren A, Holmberg L. Complete sequencing of the p53 gene provides prognostic information in breast cancer patients, particularly in relation to adjuvant systemic therapy and radiotherapy. Nat Med . 1995 Oct;1(10):1029–34.
174. Poeta ML, Manola J, Goldwasser MA, Forastiere A, Benoit N, Califano JA, et al. TP53 Mutations and Survival in Squamous-Cell Carcinoma of the Head and Neck. N Engl J Med . 2007 Dec 20;357(25):2552–61.
175. Alsner J, Sørensen SB, Overgaard J. TP53 mutation is related to poor prognosis after radiotherapy, but not surgery, in squamous cell carcinoma of the head and neck. Radiother Oncol . 2001 May;59(2):179–85.
176. Temam S, Flahault A, Périé S, Monceaux G, Coulet F, Callard P, et al. p53 Gene Status as a Predictor of Tumor Response to Induction Chemotherapy of Patients With Locoregionally Advanced Squamous Cell Carcinomas of the Head and Neck. J Clin Oncol . 2000 Jan 1;18(2):385–385.
177. Gomes AS, Ramos H, Soares J, Saraiva L. p53 and glucose metabolism: an orchestra to be directed in cancer therapy. Pharmacol Res . 2018 May;131:75–86.
178. Annibaldi A, Widmann C. Glucose metabolism in cancer cells. Curr Opin Clin Nutr Metab Care . 2010 Jul;13(4):466–70.
179. Vander Heiden MG, DeBerardinis RJ. Understanding the Intersections between Metabolism and Cancer Biology. Cell . 2017 Feb;168(4):657–69.
180. Shaw RJ. Glucose metabolism and cancer. Curr Opin Cell Biol . 2006 Dec;18(6):598–608.
181. Warburg O. On the Origin of Cancer Cells. Science (80-) . 1956 Feb 24;123(3191):309–14.
182. Lu J, Tan M, Cai Q. The Warburg effect in tumor progression: Mitochondrial oxidative metabolism as an anti-metastasis mechanism. Cancer Lett . 2015 Jan;356(2):156–64.

183. Hsu PP, Sabatini DM. Cancer Cell Metabolism: Warburg and Beyond. Cell . 2008 Sep;134(5):703–7.
184. Levine AJ, Puzio-Kuter AM. The Control of the Metabolic Switch in Cancers by Oncogenes and Tumor Suppressor Genes. Science (80-) . 2010 Dec 3;330(6009):1340–4.
185. Hanahan D, Weinberg RA. The Hallmarks of Cancer. Cell . 2000 Jan;100(1):57–70.
186. Yuneva MO, Fan TWM, Allen TD, Higashi RM, Ferraris D V., Tsukamoto T, et al. The Metabolic Profile of Tumors Depends on Both the Responsible Genetic Lesion and Tissue Type. Cell Metab . 2012 Feb;15(2):157–70.
187. Bensinger SJ, Christofk HR. New aspects of the Warburg effect in cancer cell biology. Vol. 23, Seminars in Cell and Developmental Biology. Elsevier Ltd; 2012. p. 352–61.
188. Koppenol WH, Bounds PL, Dang C V. Otto Warburg's contributions to current concepts of cancer metabolism . Vol. 11, Nature Reviews Cancer. Nature Publishing Group; 2011 [cited 2021 Mar 27]. p. 325–37.
189. Frezza C, Gottlieb E. Mitochondria in cancer: Not just innocent bystanders. Semin Cancer Biol . 2009 Feb;19(1):4–11.
190. Cairns RA, Harris IS, Mak TW. Regulation of cancer cell metabolism. Nat Rev Cancer . 2011 Feb 24 [cited 2021 Mar 27];11(2):85–95.
191. Pollard PJ, Brière JJ, Alam NA, Barwell J, Barclay E, Wortham NC, et al. Accumulation of Krebs cycle intermediates and over-expression of HIF1α in tumours which result from germline FH and SDH mutations. Hum Mol Genet . 2005 Aug 1;14(15):2231–9.
192. Papandreou I, Cairns RA, Fontana L, Lim AL, Denko NC. HIF-1 mediates adaptation to hypoxia by actively downregulating mitochondrial oxygen consumption. Cell Metab . 2006 Mar;3(3):187–97.
193. Stine ZE, Walton ZE, Altman BJ, Hsieh AL, Dang C V. MYC, Metabolism, and Cancer. Cancer Discov . 2015 Oct;5(10):1024–39.
194. Liu J, Zhang C, Hu W, Feng Z. Tumor suppressor p53 and its mutants in cancer metabolism. Cancer Lett . 2015 Jan;356(2):197–203.
195. Simabuco FM, Morale MG, Pavan ICB, Morelli AP, Silva FR, Tamura RE. p53 and metabolism: from mechanism to therapeutics. Oncotarget . 2018 May 4;9(34):23780–823.
196. Berkers CR, Maddocks ODK, Cheung EC, Mor I, Vousden KH. Metabolic Regulation by p53 Family Members. Cell Metab . 2013 Nov;18(5):617–33.
197. Kitamura N, Nakamura Y, Miyamoto Y, Miyamoto T, Kabu K, Yoshida M, et al. Mieap, a p53-Inducible Protein, Controls Mitochondrial Quality by Repairing or Eliminating Unhealthy Mitochondria. Santos J, editor. PLoS One . 2011 Jan 17;6(1):e16060.
198. Lozano G, Elledge SJ. p53 sends nucleotides to repair DNA. Nature . 2000 Mar;404(6773):24–5.
199. Kawauchi K, Araki K, Tobiume K, Tanaka N. p53 regulates glucose metabolism through an IKK-NF-κB pathway and inhibits cell transformation. Nat Cell Biol . 2008 May 6;10(5):611–8.
200. Puzio-Kuter AM. The Role of p53 in Metabolic Regulation. Genes Cancer . 2011 Apr 1;2(4):385–91.
201. Choy M-K, Movassagh M, Bennett MR, Foo RS-Y. PKB/Akt activation inhibits p53-mediated HIF1A degradation that is independent of MDM2. J Cell Physiol . 2009;n/a-n/a.
202. Feng Z, Levine AJ. The regulation of energy metabolism and the IGF-1/mTOR pathways by the p53 protein. Trends Cell Biol . 2010 Jul;20(7):427–34.
203. Faubert B, Boily G, Izreig S, Griss T, Samborska B, Dong Z, et al. AMPK Is a Negative Regulator of the Warburg Effect and Suppresses Tumor Growth In Vivo. Cell Metab . 2013 Jan;17(1):113–24.
204. Corcoran CA, Huang Y, Sheikh MS. The regulation of energy generating metabolic pathways by p53. Cancer Biol Ther . 2006 Dec 31;5(12):1610–3.

205. Kondoh H, Lleonart ME, Gil J, Wang J, Degan P, Peters G, et al. Glycolytic enzymes can modulate cellular life span. Cancer Res . 2005 Jan 1;65(1):177–85.
206. Ruiz-Lozano P, Hixon ML, Wagner MW, Flores AI, Ikawa S, Baldwin AS, et al. p53 is a transcriptional activator of the muscle-specific phosphoglycerate mutase gene and contributes in vivo to the control of its cardiac expression. Cell Growth Differ . 1999 May;10(5):295–306.
207. Vlatkovic N, Crawford K, P. Rubbi C, T. Boyd M. Tissue-Specific Therapeutic Targeting of p53 in Cancer: One Size Does Not Fit All. Curr Pharm Des . 2011 Feb 1;17(6):618–30.
208. Zhang C, Liu J, Xu D, Zhang T, Hu W, Feng Z. Gain-of-function mutant p53 in cancer progression and therapy. Lu H, editor. J Mol Cell Biol . 2020 Sep 1;12(9):674–87.
209. Freed-Pastor WA, Mizuno H, Zhao X, Langerød A, Moon S-H, Rodriguez-Barrueco R, et al. Mutant p53 Disrupts Mammary Tissue Architecture via the Mevalonate Pathway. Cell . 2012 Jan;148(1–2):244–58.
210. Zhang C, Liu J, Liang Y, Wu R, Zhao Y, Hong X, et al. Tumour-associated mutant p53 drives the Warburg effect. Nat Commun . 2013 Dec 17;4(1):2935.
211. Goel A, Mathupala SP, Pedersen PL. Glucose Metabolism in Cancer. J Biol Chem . 2003 Apr;278(17):15333–40.
212. Chavez-Perez VA, Strasberg–Rieber M, Rieber M. Metabolic utilization of exogenous pyruvate by mutant p53 (R175H) human melanoma cells promotes survival under glucose depletion. Cancer Biol Ther . 2011 Oct 27;12(7):647–56.
213. Zhou G, Wang J, Zhao M, Xie T-X, Tanaka N, Sano D, et al. Gain-of-Function Mutant p53 Promotes Cell Growth and Cancer Cell Metabolism via Inhibition of AMPK Activation. Mol Cell . 2014 Jun;54(6):960–74.
214. Mendoza-Juez B, Martínez-González A, Calvo GF, Pérez-García VM. A Mathematical Model for the Glucose-Lactate Metabolism of in Vitro Cancer Cells. Bull Math Biol . 2012 May 22;74(5):1125–42.
215. Jitschin R, Hofmann AD, Bruns H, Gießl A, Bricks J, Berger J, et al. Mitochondrial metabolism contributes to oxidative stress and reveals therapeutic targets in chronic lymphocytic leukemia. Blood . 2014 Apr 24;123(17):2663–72.
216. Bonuccelli G, Tsirigos A, Whitaker-Menezes D, Pavlides S, Pestell RG, Chiavarina B, et al. Ketones and lactate "fuel" tumor growth and metastasis. Cell Cycle . 2010 Sep 5;9(17):3506–14.
217. DeBerardinis RJ, Mancuso A, Daikhin E, Nissim I, Yudkoff M, Wehrli S, et al. Beyond aerobic glycolysis: Transformed cells can engage in glutamine metabolism that exceeds the requirement for protein and nucleotide synthesis. Proc Natl Acad Sci . 2007 Dec 4;104(49):19345–50.
218. Reitzer LJ, Wice BM, Kennell D. Evidence that glutamine, not sugar, is the major energy source for cultured HeLa cells. J Biol Chem . 1979 Apr;254(8):2669–76.
219. Twum-Ampofo J, Fu D-X, Passaniti A, Hussain A, Siddiqui MM. Metabolic targets for potential prostate cancer therapeutics. Curr Opin Oncol . 2016 May;28(3):241–7.
220. Spieth ME, Kasner DL. A tabulated summary of the FDG PET literature. J Nucl Med . 2002 Mar;43(3):441.
221. Starska K, Forma E, Jóźwiak P, Bryś M, Lewy-Trenda I, Brzezińska-Błaszczyk E, et al. Gene and protein expression of glucose transporter 1 and glucose transporter 3 in human laryngeal cancer—the relationship with regulatory hypoxia-inducible factor-1α expression, tumor invasiveness, and patient prognosis. Tumor Biol . 2015 Apr 21;36(4):2309–21.
222. Chandan VS, Faquin WC, Wilbur DC, Khurana KK. The utility of GLUT-1 immunolocalization in cell blocks. Cancer . 2006 Jan 24;108(2):124–8.

223. Reisser C, Eichhorn K, Herold-Mende C, Born AI, Bannasch P. Expression of facilitative glucose transport proteins during development of squamous cell carcinomas of the head and neck. Int J Cancer . 1999 Jan 18;80(2):194–8.
224. Ayala FRR, Rocha RM, Carvalho KC, Carvalho AL, Da Cunha IW, Lourenço SV, et al. Glut1 and Glut3 as Potential Prognostic Markers for Oral Squamous Cell Carcinoma. Molecules . 2010 Apr 1;15(4):2374–87.
225. Wigfield SM, Winter SC, Giatromanolaki A, Taylor J, Koukourakis ML, Harris AL. PDK-1 regulates lactate production in hypoxia and is associated with poor prognosis in head and neck squamous cancer. Br J Cancer . 2008 Jun 10;98(12):1975–84.
226. McFate T, Mohyeldin A, Lu H, Thakar J, Henriques J, Halim ND, et al. Pyruvate Dehydrogenase Complex Activity Controls Metabolic and Malignant Phenotype in Cancer Cells. J Biol Chem . 2008 Aug;283(33):22700–8.
227. Brizel DM, Schroeder T, Scher RL, Walenta S, Clough RW, Dewhirst MW, et al. Elevated tumor lactate concentrations predict for an increased risk of metastases in head-and-neck cancer. Int J Radiat Oncol . 2001 Oct;51(2):349–53.
228. Blatt S, Voelxen N, Sagheb K, Pabst AM, Walenta S, Schroeder T, et al. Lactate as a predictive marker for tumor recurrence in patients with head and neck squamous cell carcinoma (HNSCC) post radiation: a prospective study over 15 years. Clin Oral Investig . 2016 Nov 4;20(8):2097–104.
229. Quennet V, Yaromina A, Zips D, Rosner A, Walenta S, Baumann M, et al. Tumor lactate content predicts for response to fractionated irradiation of human squamous cell carcinomas in nude mice. Radiother Oncol . 2006 Nov;81(2):130–5.
230. Sattler UGA, Meyer SS, Quennet V, Hoerner C, Knoerzer H, Fabian C, et al. Glycolytic metabolism and tumour response to fractionated irradiation. Radiother Oncol . 2010 Jan;94(1):102–9.
231. Tripathi P, Kamarajan P, Somashekar BS, MacKinnon N, Chinnaiyan AM, Kapila YL, et al. Delineating metabolic signatures of head and neck squamous cell carcinoma: Phospholipase A2, a potential therapeutic target. Int J Biochem Cell Biol . 2012 Nov;44(11):1852–61.
232. Mims J, Bansal N, Bharadwaj MS, Chen X, Molina AJ, Tsang AW, et al. Energy Metabolism in a Matched Model of Radiation Resistance for Head and Neck Squamous Cell Cancer. Radiat Res . 2015 Mar;183(3):291–304.
233. Bonnet SS, Archer SL, Allalunis-Turner J, Haromy A, Beaulieu C, Thompson R, et al. A Mitochondria-K+ Channel Axis Is Suppressed in Cancer and Its Normalization Promotes Apoptosis and Inhibits Cancer Growth. Cancer Cell . 2007 Jan;11(1):37–51.
234. Fox CJ, Hammerman PS, Thompson CB. Fuel feeds function: energy metabolism and the T-cell response. Nat Rev Immunol . 2005 Nov 20;5(11):844–52.
235. Luengo A, Gui DY, Vander Heiden MG. Targeting Metabolism for Cancer Therapy. Cell Chem Biol . 2017 Sep;24(9):1161–80.
236. Madhok BM, Yeluri S, Perry SL, Hughes TA, Jayne DG. Targeting Glucose Metabolism. Am J Clin Oncol . 2011 Dec;34(6):628–35.
237. Zhang D, Li J, Wang F, Hu J, Wang S, Sun Y. 2-Deoxy-D-glucose targeting of glucose metabolism in cancer cells as a potential therapy. Cancer Lett . 2014 Dec;355(2):176–83.
238. Landau BR, Laszlo J, Stengle J, Burk D. Certain metabolic and pharmacologic effects in cancer patients given infusions of 2-deoxy-d-glucose. J Natl Cancer Inst . 1958 Sep;21(3):485–94.
239. Stein M, Lin H, Jeyamohan C, Dvorzhinski D, Gounder M, Bray K, et al. Targeting tumor metabolism with 2-deoxyglucose in patients with castrate-resistant prostate cancer and advanced malignancies.

Prostate . 2010 Sep 15;70(13):1388–94.

240. Raez LE, Papadopoulos K, Ricart AD, Chiorean EG, DiPaola RS, Stein MN, et al. A phase I dose-escalation trial of 2-deoxy-d-glucose alone or combined with docetaxel in patients with advanced solid tumors. Cancer Chemother Pharmacol . 2013 Feb 11;71(2):523–30.
241. Simons AL, Ahmad IM, Mattson DM, Dornfeld KJ, Spitz DR. 2-Deoxy-d-Glucose Combined with Cisplatin Enhances Cytotoxicity via Metabolic Oxidative Stress in Human Head and Neck Cancer Cells. Cancer Res . 2007 Apr 1;67(7):3364–70.
242. Simons AL, Fath MA, Mattson DM, Smith BJ, Walsh SA, Graham MM, et al. Enhanced Response of Human Head and Neck Cancer Xenograft Tumors to Cisplatin Combined With 2-Deoxy-d-Glucose Correlates With Increased 18F-FDG Uptake as Determined by PET Imaging. Int J Radiat Oncol . 2007 Nov;69(4):1222–30.
243. Dwarakanath B, Vibhuti A, Muralidhar K. Differential cytotoxicity of the glycolytic inhibitor 2-deoxy-D-glucose in isogenic cell lines varying in their p53 status. J Cancer Res Ther . 2013;9(4):686.
244. ZHANG XD, DESLANDES E, VILLEDIEU M, POULAIN L, DUVAL M, GAUDUCHON P, et al. Effect of 2-Deoxy-D-glucose on Various Malignant Cell Lines In Vitro. Anticancer Res. 2006;26(5A).
245. Sandulache VC, Ow TJ, Pickering CR, Frederick MJ, Zhou G, Fokt I, et al. Glucose, not glutamine, is the dominant energy source required for proliferation and survival of head and neck squamous carcinoma cells. Cancer . 2011 Jul 1;117(13):2926–38.
246. Sandulache VC, Skinner HD, Ow TJ, Zhang A, Xia X, Luchak JM, et al. Individualizing antimetabolic treatment strategies for head and neck squamous cell carcinoma based on TP53 mutational status. Cancer . 2012 Feb 1;118(3):711–21.
247. Yi M, Ban Y, Tan Y, Xiong W, Li G, Xiang B. 6-Phosphofructo-2-kinase/fructose-2,6-biphosphatase 3 and 4: A pair of valves for fine-tuning of glucose metabolism in human cancer. Mol Metab . 2019 Feb;20:1–13.
248. Clem B, Telang S, Clem A, Yalcin A, Meier J, Simmons A, et al. Small-molecule inhibition of 6-phosphofructo-2-kinase activity suppresses glycolytic flux and tumor growth. Mol Cancer Ther . 2008 Jan;7(1):110–20.
249. Kumar D. Regulation of glycolysis in head and neck squamous cell carcinoma. Postdoc J a J Postdr Res Postdr Aff . 2017 Jan 20 [cited 2021 Sep 7];5(1):14.
250. Botha H, Farah CS, Koo K, Cirillo N, McCullough M, Paolini R, et al. The Role of Glucose Transporters in Oral Squamous Cell Carcinoma. Biomolecules . 2021 Jul 21;11(8):1070.
251. Hitosugi T, Zhou L, Elf S, Fan J, Kang H-B, Seo JH, et al. Phosphoglycerate Mutase 1 Coordinates Glycolysis and Biosynthesis to Promote Tumor Growth. Cancer Cell . 2012 Nov;22(5):585–600.
252. Tang Y-C, Hsiao J-R, Jiang S-S, Chang J-Y, Chu P-Y, Liu K-J, et al. c-MYC-directed NRF2 drives malignant progression of head and neck cancer via glucose-6-phosphate dehydrogenase and transketolase activation. Theranostics . 2021;11(11):5232–47.
253. Fleming JC, Woo J, Moutasim K, Mellone M, Frampton SJ, Mead A, et al. HPV, tumour metabolism and novel target identification in head and neck squamous cell carcinoma. Br J Cancer . 2019 Feb 17;120(3):356–67.
254. Wong JYY, Huggins GS, Debidda M, Munshi NC, De Vivo I. Dichloroacetate induces apoptosis in endometrial cancer cells. Gynecol Oncol . 2008 Jun;109(3):394–402.
255. Vizán P, Alcarraz-Vizán G, Díaz-Moralli S, Solovjeva ON, Frederiks WM, Cascante M. Modulation of pentose phosphate pathway during cell cycle progression in human colon adenocarcinoma cell line HT29. Int J Cancer . 2009 Jun 15;124(12):2789–96.

256. Chen H, Yue J-X, Yang S-H, Ding H, Zhao R-W, Zhang S. Overexpression of transketolase-like gene 1 is associated with cell proliferation in uterine cervix cancer. J Exp Clin Cancer Res . 2009;28(1):43.
257. Varshney R, Dwarakanath B, Jain V. Radiosensitization by 6-aminonicotinamide and 2-deoxy-D-glucose in human cancer cells. Int J Radiat Biol . 2005 May 3;81(5):397–408.
258. Budihardjo II, Walker DL, Svingen PA, Buckwalter CA, Desnoyers S, Eckdahl S, et al. 6-Aminonicotinamide sensitizes human tumor cell lines to cisplatin. Clin Cancer Res . 1998 Jan;4(1):117–30.
259. Bensaad K, Tsuruta A, Selak MA, Vidal MNC, Nakano K, Bartrons R, et al. TIGAR, a p53-Inducible Regulator of Glycolysis and Apoptosis. Cell . 2006 Jul;126(1):107–20.
260. Jen KY, Cheung VG. Identification of novel p53 target genes in ionizing radiation response. Cancer Res. 2005;65(17):7666–73.
261. Rigden DJ. The histidine phosphatase superfamily: Structure and function. Biochem J. 2008;409(2):333–48.
262. Gerin I, Noël G, Bolsée J, Haumont O, Van Schaftingen E, Bommer GT. Identification of TP53-induced glycolysis and apoptosis regulator (TIGAR) as the phosphoglycolate-independent 2,3-bisphosphoglycerate phosphatase. Biochem J. 2014;458(3):439–48.
263. Bazan JF, Fletterick RJ, Pilkis SJ. Evolution of a bifunctional enzyme: 6-phosphofructo-2-kinase/fructose-2,6-bisphosphatase. Proc Natl Acad Sci . 1989 Dec 1;86(24):9642–6.
264. Lin K, Li L, Correia JJ, Pilkis SJ. Glu327 is part of a catalytic triad in rat liver fructose-2,6-bisphosphatase. J Biol Chem. 1992;267(10):6556–62.
265. Geng J, Yuan X, Wei M, Wu J, Qin Z-HH. The diverse role of TIGAR in cellular homeostasis and cancer. Free Radic Res . 2018 Dec 2;52(11–12):1240–9.
266. Okar DA, Lange AJ, Manzano À, Navarro-Sabatè A, Riera L, Bartrons R. PFK-2/FBPase-2: Maker and breaker of the essential biofactor fructose-2,6-bisphosphate. Trends Biochem Sci. 2001;26(1):30–5.
267. Sablina AA, Budanov A V, Ilyinskaya G V, Agapova LS, Kravchenko JE, Chumakov PM. The antioxidant function of the p53 tumor suppressor. Nat Med . 2005 Dec 13;11(12):1306–13.
268. Zhang YM, Liu JK, Wong TY. The DNA excision repair system of the highly radioresistant bacterium Deinococcus radiodurans is facilitated by the pentose phosphate pathway. Mol Microbiol. 2003;48(5):1317–23.
269. Bensaad K, Cheung EC, Vousden KH. Modulation of intracellular ROS levels by TIGAR controls autophagy. EMBO J . 2009 Oct 7;28(19):3015–26.
270. Cheung EC, Ludwig RL, Vousden KH. Mitochondrial localization of TIGAR under hypoxia stimulates HK2 and lowers ROS and cell death. Proc Natl Acad Sci . 2012 Dec 11;109(50):20491–6.
271. Tang J, Chen L, Qin Z, Sheng R. Structure, regulation, and biological functions of TIGAR and its role in diseases. Acta Pharmacol Sin . 2021 Jan 28;
272. Madan E, Gogna R, Kuppusamy P, Bhatt M, Pati U, Mahdi AA. TIGAR induces p53-mediated cell-cycle arrest by regulation of RB–E2F1 complex. Br J Cancer . 2012 Jul 10;107(3):516–26.
273. Cheung EC, Ludwig RL, Vousden KH. Mitochondrial localization of TIGAR under hypoxia stimulates HK2 and lowers ROS and cell death. Proc Natl Acad Sci . 2012 Dec 11;109(50):20491–6.
274. Patra KC, Hay N. The pentose phosphate pathway and cancer. Trends Biochem Sci . 2014 Aug;39(8):347–54.
275. Lee P, Vousden KH, Cheung EC. TIGAR , TIGAR , burning bright. 2014;1–9.
276. Li M, Sun M, Cao L, Gu JHJ -h., Ge J, Chen J, et al. A TIGAR-Regulated Metabolic Pathway Is Critical for Protection of Brain Ischemia. J Neurosci . 2014 May 28;34(22):7458–71.

277. Vassilev LT, Vu BT, Graves B, Carvajal D, Podlaski F, Filipovic Z, et al. In Vivo Activation of the p53 Pathway by Small-Molecule Antagonists of MDM2. Science (80-) . 2004 Feb 6;303(5659):844–8.
278. Xie J-MM, Li B, Yu H-PP, Gao Q-GG, Li W, Wu H-RR, et al. TIGAR Has a Dual Role in Cancer Cell Survival through Regulating Apoptosis and Autophagy. Cancer Res . 2014 Sep 15;74(18):5127–38.
279. Ye L, Zhao X, Lu J, Qian G, Zheng JC, Ge S. Knockdown of TIGAR by RNA interference induces apoptosis and autophagy in HepG2 hepatocellular carcinoma cells. Biochem Biophys Res Commun . 2013 Jul;437(2):300–6.
280. Li B, Wang Z, Xie J, Wang G, Qian L, Guan X, et al. TIGAR knockdown enhanced the anticancer effect of aescin via regulating autophagy and apoptosis in colorectal cancer cells. Acta Pharmacol Sin . 2019 Jan 16;40(1):111–21.
281. AĞCA CA, SHAREEF OH. Knockdown of TIGAR Induces Apoptosis and Autophagy with Modulates NF-κB and HO-1 Expression in A549 Lung Cancer Cells. J Inst Sci Technol . 2019 Mar 1;310–20.
282. Toufektchan E, Toledo F. The Guardian of the Genome Revisited: p53 Downregulates Genes Required for Telomere Maintenance, DNA Repair, and Centromere Structure. Cancers (Basel) . 2018 May 6;10(5):135.
283. Krause CJ, Carey TE, Ott RW, Hurbis C, McClatchey KD, Regezi JA. Human Squamous Cell Carcinoma: Establishment and Characterization of New Permanent Cell Lines. Arch Otolaryngol - Head Neck Surg . 1981 Nov 1;107(11):703–10.
284. Lin CJ, Grandis JR, Carey TE, Gollin SM, Whiteside TL, Koch WM, et al. Head and neck squamous cell carcinoma cell lines: Established models and rationale for selection. Head Neck . 2007 Feb;29(2):163–88.
285. Sano D, Xie T-X, Ow TJ, Zhao M, Pickering CR, Zhou G, et al. Disruptive TP53 Mutation Is Associated with Aggressive Disease Characteristics in an Orthotopic Murine Model of Oral Tongue Cancer. Clin Cancer Res . 2011 Nov 1;17(21):6658–70.
286. Bradford CR, Zacks SE, Androphy EJ, Gregoire L, Lancaster WD, Carey TE. Human Papillomavirus DNA Sequences in Cell Lines Derived from Head and Neck Squamous Cell Carcinomas. Otolaryngol Neck Surg . 1991 Mar;104(3):303–10.
287. Bouaoun L, Sonkin D, Ardin M, Hollstein M, Byrnes G, Zavadil J, et al. TP53 Variations in Human Cancers: New Lessons from the IARC TP53 Database and Genomics Data. Hum Mutat . 2016 Sep 1 [cited 2021 Mar 11];37(9):865–76.
288. Dearth LR, Qian H, Wang T, Baroni TE, Zeng J, Chen SW, et al. Inactive full-length p53 mutants lacking dominant wild-type p53 inhibition highlight loss of heterozygosity as an important aspect of p53 status in human cancers. Carcinogenesis . 2007 Feb;28(2):289–98.
289. Mizuarai S, Yamanaka K, Kotani H. Mutant p53 Induces the GEF-H1 Oncogene, a Guanine Nucleotide Exchange Factor-H1 for RhoA, Resulting in Accelerated Cell Proliferation in Tumor Cells. Cancer Res . 2006 Jun 15;66(12):6319–26.
290. Scian MJ, Stagliano KERR, Deb D, Ellis MA, Carchman EH, Das A, et al. Tumor-derived p53 mutants induce oncogenesis by transactivating growth-promoting genes. Oncogene . 2004 May 12 [cited 2021 Mar 11];23(25):4430–43.
291. Hauser U, Balz V, Carey TE, Grénman R, van Lierop A, Scheckenbach K, et al. Reliable detection of p53 aberrations in squamous cell carcinomas of the head and neck requires transcript analysis of the entire coding region. Head Neck . 2002 Sep;24(9):868–73.
292. Frebourg T, Kassel J, Lam KT, Gryka MA, Barbier N, Andersen TI, et al. Germ-line mutations of the p53 tumor suppressor gene in patients with high risk for cancer inactivate the p53 protein. Proc Natl Acad

Sci . 1992 Jul 15;89(14):6413–7.

293. Monti P, Perfumo C, Bisio A, Ciribilli Y, Menichini P, Russo D, et al. Dominant-Negative Features of Mutant TP53 in Germline Carriers Have Limited Impact on Cancer Outcomes. Mol Cancer Res . 2011 Mar;9(3):271–9.
294. Yan B, Yang X, Lee T-LL, Friedman J, Tang J, Van Waes C, et al. Genome-wide identification of novel expression signatures reveal distinct patterns and prevalence of binding motifs for p53, nuclear factor-κB and other signal transcription factors in head and neck squamous cell carcinoma. Genome Biol . 2007 May 11 [cited 2021 Mar 11];8(5):R78.
295. Brenner JC, Graham MP, Kumar B, Saunders LM, Kupfer R, Lyons RH, et al. Genotyping of 73 UM-SCC head and neck squamous cell carcinoma cell lines. Head Neck . 2009;NA-NA.
296. Friedman J, Nottingham L, Duggal P, Pernas FG, Yan B, Yang XP, et al. Deficient TP53 Expression, Function, and Cisplatin Sensitivity Are Restored by Quinacrine in Head and Neck Cancer. Clin Cancer Res . 2007 Nov 15;13(22):6568–78.
297. Divakaruni AS, Paradyse A, Ferrick DA, Murphy AN, Jastroch M. Analysis and Interpretation of Microplate-Based Oxygen Consumption and pH Data. In 2014. p. 309–54.
298. Guo S, Olm-Shipman A, Walters A, Urciuoli WR, Devito S, Nadtochiy SM, et al. A Cell-Based Phenotypic Assay to Identify Cardioprotective Agents. Circ Res . 2012 Mar 30;110(7):948–57.
299. Theparambil SM, Weber T, Schmälzle J, Ruminot I, Deitmer JW. Proton Fall or Bicarbonate Rise. J Biol Chem . 2016 Sep;291(36):19108–17.
300. Shechter Y, Ron A. Effect of depletion of phosphate and bicarbonate ions on insulin action in rat adipocytes. J Biol Chem . 1986 Nov;261(32):14945–50.
301. Lundholt BK, Scudder KM, Pagliaro L. A Simple Technique for Reducing Edge Effect in Cell-Based Assays. J Biomol Screen . 2003 Oct 25;8(5):566–70.
302. Pelletier M, Billingham LK, Ramaswamy M, Siegel RM. Extracellular Flux Analysis to Monitor Glycolytic Rates and Mitochondrial Oxygen Consumption. In 2014. p. 125–49.
303. Hill BG, Benavides GA, Lancaster JJR, Ballinger S, Dell'Italia L, Zhang J, et al. Integration of cellular bioenergetics with mitochondrial quality control and autophagy. Biol Chem . 2012 Dec 1 [cited 2021 Mar 16];393(12):1485–512.
304. Wu M, Neilson A, Swift AL, Moran R, Tamagnine J, Parslow D, et al. Multiparameter metabolic analysis reveals a close link between attenuated mitochondrial bioenergetic function and enhanced glycolysis dependency in human tumor cells. Am J Physiol Physiol . 2007 Jan;292(1):C125–36.
305. Agilent Technologies. Agilent Technologies Agilent Seahorse XF Glycolysis Stress Test Kit User Guide. 2019;
306. Mittal V. Improving the efficiency of RNA interference in mammals. Nat Rev Genet . 2004 May;5(5):355–65.
307. Berridge MV, Tan AS. Characterization of the Cellular Reduction of 3-(4,5-dimethylthiazol-2-yl)-2,5-diphenyltetrazolium bromide (MTT): Subcellular Localization, Substrate Dependence, and Involvement of Mitochondrial Electron Transport in MTT Reduction. Arch Biochem Biophys . 1993 Jun;303(2):474–82.
308. Plumb JA, Milroy R, Kaye SB. Effects of the pH Dependence of 3-(4,5-Dimethylthiazol-2-yl)-2,5-diphenyltetrazolium Bromide-Formazan Absorption on Chemosensitivity Determined by a Novel Tetrazolium-based Assay. Cancer Res . 1989 Aug 1 [cited 2021 Mar 19];49(16):4435–40.
309. Franken NAP, Rodermond HM, Stap J, Haveman J, van Bree C. Clonogenic assay of cells in vitro. Nat Protoc . 2006 Dec 21;1(5):2315–9.

310. Chang HW, Lee M, Lee YS, Kim SH, Lee JC, Park JJ, et al. p53-dependent glutamine usage determines susceptibility to oxidative stress in radioresistant head and neck cancer cells. Cell Signal . 2021 Jan;77:109820.
311. Tanaka N, Zhao M, Tang L, Patel AA, Xi Q, Van HT, et al. Gain-of-function mutant p53 promotes the oncogenic potential of head and neck squamous cell carcinoma cells by targeting the transcription factors FOXO3a and FOXM1. Oncogene . 2018 Mar 22;37(10):1279–92.
312. MD. W. Tumour Metabolism in Squamous Cell Carcinoma of the Head & Neck: Consequences & Potential Therapeutic Implications of TP53 Mutation. University of Liverpool; 2017.
313. Arya AK, El-Fert A, Devling T, Eccles RM, Aslam MA, Rubbi CP, et al. Nutlin-3, the small-molecule inhibitor of MDM2, promotes senescence and radiosensitises laryngeal carcinoma cells harbouring wild-type p53. Br J Cancer . 2010 Jul 29;103(2):186–95.
314. Kato S, Han S-Y, Liu W, Otsuka K, Shibata H, Kanamaru R, et al. Understanding the function–structure and function–mutation relationships of p53 tumor suppressor protein by high-resolution missense mutation analysis. Proc Natl Acad Sci . 2003 Jul 8;100(14):8424–9.
315. Alexandrov LB, Nik-Zainal S, Wedge DC, Aparicio SAJR, Behjati S, Biankin A V., et al. Signatures of mutational processes in human cancer. Nature . 2013 Aug 22;500(7463):415–21.
316. NW. F. The Functional and Clinical Consequences of TP53 Mutations in Cancer. University of Toronto; 2019.
317. (IARC) TIA for R on C. C176F . Available from: https://p53.iarc.fr/TP53GeneVariations.aspx
318. Warburg O. The Metabolism of Carcinoma Cells. J Cancer Res . 1925 Mar 1;9(1):148–63.
319. Gleeson LE, O'Leary SM, Ryan D, McLaughlin AM, Sheedy FJ, Keane J. Cigarette Smoking Impairs the Bioenergetic Immune Response to Mycobacterium tuberculosis Infection. Am J Respir Cell Mol Biol . 2018 Nov;59(5):572–9.
320. Xie N, Tan Z, Banerjee S, Cui H, Ge J, Liu R-M, et al. Glycolytic Reprogramming in Myofibroblast Differentiation and Lung Fibrosis. Am J Respir Crit Care Med . 2015 Dec 15;192(12):1462–74.
321. Nojima I, Eikawa S, Tomonobu N, Hada Y, Kajitani N, Teshigawara S, et al. Dysfunction of CD8 + PD-1 + T cells in type 2 diabetes caused by the impairment of metabolism-immune axis. Sci Rep . 2020 Dec 10;10(1):14928.
322. McGarry T, Biniecka M, Gao W, Cluxton D, Canavan M, Wade S, et al. Resolution of TLR2-induced inflammation through manipulation of metabolic pathways in Rheumatoid Arthritis. Sci Rep . 2017 Mar 22;7(1):43165.
323. Lu H, Li X, Fan Z. Abstract 5409: Cetuximab downregulates lactate dehydrogenase-A, leading to inhibition of glycolysis and reversal of the Warburg effect in HNSCC cells. In: Molecular and Cellular Biology . American Association for Cancer Research; 2013. p. 5409–5409.
324. Ohashi T, Aoki M, Tomita H, Akazawa T, Sato K, Kuze B, et al. M2-like macrophage polarization in high lactic acid-producing head and neck cancer. Cancer Sci . 2017 Jun 19;108(6):1128–34.
325. de Andrade Barreto E, de Souza Santos PT, Bergmann A, de Oliveira IM, Wernersbach Pinto L, Blanco T, et al. Alterations in glucose metabolism proteins responsible for the Warburg effect in esophageal squamous cell carcinoma. Exp Mol Pathol . 2016 Aug;101(1):66–73.
326. Krupar R, Robold K, Gaag D, Spanier G, Kreutz M, Renner K, et al. Immunologic and metabolic characteristics of HPV-negative and HPV-positive head and neck squamous cell carcinomas are strikingly different. Virchows Arch . 2014 Sep 16;465(3):299–312.
327. Green MR, Hughes H, Sambrook J, MacCallum P. Molecular cloning: a laboratory manual. In: Molecular cloning: a laboratory manual. 2012. p. 1890.

328. Warburton HE, Brady M, Vlatković N, Linehan WM, Parsons K, Boyd MT. p53 Regulation and Function in Renal Cell Carcinoma. Cancer Res . 2005 Aug 1;65(15):6498–503.
329. Hanson RL, Porter JR, Batchelor E. Protein stability of p53 targets determines their temporal expression dynamics in response to p53 pulsing. J Cell Biol . 2019 Apr 1;218(4):1282–97.
330. C242S . Available from: https://ckb.jax.org/geneVariant/show?geneVariantId=27041
331. Jordan JJ, Inga A, Conway K, Edmiston S, Carey LA, Wu L, et al. Altered-Function p53 Missense Mutations Identified in Breast Cancers Can Have Subtle Effects on Transactivation. Mol Cancer Res . 2010 May;8(5):701–16.
332. Friedman J, Nottingham L, Duggal P, Pernas FG, Yan B, Xin PY, et al. Deficient TP53 Expression, Function, and Cisplatin Sensitivity Are Restored by Quinacrine in Head and Neck Cancer. Clin Cancer Res . 2007 Nov 15 [cited 2021 Mar 11];13(22):6568–78.
333. Duan J, Friedman J, Nottingham L, Chen Z, Ara G, Van Waes C. Nuclear factor-κB p65 small interfering RNA or proteasome inhibitor bortezomib sensitizes head and neck squamous cell carcinomas to classic histone deacetylase inhibitors and novel histone deacetylase inhibitor PXD101. Mol Cancer Ther . 2007 Jan;6(1):37–50.
334. Hoffman-Luca CG, Yang C-Y, Lu J, Ziazadeh D, McEachern D, Debussche L, et al. Significant Differences in the Development of Acquired Resistance to the MDM2 Inhibitor SAR405838 between In Vitro and In Vivo Drug Treatment. Gartel AL, editor. PLoS One . 2015 Jun 12;10(6):e0128807.
335. Brady M, Vlatković N, Boyd MT. Regulation of p53 and MDM2 Activity by MTBP. Mol Cell Biol . 2005 Jan 15;25(2):545–53.
336. Mikawa T, Maruyama T, Okamoto K, Nakagama H, Lleonart ME, Tsusaka T, et al. Senescence-inducing stress promotes proteolysis of phosphoglycerate mutase via ubiquitin ligase Mdm2. J Cell Biol . 2014 Mar 3;204(5):729–45.
337. Jiang X, Sun Q, Li H, Li K, Ren X. The role of phosphoglycerate mutase 1 in tumor aerobic glycolysis and its potential therapeutic implications. Int J Cancer . 2014 Nov 1;135(9):1991–6.
338. Riscal R, Le Cam L, Linares LK. Chromatin-bound MDM2, a new player in metabolism. Mol Cell Oncol. 2016;3(5).
339. Riscal R, Schrepfer E, Arena G, Cissé MY, Bellvert F, Heuillet M, et al. Chromatin-Bound MDM2 Regulates Serine Metabolism and Redox Homeostasis Independently of p53. Mol Cell . 2016 Jun;62(6):890–902.
340. Lukashchuk N, Vousden KH. Ubiquitination and Degradation of Mutant p53. Mol Cell Biol . 2007 Dec 1;27(23):8284–95.
341. Zheng T, Wang J, Zhao Y, Zhang C, Lin M, Wang X, et al. Spliced MDM2 isoforms promote mutant p53 accumulation and gain-of-function in tumorigenesis. Nat Commun . 2013 Dec 20;4(1):2996.
342. Midgley CA, Lane DP. p53 protein stability in tumour cells is not determined by mutation but is dependent on Mdm2 binding. Oncogene . 1997 Sep 18;15(10):1179–89.
343. Kubbutat MHGG, Jones SN, Vousden KH. Regulation of p53 stability by Mdm2. Nature . 1997 May;387(6630):299–303.
344. Haupt Y, Maya R, Kazaz A, Oren M. Mdm2 promotes the rapid degradation of p53. Nature . 1997 May;387(6630):296–9.
345. Manfredi JJ. The Mdm2-p53 relationship evolves: Mdm2 swings both ways as an oncogene and a tumor suppressor. Genes Dev . 2010 Aug 1;24(15):1580–9.
346. Brown DR, Thomas CA, Deb SP. The human oncoprotein MDM2 arrests the cell cycle: Elimination of its cell-cycle-inhibitory function induces tumorigenesis. EMBO J . 1998 May 1;17(9):2513–25.

347. Ren F, Wu H, Lei Y, Zhang H, Liu R, Zhao Y, et al. Quantitative proteomics identification of phosphoglycerate mutase 1 as a novel therapeutic target in hepatocellular carcinoma. Mol Cancer . 2010;9(1):81.
348. LIU L, WANG S, ZHANG Q, DING Y. Identification of potential genes/proteins regulated by Tiam1 in colorectal cancer by microarray analysis and proteome analysis. Cell Biol Int . 2008 Oct;32(10):1215–22.
349. Tennant DA, Duran R V., Boulahbel H, Gottlieb E. Metabolic transformation in cancer. Carcinogenesis . 2009 Aug 1;30(8):1269–80.
350. Tennant DA, Durán RVR V., Gottlieb E. Targeting metabolic transformation for cancer therapy. Nat Rev Cancer . 2010 Apr 19 [cited 2021 Mar 28];10(4):267–77.
351. Mikawa T, LLeonart ME, Takaori-Kondo A, Inagaki N, Yokode M, Kondoh H. Dysregulated glycolysis as an oncogenic event. Cell Mol Life Sci . 2015 May 22;72(10):1881–92.
352. Aykul S, Martinez-Hackert E. Determination of half-maximal inhibitory concentration using biosensor-based protein interaction analysis. Anal Biochem . 2016 Sep;508:97–103.
353. Pang Y-Y, Wang T, Chen F-Y, Wu Y-L, Shao X, Xiao F, et al. Glycolytic inhibitor 2-deoxy- <scp>d</scp> -glucose suppresses cell proliferation and enhances methylprednisolone sensitivity in non-Hodgkin lymphoma cells through down-regulation of HIF-1α and c-MYC. Leuk Lymphoma . 2015 Jun 3;56(6):1821–30.
354. Sharma PK, Dwarakanath BS, Varshney R. Radiosensitization by 2-deoxy-D-glucose and 6-aminonicotinamide involves activation of redox sensitive ASK1-JNK/p38MAPK signaling in head and neck cancer cells. Free Radic Biol Med . 2012 Oct;53(7):1500–13.
355. Herken H, Voss P, Brade W, Kolbe H. Induction of glucose-6-phosphate dehydrogenase and 6-phosphogluconate dehydrogenase in the regenerating kidney after lesions by drugs. Naunyn-Schmiedebergs Arch f�r Pharmakologie . 1970;267(4):297–306.
356. Köhler E, Barrach H-J, Neubert D. Inhibition of NADP dependent oxidoreductases by the 6-aminonicotinamide analogue of NADP. FEBS Lett . 1970 Feb 16;6(3):225–8.
357. Kaushik N, Kaushik NK, Choi EH, Kim JH. Blockade of Cellular Energy Metabolism through 6-Aminonicotinamide Reduces Proliferation of Non-Small Lung Cancer Cells by Inducing Endoplasmic Reticulum Stress. Biology (Basel) . 2021 Oct 22;10(11):1088.
358. Liu C-L, Hsu Y-C, Lee J-J, Chen M-J, Lin C-H, Huang S-Y, et al. Targeting the pentose phosphate pathway increases reactive oxygen species and induces apoptosis in thyroid cancer cells. Mol Cell Endocrinol . 2020 Jan;499:110595.
359. Chen X, Xu Z, Zhu Z, Chen A, Fu G, Wang Y, et al. Modulation of G6PD affects bladder cancer via ROS accumulation and the AKT pathway in vitro. Int J Oncol . 2018 Jul 25;
360. Sharma PK, Bhardwaj R, Dwarakanath BS, Varshney R. Metabolic oxidative stress induced by a combination of 2-DG and 6-AN enhances radiation damage selectively in malignant cells via non-coordinated expression of antioxidant enzymes. Cancer Lett . 2010 Sep;295(2):154–66.
361. Halestrap AP. The mitochondrial pyruvate carrier. Kinetics and specificity for substrates and inhibitors. Biochem J . 1975 Apr 1;148(1):85–96.
362. Corbet C, Bastien E, Draoui N, Doix B, Mignion L, Jordan BF, et al. Interruption of lactate uptake by inhibiting mitochondrial pyruvate transport unravels direct antitumor and radiosensitizing effects. Nat Commun . 2018 Dec 23;9(1):1208.
363. Li Y, Li XX, Kan Q, Zhang M, Li XX, Xu R, et al. Mitochondrial pyruvate carrier function is negatively linked to Warburg phenotype in vitro and malignant features in esophageal squamous cell carcinomas.

Oncotarget . 2017 Jan 3;8(1):1058–73.

364. Stockwin LH, Yu SX, Borgel S, Hancock C, Wolfe TL, Phillips LR, et al. Sodium dichloroacetate selectively targets cells with defects in the mitochondrial ETC. Int J Cancer . 2010 Jun 7;127(11):2510–9.
365. Zwicker F, Kirsner A, Peschke P, Roeder F, Debus J, Huber PE, et al. Dichloroacetate induces tumor-specific radiosensitivity in vitro but attenuates radiation-induced tumor growth delay in vivo. Strahlentherapie und Onkol . 2013 Aug 23;189(8):684–92.
366. Cook KM, Shen H, McKelvey KJ, Gee HE, Hau E. Targeting Glucose Metabolism of Cancer Cells with Dichloroacetate to Radiosensitize High-Grade Gliomas. Int J Mol Sci . 2021 Jul 6;22(14):7265.
367. de Mey S, Dufait I, Jiang H, Corbet C, Wang H, Van De Gucht M, et al. Dichloroacetate Radiosensitizes Hypoxic Breast Cancer Cells. Int J Mol Sci . 2020 Dec 9;21(24):9367.
368. Stacpoole PW, Henderson GN, Yan Z, Cornett R, James MO. Pharmacokinetics, Metabolism, and Toxicology of Dichloroacetate. Drug Metab Rev . 1998 Jan 22;30(3):499–539.
369. Crabtree HG. Observations on the carbohydrate metabolism of tumours. Biochem J . 1929 Jan 1;23(3):536–45.
370. Ben Sahra I, Laurent K, Giuliano S, Larbret F, Ponzio G, Gounon P, et al. Targeting Cancer Cell Metabolism: The Combination of Metformin and 2-Deoxyglucose Induces p53-Dependent Apoptosis in Prostate Cancer Cells. Cancer Res . 2010 Mar 15;70(6):2465–75.
371. Okoshi R, Ozaki T, Yamamoto H, Ando K, Koida N, Ono S, et al. Activation of AMP-activated Protein Kinase Induces p53-dependent Apoptotic Cell Death in Response to Energetic Stress. J Biol Chem . 2008 Feb;283(7):3979–87.
372. Gowans GJ, Hardie DG. AMPK: a cellular energy sensor primarily regulated by AMP. Biochem Soc Trans . 2014 Feb 1;42(1):71–5.
373. Hawley SA, Boudeau J, Reid JL, Mustard KJ, Udd L, Mäkelä TP, et al. Complexes between the LKB1 tumor suppressor, STRAD alpha/beta and MO25 alpha/beta are upstream kinases in the AMP-activated protein kinase cascade. J Biol . 2003;2(4):28.
374. Xing Y, Musi N, Fujii N, Zou L, Luptak I, Hirshman MF, et al. Glucose Metabolism and Energy Homeostasis in Mouse Hearts Overexpressing Dominant Negative α2 Subunit of AMP-activated Protein Kinase. J Biol Chem . 2003 Aug;278(31):28372–7.
375. Hardie DG. Minireview: The AMP-Activated Protein Kinase Cascade: The Key Sensor of Cellular Energy Status. Endocrinology . 2003 Dec 1;144(12):5179–83.
376. Vousden KH, Lu X. Live or let die: the cell's response to p53. Nat Rev Cancer . 2002 Aug;2(8):594–604.
377. Sionov RV, Haupt Y. The cellular response to p53: the decision between life and death. Oncogene . 1999 Nov 4;18(45):6145–57.
378. Jones RG, Plas DR, Kubek S, Buzzai M, Mu J, Xu Y, et al. AMP-Activated Protein Kinase Induces a p53-Dependent Metabolic Checkpoint. Mol Cell . 2005 Apr;18(3):283–93.
379. Frederick M, Skinner HD, Kazi SA, Sikora AG, Sandulache VC. High expression of oxidative phosphorylation genes predicts improved survival in squamous cell carcinomas of the head and neck and lung. Sci Rep . 2020 Dec 14;10(1):6380.
380. Wu Z-H, Tang Y, Zhou Y. A Metabolic Gene Signature to Predict Overall Survival in Head and Neck Squamous Cell Carcinoma. Contreras C, editor. Mediators Inflamm . 2020 Dec 30;2020:1–12.
381. Osman AA, Neskey DM, Katsonis P, Patel AA, Ward AM, Hsu T-K, et al. Evolutionary Action Score of TP53 Coding Variants Is Predictive of Platinum Response in Head and Neck Cancer Patients. Cancer Res . 2015 Apr 1;75(7):1205–15.
382. Sano D, Xie T-XT-X, Ow TJ, Zhao M, Pickering CR, Zhou GG, et al. Disruptive TP53 Mutation Is Associated

with Aggressive Disease Characteristics in an Orthotopic Murine Model of Oral Tongue Cancer. Clin Cancer Res . 2011 Nov 1;17(21):6658–70.

383. Neskey DM, Osman AA, Ow TJ, Katsonis P, McDonald T, Hicks SC, et al. Evolutionary action score of TP53 identifies high-risk mutations associated with decreased survival and increased distant metastases in head and neck cancer. Cancer Res. 2015;75(7):1527–36.
384. Skinner HD, Sandulache VC, Ow TJ, Meyn RE, Yordy JS, Beadle BM, et al. TP53 Disruptive Mutations Lead to Head and Neck Cancer Treatment Failure through Inhibition of Radiation-Induced Senescence. Clin Cancer Res . 2012 Jan 1 [cited 2021 Mar 11];18(1):290–300.
385. Aas' T, B0rresen A-L, Gejsler S, Rgiti' B!, Sm E, Th-S0rensen !, et al. Specific PS3 mutations are associated with de novo resistance to doxorubicin in breast cancer patients. 1996 [cited 2021 Oct 14];
386. Cadwell C, Zambetti GP. The effects of wild-type p53 tumor suppressor activity and mutant p53 gain-of-function on cell growth. Gene . 2001 Oct;277(1–2):15–30.
387. Pascale RM, Calvisi DF, Simile MM, Feo CF, Feo F. The Warburg Effect 97 Years after Its Discovery. Cancers (Basel) . 2020 Sep 30;12(10):2819.
388. Bricker DK, Taylor EB, Schell JC, Orsak T, Boutron A, Chen Y-C, et al. A Mitochondrial Pyruvate Carrier Required for Pyruvate Uptake in Yeast, Drosophila , and Humans. Science (80-) . 2012 Jul 6;337(6090):96–100.
389. Schell JC, Olson KA, Jiang L, Hawkins AJ, Van Vranken JG, Xie J, et al. A Role for the Mitochondrial Pyruvate Carrier as a Repressor of the Warburg Effect and Colon Cancer Cell Growth. Mol Cell . 2014 Nov;56(3):400–13.
390. Rauckhorst AJ, Taylor EB. Mitochondrial pyruvate carrier function and cancer metabolism. Curr Opin Genet Dev . 2016 Jun;38:102–9.
391. Tan AS, Baty JW, Dong L-F, Bezawork-Geleta A, Endaya B, Goodwin J, et al. Mitochondrial Genome Acquisition Restores Respiratory Function and Tumorigenic Potential of Cancer Cells without Mitochondrial DNA. Cell Metab . 2015 Jan;21(1):81–94.
392. Han YH, Kim SH, Kim SZ, Park WH. Antimycin A as a mitochondrial electron transport inhibitor prevents the growth of human lung cancer A549 cells. Oncol Rep . 2008 Sep;20(3):689–93.
393. Vacanti NM, Divakaruni AS, Green CR, Parker SJ, Henry RR, Ciaraldi TP, et al. Regulation of Substrate Utilization by the Mitochondrial Pyruvate Carrier. Mol Cell . 2014 Nov;56(3):425–35.
394. Yang C, Ko B, Hensley CT, Jiang L, Wasti AT, Kim J, et al. Glutamine Oxidation Maintains the TCA Cycle and Cell Survival during Impaired Mitochondrial Pyruvate Transport. Mol Cell . 2014 Nov;56(3):414–24.
395. Paradies G, Capuano F, Palombini G, Galeotti T, Papa S. Transport of pyruvate in mitochondria from different tumor cells. Cancer Res . 1983 Nov;43(11):5068–71.
396. Eboli ML, Paradies G, Galeotti T, Papa S. Pyruvate transport in tumour-cell mitochondria. Biochim Biophys Acta - Bioenerg . 1977 Apr;460(1):183–7.
397. Zhong Y, Li XX, Yu D, Li XX, Li Y, Long Y, et al. Application of mitochondrial pyruvate carrier blocker UK5099 creates metabolic reprogram and greater stem-like properties in LnCap prostate cancer cells in vitro. Oncotarget . 2015 Nov 10;6(35):37758–69.
398. Florio R, De Lellis L, Veschi S, Verginelli F, di Giacomo V, Gallorini M, et al. Effects of dichloroacetate as single agent or in combination with GW6471 and metformin in paraganglioma cells. Sci Rep . 2018 Dec 11;8(1):13610.
399. Dai Y, Xiong X, Huang G, Liu J, Sheng S, Wang H, et al. Dichloroacetate Enhances Adriamycin-Induced Hepatoma Cell Toxicity In Vitro and In Vivo by Increasing Reactive Oxygen Species Levels. Lebedeva I

V., editor. PLoS One . 2014 Apr 11;9(4):e92962.

400. Lin G, Hill DK, Andrejeva G, Boult JKR, Troy H, Fong A-CLFWT, et al. Dichloroacetate induces autophagy in colorectal cancer cells and tumours. Br J Cancer . 2014 Jul 3;111(2):375–85.
401. Oren M, Rotter V. Mutant p53 Gain-of-Function in Cancer. Cold Spring Harb Perspect Biol . 2010 Feb 1;2(2):a001107–a001107.
402. Van Oijen MGCT, Slootweg PJ. Gain-of-function mutations in the tumor suppressor gene p53. Clin Cancer Res . 2000 Jun;6(6):2138–45.
403. Blandino G, Levine AJ, Oren M. Mutant p53 gain of function: differential effects of different p53 mutants on resistance of cultured cells to chemotherapy. Oncogene . 1999 Jan 20;18(2):477–85.
404. Yi Y, Chen D, Ao J, Sun S, Wu M, Li X, et al. Metformin Promotes AMP-activated Protein Kinase-independent Suppression of ΔNp63α Protein Expression and Inhibits Cancer Cell Viability. J Biol Chem . 2017 Mar;292(13):5253–61.
405. Forastiere A, Weber R, Ang K. Treatment of Head and Neck Cancer. N Engl J Med . 2008 Mar 6;358(10):1076–8.
406. Forastiere AA, Trotti A, Pfister DG, Grandis JR. Head and neck cancer: Recent advances and new standards of care. J Clin Oncol . 2006 Jun 10;24(17):2603–5.
407. Faubert B, Solmonson A, DeBerardinis RJ. Metabolic reprogramming and cancer progression. Science (80-) . 2020 Apr 10;368(6487):eaaw5473.
408. Gandhi N, Das G. Metabolic Reprogramming in Breast Cancer and Its Therapeutic Implications. Cells . 2019 Jan 26;8(2):89.
409. Yoshida GJ. Metabolic reprogramming: the emerging concept and associated therapeutic strategies. J Exp Clin Cancer Res . 2015 Dec 6;34(1):111.
410. Vaupel P, Schmidberger H, Mayer A. The Warburg effect: essential part of metabolic reprogramming and central contributor to cancer progression. Int J Radiat Biol . 2019 Jul 3;95(7):912–9.
411. Sun RC, Fadia M, Dahlstrom JE, Parish CR, Board PG, Blackburn AC. Reversal of the glycolytic phenotype by dichloroacetate inhibits metastatic breast cancer cell growth in vitro and in vivo. Breast Cancer Res Treat . 2010 Feb 19;120(1):253–60.
412. Wilkie MD, Anaam EA, Lau AS, Rubbi CP, Jones TM, Boyd MT, et al. TP53 mutations in head and neck cancer cells determine the Warburg phenotypic switch creating metabolic vulnerabilities and therapeutic opportunities for stratified therapies. Cancer Lett . 2020 May;478:107–21.
413. Wilkie MD, Anaam EA, Lau AS, Rubbi CP, Vlatkovic N, Jones TM, et al. Metabolic Plasticity and Combinatorial Radiosensitisation Strategies in Human Papillomavirus-Positive Squamous Cell Carcinoma of the Head and Neck Cell Lines. Cancers (Basel) . 2021 Sep 28;13(19):4836.
414. Kamp WM, Wang P, Hwang PM. TP53 mutation, mitochondria and cancer. Curr Opin Genet Dev . 2016 Jun;38:16–22.
415. Won KY, Lim S-JJ, Kim GY, Kim YW, Han S-AA, Song JY, et al. Regulatory role of p53 in cancer metabolism via SCO2 and TIGAR in human breast cancer. Hum Pathol . 2012 Feb;43(2):221–8.
416. Shen M, Zhao X, Zhao L, Shi L, An S, Huang G, et al. Met is involved in TIGAR-regulated metastasis of non-small-cell lung cancer. Mol Cancer . 2018 Dec 12;17(1):88.
417. Fendt S-M, Lunt SY. Dynamic ROS Regulation by TIGAR: Balancing Anti-cancer and Pro-metastasis Effects. Cancer Cell . 2020 Feb;37(2):141–2.
418. Elstrom RL, Bauer DE, Buzzai M, Karnauskas R, Harris MH, Plas DR, et al. Akt Stimulates Aerobic Glycolysis in Cancer Cells. Cancer Res . 2004 Jun 1;64(11):3892–9.
419. Gottschalk S, Anderson N, Hainz C, Eckhardt SG, Serkova NJ. Imatinib (STI571)-Mediated Changes in

Glucose Metabolism in Human Leukemia BCR-ABL-Positive Cells. Clin Cancer Res . 2004 Oct 1;10(19):6661–8.

420. Yizhak K, Le Dévédec SE, Rogkoti VM, Baenke F, Boer VC, Frezza C, et al. A computational study of the Warburg effect identifies metabolic targets inhibiting cancer migration. Mol Syst Biol . 2014 Aug;10(8):744.
421. Meng M-B, Wang H-H, Guo W-H, Wu Z-Q, Zeng X-L, Zaorsky NG, et al. Targeting pyruvate kinase M2 contributes to radiosensitivity of non-small cell lung cancer cells in vitro and in vivo. Cancer Lett . 2015 Jan;356(2):985–93.
422. Vander Heiden MG, Cantley LC, Thompson CB, Heiden MGV, Cantley LC, Thompson CB. Understanding the Warburg Effect: The Metabolic Requirements of Cell Proliferation. Science (80-) . 2009 May 22 [cited 2021 Mar 27];324(5930):1029–33.
423. Porporato PE, Filigheddu N, Pedro JMB-S, Kroemer G, Galluzzi L. Mitochondrial metabolism and cancer. Cell Res . 2018 Mar 8;28(3):265–80.
424. Hussain SP, Amstad P, He P, Robles A, Lupold S, Kaneko I, et al. p53-Induced Up-Regulation of MnSOD and GPx but not Catalase Increases Oxidative Stress and Apoptosis. Cancer Res . 2004 Apr 1;64(7):2350–6.
425. Norberg E, Orrenius S, Zhivotovsky B. Mitochondrial regulation of cell death: Processing of apoptosis-inducing factor (AIF). Biochem Biophys Res Commun . 2010 May;396(1):95–100.
426. Vakifahmetoglu-Norberg H, Ouchida AT, Norberg E. The role of mitochondria in metabolism and cell death. Biochem Biophys Res Commun . 2017 Jan;482(3):426–31.
427. Eriksson M, Ambroise G, Ouchida AT, Lima Queiroz A, Smith D, Gimenez-Cassina A, et al. Effect of Mutant p53 Proteins on Glycolysis and Mitochondrial Metabolism. Mol Cell Biol . 2017 Dec 15;37(24).
428. Cheung EC, Athineos D, Lee P, Ridgway RA, Lambie W, Nixon C, et al. TIGAR Is Required for Efficient Intestinal Regeneration and Tumorigenesis. Dev Cell . 2013 Jun;25(5):463–77.
429. Lee P, Hock AK, Vousden KH, Cheung EC. p53- and p73-independent activation of TIGAR expression in vivo. Cell Death Dis . 2015 Aug 6;6(8):e1842–e1842.
430. Zou S, Rao Y, Chen W. miR-885-5p plays an accomplice role in liver cancer by instigating TIGAR expression via targeting its promoter. Biotechnol Appl Biochem . 2019 Sep 27;66(5):763–71.
431. Maschek G, Savaraj N, Priebe W, Braunschweiger P, Hamilton K, Tidmarsh GF, et al. 2-Deoxy-d-glucose Increases the Efficacy of Adriamycin and Paclitaxel in Human Osteosarcoma and Non-Small Cell Lung Cancers In Vivo. Cancer Res . 2004 Jan 1;64(1):31–4.
432. Magno L, Terraneo F, Bertoni F, Tordiglione M, Bardelli D, Rosignoli MT, et al. Double-blind randomized study of lonidamine and radiotherapy in head and neck cancer. Int J Radiat Oncol . 1994 Apr;29(1):45–55.
433. Colella E, Merlano M, Blengio F, Angelini F, Ausili Cefaro GP, Scasso F, et al. Randomised phase II study of methotrexate (MTX) versus methotrexate plus lonidamine (MTX + LND) in recurrent and/or metastatic carcinoma of the head and neck. Eur J Cancer . 1994 Jan;30(7):928–30.
434. Wilkie M, Lau A, Vlatkovic N, Jones T, Boyd M. Tumour metabolism in squamous cell carcinoma of the head and neck: an in-vitro study of the consequences of TP53 mutation and therapeutic implications. Lancet . 2015 Feb;385:S101.
435. Martinez Marignac V, Smith S, Toban N, Bazile M, Aloyz R. Resistance to Dasatinib in primary chronic lymphocytic leukemia lymphocytes involves AMPK-mediated energetic re-programming. Oncotarget . 2013 Dec 31;4(12):2550–66.
436. Martinez-Outschoorn UE, Goldberg AF, Lin Z, Ko Y-H, Flomenberg N, Wang C, et al. Anti-estrogen

resistance in breast cancer is induced by the tumor microenvironment and can be overcome by inhibiting mitochondrial function in epithelial cancer cells. Cancer Biol Ther . 2011 Nov 15;12(10):924–38.

437. Wang J, Duan Z, Nugent Z, Zou JX, Borowsky AD, Zhang Y, et al. Reprogramming metabolism by histone methyltransferase NSD2 drives endocrine resistance via coordinated activation of pentose phosphate pathway enzymes. Cancer Lett . 2016 Aug;378(2):69–79.
438. Tai G, Zhang H, Du J, Chen G, Huang J, Yu J, et al. TIGAR overexpression diminishes radiosensitivity of parotid gland fibroblast cells and inhibits IR-induced cell autophagy. Int J Clin Exp Pathol . 2015;8(5):4823–9.
439. Qian S, Li J, Hong M, Zhu Y, Zhao H, Xie Y, et al. TIGAR cooperated with glycolysis to inhibit the apoptosis of leukemia cells and associated with poor prognosis in patients with cytogenetically normal acute myeloid leukemia. J Hematol Oncol . 2016 Dec 25;9(1):128.
440. Cruz-Gregorio A, Martínez-Ramírez I, Pedraza-Chaverri J, Lizano M. Reprogramming of Energy Metabolism in Response to Radiotherapy in Head and Neck Squamous Cell Carcinoma. Cancers (Basel) . 2019 Feb 5;11(2):182.
441. Circu ML, Aw TY. Reactive oxygen species, cellular redox systems, and apoptosis. Free Radic Biol Med . 2010 Mar 15;48(6):749–62.
442. Brand KA, Hermfisse U. Aerobic glycolysis by proliferating cells: a protective strategy against reactive oxygen species 1. FASEB J . 1997 Apr;11(5):388–95.
443. Zhivotovsky B, Joseph B, Orrenius S. Tumor radiosensitivity and apoptosis. Exp Cell Res . 1999 Apr;248(1):10–7.
444. Gillet J-P, Varma S, Gottesman MM. The Clinical Relevance of Cancer Cell Lines. JNCI J Natl Cancer Inst . 2013 Apr 3;105(7):452–8.
445. Majmundar AJ, Wong WJ, Simon MC. Hypoxia-Inducible Factors and the Response to Hypoxic Stress. Mol Cell . 2010 Oct;40(2):294–309.
446. Park GB, Chung YH, Kim D. 2-Deoxy-D-glucose suppresses the migration and reverses the drug resistance of colon cancer cells through ADAM expression regulation. Anticancer Drugs . 2017 Apr;28(4):410–20.
447. De Lena M, Lorusso V, Latorre A, Fanizza G, Gargano G, Caporusso L, et al. Paclitaxel, cisplatin and lonidamine in advanced ovarian cancer. A phase II study. Eur J Cancer . 2001 Feb;37(3):364–8.
448. Portatone L, Lombardi A, Antilli A, Cruciani AR, Magliacani V, Mugnaini L, et al. Treatment of Inoperable Non-small Cell Lung Carcinoma Stage IIIB and IV with Cisplatin, Epidoxorubicin, Vindesine and Lonidamine: A Phase II Study. Tumori J . 1999 Jul 17;85(4):239–42.
449. Pacini P, Rinaldini M, Algeri R, Guarneri A, Tucci E, Barsanti G, et al. FEC (5-fluorouracil, epidoxorubicin and cyclophosphamide) versus EM (epidoxorubicin and mitomycin-C) with or without lonidamine as first-line treatment for advanced breast cancer. A multicentric randomised study. Final results. Eur J Cancer . 2000 May;36(8):966–75.
450. Berruti A, Bitossi R, Gorzegno G, Bottini A, Alquati P, De Matteis A, et al. Time to Progression in Metastatic Breast Cancer Patients Treated With Epirubicin Is Not Improved by the Addition of Either Cisplatin or Lonidamine: Final Results of a Phase III Study With a Factorial Design. J Clin Oncol . 2002 Oct 15;20(20):4150–9.
451. Mohanti BK, Rath GK, Anantha N, Kannan V, Das BS, Chandramouli BAR, et al. Improving cancer radiotherapy with 2-deoxy-d-glucose: phase I/II clinical trials on human cerebral gliomas. Int J Radiat Oncol . 1996 Apr;35(1):103–11.

452. Garon EB, Christofk HR, Hosmer W, Britten CD, Bahng A, Crabtree MJ, et al. Dichloroacetate should be considered with platinum-based chemotherapy in hypoxic tumors rather than as a single agent in advanced non-small cell lung cancer. J Cancer Res Clin Oncol . 2014 Mar 18;140(3):443–52.
453. Dunbar EM, Coats BS, Shroads AL, Langaee T, Lew A, Forder JR, et al. Phase 1 trial of dichloroacetate (DCA) in adults with recurrent malignant brain tumors. Invest New Drugs . 2014 Jun 3;32(3):452–64.
454. Chu QS-C, Sangha R, Spratlin J, J. Vos L, Mackey JR, McEwan AJB, et al. A phase I open-labeled, single-arm, dose-escalation, study of dichloroacetate (DCA) in patients with advanced solid tumors. Invest New Drugs . 2015 Jun 13;33(3):603–10.
455. Chang DT. Phase I Trial of Metabolic Reprogramming Therapy for Treatment of Recurrent Head and Neck Cancers . Clinicaltrials.Gov. 2010 [cited 2021 Oct 7]. p. 8/1/2010-2/1/2013.
456. Dwarakanath B, Singh D, Banerji A, Sarin R, Venkataramana N, Jalali R, et al. Clinical studies for improving radiotherapy with 2-deoxy-D-glucose: Present status and future prospects. J Cancer Res Ther . 2009;5(9):21.
457. Gray LH, Conger AD, Ebert M, Hornsey S, Scott OCA. The Concentration of Oxygen Dissolved in Tissues at the Time of Irradiation as a Factor in Radiotherapy. Br J Radiol . 1953 Dec;26(312):638–48.
458. Moulder JE, Rockwell S. Tumor hypoxia: its impact on cancer therapy. Cancer Metastasis Rev . 1987;5(4):313–41.
459. Nath S, Devi GR. Three-dimensional culture systems in cancer research: Focus on tumor spheroid model. Pharmacol Ther . 2016 Jul;163:94–108.
460. Freyer JP. Role of Necrosis in Regulating the Growth Saturation of Multicellular Spheroids. Cancer Res . 1988 May 1;48(9):2432–9.
461. Schwachöfer JH, Acker H, Crooijmans RP, Van Gasteren JJ, Holtermann G, Hoogenhout J, et al. Oxygen tensions in two human tumor cell lines grown and irradiated as multicellular spheroids. Anticancer Res . 11(1):273–9.
462. Hidalgo M, Amant F, Biankin A V., Budinská E, Byrne AT, Caldas C, et al. Patient-Derived Xenograft Models: An Emerging Platform for Translational Cancer Research. Cancer Discov . 2014 Sep;4(9):998–1013.
463. Tentler JJ, Tan AC, Weekes CD, Jimeno A, Leong S, Pitts TM, et al. Patient-derived tumour xenografts as models for oncology drug development. Nat Rev Clin Oncol . 2012 Jun 17;9(6):338–50.
464. Okada S, Vaeteewoottacharn K, Kariya R. Establishment of a Patient-Derived Tumor Xenograft Model and Application for Precision Cancer Medicine. Chem Pharm Bull . 2018;66(3):225–30.
465. Aparicio S, Hidalgo M, Kung AL. Examining the utility of patient-derived xenograft mouse models. Nat Rev Cancer . 2015 May 24;15(5):311–6.
466. Yates LR, Knappskog S, Wedge D, Farmery JHR, Gonzalez S, Martincorena I, et al. Genomic Evolution of Breast Cancer Metastasis and Relapse. Cancer Cell . 2017 Aug;32(2):169-184.e7.
467. Mroz EA, Rocco JW. MATH, a novel measure of intratumor genetic heterogeneity, is high in poor-outcome classes of head and neck squamous cell carcinoma. Oral Oncol . 2013 Mar;49(3):211–5.
468. Mroz EA, Tward AD, Pickering CR, Myers JN, Ferris RL, Rocco JW. High intratumor genetic heterogeneity is related to worse outcome in patients with head and neck squamous cell carcinoma. Cancer . 2013 Aug 15;119(16):3034–42.
469. Salk JJ, Fox EJ, Loeb LA. Mutational Heterogeneity in Human Cancers: Origin and Consequences. Annu Rev Pathol Mech Dis . 2010 Jan;5(1):51–75.
470. Dexter DL, Kowalski HM, Blazar BA, Fligiel Z, Vogel R, Heppner GH. Heterogeneity of tumor cells from a single mouse mammary tumor. Cancer Res . 1978 Oct;38(10):3174–81.

471. Fidler I, Kripke M. Metastasis results from preexisting variant cells within a malignant tumor. Science (80-) . 1977 Aug 26;197(4306):893–5.
472. Håkansson L, Tropé C. ON THE PRESENCE WITHIN TUMOURS OF CLONES THAT DIFFER IN SENSITIVITY TO CYTOSTATIC DRUGS. Acta Pathol Microbiol Scand Sect A Pathol . 2009 Aug 15;82A(1):35–40.
473. Kobayashi K, Yoshimoto S, Ando M, Matsumoto F, Murakami N, Omura G, et al. Full-coverage TP53 deep sequencing of recurrent head and neck squamous cell carcinoma facilitates prognostic assessment after recurrence. Oral Oncol . 2021 Feb;113:105091.
474. Przybyla L, Gilbert LA. A new era in functional genomics screens. Nat Rev Genet . 2021 Sep 20;
475. Chandel V, Sharma PP, Nayar SA, Jha NK, Jha SK, Rathi B, et al. In silico identification of potential inhibitor for TP53-induced glycolysis and apoptosis regulator in head and neck squamous cell carcinoma. 3 Biotech . 2021 Mar 7;11(3):117.
476. Poyya J, Kumar DJ, Nagendra HG, Dinesh B, Aditya Rao SJ, Joshi CG. Receptor based virtual screening of potential novel inhibitors of tigar [TP53 (tumour protein 53)-induced glycolysis and apoptosis regulator. Med Hypotheses . 2021 Nov;156:110683.
477. Szymański P, Markowicz M, Mikiciuk-Olasik E. Adaptation of High-Throughput Screening in Drug Discovery—Toxicological Screening Tests. Int J Mol Sci . 2011 Dec 29;13(1):427–52.
478. Zhu J, Zheng Y, Zhang H, Sun H. Targeting cancer cell metabolism: The combination of metformin and 2-Deoxyglucose regulates apoptosis in ovarian cancer cells via p38 MAPK/JNK signaling pathway. Am J Transl Res . 2016;8(11):4812–21.
479. Mert I, Chhina J, Allo G, Dai J, Seward S, Carey MS, et al. Synergistic effect of MEK inhibitor and metformin combination in low grade serous ovarian cancer. Gynecol Oncol . 2017 Aug;146(2):319–26.
480. Zhao J, Ma Y, Zhang Y, Fu B, Wu X, Li Q, et al. Low-dose 2-deoxyglucose and metformin synergically inhibit proliferation of human polycystic kidney cells by modulating glucose metabolism. Cell Death Discov . 2019 Dec 11;5(1):76.
481. Lu S-L, Herrington H, Wang X-J. Mouse models for human head and neck squamous cell carcinomas. Head Neck . 2006 Oct;28(10):945–54.
482. Patel SG, Lydiatt WM. Staging of head and neck cancers: Is it time to change the balance between the ideal and the practical? J Surg Oncol . 2008 Jun 15;97(8):653–7.
483. Kobayashi K, Yoshimoto S, Matsumoto F, Ando M, Murakami N, Omura G, et al. All-Exon TP53 Sequencing and Protein Phenotype Analysis Accurately Predict Clinical Outcome after Surgical Treatment of Head and Neck Squamous Cell Carcinoma. Ann Surg Oncol . 2019 Jul 21;26(7):2294–303.
484. Pettitt AR, Jackson R, Carruthers S, Dodd J, Dodd S, Oates M, et al. Alemtuzumab in Combination With Methylprednisolone Is a Highly Effective Induction Regimen for Patients With Chronic Lymphocytic Leukemia and Deletion of TP53 : Final Results of the National Cancer Research Institute CLL206 Trial. J Clin Oncol . 2012 May 10;30(14):1647–55.
485. Dutta S, Pregartner G, Rücker FG, Heitzer E, Zebisch A, Bullinger L, et al. Functional Classification of TP53 Mutations in Acute Myeloid Leukemia. Cancers (Basel) . 2020 Mar 10;12(3):637.
486. Hou H, Qin K, Liang Y, Zhang C, Liu D, Jiang H, et al. Concurrent TP53 mutations predict poor outcomes of EGFR-TKI treatments in Chinese patients with advanced NSCLC. Cancer Manag Res . 2019 Jun;Volume 11:5665–75.
487. Kron A, Alidousty C, Scheffler M, Merkelbach-Bruse S, Seidel D, Riedel R, et al. Impact of TP53 mutation status on systemic treatment outcome in ALK-rearranged non-small-cell lung cancer. Ann Oncol . 2018

Oct;29(10):2068–75.

488. Ungerleider NA, Rao SG, Shahbandi A, Yee D, Niu T, Frey WD, et al. Breast cancer survival predicted by TP53 mutation status differs markedly depending on treatment. Breast Cancer Res . 2018 Dec 1;20(1):115.
489. Roulland-Dussoix D, Henry A, Lemercier B. Detection of mycoplasmas in cell cultures by PCR: a one year study. J Microbiol Methods . 1994 Feb;19(2):127–34.
490. Young L, Sung J, Stacey G, Masters JR. Detection of Mycoplasma in cell cultures. Nat Protoc . 2010 May 22;5(5):929–34.
491. Rawadi G, Dussurget O. Advances in PCR-based detection of mycoplasmas contaminating cell cultures. Genome Res . 1995 Feb 1;4(4):199–208.
492. van Kuppeveld FJM, Van der Logt JTM, Angulo AF, Van Zoest MJ, Quint WGV, Niesters HGM, et al. Genus- and species-specific identification of mycoplasmas by 16S rRNA amplification. Appl Environ Microbiol. 1992;58(8):2606–15.

6. Appendix

6.1. Cell line authentication and optimisation

6.1.1. STR profiling

Short Tandem Repeat (STR) profiling of all cell lines used in this study was conducted with the assistance of Dr Lakis Liloglou (University of Liverpool). Prior to use in experiments, all cell lines were subjected to STR profiling to verify their identity, as determined by comparison with published profiles for each individual cell line.

Firstly, genomic DNA was isolated from cells. Extraction of genomic DNA was performed using Qiagen's DNeasy® Blood & Tissue Kit as per the manufacturer's instructions. A maximum of 5 x 10^6 cells were trypsinised and centrifuged for 5 min at 300 x g as described in section 2.2.4. The cell pellet was then re-suspended in 200µl of PBS before 20 µl proteinase K was added. 200 µl Buffer AL (which contains a chaotropic salt) before mixing thoroughly with a vortex. Samples were incubated at 56°C for 10 min. 200 µl of molecular biology grade ethanol was added and the samples were mixed thoroughly by vortexing before being transferred into a mini spin column placed in a 2 ml collection tube. The mixture was centrifuged at ≥6000 x g for 1 min, then the flow-through and collection tube were discarded. The spin column was placed in a new 2 ml collection tube before adding 500 µl of Buffer AW1, which contains a higher proportion of ethanol to remove excess salt and improve the pH conditions. Centrifugation at ≥6000 x g for 1 min was carried out before discarding the flow-through and collection tube. The spin column was placed in a new 2 ml collection tube before adding 500 µl of Buffer AW2, the mixture was centrifuged at ≥20,000 x g for 3 min to remove digested proteins or other impurities. The flow-through and collection tube were then discarded. After transferring the spin column to a 2 ml microcentrifuge tube, the DNA was eluted by adding 200 µl Buffer AE to the centre of the spin column membrane. Buffer AE contains Tris and EDTA which functions to rehydrate the nucleic acids and release DNA from the silica membrane. The mixture was then incubated for 1 minute at room temperature before being centrifuged again for 1 minute at ≥6000 x g. DNA concentration was determined using a NanoDrop™ One/One^C Microvolume UV-Vis Spectrophotometer (Thermo Scientific™) at 260/280 nm wavelength. Samples were then serially diluted with deionised water to achieve a DNA concentration of 10-30 ng/µl in preparation for the subsequent process of STR profiling.

The GenePrint® 10 System (Promega, Southampton, UK) was used for PCR and STR profiling which were performed as per the manufacturer's instructions. The required amount of PCR amplification mix (9 µl/reaction) was added to each labelled PCR tube, consisting of 6 µl deionised water, 2µl of master mix and 1µl of primer pair mix. 1µl sample template DNA was added to the respective tubes, as well as 1µl of the negative control (deionised water) and positive control (GenePrint® 10 control). Tubes were centrifuged for 5 seconds before being placed into a Px2 thermal cycler (Thermo Fisher Scientific) to perform the following thermal cycle:

- 96°C – 1 minute
- 94°C – 15 seconds
- 60°C – 30 seconds
- 72°C – 45 seconds

  } 35 cycles

- 72°C – 20 minutes
- 4°C – hold

Following amplification, a loading cocktail was prepared by combining and mixing 9.5µl of Hi-Di™ formamide and 0.5µl of the GenePrint® 10 Internal Lane Standard (ILS) 600 for 15 seconds. PCR product was diluted 1:5 with Tris-HCL EDTA (TE) buffer, before 1µl of the diluted PCR product or 1µl of GenePrint® 10 Allelic Ladder Mix for the positive control) was added to 10µl of the formamide/ILS 600 mix in each PCR strip tube. Tubes were sealed and centrifuged to remove air bubbles. Samples were then denatured at 95°C for two minutes, and then immediately chilled on ice for a further two minutes. Samples were subsequently transferred to the Applied Biosystems 3130 Genetic Analyser (Thermo Fisher Scientific) for processing, and GeneMapper® software (Thermo Fisher Scientific) was used to analyse data.

6.1.2. Mycoplasma testing

Mycoplasmas are a group of bacteria that lack a cell wall around the cell membrane. They induce changes in growth rate, cell metabolism and morphology (489). Since mycoplasmas are not so easy to detect as other bacteria, mould or yeast, mycoplasma contamination is characteristically unapparent macroscopically or microscopically and can affect any parameter measured in cell culture or in laboratory investigations, and the experimental findings obtained from Mycoplasma-infected cell culture may be

unreliable (284,490). The prevalence of such contaminations ranges from 5 to 87% (491). Therefore, frequent detection of mycoplasmas in cell culture is essential for cell-based assays. Due to its rapidity and sensitivity, the PCR method is commonly used to detect mycoplasma contamination in cell cultures (491,492).

Screening for mycoplasma contamination was performed as a service at the University of Liverpool with the assistance of Mr Steven Hoang (Technician support, University of Liverpool) using e-Myco™ mycoplasma PCR detection kit (ChemBio, UK) to detect mycoplasma-specific sequences. Cells were left without being passaged or having the media changed for at least 3 days before being harvested using trypsin-EDTA, as described in section 2.2.3. 1ml of cell suspension, at a minimum cell count of $5x10^4$/ml, was transferred to an Eppendorf® 1.5ml microcentrifuge tube. Following centrifugation at 7,000 RPM (Eppendorf 5424R refrigerated microcentrifuge) see comment below for 5 minutes, the supernatant was carefully removed, and the cells were resuspended in 1ml of sterile PBS and washed twice. Cells were then resuspended in 100µl of sterile PBS, heated for 10 minutes at 95°C in a heat block, and vortexed for 5-10 seconds, before being centrifuged at 13,000 RPM (Eppendorf 5424R refrigerated microcentrifuge) for two minutes. The supernatant was then removed and 100µl of the supernatant was aliquoted into a new Eppendorf® 1.5ml microcentrifuge tube. Next, 10µl of each sample was mixed with 10µl of DNase/RNase-free distilled water in an e-Myco™ reaction tube. 20µl of DNase/RNase-free Distilled water was used as a negative control, while 10µl of e-Myco™ control DNA was mixed with 10µl DNase/RNase-free Distilled water and used as a positive control. Samples were lightly vortexed and centrifuged before loading into a Px2 thermal cycler (Thermo Fisher Scientific), which was used to perform the following PCR:

- 94°C – 1 minute
- 94°C – 30 seconds
- 60°C – 20 seconds
- 72°C – 1 minute

  } 35 cycles

- 72°C – 5 minutes

2g of agarose was fully dissolved in 100ml of Tris base, acetic acid and EDTA (TAE) buffer and allowed to cool before being slowly poured into a sealed gel cast to set. Next, the sealing tape and the comb were removed, and the assembled gel was submerged in TAE buffer inside Sub-Cell® GT tank. 15µl of DNA size ladder, samples and controls

were loaded, and the gel was run at 100V for 35 minutes. DNA bands were imaged using ChemiDoc MP Imaging System (Bio-Rad), enabled by the presence of 0.5µg/ml of ethidium bromide in the agarose gel. Figure 6.1. is a representative of the regular mycoplasma test results confirming that the UM-SCC cells used in this research were mycoplasma-negative. If cell lines were found to be positive for mycoplasma contamination, alternative stocks were tested for the presence of mycoplasma contamination before being used. Contaminated cells were treated as detailed in 6.2.

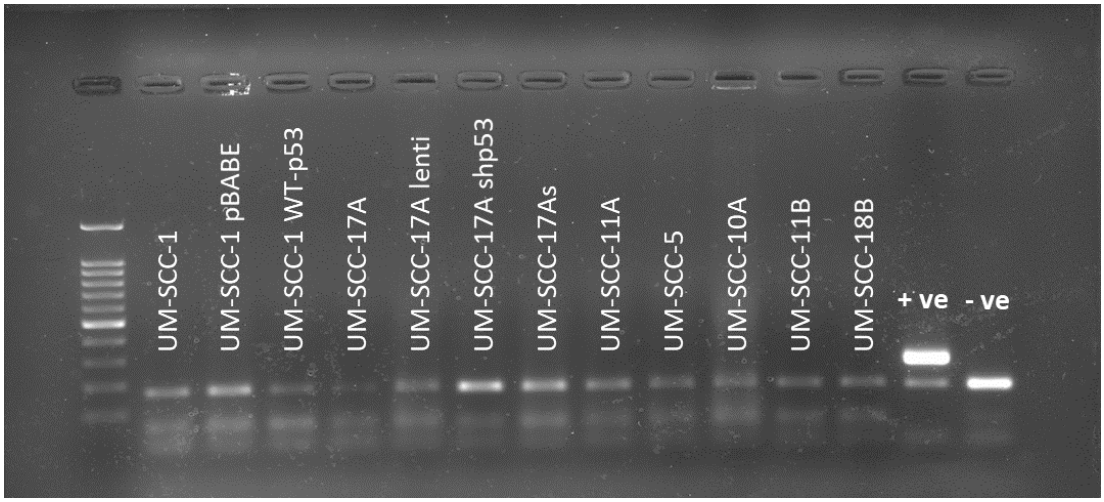

Figure 6.1.: A representative of the regular mycoplasma test results confirming that the UM-SCC cells used in this research were mycoplasma-negative.

6.2. Treatment of mycoplasma contamination in cell culture

Cells contaminated with mycoplasma were treated with Plasmocin™ (Invivogen). This compound contains two bactericidal components, one of which interferes with ribosome translation, targeting the protein synthesis machinery, while the other targets DNA replication. Plasmocin™ was used at a final concentration of 25 µg/ml in a complete media as follows: medium from the contaminated cells was removed and washed twice with PBS. Cells were passaged into a complete medium containing Plasmocin™ at an appropriate dilution depending on the growth rate of the contaminated cells (typically 1:10 split ratio). The medium was replaced or a passage was performed into a fresh complete medium containing Plasmocin™ every 3-4. The process was repeated for at least two weeks (typically 4 passages). Cells were then examined the cells as described in section 6.1.2. to confirm mycoplasma eradication.

6.3. Plasmids maps

(A)

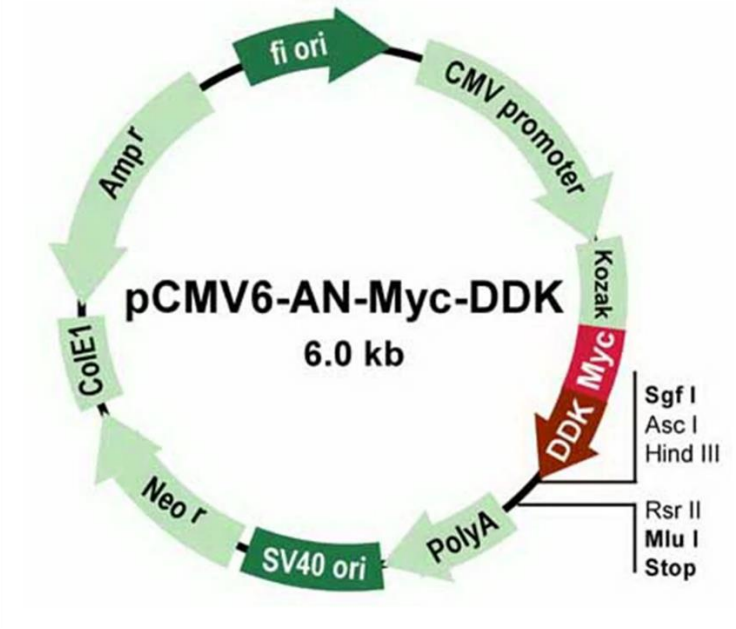

(B)

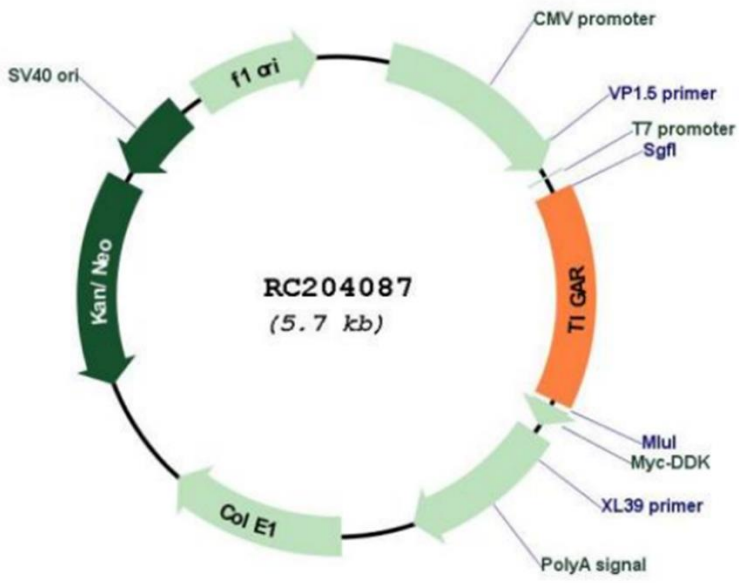

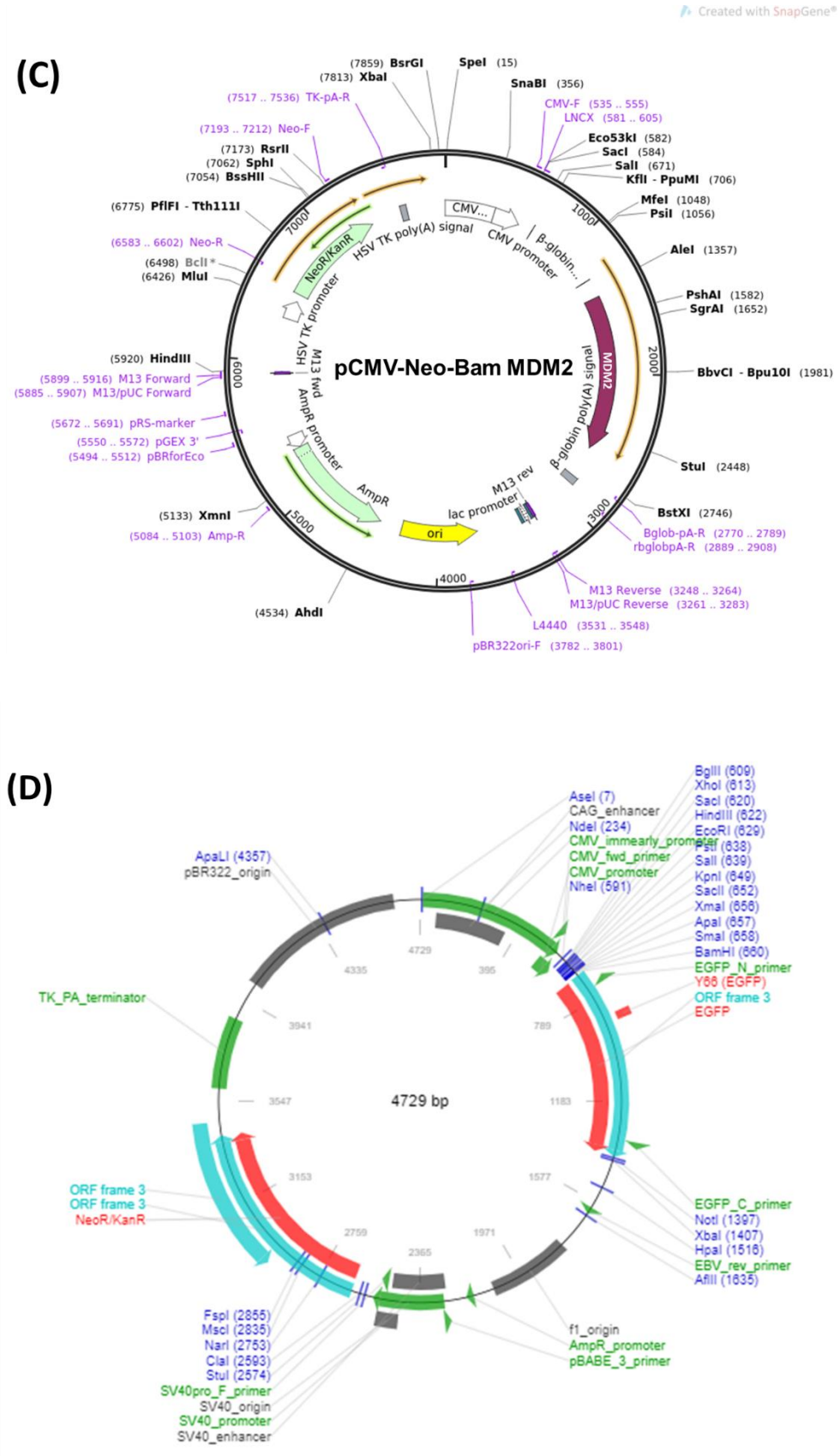

Figure 6.2.: Maps of the plasmids used: (A) pCMV6-AN-Myc-DDK Mammalian Expression Vector, **(B)** Myc-DDK-tagged-Human TIGAR open reading frame 5 clone, **(C)** pCMV-Neo-Bam MDM2 and **(D)** pEGFP-N3 plasmid.

6.4. Sanger sequencing of TIGAR plasmid

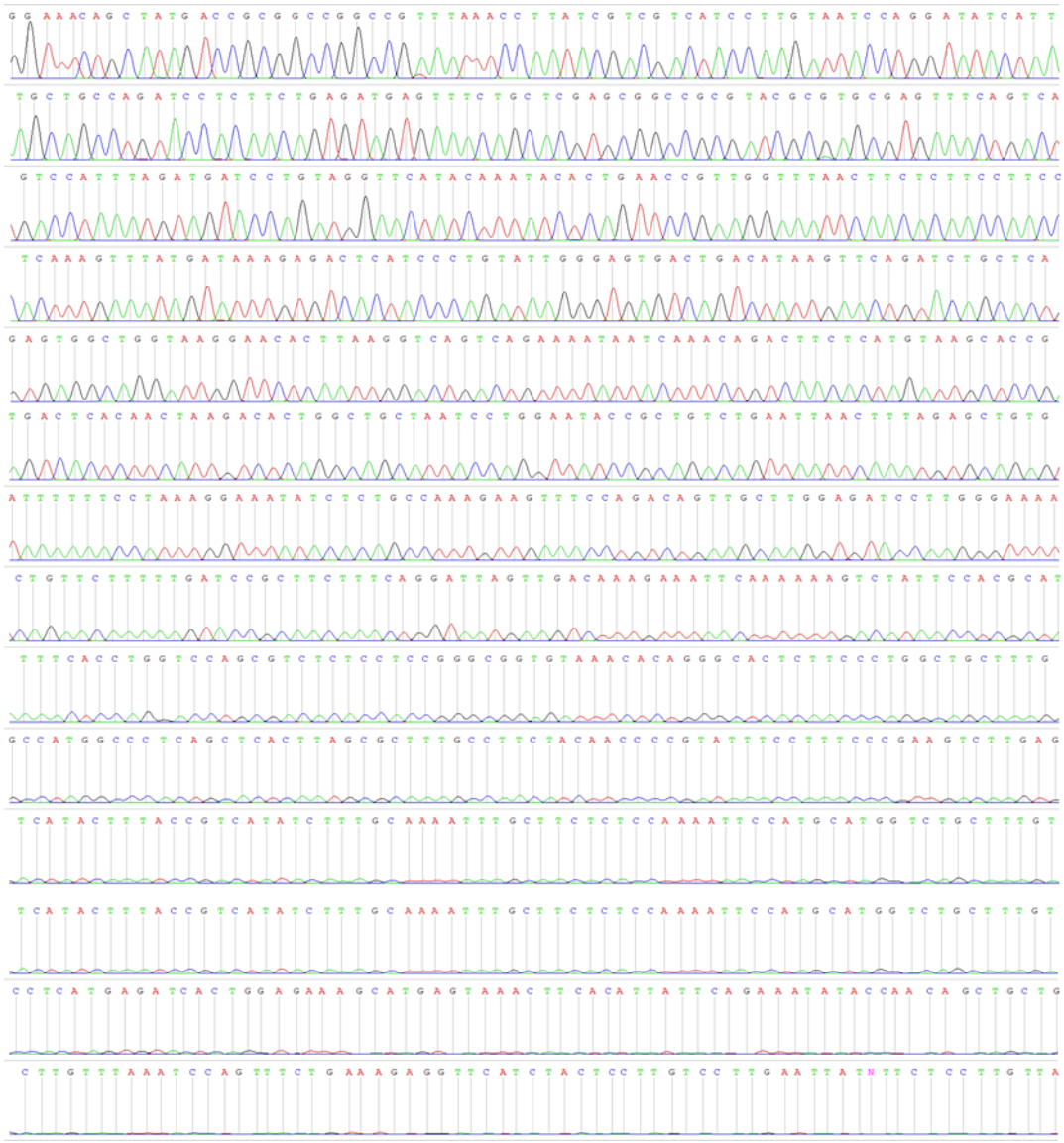

Figure 6.3.: A four-colour DNA sequencing chromatogram of the Myc-DDK-tagged-Human TIGAR open reading frame 5 clone, generated using the Sanger sequencing service by Source BioScience lab (Nottingham, UK).